Muscarinic receptor antagonism activates TRPM3 channels to augment mitochondrial function and provide neuroprotection

by

Sanjana Chauhan

A THESIS

SUBMITTED TO THE FACULTY OF GRADUATE STUDIES

IN PARTIAL FULFILLMENT OF THE REQUIREMENTS FOR THE DEGREE OF

DOCTOR OF PHILOSOPHY

DEPARTMENT OF PHARMACOLOGY AND THERAPEUTICS

RADY FACULTY OF HEALTH SCIENCES

UNIVERSITY OF MANITOBA

WINNIPEG, MANITOBA

ABSTRACT

Peripheral neuropathy, commonly associated with diabetes, chemotherapy, and HIV- induced nerve damage, leads to progressive sensory deficits and nerve dysfunction. While muscarinic acetylcholine type 1 receptor (M_1R) antagonism promotes sensory axon repair, the mechanisms underlying its neuroprotective effects remained unclear. Transient receptor potential melastatin-3 (TRPM3), a heat-sensitive cation channel, plays a crucial role in calcium signaling, mitochondrial function and neuronal metabolism, positioning it as a potential mediator of M_1R antagonist-driven neuroprotection. This thesis investigated the mechanistic link between M_1R antagonism and TRPM3 activation and explored the therapeutic potential of TRPM3 modulation in sensory axon regeneration.

M_1R antagonists pirenzepine (PZ) and muscarinic toxin 7 (MT7) enhanced TRPM3-mediated Ca^{2+} influx in dorsal root ganglion (DRG) neurons, an effect that was abolished by TRPM3 inhibitors or extracellular Ca^{2+} removal. TRPM3 activation using CIM0216 and pregnenolone sulfate (PS) elevated intracellular Ca^{2+}, promoted AMP-activated protein kinase (AMPK) phosphorylation via the Ca^{2+}/calmodulin-dependent protein kinase kinase β (CaMKKβ) pathway, leading to enhanced mitochondrial function, glycolysis, and tricarboxylic acid (TCA) cycle activity. Further analysis established that M_1R antagonism stimulated TRPM3 by inhibiting phosphatidylinositol 4,5-bisphosphate (PIP_2) hydrolysis, facilitating sustained calcium signaling and metabolic enhancement. TRPM3 knockdown via adeno-associated virus (AAV)-mediated shRNA suppressed the neurite-promoting effects of M_1R antagonists, confirming its essential role in axonal plasticity.

To assess whether these findings translated to an *in vivo* setting, the streptozotocin (STZ)-induced diabetic neuropathy model was utilized, which recapitulated key sensory impairments such as mechanical allodynia, slowed motor nerve conduction velocity (MNCV), and thermal hypoalgesia. PZ treatment restored sensory function in diabetic mice, but co-administration of TRPM3 inhibitors (isosakuranetin and primidone) abolished these improvements, confirming that M_1R-mediated neuroprotection was TRPM3-dependent. Despite the emergence of sensory impairments at 16 weeks post-STZ induction, corneal nerve loss was less pronounced than expected, suggesting a gradual progression of neuropathy, where functional impairments preceded structural degeneration. However, TRPM3 inhibition significantly reduced corneal nerve density, further highlighting its potential role in sensory fiber maintenance. This thesis established TRPM3 as a key modulator of sensory axon regeneration via Ca^{2+}-dependent AMPK signaling, demonstrating its potential as a therapeutic target for peripheral neuropathy and neurodegenerative disorders.

ACKNOWLEDGEMENTS

Completing this doctoral thesis has been one of the most challenging yet rewarding experiences of my life. This journey would not have been possible without the unwavering support of my lab mates, friends, and family, to whom I am immensely grateful.

First and foremost, I extend my deepest gratitude to my supervisor and mentor, Dr. Paul Fernyhough. His steadfast support over the past six years has been instrumental in shaping my academic and personal growth. He not only equipped me with the knowledge and confidence to present my research in front of large audiences but also fostered resilience and strength within me. His transparency and open-door policy created an environment where I could freely share my thoughts and challenges. Dr. Fernyhough not only guided me academically but walked alongside me at every step of my Ph.D. journey, ensuring I reached the finish line. From writing research proposals and manuscripts to troubleshooting experimental setups, he was always available, despite his busy schedule. I am profoundly indebted to him.

I sincerely appreciate Dr. Nigel A. Calcutt for mentoring me during my three-month tenure as a visiting scholar at UCSD. His guidance made adapting to a new city, research environment, and animal techniques seamless. I am also grateful to the UCSD lab members for their warm welcome and support, which helped me quickly integrate and learn new experimental methods.

I am equally grateful to my thesis committee members, Dr. Michael F. Jackson, and Dr. Jillian Stobart, for their invaluable feedback and encouragement throughout my doctoral journey. Dr. Jackson's insights pushed me to look at the bigger picture and explore alternative approaches to my research questions. Dr. Stobart's challenging yet insightful questions helped shape my research direction, and her guidance in calcium analysis was instrumental in refining my work. Their mentorship and support during progress meetings and beyond have been truly invaluable.

This achievement would not have been possible without the support of past and present members of Dr. Fernyhough's lab. Thank you, Shayan, Pranav, Reza, Ruth, Farhana, Zaved, Terra, and Karmen, for fostering a supportive and engaging lab environment. A special mention to Shayan and Pranav, with whom I shared the highs and lows of this Ph.D. journey. I would also like to express my gratitude to Darrell for his relentless support in maintaining the lab, assisting with animal handling, and ensuring the smooth operation of my experiments. My heartfelt thanks also go to Kelly for handling every administrative aspect of my Ph.D. with efficiency, making the process seamless.

My family and friends have been my foundation of strength and support. The unconditional love, encouragement, and sacrifices of my parents, Mr. Rajinder Kumar and Mrs. Ravinderjit Kaur, have shaped me into the person I am today. My younger brother Sandeep Kumar is the reason I dare to chase my dreams, and I am grateful for his constant encouragement and belief in me. I would also like to acknowledge my dear friend, Keshav Narayan, at SBRC. From the very first day of my Ph.D., he has been my unwavering support, helping me face challenges head-on and navigate the ups and downs of this journey with resilience. To my friends back home in India—Dr. Swarnendra Singh, Neetu, Monika, and Sonika - thank you for being my emotional anchors, always available to listen and support me, no matter the distance. Your presence, even from miles away, has been invaluable.

Lastly, my gratitude extends to Karen and Janelle for their administrative support and to the funding agencies that supported my research project. This journey has been a collective effort, and I am deeply grateful to everyone who played a role in shaping this significant milestone in my life.

Table of Contents

List of Abbreviations, Symbols and Nomenclature

Abbreviation	Definition
ACC	Acetyl-CoA carboxylases
Ach	Acetylcholine
AGEs	Advanced glycation end products
AMPK	AMP-activated protein kinase
ATP	Adenosine triphosphate
AUC	Area under the curve
BDNF	Brain-derived neurotrophic factor
CaM	Calmodulin
CaMKKβ	Ca^{2+}/calmodulin-dependent protein kinase kinase β
CBS	Cystathione β-synthase
CCAC	Canadian Committee on Animal Care
CCM	Corneal confocal microscopy
CCM	Corneal confocal microscopy
CIPN	Chemotherapy-induced peripheral neuropathy
CNS	Central nervous system
COX-2	Cyclooxygenase-2
CXCL12	C-X-C Motif Chemokine Ligand 12
CXCR4	C-X-C chemokine receptor type 4
DAG	Diacylglycerol
DEE	Developmental and epileptic encephalopathies
DM	Diabetes mellitus
DRG	Dorsal root ganglion
DSPN	Diabetic sensorimotor polyneuropathy
eEF2K	Eukaryotic elongation factor 2 kinase
ER	Endoplasmic reticulum
F-6-P	Fructose-6-phosphate
FADH2	Flavin adenine dinucleotide
FBS	Fetal bovine serum
GABA	Gamma-aminobutyric acid
GAP43	Growth-associated protein 43
GLUT1	Glucose transporter type 1
GLUT3	Glucose transporter type 3
GLUT4	Glucose transporter type 4
GPCR	G protein-coupled receptor
HDL	High-density lipoprotein
HFD	High-fat diet
HIV-DSP	HIV-associated distal sensory polyneuropathy
HLA	Human leukocyte antigen
IDF	International Diabetes Federation
IDH	Isocitrate dehydrogenase

IENF	Intraepidermal nerve fiber
IGT	Impaired glucose tolerance
IL-6	Interleukin-6
IP3	Inositol trisphosphate
IP3Rs	Inositol 1,4,5-trisphosphate receptors
KCC2	Potassium-chloride cotransporter 2
LDL	Low-density lipoprotein
M1R	Muscarinic acetylcholine type 1 receptor
MAMs	Mitochondria-associated membranes
MAPK	Mitogen-activated protein kinase
MCU	Mitochondrial Ca^{2+} uniporter
MDA	Malondialdehyde
MGO	Methylglyoxal
MHC	Major histocompatibility complex
MMP	Mitochondrial membrane potential
MT7	Muscarinic toxin 7
mTORC1	Mammalian target of rapamycin complex 1
mtTFA	Mitochondrial transcription factor A
NADPH	Nicotinamide adenine dinucleotide
NCV	Nerve conduction velocity
NF-κB	Nuclear factor kappa-light-chain-enhancer of activated B cells
NO	Nitric oxide
NOD	Non-obese diabetic
OCR	Oxygen consumption rate
OXPHOS	Oxidative phosphorylation
PAD	Peripheral artery disease
PAI-1	Plasminogen activator inhibitor-1
PBS	Phosphate buffer saline
pChAT	Peripheral form of choline acetyltransferase
PDH	Pyruvate dehydrogenase
PDN	Painful diabetic neuropathy
PFKFB3	6-Phosphofructo-2-kinase/fructose-2,6-biphosphatase 3
PGC-1α	Peroxisome proliferator-activated receptor-γ coactivator 1α
PIP2	Phosphatidylinositol 4,5-bisphosphate
PIP3	Phosphatidylinositol (3,4,5)-trisphosphate
PKC	Protein kinase C
PLC	Phospholipase C
PNS	Peripheral nervous system
PS	Pregnenolone sulphate
PTEN	Phosphatase and tensin homolog
PWT	Paw withdrawal threshold
PZ	Pirenzepine
ROI	Region of interest
ROS	Reactive oxygen species
RyRs	Ryanodine receptors

SERCA	Sarco/endoplasmic reticulum Ca^{2+} ATPase
STZ	Streptozotocin
T1DM	Type 1 diabetes mellitus
T2DM	Type 2 diabetes mellitus
TCA	Tricarboxylic acid
TNF-α	Tumor necrosis factor-α
TNF-β	Tumor necrosis factor-β
TrkB	Tropomyosin receptor kinase B
TRP	Transient receptor potential
TRPM3	Transient receptor potential melastatin-3
UDP-GlcNAc	Uridine diphosphate N-acetylglucosamine
ULK1	Unc-51-like autophagy-activating kinases 1
VDACs	Voltage-dependent anion channels
VGCCs	Voltage-gated Ca^{2+} channels
VGSCs	Voltage-gated sodium channels
VSD	Voltage-sensing domain
α-KGDH	α-Ketoglutarate dehydrogenase
β-SID	β-subunit interacting domain

List of Figures and Tables

Figures

Supplementary figures

Tables

Chapter 1

Background and literature review

1.1 Diabetes mellitus

Diabetes mellitus (DM) is a significant metabolic disorder with profound global health implications. Central to its pathophysiology are hyperglycemia and insulin resistance, which play crucial roles in disease progression and its complications (Nathan *et al.*, 2006). Chronic hyperglycemia, a hallmark of DM, leads to long-term damage, dysfunction, and failure of various organs, including the retina, kidneys, peripheral nerves, cardiovascular system, and blood vessels (Brownlee, 2001; Nathan *et al.*, 2006). There are two primary forms of diabetes: Type 1 diabetes mellitus (T1DM) and Type 2 diabetes mellitus (T2DM). T1DM, also known as insulin-dependent DM, constitutes 5-10% of DM cases, resulting from autoimmune destruction of pancreatic β-cells, leading to absolute insulin deficiency. This autoimmune process is mediated by T cells and involves multiple autoantigens, including insulin, glutamic acid decarboxylase (Agarwal *et al.*, 2018), and islet antigen-2 (IA-2) (Atkinson *et al.*, 2014; Bluestone *et al.*, 2015). T1DM primarily results from environmental triggers, such as viral infections and dietary factors, which initiate the autoimmune response. Although genetic predisposition plays a relatively minor role, certain polymorphisms, including those in the major histocompatibility complex (MHC) and human leukocyte antigen (HLA), influence the risk for T1DM. In contrast, T2DM, or insulin-independent DM, which accounts for 90-95% of DM cases, involves a more complex interplay between genetics and lifestyle factors (DeFronzo, 2004). T2DM is primarily characterized by peripheral insulin resistance combined with inadequate compensatory insulin secretion. Metabolic factors, particularly obesity, play a significant role in T2DM by contributing to insulin resistance. The

accumulation of ectopic fat in liver and muscle tissues interferes with insulin signaling pathways, resulting in decreased glucose uptake and increased hepatic glucose production. Initially, compensatory hyperinsulinemia maintains normoglycemic conditions, but over time, β-cell dysfunction ensues, leading to overt hyperglycemia (Gerich, 2003). The coexistence of impaired insulin secretion and insulin action defects in patients often complicates the identification of the primary cause of hyperglycemia in individual cases (Rossi, 2010). This hyperglycemic state is frequently associated with clinical symptoms such as polyuria, polydipsia, weight loss, and blurred vision (Kitabchi *et al.*, 2009).

1.2 Diabetic sensorimotor polyneuropathy

Diabetic sensorimotor polyneuropathy (DSPN) is a significant and prevalent complication of DM, characterized by a complex interplay of metabolic and vascular factors that result in widespread peripheral nerve damage (Callaghan *et al.*, 2012). Affecting up to 50% of individuals with diabetes, DSPN is initiated by chronic hyperglycemia, which sets off a cascade of biochemical disturbances and profoundly impacts quality of life (Feldman *et al.*, 2019). Sustained elevated blood glucose levels promote the accumulation of advanced glycation end products (AGEs) and reactive oxygen species (ROS), culminating in oxidative stress and chronic inflammation (Pedreanez *et al.*, 2024). These processes collectively disrupt neuronal integrity and function, manifesting through pain, sensory loss, and motor dysfunction (Smith *et al.*, 2022). The condition typically presents with a "stocking-glove" distribution of sensory deficits, where the hands and feet are most commonly affected, and the sensory loss often follows a length-dependent pattern, progressing proximally over time (Callaghan *et al.*, 2012; Palumbo *et al.*, 1978). This loss of protective sensation is particularly concerning as it severely compromises balance and the ability

to detect injuries, increasing the risk of foot ulcers (Armstrong and Lavery, 1998). These ulcers, if not properly managed, can lead to infections and, in severe cases, limb amputations.

Despite the widespread prevalence of DSPN, it is often underdiagnosed or inconsistently diagnosed, largely due to variable endpoint measurement methods, differing DSPN definitions, and the diverse types of patients studied (Steinmetz, 2024). Neurological signs and electrophysiological measurements are critical tools in diagnosing DSPN (Kambiz *et al.*, 2015; Mulder *et al.*, 1961; Pirart, 1977; Tuncer *et al.*, 2011), yet the lack of standardized criteria complicates the identification of the condition. The current treatment strategies focus primarily on glycemic control and pain management (Feldman *et al.*, 2019). However, these approaches are not effective in halting the progression of DSPN, underscoring the urgent need for early diagnosis, prevention, and more comprehensive treatment options. At this time, there is no disease-modifying therapy available to patients.

The risk and severity of DSPN are closely correlated with the duration of diabetes and the degree of glycemic control, highlighting the importance of stringent blood glucose management to mitigate the condition's progression (Staehelin Jensen, 2023). Furthermore, DSPN often coexists with autonomic neuropathy, another underdiagnosed condition that affects the autonomic nervous system, leading to abnormalities in cardiovascular, gastrointestinal, and genitourinary function (Vinik *et al.*, 2003). This autonomic involvement augments the complexity of neuropathic damage, as it impacts blood flow and homeostatic balance, thereby aggravating nerve degeneration. In addition to sensory nerve impairment, DSPN also affects motor nerves, leading to symptoms such as foot drop and distal muscle weakness (Callaghan *et al.*, 2012). This further exacerbates the patient’s risk of falls and injuries, emphasizing the necessity for early intervention and

comprehensive management strategies to prevent severe complications and improve patient outcomes (Chong and Hester, 2007).

1.3 Epidemiology - Economic and social burden of DSPN

DSPN represents a critical and expanding global health challenge, intricately linked to the escalating prevalence of diabetes mellitus, affecting nearly 50% of all diabetic patients globally (Steinmetz, 2024). The International Diabetes Federation (IDF) reports that as of 2021, approximately 537 million adults aged 20-79 years were living with diabetes, equating to 1 in 10 adults globally (Magliano *et al.*, 2021). This number is expected to rise to 643 million by 2030 and 783 million by 2045, with over three-quarters of these individuals residing in low and middle-income countries, where healthcare infrastructure may be less capable of effectively managing chronic complications, such as DSPN. The epidemiology of DSPN is fraught with challenges, particularly in terms of population selection and the definition of neuropathy. Despite these challenges, DSPN remains a widespread condition with a considerable impact on public health, particularly due to its association with a compromised quality of life and the substantial economic burden it imposes (Sloan *et al.*, 2021). The annual global expenditure on treating diabetic neuropathy and its complications is substantial, amounting to billions of dollars. For example, in 2003, the cost in the United States alone was estimated at US$11 billion, highlighting the significant financial burden associated with this condition (Gordois *et al.*, 2003).

Several epidemiological studies have attempted to evaluate the incidence and prevalence of diabetic neuropathy across different populations, with a focus on both T1DM and T2DM. The prevalence of DSPN is notably higher in individuals with T2DM, with an incidence of approximately 6,100 per 100,000 person-years, compared to 2,800 per 100,000 person-years in

those with T1DM (Ang *et al.*, 2014; Martin *et al.*, 2014; Pop-Busui *et al.*, 2013). This higher prevalence in T2DM is attributed to several factors, including differences in the age of onset of diabetes and variations in the underlying pathophysiology. Moreover, as the duration of diabetes increases, so does the likelihood of developing neuropathy. For instance, in a longitudinal study, the prevalence of diabetic neuropathy in patients with T2DM increased from 8% to 42% over a 10-year monitoring period (Partanen *et al.*, 1995). Regional studies highlight significant variations in prevalence, underscoring the disproportionate impact of DSPN in certain populations. For instance, a study in eastern Libya reported a prevalence of 42.2% among diabetic individuals, underscoring the heightened burden in North Africa (Garoushi *et al.*, 2019). Similarly, in Europe, North America, and Caribbean regions, where the diabetic population was estimated at 40-50 million in 2021, projections suggest this number will rise to approximately 70 million by 2045 (IDF report, 2021). With approximately half of these patients likely to suffer from peripheral neuropathy, the burden of DSPN in these regions is expected to grow exponentially (Newlin Lew *et al.*, 2022).

The clinical management of DSPN is further complicated by the fact that less than one-third of physicians accurately recognize its signs, leading to high rates of undiagnosed cases (Ziegler *et al.*, 2018). This lack of early detection contributes significantly to the morbidity and mortality associated with diabetes. Up to 50% of patients with DSPN are asymptomatic, which means they often remain undiagnosed and are consequently at greater risk of insensate injuries, which can lead to severe complications such as foot ulcers and amputations (Karthiksaravanan and Meriton, 2024). The global economic burden of diabetes is immense, with diabetes-related health expenditures reaching at least USD 966 billion in 2021, a 316% increase over the past 15 years (Magliano *et al.*, 2021). DSPN contributes significantly to this financial strain due to the costs

associated with managing its complications, particularly foot ulcers and amputations. Diabetic foot ulcers are estimated to affect 9.1 to 26.1 million people annually, often leading to amputations (Stancu *et al.*, 2022). Amputations due to DSPN are associated with a high mortality rate, with up to 30.5% of patients dying within five years post-amputation (Armstrong *et al.*, 2020). The impact of DSPN on quality of life is profound. Chronic painful DSPN, which affects up to 25% of diabetic individuals, significantly reduces patient's quality of life due to persistent pain and disability (Sharma and Rayman, 2023).

The prevalence of DSPN is also notable in populations with impaired glucose tolerance (IGT), which includes 541 million adults worldwide (Magliano *et al.*, 2021). These individuals are at a high risk of developing type 2 diabetes, and subsequently, DSPN, if preventive measures are not effectively implemented. In countries with large diabetic populations, such as China, India, and the United States—where 115 million, 73 million, and 30 million people, respectively, have diabetes, the management and prevention of DSPN are of critical importance (Feldman *et al.*, 2019). Given the significant global burden, it is crucial to deploy effective treatment strategies for DSPN in order to minimize the impact on quality of life as well as reduce the healthcare burden.

1.4 Dorsal root ganglion and nerve abnormalities in DSPN: Bridging human studies and animal insights

In DSPN, the dorsal root ganglia (DRG) serve as critical sensory relay centers within the peripheral nervous system (Berta *et al.*, 2017). These ganglia are integral to the modulation and transmission of sensory signals, and in DSPN, they undergo significant pathological changes due to metabolic disturbances, such as hyperglycemia (Miyashita *et al.*, 2023). These alterations in DRG function are key contributors to the sensory deficits and complex neurodegenerative processes observed in

DSPN, underscoring their importance in the disease's pathophysiology (Bhandari *et al.*, 2021; Krames, 2014). Located along the spinal column, these ganglia house the cell bodies of sensory neurons that extend their axons into both peripheral tissues and the spinal cord or brainstem (Berta *et al.*, 2017). The sensory neurons within the DRG are responsible for detecting a variety of stimuli, including mechanical pressure, temperature, pain, and proprioceptive information, and for converting these stimuli into electrical signals that can be interpreted by the CNS (Krames, 2014). DRG neurons are diverse, comprising several subpopulations that differ in their size, myelination, and function. These subpopulations can be broadly categorized based on their fiber types: unmyelinated small diameter C fibers, thinly myelinated Aδ fibers, myelinated Aβ fibers, and large myelinated proprioceptors known as Aα fibers (Haberberger *et al.*, 2023). Each of these fiber types is specialized to respond to specific types of stimuli, for instance C fibers, which are the most numerous, are primarily involved in transmitting nociceptive and thermal information, while Aβ fibers are involved in detecting touch and vibration (Figure 1.1).

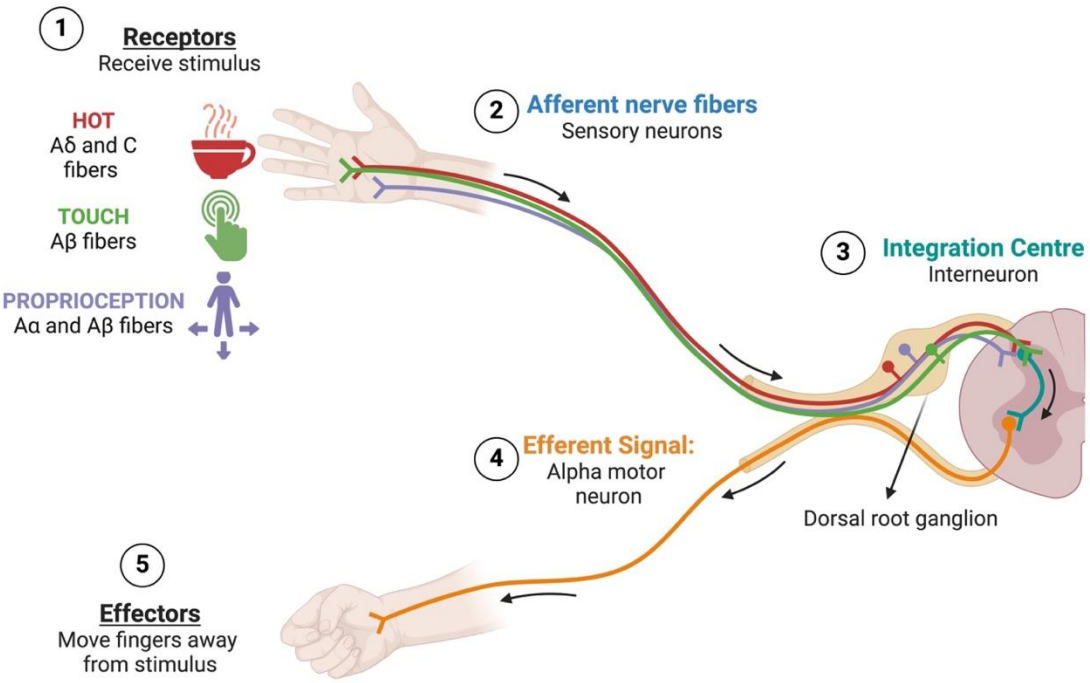

Figure 1.1. Sensory signal flow and reflexive motor Output. This figure depicts the pathways involved in detecting and responding to noxious and non-noxious stimuli. Specific receptors in the skin and muscles sense various stimuli: Aδ fibers transmit sharp pain from hot stimuli, while C fibers carry dull, slow pain signals. Touch stimuli, including light touch and pressure, are transmitted via Aβ fibers, and proprioception-sensing body position and movement, is detected by Aα and Aβ fibers. Sensory (afferent) neurons relay these signals to the dorsal root ganglion (DRG) and into the spinal cord, where interneurons in the integration center process the input. Motor (efferent) signals are then sent via alpha motor neurons to effectors, such as hand or arm muscles, which execute responses like withdrawing from a harmful stimulus. This reflex arc highlights the body's rapid processing of sensory input to produce protective motor responses. *Created with BioRender.*

Anatomically, DRG neurons are surrounded by satellite glial cells and are exposed to a high blood flow, but they lack a robust neurovascular barrier, making them particularly prone to injury from circulating toxins and metabolic imbalances seen in diabetes (Abram *et al.*, 2006; Jimenez-Andrade *et al.*, 2008; Sapunar *et al.*, 2012; Zochodne and Ho, 1991). Hyperglycemia is believed to directly target these neurons, initiating a cascade of degenerative changes. DSPN typically presents with sensory deficits that follow a “stocking and glove” distribution, progressing from the distal extremities toward more proximal regions (Brown and Asbury, 1984; Sharma and Rayman, 2023) . This pattern suggests a dying-back mechanism, where longer axons are affected first, leading to a retrograde degeneration that may ultimately compromise the neuronal cell bodies within the DRG. To better understand these processes, rodent models of T1DM and T2DM have been extensively used to replicate many of the early functional and structural abnormalities observed in human DSPN (Feldman *et al.*, 2019). These models, including the BioBreeding/Worcester (BB/Wor) rat and the Ins2Akita mouse, demonstrate early functional and structural abnormalities such as the slowing of motor and sensory nerve conduction velocities

(MNCV and SNCV), sensory disturbances such as allodynia and hyperalgesia, and the eventual progression to sensory loss; mirroring the early stages of human DSPN (Kamiya *et al.*, 2009; Stevens *et al.*, 2004).

In streptozotocin (STZ) induced T1DM rats, for example, there is a progressive decline in the synthesis and export of neurofilament polymers, resulting from aberrant phosphorylation at specific sites within the neurofilament protein structure (Fernyhough *et al.*, 1999). This improper phosphorylation disrupts neurofilament assembly and compromises the structural integrity of sensory axons. This mirrors the neurofilament depletion observed in human DSPN (Maalmi *et al.*, 2023). Structurally, rodent models also replicate several features of early nerve pathology observed in humans, including reduced density of epidermal and corneal small sensory nerve fibers, myelin thinning, and a reduction in the size of large, myelinated axons (Dhage *et al.*, 2021; Misra *et al.*, 2015; Wang *et al.*, 2015; Ziegler *et al.*, 2014). However, despite these parallels, rodent models often fall short in replicating the late-stage structural pathology of human DSPN, particularly the extensive loss of fibers, Schwann cell pathology and segmental demyelination that are prominent in advanced human cases (Dunnigan *et al.*, 2013; Gumy *et al.*, 2008; Mizisin *et al.*, 1998; Willows *et al.*, 2023). While mild myelin thinning and occasional segmental demyelination (only observed in the BB rat model of type 1 diabetes) have been observed in rodents, they generally do not exhibit the severe Schwann cell damage seen in humans (Jin *et al.*, 2021). The reported variability in neuropathy measures among different models highlight the intricate and varied nature of DSPN progression, which can be influenced by factors such as background strain, diet composition, insulin/C-peptide deficiency, and coexisting conditions such as hyperglycemia and hypertension (Singh *et al.*, 2024). Despite these limitations, rodent models provide a controlled environment to explore early molecular events that may not be as easily studied in humans. For example, the

downregulation of growth-associated proteins such as growth-associated protein 43 (GAP43) and the upregulation of inhibitory factors such as phosphatase and tensin homolog (PTEN) in rodent models highlight the degenerative phenotype specific to diabetes, underscoring the role of metabolic and neurotrophic dysfunctions in driving DSPN (Maeda *et al.*, 1996; Singh *et al.*, 2014). Additionally, advancements in diagnostic techniques, such as corneal confocal microscopy (CCM) and intraepidermal nerve fiber (IENF) density measurements, have enhanced our ability to monitor small fiber neuropathy and DRG neuronal health in these models (Chen *et al.*, 2015; Dhage *et al.*, 2021). This, in turn, provides a more comprehensive understanding of DSPN's progression, ultimately aiding in bridging the gap between early and late-stage disease observed in humans.

1.5 Painful diabetic peripheral neuropathy (PDN)

Painful diabetic peripheral neuropathy (PDN) represents a significant complication found in persons with DSPN, affecting approximately 20–30% of individuals with neuropathy (Preston *et al.*, 2023). It is characterized by chronic neuropathic pain, which can severely impact quality of life, sleep, and mental health. While DSPN typically involves progressive axonal loss and sensory deficits, the painful phenotype is characterized by paradoxical sensory abnormalities, including spontaneous pain, mechanical allodynia, and thermal hypoalgesia (Pacifico *et al.*, 2023). The underlying pathophysiology of neuropathic pain in PDN extends beyond peripheral nerve degeneration, involving anatomical and functional alterations at multiple levels of the pain pathway, including the DRG, dorsal horn of the spinal cord, and brain. Chronic hyperglycemia leads to oxidative stress, mitochondrial dysfunction, and impaired protein homeostasis within the DRG, triggering upregulation of voltage-gated sodium channels such as Nav1.7 and Nav1.8 (Jayaraj *et al.*, 2018). Studies indicate that Nav1.8 is expressed in approximately 75% of DRG sensory neurons, including over 90% of C-fiber nociceptors, as well as certain Aδ-nociceptors and

Aβ afferents (Shields *et al.,* 2012). The hyperexcitability of sensory neurons in PDN is largely driven by dysregulated Nav1.8, which plays a crucial role in pain signaling (Jayaraj *et al.*, 2018). This dysregulation leads to increased spontaneous firing of nociceptive neurons, causing persistent pain even in the absence of external stimuli.

In experimental models of PDN, tactile allodynia has been extensively studied using high-fat diet (HFD) mouse models, where mechanical allodynia develops as a hypersensitivity to mechanical stimuli such as light touch. This phenomenon is linked to the hyperexcitability of Nav1.8-positive DRG neurons, driven by C-X-C motif chemokine 12 (CXCL12)/ C-X-C chemokine receptor type 4 (CXCR4) signaling (Jayaraj *et al.,* 2018). By targeting the CXCR4 signaling pathway, researchers have been able to both prevent and reverse mechanical allodynia, suggesting a potential therapeutic avenue for managing pain in PDN. A critical factor contributing to PDN is the complex interplay between keratinocytes and sensory neurons. Recent research on keratinocyte-derived exosomes (KDEs) has revealed their involvement in axon degeneration and neuropathic pain development (Coy-Dibley *et al.*, 2024). Using a HFD mouse model of PDN, KDEs were successfully characterized and isolated, revealing significant alterations in their proteomic and microRNA composition. Notably, pathways associated with axon guidance and synaptic transmission were found to be dysregulated in KDEs from HFD-fed mice, implicating their role in neuropathic pain. *In vivo* tracking of KDEs demonstrated that these exosomes are retrogradely trafficked into DRG neurons, indicating bi-directional communication between keratinocytes and sensory neurons. This suggests that KDEs contribute to axon degeneration and maladaptive pain signaling, opening new possibilities for targeting KDE-mediated mechanisms in the development of topical interventions for PDN. Additionally, some ion channels, including transient receptor potential (TRP) channels such as TRPV1 and TRPA1, are implicated in pain

hypersensitivity by amplifying nociceptive signaling (Gao *et al.*, 2024). Despite the complexity of the underlying mechanisms in PDN, ongoing research continues to explore new strategies to alleviate pain and identify novel molecular targets for effective therapeutic interventions in diabetic neuropathy.

1.6 Pathogenesis of DSPN: Crosstalk between metabolic pathways

1.6.1 Hyperglycemia & lipid abnormalities

Peripheral neurons that innervate the feet, are among the longest cells in the human body. These sensory neurons are heavily reliant on a robust vascular supply, functional mitochondria, and tightly regulated glucose and lipid metabolism to meet their substantial energy requirements (Galiero *et al.*, 2023; Rawat and Morrison, 2021). Neurons, even in a quiescent state, demand constant energy to sustain membrane potential, propagate action potentials, and recycle neurotransmitters (Li and Sheng, 2022). This high metabolic demand underscores the importance of efficient bioenergetic processes, which involve the uptake and regulated catabolism of glucose and fatty acids (Petersen *et al.*, 2022) to generate ATP. Neurons primarily absorb glucose via the insulin-independent glucose transporter 3 (GLUT3), which is metabolized through glycolysis into pyruvate (Peng *et al.*, 2021). Under aerobic conditions, pyruvate enters the tricarboxylic acid (TCA) cycle and oxidative phosphorylation (OXPHOS), generating up to 32 ATP molecules per glucose molecule. This pathway is critical for sustaining neuronal activity and energy homeostasis (Wilson, 2017). However, in DSPN, these tightly regulated metabolic pathways become overwhelmed, leading to the activation of auxiliary metabolic routes such as the polyol and hexosamine pathways (Mizukami and Osonoi, 2020). These metabolic shifts, while initially adaptive in managing excess glucose, contribute to long-term bioenergetic dysfunction by

promoting the generation of ROS, increasing inflammatory responses, and driving mitochondrial dysfunction (Román-Pintos *et al.*, 2016) .

Hyperglycemia triggers the activation of multiple metabolic pathways, beginning with the polyol pathway, which is highly active in cells such as neurons that do not effectively regulate glucose uptake (Chung *et al.*, 2003). In this pathway, the enzyme aldose reductase catalyzes the first step and reduces excess glucose to sorbitol. This reaction utilizes nicotinamide adenine dinucleotide (NADPH) as a cofactor, which is essential for maintaining cellular redox balance and regenerating reduced glutathione, a major antioxidant. However, the accumulation of sorbitol within cells, due to its limited ability to diffuse across membranes, results in osmotic stress, drawing water into the cells and causing swelling. This osmotic imbalance can lead to cellular damage, particularly affecting Schwann cells, which are critical for nerve conduction. The disruption of Schwann cells impairs nerve signal transmission, contributing to sensory deficits observed in DSPN. Additionally, the conversion of sorbitol to fructose by sorbitol dehydrogenase consumes NAD+, disrupting the NADH/NAD+ ratio and contributing to oxidative stress (Pang *et al.*, 2020). The depletion of NADPH further reduces the capacity to regenerate glutathione, exacerbating oxidative damage to nerve cells, including those in the DRG. Simultaneously, hyperglycemia promotes the diversion of glucose into the hexosamine pathway, where fructose-6-phosphate (F-6-P) is converted to glucosamine-6-phosphate via the enzyme glutamine aminotransferase (GFAT). This pathway ultimately generates uridine diphosphate N-acetylglucosamine (UDP-GlcNAc), which typically functions in proteoglycan synthesis and the O-linked glycosylation of proteins (Paneque *et al.*, 2023). However, in the context of DSPN, a portion of UDP-GlcNAc is aberrantly directed toward transcription factors such as Sp-1 (Zhu *et al.*, 2023). Sp-1 regulates crucial metabolic and inflammatory pathways, including insulin and lipid

homeostasis, and influences the expression of tumor necrosis factor-β (TNF-β) and plasminogen activator inhibitor-1 (PAI-1) (Figure 1.2). These molecular alterations drive persistent inflammation, elevated oxidative stress, and activation of neurodegenerative pathways, leading to targeted degeneration of sensory neurons and Schwann cells within the peripheral nervous system.

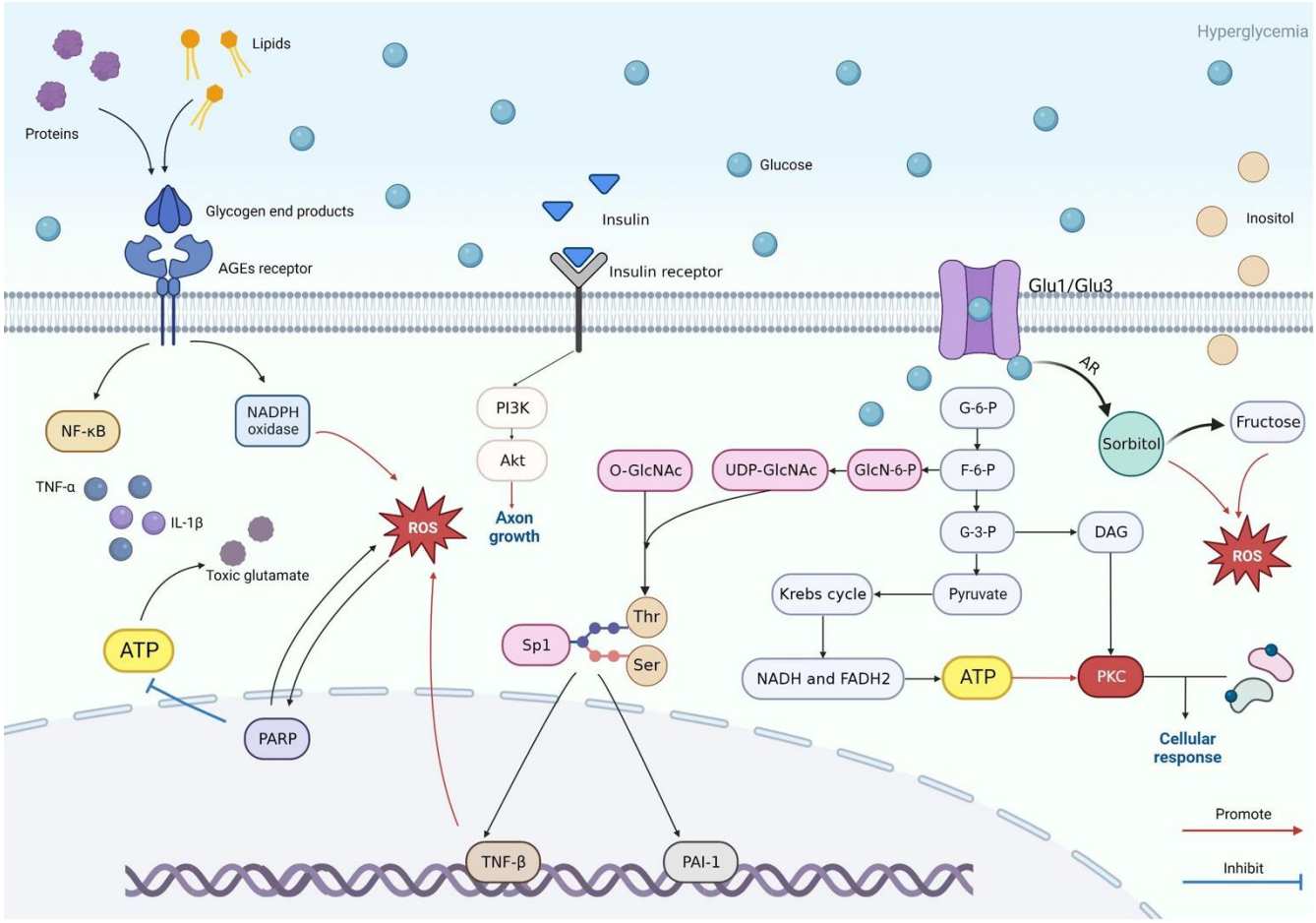

Figure 1.2. Hyperglycemia-driven pathways contributing to DSPN. Under hyperglycemic conditions, elevated glucose levels enter cells through glucose transporters and are shunted into multiple metabolic pathways. Excess glucose is converted into sorbitol and fructose via the polyol pathway, generating reactive oxygen species (ROS). Increased glucose also promotes the formation of advanced glycation end-products

(AGEs), activating their receptor (Burglen *et al.*) and stimulating NADPH oxidase, NF-κB, and pro-inflammatory cytokines. The hexosamine pathway modifies transcription factors (e.g., Sp1), altering gene expression of factors like TNF-β. Elevated diacylglycerol (DAG) activates protein kinase C (PKC), influencing cellular responses. Collectively, these intertwined mechanisms lead to oxidative stress, inflammation, and disrupted cellular function. *Adapted from Zhu, Jinxi et al. 2024* and added explanation to the figure legend (Zhu *et al.*, 2023), Frontiers in Endocrinology under the terms of the CC BY 4.0 license.

Hyperglycemia continues to drive this detrimental cycle, as elevated glucose levels result in the non-enzymatic binding of glucose to amino residues of various structural and functional proteins, leading to the formation of advanced glycation end-products (AGEs) (Wada and Yagihashi, 2005) (Figure 1.2). These products, which are toxic to neural tissues (Kikuchi *et al.*, 1999), have been linked to pain and hyperalgesia in individuals with diabetes (Bierhaus *et al.*, 2012). One major mediator of this hyperalgesia is methylglyoxal (MGO), a highly reactive dicarbonyl metabolite that accumulates in diabetes due to impaired glyoxalase-1 activity in the PNS. Elevated MGO levels have been observed in patients with painful diabetic neuropathy (Bierhaus *et al.*, 2012), although conflicting results exist (Hansen *et al.*, 2015). MGO contributes to pain through post-translational modification of voltage-gated sodium channels (VGSCs), particularly Nav1.8. By modifying arginine residues within Nav1.8's inactivation domain, MGO induces a depolarizing shift in the voltage dependence of fast inactivation, causing hyperexcitability of nociceptors. In addition to the role of MGO, another major consequence of hyperglycemia is the deposition of AGEs within neural tissues. The deposition of AGEs has been observed in the nerves of diabetic patients and animal models of diabetes. When AGEs bind to their specific receptors (Burglen *et al.*, 2023) they trigger modifications in gene expression and intracellular signaling pathways,

resulting in the secretion of pro-inflammatory molecules and free radicals (Koerich *et al.*, 2023). This AGE-RAGE interaction not only amplifies inflammatory responses but also stimulates oxidative stress, which perpetuates neural damage. The other major contributor to the development of DSPN is protein kinase C (PKC), which is linked to normal nerve function (Way *et al.*, 2001). Aberrant regulation of PKC activity under hyperglycemia contributes to DSPN pathogenesis (Figure 1.2). Glucose is converted to diacylglycerol (DAG), a substrate for PKC-β, increasing vascular permeability and dysfunction (Geraldes and King, 2010). The pathological consequences of hyperglycemia are diverse and extensive, leading to pronounced nerve damage and dysfunction.

Lipids play a significant role in this progression, where both hyperlipidemia and dyslipidemia exacerbate DSPN in conjunction with hyperglycemia. Under normal physiological conditions, long-chain fatty acids enter the β-oxidation pathway, with each cycle producing one molecule of acetyl-CoA. However, in diabetes, the increased substrate load saturates the transport system, leading to the conversion of excess acetyl-CoA into acylcarnitines (Mu *et al.*, 2022). The buildup of these acylcarnitines is toxic to both DRG neurons and Schwann cells. Dyslipidemia, marked by elevated triglycerides and LDL cholesterol levels and reduced HDL cholesterol, further promotes vascular inflammation and oxidative stress, impairing blood flow and activating inflammatory pathways in the peripheral nervous system (Rumora *et al.*, 2018). The synergistic interaction between hyperlipidemia, dyslipidemia, and hyperglycemia amplifies metabolic instability, driving oxidative stress, inflammatory molecule secretion, and nerve degeneration, underscoring the importance of managing both glucose and lipid levels in diabetic patients to mitigate DSPN progression and improve neural health.

1.6.2 Vascular complications in DSPN

In DSPN, vascular dysfunction has emerged as a central element in the progression of the disease. While there is some variability in studies regarding the role of blood flow in the early stages of DSPN, mounting evidence supports the critical involvement of both microvascular and macrovascular complications in accelerating nerve damage (Li *et al.*, 2022). These vascular disturbances are intricately linked to chronic hyperglycemia, which drives a cascade of metabolic dysfunction, oxidative stress, and inflammation, leading to both impaired nerve perfusion and progressive nerve degeneration. Chronic hyperglycemia serves as the primary trigger for vascular dysfunction in DSPN, initiating metabolic dysregulation that impacts both the small blood vessels (microvasculature) and larger arteries (macrovasculature) (Cade, 2008). One of the key mechanisms through which hyperglycemia contributes to vascular damage is by disrupting endothelial nitric oxide (NO) production (Meza *et al.*, 2019). NO, a critical vasodilator responsible for maintaining vascular tone and regulating blood flow, is diminished in DSPN due to oxidative stress and inflammation triggered by persistent high glucose levels. The resulting endothelial dysfunction leads to reduced bioavailability of NO, which contributes to vasoconstriction and impaired blood flow to peripheral nerves (Kolluru *et al.*, 2012). This reduction in nerve perfusion results in chronic ischemia, depriving the nerves of essential oxygen and nutrients (Cameron *et al.*, 2001). The combination of reduced blood flow and metabolic stress accelerates axonal degeneration and impairs Schwann cells, which play a key role in myelination and nerve repair. Animal studies reinforce the role of vascular dysfunction in DSPN. For example, STZ-diabetic mice and db/db mice exhibit impaired blood flow and vascularization in their sciatic nerves (Himeno *et al.*, 2011), providing direct evidence of how vascular disturbances manifest in peripheral nerve tissues. However, it remains debated whether vascular pathology is the main driver of nerve degeneration in DSPN.

Microvascular complications are particularly prominent in DSPN, marked by structural abnormalities in the capillaries that supply the peripheral nerves (Khawaja *et al.*, 2000; Powell *et al.*, 1985). The thickening of the capillary basement membrane, a hallmark of diabetic microangiopathy, results in impaired oxygen and nutrient delivery to the nerves. Studies have shown that capillary density is significantly reduced in DSPN patients, contributing to chronic ischemic injury (Tesfaye *et al.*, 2005). This hypoxia not only exacerbates nerve dysfunction but also impairs the nerve's ability to regenerate. In addition, the loss of autonomic regulation in the microvasculature, often seen in DSPN, further impairs the ability of blood vessels to adjust blood flow in response to changing metabolic demands (Beggs *et al.*, 1992). This inability of the neuropathic nerve to increase its blood flow, as demonstrated by studies showing a lack of increased sural nerve conduction velocity following exercise, underscores the critical role of vascular factors in DSPN (Cameron and Cotter, 2001). Macrovascular complications such as atherosclerosis and peripheral artery disease (PAD) also play a significant role in worsening vascular dysfunction in DSPN (Soyoye *et al.*, 2021). Hyperglycemia-induced activation of PKC via the accumulation of DAG is a key pathway through which vascular inflammation and endothelial dysfunction are amplified (Himeno *et al.*, 2011). The overactivation of PKC leads to increased vascular permeability, endothelial cell dysfunction, and the formation of atherosclerotic plaques (Qin *et al.*, 2023). These plaques obstruct blood flow, worsening the ischemic environment and accelerating nerve degeneration. PAD, which frequently coexists with DSPN, creates a vicious cycle of nerve hypoxia and ischemic injury. The presence of atherosclerotic plaques not only impairs the delivery of oxygen and nutrients to the nerves but also triggers further inflammatory processes that leads to both vascular and neural damage (Esper *et al.*, 2006). The overall impact of these vascular disturbances is profound, leading to a detrimental cycle of chronic ischemia,

reduced nerve repair capacity, and worsening neuropathy symptoms, including pain, sensory loss, and motor dysfunction. The inability of the ischemic nerves to regenerate in this environment significantly contributes to the progressive nature of DSPN.

1.6.3 Molecular and Cellular Mechanisms Driving DSPN

1.6.3.1 Mitochondrial dysfunction in DSPN pathology

Mitochondrial dysfunction is a well-established feature in DSPN, with structural abnormalities consistently documented across multiple animal models and human studies (Fernyhough and McGavock, 2014). Mitochondria, as dynamic organelles, are vital for several cellular processes, most notably ATP generation through oxidative phosphorylation, but also calcium (Ca^{2+}) homeostasis and the regulation of apoptotic pathways (Wang *et al.*, 2023). Their structural integrity, defined by a double membrane system comprising the outer and inner membranes, is critical for maintaining cellular energy homeostasis. The outer membrane contains voltage-dependent anion channels (VDACs), which allow for the exchange of ions and small molecules, while also playing roles in lipid synthesis and the import of mitochondrial precursors (Varughese *et al.*, 2021) (Figure 1.3). In contrast, the inner membrane is more specialized and impermeable, embedding transport proteins crucial for metabolite exchange, and houses the electron transport chain (ETC), which is integral to ATP production (Mannella, 2020). The extensive folding of the inner membrane into cristae optimizes ATP production by increasing the surface area available for ETC and ATP synthase complexes. Within the matrix, the TCA cycle generates NADH and FADH2, which donate electrons to the ETC, driving oxidative phosphorylation. The matrix also contains mitochondrial DNA (mtDNA), ribosomes, and enzymes that support mtDNA replication

and transcription, indicating the organelle's endosymbiotic origins and intricate communication with nuclear processes (Matsushima and Kaguni, 2012).

In DSPN, mitochondria exhibit a complex and heterogeneous response, varying by cell type and affected regions. In diabetic feline models, particularly in the sural nerve, dystrophic axons contain both abnormally enlarged and normal mitochondria, suggesting a selective vulnerability, especially in distal axonal segments where the pathological enlargement of mitochondria is more pronounced (Mizisin *et al.*, 2007). Similarly, in rodent models of type 1 diabetes, such as STZ-treated and BioBreeding (Kalichman *et al.*, 1998) rats, Schwann cells, essential for axonal support, display significant mitochondrial ultrastructural abnormalities, while axons and neuronal perikarya show relatively normal mitochondrial profiles (Kalichman *et al.*, 1998; Kamiya *et al.*, 2006). This selective vulnerability of Schwann cells to mitochondrial dysfunction likely contributes to the progression of DSPN, as these cells play a critical role in maintaining axonal health and function. Interestingly, in type 2 diabetic models such as the db/db mouse, which mimics obesity-induced diabetes, an increased density of mitochondria in DRG sensory axons has been observed, yet these mitochondria appear to have a normal ultrastructure (Kamiya *et al.*, 2006). This suggests that mitochondrial proliferation may occur as a compensatory mechanism in response to metabolic stress, without overt structural damage (Galloway and Yoon, 2013). In contrast, type 1 diabetic models, such as the non-obese diabetic (NOD) mouse and STZ-treated mice, as well as the Akita mouse, consistently exhibit an accumulation of small, hyperdense mitochondria (Schmidt *et al.*, 2009; Schmidt *et al.*, 2008; Schroer *et al.*, 1992). These smaller mitochondria often aggregate in post-synaptic dendrites, forming tightly packed clusters without intervening cytoplasm, indicative of increased mitochondrial fission in response to the diabetic environment (Seager *et al.*, 2020). The aggregation of dysfunctional mitochondria in synaptic regions may impair synaptic

transmission and energy metabolism, further escalating the neurodegenerative processes observed in DSPN.

At a functional level, respiratory chain activity is markedly reduced in DSPN (Chowdhury *et al.*, 2010; Roy Chowdhury *et al.*, 2012). Depolarization of the mitochondrial inner membrane has been observed in acutely isolated adult DRG sensory neurons from STZ-diabetic rats (Huang *et al.*, 2003; Srinivasan *et al.*, 2000). This depolarization impairs ATP production, disrupts Ca^{2+} homeostasis, and increases ROS generation, all of which contribute to mitochondrial dysfunction and cellular stress. Research, including our work and studies conducted by the Dobrowsky laboratory, has employed various methodologies to demonstrate that mitochondrial respiratory chain activity is diminished in DRG neurons in both type 1 and type 2 diabetic rodent models (Akude *et al.*, 2011; Chowdhury *et al.*, 2010; Ma *et al.*, 2014). A decline in oxidative phosphorylation (OXPHOS) efficiency directly compromises ATP production, limiting neuronal energy reserves required for maintaining membrane potential, synaptic transmission, and ion homeostasis. Proteomic analyses using stable isotope labeling with amino acids in cell culture (SILAC) have identified a significant downregulation of proteins involved in oxidative phosphorylation and the tricarboxylic acid (TCA) cycle in DRG mitochondria of STZ-diabetic rats (Akude *et al.*, 2011; Chowdhury *et al.*, 2011). These proteomic alterations align with findings from cardiac and skeletal muscle tissues in diabetic models, where key transcriptional regulators of mitochondrial function, such as nuclear respiratory factor 1 (NRF-1) and peroxisome proliferator-activated receptor gamma coactivator 1-alpha (PGC-1α), are downregulated (Bugger *et al.*, 2009; Mootha *et al.*, 2003). The convergence of mitochondrial impairments across multiple tissues highlights the systemic impact of diabetes on energy metabolism and cellular resilience.

Further investigation into mitochondrial physiology has revealed that ATP synthase inhibition via oligomycin administration results in significant hyperpolarization of the mitochondrial inner membrane in neurons from diabetic rats compared to controls (Akude *et al.*, 2011). In healthy neurons, ATP synthase inhibition typically induces a transient hyperpolarization, followed by a compensatory response facilitated by uncoupling proteins (UCPs). However, diabetic neurons exhibit a prolonged hyperpolarization with an impaired recovery phase, suggesting an inability to regulate mitochondrial membrane potential effectively (Chowdhury *et al.*, 2013). This maladaptive response may stem from insufficient expression or functional impairment of UCPs, leading to suboptimal ROS modulation and increased susceptibility to oxidative damage (Vincent *et al.*, 2004). The disruption of lipid peroxidation pathways further exacerbates mitochondrial membrane instability, compounding neuronal dysfunction in DSPN.

While Schwann cells (SCs) are selectively vulnerable to mitochondrial dysfunction, evidence shows that such dysfunction is not limited to neurons alone. SCs play a critical role in maintaining neuronal integrity and function, making their mitochondrial health essential for overall nervous system stability. SILAC and pathway analysis of cultured primary Schwann cells under hyperglycemic conditions indicated that proteins associated with mitochondrial dysfunction, oxidative phosphorylation, TCA cycle, and detoxification were significantly increased in expression (Zhang *et al.*, 2010). Mitochondrial respiration assays in intact SCs have demonstrated that hyperglycemia increases overall oxygen consumption while decreasing the efficiency of coupled respiration, indicative of a metabolic shift toward uncoupled mitochondrial activity and reduced ATP synthesis efficiency. These findings underscore the systemic nature of mitochondrial dysfunction in diabetes and its critical role in the development of DSPN.

Mitochondrial dysfunction in DSPN has also been investigated in human studies. Confocal microscopy analysis of skin biopsies from patients with diabetes and sensory neuropathy revealed a significant reduction in the expression of Complex IV components in intraepidermal nerve fibers (IENFs) and subpapillary dermal fibers, compared to non-diabetic controls (Casanova-Molla *et al.*, 2012). This reduction in Complex IV expression occurred before significant fiber loss, suggesting that mitochondrial dysfunction may precede overt neurodegeneration. However, contradictory findings have emerged from a novel 3D imaging study, which demonstrated enhanced mitochondrial volumes within IENFs of patients with diabetic neuropathy (Hamid *et al.*, 2014). This discrepancy may reflect different stages of DSPN progression, where early-stage disease is characterized by reduced mitochondrial function, followed by a compensatory increase in mitochondrial volume in response to elevated energy demands during later stages of disease. These observations suggest a dynamic adaptation of mitochondria in response to metabolic stress in DSPN, highlighting the need for further investigation into the temporal progression of mitochondrial abnormalities in diabetes.

1.6.3.2 Calcium imbalance in DSPN progression

Ca^{2+} dyshomeostasis in DSPN is a hallmark of the pathophysiological mechanisms underpinning neuronal dysfunction in diabetes, where the finely tuned regulation of intracellular Ca^{2+} is profoundly disrupted (Fernyhough and Calcutt, 2010). Ca^{2+} serve as critical intracellular second messengers, regulating a range of neuronal processes including neurotransmission, excitability, and cell survival (Klocke *et al.*, 2023). Under normal conditions, cellular Ca^{2+} homeostasis is tightly regulated by a coordinated system of Ca^{2+} channels, transporters, and buffers across various intracellular compartments, notably the cytosol, endoplasmic reticulum (ER), and mitochondria (Ureshino *et al.*, 2019). However, chronic hyperglycemia associated with diabetes severely alters

this intricate regulatory network, leading to Ca^{2+} mishandling and subsequent neuronal degeneration in DSPN.

The ER plays a central role in maintaining Ca^{2+} balance (Clapham, 2007). It acts as the primary intracellular Ca^{2+} store, where Ca^{2+} is sequestered via the action of sarco/endoplasmic reticulum Ca^{2+} ATPase (SERCA) pumps. These pumps are responsible for transporting Ca^{2+} from the cytosol into the ER lumen, where the concentration of free Ca^{2+} reaches millimolar levels (0.5 – 1.0 mM). This Ca^{2+} reserve is released in response to various physiological stimuli, with inositol 1,4,5-trisphosphate receptors (IP3Rs) and ryanodine receptors (RyRs) mediating its release to the cytosol, thereby activating a cascade of Ca^{2+}-dependent processes critical for neuronal activity, such as neurotransmitter release and long-term potentiation. In DSPN, however, oxidative stress induced by sustained hyperglycemia results in structural and functional damage to the SERCA pumps, reducing their efficacy (Zherebitskaya *et al.*, 2012). This leads to a diminished ER Ca^{2+} load, which not only impairs Ca^{2+} release but also compromises the signaling capacity of ER-resident chaperones involved in protein folding and stress responses. Notably, chaperone-targeting therapies have shown promise in mitigating DPN (diabetic peripheral neuropathy) related damage. In particular, modulation of heat shock proteins (Hsp) has been proposed as a potential therapeutic approach, with inhibitors such as KU-32 demonstrating protective effects. KU-32 and KU-596, C-terminal Hsp90 inhibitors, enhanced mitochondrial bioenergetics in sensory neurons, improved intra-epidermal nerve fiber density, deceased the inflammatory transcriptome, and reversed physiological deficits associated with diabetic neuropathy (Ma *et al.*, 2015; Urban *et al.*, 2012).

Moreover, the reduction in ER Ca^{2+} stores has far-reaching effects on intracellular signaling dynamics. In sensory neurons affected by DSPN, the ability of the ER to release Ca^{2+} via IP3Rs and RyRs is significantly compromised, leading to a reduction in Ca^{2+} transients essential for rapid

neuronal responses (Hernández-Beltrán *et al.*, 2013). This impairment in Ca^{2+} signaling is exacerbated by the decrease in SERCA activity, which slows the reuptake of Ca^{2+} into the ER following its release. As a result, there is a sustained elevation in cytosolic Ca^{2+} concentration ($[Ca^{2+}]i$), which triggers maladaptive cellular responses. Prolonged elevations in $[Ca^{2+}]i$ lead to the activation of Ca^{2+}-dependent enzymes, such as calpains and caspases, which degrade cytoskeletal proteins and initiate apoptotic signaling cascades (Klocke *et al.*, 2023). While these processes can cause structural and functional impairments, evidence for DRG neuronal loss in diabetic neuropathy remains limited (Schmidt *et al.*, 1997). Mitochondria, which are also key players in cellular Ca^{2+} regulation, become compromised in the context of diabetic neuropathy. Mitochondria are responsible for buffering cytosolic Ca^{2+}, particularly during periods of high neuronal activity, by taking up Ca^{2+} through the mitochondrial Ca^{2+} uniporter (MCU) (Ryan *et al.*, 2020) (Figure 1.3). This Ca^{2+} influx into mitochondria is crucial for the regulation of metabolic enzymes within the Krebs cycle, which in turn enhances ATP production to meet the heightened energy demands of neurons (Boyman *et al.*, 2020). In DSPN, mitochondrial Ca^{2+} handling is severely impaired, leading to Ca^{2+} overload within the organelle (George *et al.*, 2022). This overload disrupts mitochondrial function, leading to a reduction in ATP synthesis and the accumulation of ROS, which further damages cellular structures.

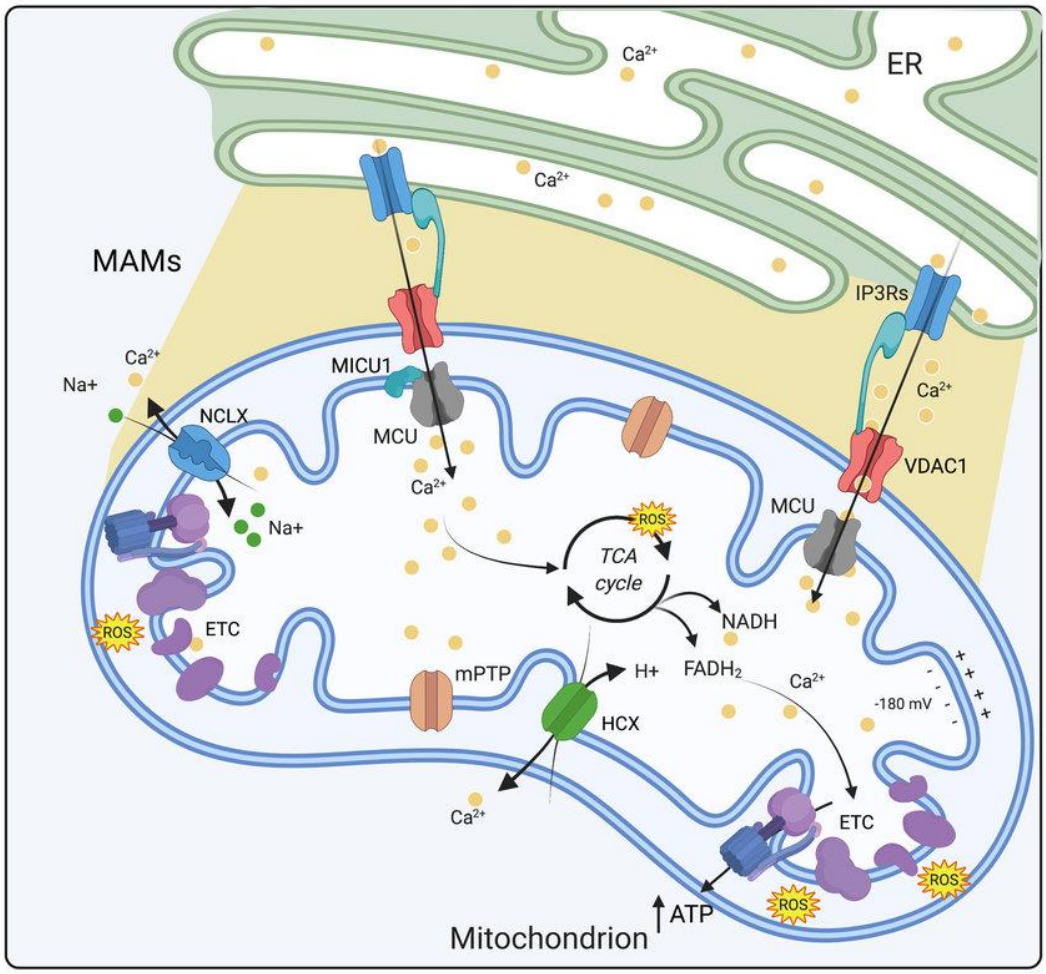

Figure 1.3. **Mitochondrial Ca^{2+} homeostasis**. mCa^{2+} homeostasis is tightly regulated by influx and efflux mechanisms. Ca^{2+} enters into the mitochondrial matrix via MCU and through a high electronegative potential (−180 mV) while its extrusion depends on NCLX and HCX exchangers. Within the matrix, Ca^{2+} stimulates the activity of three dehydrogenases of the Krebs cycle and ATP production. Ca^{2+} ions are depicted as yellow dots. Abbreviations: ER, endoplasmic reticulum; MAMs, mitochondria associated membranes; ETC, electron transport chain; MCU, mitochondrial Ca^{2+} uniporter; VDAC1, voltage-dependent anion channel 1; ATP, adenosine triphosphate; MICU1, mitochondrial Ca^{2+} uptake 1; IP3Rs, inositol-1,4,5-trisphosphate receptors; ROS, reactive oxygen species; mPTP, mitochondrial permeability transition pore; NCLX, Na+/Ca^{2+} exchanger; HCX, H+/Ca^{2+} exchanger. Adapted from Modesti, L. et al. 2021, (Modesti *et al.*, 2021), Cells, MDPI under the terms of the CC BY 4.0 license.

The dysfunction of mitochondria in DSPN is closely linked to the disruption of Ca^{2+} signaling at mitochondria-associated membranes (MAMs), the specialized contact sites between the ER and mitochondria (Giorgi *et al.*, 2015). MAMs facilitate the efficient transfer of Ca^{2+} from the ER to mitochondria (Figure 1.3). In diabetic conditions, however, the function of MAMs is diminished, leading to impaired Ca^{2+} transfer and a further reduction in mitochondrial ATP production (Dia *et al.*, 2020). This disruption exacerbates the energy crisis within sensory neurons, which are highly dependent on mitochondrial ATP for maintaining membrane potential and supporting active transport processes. While mitochondrial dysfunction compromises energy balance in sensory neurons, there is currently no evidence of apoptotic signaling in DRG neurons (Verkhratsky and Fernyhough, 2008).

The disturbances in Ca^{2+} homeostasis within sensory neurons also extend to the plasma membrane, where voltage-gated Ca^{2+} channels mediate Ca^{2+} entry in response to neuronal depolarization. In DSPN, alterations in the expression and function of these channels have been observed, with increased density of both low- and high-threshold Ca^{2+} currents reported in diabetic sensory neurons (Nilius *et al.*, 2006). However, despite this increase in channel density, depolarization-induced Ca^{2+} transients are often depressed, particularly in neurons with long axons, such as those from the lumbar DRG (Huang *et al.*, 2002; Kostyuk *et al.*, 1995). This paradoxical reduction in Ca^{2+} transients may be attributed to enhanced Ca^{2+}-dependent inactivation of Ca^{2+} channels, a process likely exacerbated by elevated resting $[Ca^{2+}]i$ levels in diabetic neurons. Ca^{2+} dyshomeostasis in DSPN reflects a multifaceted breakdown of the systems responsible for maintaining intracellular Ca^{2+} balance. The interconnected failures of the ER, mitochondria, and plasma membrane Ca^{2+} channels highlight the complexity of Ca^{2+} regulation in neurons and underscore the critical role of Ca^{2+} signaling in neuronal survival and function.

1.7 AMP-activated protein kinase (AMPK)

1.7.1 AMPK structure and function

The Ca^{2+} sensitive AMP-activated protein kinase (AMPK) functions as a central metabolic sensor, orchestrating cellular responses to energy stress by modulating a variety of biochemical processes. Structurally, AMPK is a heterotrimer composed of a catalytic α subunit (α1 or α2) and regulatory β (β1 or β2) and γ subunits (γ1, γ2, or γ3), with the γ subunit containing four cystathione β-synthase (CBS) repeats that bind AMP, ADP, and ATP (Ross *et al.,* 2016) (Figure 1.4). This structural arrangement allows AMPK to detect shifts in cellular energy status, particularly changes in the ATP/AMP ratio, and subsequently adjust its activity (Chen *et al.*, 2012; Xiao *et al.*, 2011). Under conditions of diminished ATP, AMP binds competitively to the CBS domains, enhancing AMPK's basal activity and facilitating the phosphorylation of the α subunit at Thr172 by upstream kinases, such as liver kinase B1 (LKB1) (Woods *et al.,* 2003) and $Ca^{2+/}$calmodulin-dependent protein kinase kinase β (CaMKKβ) (Hawley *et al.,* 2005). Phosphorylation at this site increases AMPK activity by approximately 100-fold, setting off a cascade of downstream effects that collectively promote catabolic pathways to restore ATP levels while suppressing anabolic processes that consume energy (Woods *et al.*, 2003).

Once activated, AMPK initiates metabolic shifts by phosphorylating key enzymes across multiple pathways. In glucose metabolism, AMPK modulates enzymes that facilitate glucose uptake and glycolysis, such as TBC1 domain family member 1 (TBC1D1) and thioredoxin-interacting protein (TXNIP), which control glucose transporter type 4 (GLUT4) and glucose transporter type 1 (GLUT1) activity (Hardie, 2013). AMPK also enhances glycolytic flux by phosphorylating 6-phosphofructo-2-kinase (PFKFB3) and inhibits glycogen synthesis via modulation of glycogen

synthase. In lipid metabolism, AMPK activation results in the phosphorylation and inhibition of of acetyl-CoA carboxylases (ACC1 and ACC2), the enzymes responsible for producing malonyl CoA. This results in decreased intracellular malonyl CoA levels. Since malonyl CoA is a potent inhibitor of carnitine palmitoyltransferase 1 (CPT1), its reduction removes this inhibition, allowing CPT1 to facilitate the transport of long-chain fatty acids into the mitochondria for β-oxidation. Thus, AMPK activation indirectly promotes fatty acid oxidation by decreasing malonyl CoA and enabling mitochondrial fatty acid uptake (Kim *et al.*, 2016). Furthermore, AMPK restricts protein synthesis by phosphorylating the mammalian target of rapamycin complex 1 (mTORC1) and eukaryotic elongation factor 2 kinase (eEF2K), thus inhibiting pathways dependent on S6 kinase (S6K1) (Inoki *et al.*, 2003; Leprivier *et al.*, 2013). Collectively, these effects shift cellular metabolism to an energy-conserving mode that supports ATP regeneration.

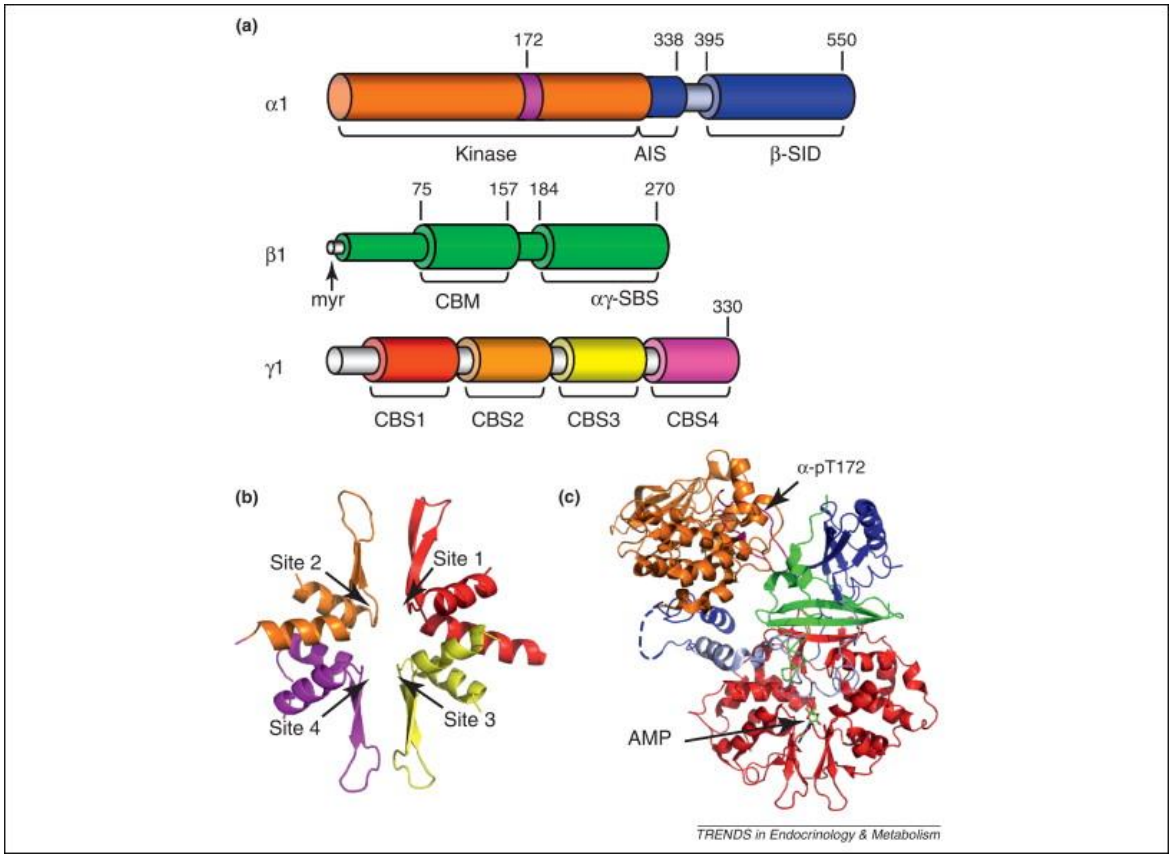

Figure 1.4. AMPK domains and structure. (a) Domain organization of AMPK subunits. Residue numbering refers to human α1, β1 and γ1 isoforms. The α subunit consists of an N-terminal kinase domain, an autoinhibitory sequence (Ang *et al.*) and a β-subunit interacting domain (β-SID). The β subunit is N-terminally myristoylated (myr) and contains a mid-molecule carbohydrate-binding module (CBM) and C-terminal αγ subunit-binding sequence (SBS). The γ subunit contains four cystathione β-synthase (CBS) domains, paired (1+2 and 3+4) to form two Bateman modules. (b) Tetrad organization of CBS domains in the γ-subunit, colored as in (a), showing locations of nucleotide binding sites (black arrows). (c) Structure of the mammalian AMPK regulatory core and kinase domain [PDB 2Y94: rat α1 (7–299)/(331–469)/(524–548), human β1 (198–272) (green), rat γ1 (23–326) (red)]; α-subunit regions are colored as in (a). AMP bound at γ site 3 is evident. *Reprinted from "AMPK functions as an adenylate charge-regulated protein kinase", Vol 23, Jonathan S. et.al. 2012, with permission from Elsevier (Oakhill et al., 2012).*

A key role of AMPK is in mitochondrial biogenesis, achieved primarily through its interaction with peroxisome proliferator-activated receptor gamma coactivator-1α (PGC-1α), a transcriptional coactivator that stimulates the transcription of mitochondrial genes (Rodgers *et al.*, 2008). PGC-1α enhances mitochondrial DNA replication and activates nuclear respiratory factors (NRF1 and NRF2), which in turn stimulate mitochondrial transcription factor A (mtTFA) to drive mitochondrial DNA transcription (Feige and Auwerx, 2007; Rodgers *et al.*, 2008). Phosphorylation of PGC-1α by AMPK enhances this pathway, leading to increased mitochondrial biogenesis and oxidative phosphorylation capacity. This AMPK-PGC-1α regulatory axis is particularly critical in cells with high energy demands, such as neurons, where it supports ATP production and counters oxidative stress by upregulating antioxidant genes (Feige and Auwerx, 2007; Jäger *et al.*, 2007; Roy Chowdhury *et al.*, 2012).

1.7.2 AMPK abnormalities in DSPN

In DSPN, AMPK signaling is profoundly impaired, which has been linked to mitochondrial dysfunction and neuropathic deficits (Roy Chowdhury *et al.*, 2012). In diabetic models, such as STZ-induced diabetic rats, reduced AMPK phosphorylation correlates with mitochondrial depolarization, diminished mitochondrial biogenesis, and increased vulnerability to neuronal injury (Aghanoori *et al.*, 2019; Chowdhury *et al.*, 2013; Roy Chowdhury *et al.*, 2012). Therapeutic strategies to restore AMPK activity, such as the administration of resveratrol, reverse these defects by enhancing AMPK signaling, thereby promoting mitochondrial polarization and stimulating axonal outgrowth (Dasgupta and Milbrandt, 2007; Roy Chowdhury *et al.*, 2012). Resveratrol, a potent antioxidant, has also demonstrated efficacy in mitigating oxidative stress, which is a central pathological feature in diabetic neuropathy (Kumar and Sharma, 2010). In STZ-induced diabetic rats, resveratrol treatment significantly ameliorated neuropathic symptoms, including reductions in motor nerve conduction velocity (MNCV) deficits, nerve blood flow impairments, and thermal hyperalgesia. These protective effects were associated with decreased levels of oxidative stress markers, such as malondialdehyde (MDA) and peroxynitrite, alongside increased catalase activity. Resveratrol also reduced DNA fragmentation in sciatic nerve, as demonstrated by fewer TUNEL-positive cells, highlighting its neuroprotective potential through DNA preservation (Kumar *et al.*, 2007). Additionally, resveratrol targets inflammatory pathways by inhibiting the nuclear factor kappa-light-chain-enhancer of activated B cells (NF-κB) signaling cascade, which is often upregulated in diabetic neuropathy due to oxidative stress and AGE formation. This inhibition reduces pro-inflammatory mediators such as cyclooxygenase-2 (COX-2), TNF-α, and interleukin-6 (IL-6), while also decreasing oxidative damage markers such as MDA, highlighting its neuroprotective potential in diabetic neuropathy.

The activation of AMPK by CaMKKβ is of particular interest due to its Ca^{2+} dependency. Unlike LKB1, which is primarily activated by changes in the AMP ratio, CaMKKβ responds to increases in intracellular Ca^{2+} levels, allowing AMPK to be activated independently of cellular energy status (Amato and Man, 2011). This mechanism is especially pertinent in neurons, where Ca^{2+} fluctuations are frequent and critical for various signaling cascades. CaMKKβ-mediated AMPK activation enables cells to respond rapidly to changes in intracellular Ca^{2+}, thereby supporting essential functions such as mitochondrial biogenesis and the maintenance of mitochondrial function. In this capacity, AMPK aids neuronal survival and promotes axonal growth, providing a neuroprotective effect in environments where energy homeostasis is compromised, such as in DSPN (Roy Chowdhury *et al.*, 2012; Saleh *et al.*, 2020). AMPK also contributes to neuronal health through its role in autophagy and mitophagy. Specifically, AMPK activation of Unc-51-like autophagy-activating kinases 1(ULK1) initiates autophagy, facilitating the removal of damaged organelles and thus mitigating oxidative stress (Egan *et al.*, 2011; Greer *et al.*, 2007).

AMPK's significance extends beyond neurons to systemic metabolic health, where it has beneficial effects in various tissues. Pharmacological activators of AMPK, such as metformin and AICAR, have demonstrated improved nerve conduction velocity, reduced inflammation, and normalized mitochondrial function in diabetic models, suggesting potential applications for AMPK activation in DSPN (Li *et al.*, 2007; Owen *et al.*, 2000; Russell *et al.*, 2004). These effects are likely mediated through the AMPK-PGC-1α axis, which supports mitochondrial biogenesis, enhances ATP production, and decreases oxidative stress (Choi *et al.*, 2014). By restoring cellular energy homeostasis and reducing oxidative damage, the AMPK-PGC-1α axis offer a therapeutic strategy to protect from neurodegeneration and improve outcomes in DSPN. Recent studies have

identified the muscarinic acetylcholine type 1 receptor (M_1R) as a key regulator of AMPK activity in animal models of diabetic neuropathy (Calcutt *et al.*, 2017). Inhibition of M_1R leads to robust activation of AMPK, which in turn confers protection against neuropathy in both type 1 and type 2 diabetes models.

1.8 Role of M_1R in nerve repair

1.8.1 GPCR pharmacology and M_1R structure

G protein-coupled receptors (GPCRs) form one of the most extensive and varied families of membrane proteins, acting as vital mediators of cellular communication (Weis and Kobilka, 2018). GPCRs are activated by a broad range of ligands, including neurotransmitters, hormones, and other signaling molecules, making them indispensable for maintaining cellular homeostasis (Latorraca *et al.*, 2017; Zhang *et al.*, 2024). Among GPCRs, the muscarinic acetylcholine receptors (mAChRs) stand out as a highly conserved class of GPCR that are pivotal for their critical involvement in the central and peripheral nervous systems (Kruse *et al.*, 2014). These receptors are divided into five subtypes: M1, M2, M3, M4, and M5. Each subtype is distinguished by its unique G protein-coupling preferences. The M1, M3, and M5 subtypes are primarily associated with Gq/11 proteins, leading to the activation of phospholipase C (PLC), which subsequently increases intracellular Ca^{2+} signaling. In contrast, M2 and M4 receptors couple with Gi/o proteins, which inhibit adenylyl cyclase and reduce cyclic AMP levels, creating distinct physiological effects across various tissues (Hulme *et al.*, 1990). Among the five subtypes, the M_1R exhibits a key role in shaping cognitive and sensory processes (Zhao *et al.*, 2018). Insights from M_1R knockout ($M_1R^{-/-}$) mice further underscore its importance. These mice exhibit deficits in mitogen-activated protein kinase (MAPK) pathway activation, a critical signaling cascade for synaptic plasticity and cognition, particularly in hippocampal and cortical neurons (Wess *et al.*,

2007). Behaviorally, $M_1R^{-/-}$ mice perform similarly to wild-type controls in certain cognitive tasks, such as the Morris water maze, indicating that M_1R is dispensable for basic memory formation or stability. However, under specific experimental conditions, such as non-matching-to-sample working memory tasks or fear-conditioning paradigms, these mice demonstrate significant impairments, suggesting that M_1R is essential for higher-order cognitive processes requiring cortical-hippocampal interactions (Gould *et al.*, 2015). M_1R is a Gq-coupled receptor that, when activated by acetylcholine (ACh) leads to the breakdown of phosphatidylinositol 4,5-bisphosphate (PIP_2) through the action of PLCβ (Falkenburger *et al.*, 2010) (Figure 1.5). This breakdown generates two important secondary messengers: inositol trisphosphate (IP_3) and diacylglycerol (DAG). IP_3 binds to its receptors (IP_3Rs) on the ER, stimulating the release of Ca^{2+} from the ER into the cytosol (Berridge and Irvine, 1989). Concurrently, DAG activates PKC. Together, these signaling mechanisms orchestrate a variety of neuronal processes that are essential for neural development and functional maintenance, particularly axonal plasticity, which is indispensable for proper neuronal circuitry and synapse formation (Callender and Newton, 2017; Nishizuka, 1995).

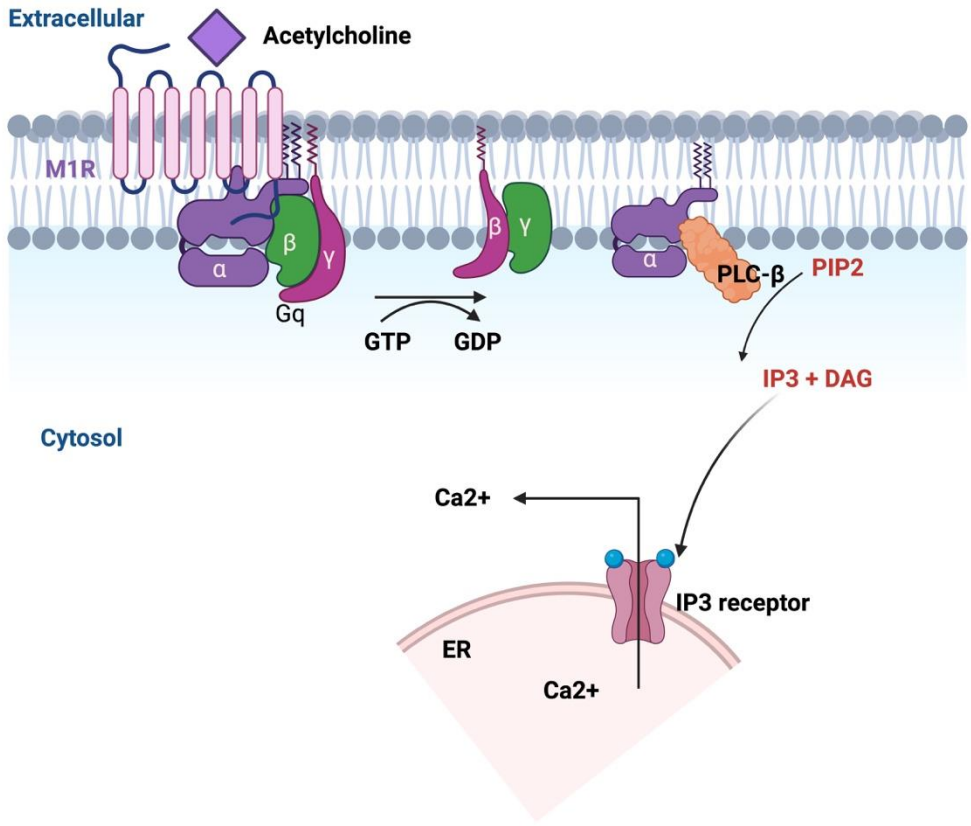

Figure 1.5. **Schematic of M1 muscarinic receptor (M_1R) signaling via the Gq protein pathway**. When acetylcholine (ACh) binds to M_1R, the Gq heterotrimeric protein (α, β, γ) becomes activated, exchanging GDP for GTP on the α-subunit. The activated Gqα then stimulates phospholipase C-β (PLC-β), which cleaves the membrane lipid phosphatidylinositol 4,5-bisphosphate (PIP_2) into two second messengers: inositol 1,4,5-trisphosphate (IP_3) and diacylglycerol (DAG). IP_3 diffuses through the cytosol and binds to IP_3 receptors on the endoplasmic reticulum (ER), triggering Ca^{2+} ion (Ca^{2+}) release into the cytosol. Increased cytosolic Ca^{2+}, along with DAG, mediate downstream signaling events that lead to various cellular responses. *Created with BioRender*.

1.8.2 M_1R signaling: protection against dying-back neuropathy

ACh is an essential neurotransmitter that modulates multiple aspects of neuronal function, including the fine-tuning of synaptic transmission and neuronal development (Picciotto *et al.*, 2012). A key role of ACh during development is its impact on axonal sprouting, especially in neurons, where it influences growth cone motility and cytoskeletal rearrangement (Rüdiger and Bolz, 2008). Growth cones, found at the tips of extending axons and dendrites, are dynamic structures that respond to extracellular signals to guide neurons toward their target destinations (Erskine and McCaig, 1995). This motility is fundamental for the proper formation of neural circuits, as it allows for the precise wiring of neuronal connections during development. M_1R, through its modulation of Ca^{2+} signaling within the growth cone, plays a vital role in controlling the dynamics of the cytoskeleton, particularly the actin filaments (Bernstein and Bamburg, 2003; Erskine and McCaig, 1995; Sabbir *et al.*, 2018; Young and Poo, 1983). Upon ACh activation, M_1R initiates a cascade that triggers the release of Ca^{2+}, which then interacts with proteins regulating actin polymerization. This regulation is essential for the movement, extension, or retraction of the growth cone, ensuring that neurons establish appropriate synaptic connections in response to environmental cues.

These mechanisms, while critical during early development, are re-engaged in the adult nervous system following injury, forming the foundation of neuronal regeneration (O'Donovan, 2016). Neuronal regeneration broadly encompasses several cellular processes - including neurite outgrowth, axonal regeneration, dendritic remodeling, and synaptogenesis. Neurite outgrowth is often the first step, referring to the extension of projections from the neuronal soma, which later specialize into axons or dendrites. Axonal regeneration follows in damaged neurons, involving the re-formation of growth cones at the injury site and directed regrowth toward original or new targets (Mahar and Cavalli, 2018). Dendritic regeneration, in parallel, restores the ability of neurons to

receive synaptic input. Collateral sprouting, a process in which axons branch and extend toward new targets in response to injury or external cues, is a cornerstone of neural plasticity and controls fields of innervation (Hagg, 2006). Unlike axonal regeneration, which involves injured neurons regrowing their axons, collateral sprouting is driven by uninjured neighboring neurons attempting to compensate for the loss of axonal activity or synaptic input in denervated regions (Lemaitre *et al.*, 2020). This distinction is crucial: while both processes involve neurite extension, their origin and triggers differ.

A growing body of research has revealed that endogenous cholinergic signaling can impose a tonic suppression on neurite outgrowth in mature neurons, a finding that has critical implications for therapeutic strategies targeting neuro-regenerative pathways (Calcutt *et al.*, 2017). Research conducted across diverse models, including *Aplysia*, *Xenopus*, and mammalian embryonic neurons, has revealed that ACh released from growth cones modulates Ca^{2+}-dependent motility through nicotinic and muscarinic receptors (Erskine and McCaig, 1995; Young and Poo, 1983). Activation of nicotinic receptors promotes neurite outgrowth, whereas muscarinic receptor signaling, especially mediated by M_1R, exerts an inhibitory effect. This suppression is largely attributed to Ca^{2+} mobilization from internal stores as well as M_1R-mediated activation of Gα signaling, which inhibits actin filament dynamics, imposing constraints on growth cone motility (Sabbir *et al.*, 2018). In mammals, sensory neurons synthesize and secrete ACh and express key components of cholinergic signaling, including the peripheral form of choline acetyltransferase (pChAT) (Bellier and Kimura, 2007). Immunohistochemical staining of IENFs in the skin confirms the presence of pChAT in nerve endings (Hanada *et al.*, 2013). These neurons also exhibit multiple muscarinic receptors, with notably low acetylcholinesterase activity (Bellier and Kimura, 2007; Bernardini *et al.*, 2004). Together, these features establish a functional endogenous

cholinergic system within sensory neurons, which tonically suppresses neurite outgrowth in adult neurons. Our *in vitro* assays using DRG neurons replicate this sprouting behavior, providing a robust model for studying axonal plasticity under conditions mimicking *in vivo* environments (Smith and Skene, 1997). This model further serves as a predictive tool for assessing the therapeutic potential of drugs aimed at enhancing IENF density and corneal sensory nerve fiber restoration.

Muscarinic receptor antagonists, such as pirenzepine (PZ) and muscarinic toxin 7 (MT7), have demonstrated significant promise in overcoming ACh-induced suppression of neurite outgrowth (Calcutt *et al.*, 2017; Jolivalt *et al.*, 2020; Sabbir *et al.*, 2018; Saleh *et al.*, 2020). PZ is a competitive orthosteric antagonist that binds to the active site of M_1R, blocking the interaction of ACh and preventing downstream signaling (el-Fakahany *et al.*, 1986). In contrast, MT7, derived from Green Mamba snake toxin, acts as a negative allosteric modulator and exhibits remarkable specificity for M_1R (Kukkonen *et al.*, 2004). Previous studies have highlighted the potential of M_1R antagonism in promoting neurite outgrowth and mitigating neuropathic conditions. Inhibition of M_1R, particularly with antagonists such as MT7, counteracted ACh-induced constraints on neurite extension, facilitating enhanced growth (Calcutt *et al.*, 2017). M_1R knockout (KO) mice exhibit notable resilience to diabetic neuropathy, highlighting M_1R's pivotal role in neuroprotective pathways (Calcutt *et al.*, 2017). However, investigations reveal no evidence of diabetes-induced alterations in muscarinic receptor signaling. Specifically, ChAT activity and M_1R mRNA levels in diabetic models remain unchanged, suggesting that the susceptibility conferred by M_1R is independent of changes in ACh synthesis or receptor expression, thereby adding complexity to its involvement in neuronal maintenance and injury response.

A critical mechanistic insight into M_1R's function relates to its modulation of M-currents - a class of voltage-gated potassium currents (mediated by KCNQ/Kv7 channels) that are active near the resting membrane potential and serve to limit neuronal excitability (Galvin *et al.*, 2020). Activation of M_1R inhibits M-current activity, leading to membrane depolarization and enhanced excitability, which may exacerbate pain signaling and neuronal stress. Conversely, M_1R antagonism relieves this suppression, resulting in increased M-current amplitude, membrane hyperpolarization, and reduced likelihood of action potential generation (Naznin *et al.*, 2022). This neurophysiological modulation represents a key pathway through which M_1R antagonists mitigate hyperexcitability in neuropathic conditions. Beyond their electrophysiological effects, recent studies have illuminated the importance of the AMPK/PGC-1α signaling axis in M_1R-mediated regulation of neuronal energy homeostasis and growth (Saleh *et al.*, 2020). Blocking M_1R with MT7 activates the CaMKKβ-AMPK pathway in sensory neurons, which enhances mitochondrial bioenergetics. These processes are critical for meeting the high energy demands associated with neurite extension and cytoskeletal reorganization. Intriguingly, this mechanism appears spatially localized as topical application of MT7 reversed the loss of sensory nerves in the cornea in animal models of neuropathy (Calcutt *et al.*, 2017; Saleh *et al.*, 2020). In a model of chemotherapy-induced peripheral neuropathy (CIPN) when applied topically to one eye, MT7 resulted in enhanced AMPK activation only in the ipsilateral trigeminal ganglion, underscoring the localized effect of M_1R antagonism on sensory nerve regeneration (Saleh *et al.*, 2020).

1.8.3 Therapeutic implications of M_1R antagonism in diverse neuropathies

Beyond diabetic neuropathy, studies have extended these findings to other neuropathic conditions such as CIPN, and human immunodeficiency virus-associated distal sensory polyneuropathy (HIV-DSP), despite differing etiologies. The potential for M_1R antagonists to address CIPN is

particularly compelling given the widespread and debilitating nature of CIPN, which affects more than 80% of patients receiving standard-dose anticancer therapies (Lee *et al.*, 2024). CIPN, characterized by distal axonal degeneration and reduced IENF density, shares significant pathological similarities with diabetic neuropathy, including mitochondrial dysfunction, axonal swelling, and impaired axonal transport. Schwann cell dedifferentiation and altered axonal transport exacerbate these effects, causing debilitating sensory symptoms, including pain, hyperalgesia, and allodynia. As M_1R inhibition exerts a neuroprotective role in diabetic neuropathy, given that CIPN also causes nerve defects, daily intraperitoneal injections of benztropine, which targets both M_1R and M_3R, prevents sensory deficits, prevented tactile allodynia and preserved nerve conduction velocity (Cerles *et al.*, 2019; Saleh *et al.*, 2020). In HIV-associated neuropathy, the HIV-TAT (trans-activator of transcription) protein exacerbates mitochondrial dysfunction and axonal damage, resulting in distal sensory deficits, including pain, tactile allodynia, and thermal hypoalgesia (Han *et al.*, 2021). These neuropathies converge on common mechanisms such as distal dying-back of axons, reduced IENF density, impaired mitochondrial function, and axonal transport deficits as of DSPN. In the doxycycline-inducible HIV-TAT transgenic mouse model, systemic administration of PZ preserved corneal nerve density and prevented tactile and thermal deficits by mitigating mitochondrial dysfunction caused by TAT expression (Han *et al.*, 2021).

The efficacy of these drugs has been demonstrated across various *in vitro* and *in vivo* models. *In vitro* studies using DRG neurons have shown that M_1R antagonists enhance mitochondrial respiration and promote neurite outgrowth, highlighting their role in reversing neuropathy at the cellular level (Calcutt *et al.*, 2017; Saleh *et al.*, 2020). *In vivo*, STZ-induced type 1 diabetes and db/db mouse models for type 2 diabetes have been used to evaluate systemic and

topical delivery of these agents (Jolivalt *et al.*, 2020; Jolivalt *et al.*, 2022). Subcutaneous administration of oxybutynin reversed tactile and thermal deficits, while topical application of MT7 and oxybutynin restored corneal nerve density and prevented IENF loss (Calcutt *et al.*, 2017; Casselini *et al.*, 2024).

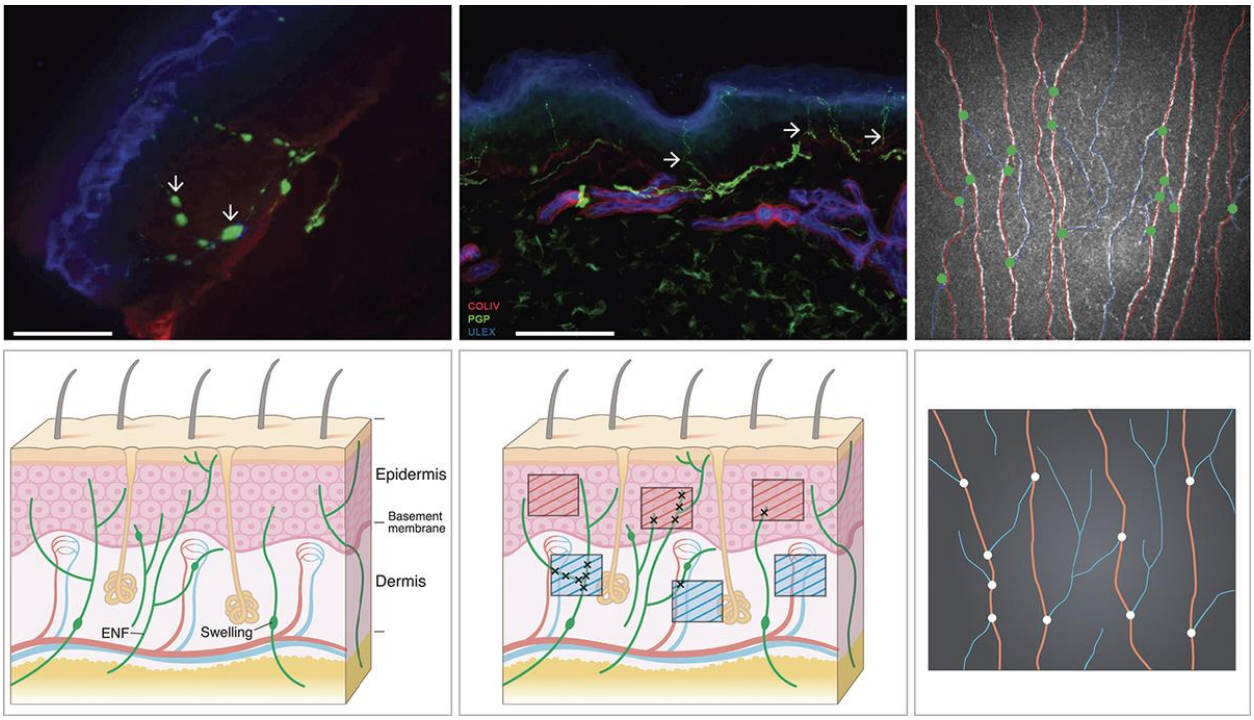

Figure 1.6. **Morphological assessment of key small fiber parameters on skin biopsy and CCM**. Upper panel: skin biopsy and CCM analysis in a diabetic patient. Left: examples of axonal swellings on IENFs (green). Arrows: axonal swellings, defined as enlargement on an IENF exceeding 1.5 mm. Scale bar 5 30 mm. Middle: IENFs stained with PGP 9.5 (green), Collagen IV, and ULEX (blood vessels). Arrows: IENFDs, defined as nerve fibers visible both in the dermis and the epidermis. Scale bar 100 mm. Right: example of a CCM image. Red-traced nerve fibers: CNFD (main nerve fibers); blue-traced fibers: CNFL (branched nerve fibers); green dots: branch points. Corneal confocal microscopy image is 400 3 400 mm.

Lower panel: schematic representations of the main structures in the upper skin and of a typical CCM image. Left: visualization of how IENFs are quantified. The nerve fibers (green) must be visible at both the upper dermis and epidermis and therefore intersect the basement membrane. Axonal swellings are represented on some of the IENFs (definition of axonal swellings varies among studies, eg, enlargements exceeding 1.5 mm in diameter or enlargements at least 3 times the diameter of the afferent nerve fiber). Middle: visualization of how epidermal NFLD (red boxes) and dermal NFLD (blue boxes) is quantified using stereology. Briefly, stereological software (newCAST; Visiopharm, Hoersholm, Denmark) superimposes 3D counting boxes on the computer screen together with "counting lines" inside the box, representing the place where the focal plane and a virtual plane intersect. The counting is performed under live microscopy, and the counting lines move inside the box as the investigator moves along the z-axis. Every time a nerve fiber in focus intersects with a counting line, the nerve is marked, and the software estimates their length. Right: schematic representation of a CCM image, showing main nerve fibers (red), branched nerve fibers (Bluestone *et al.*), and branch points (white dots). CCM, corneal confocal microscopy; CNFD, corneal nerve fiber density; CNFL, corneal nerve fiber length; IENFD, intraepidermal nerve fiber density; NFLD, nerve fiber length density. *Reprinted from "Structural, functional, and symptom relations in painful distal symmetric polyneuropathies: a systematic review", Pall Karlsson et.al. 2019, with permission from Wolters Kluwer Health, Inc.- Pain (Karlsson et al., 2019).*

The efficacy of M_1R antagonists is measured through key endpoints that reflect structural, functional, and metabolic recovery. Structural endpoints include IENF density in skin biopsies and corneal nerve density measured via corneal confocal microscopy (Figure 1.6), both of which are critical indicators of sensory nerve integrity (Calcutt *et al.*, 2017; Jolivalt *et al.*, 2022). Functional endpoints, such as tactile allodynia and thermal hypoalgesia assessed using von Frey filaments and hot plate tests, respectively, provide direct measures of sensory recovery. Metabolic endpoints,

including enhanced mitochondrial respiration, ATP production, and activation of the AMPK-PGC-1α axis, highlight the bioenergetic improvements conferred by these treatments (Saleh *et al.*, 2020). Human studies have further validated the translational potential of M_1R antagonists. A randomized, double-blind, placebo-controlled trial of topical oxybutynin in patients with type 2 diabetes and confirmed peripheral neuropathy demonstrated significant increases in IENF density, reduced neuropathic pain, and improved quality-of-life scores (Casselini *et al.*, 2024). This study underscores the clinical relevance of muscarinic receptor antagonists in reversing neuropathy symptoms. Moreover, the ability of these drugs to target shared mechanisms across DSPN, CIPN, and HIV-DSP suggests their potential for broad therapeutic applications. The evidence from preclinical and clinical studies supports the central role of mitochondrial bioenergetics and cytoskeletal organization in neuropathy treatment. By addressing these fundamental processes, M_1R antagonists not only restore sensory function and structural integrity but also pave the way for targeted therapies that minimize systemic side effects. The success of both systemic and topical delivery underscores their versatility and adaptability to different clinical scenarios, making them a pivotal component of the therapeutic landscape for peripheral neuropathies.

1.9 TRPM3: A key player in sensory perception

1.9.1 Structure and function

Transient Receptor Potential (TRP) channels are a large family of ion channels that play a vital role in sensory perception and a variety of physiological processes in the human body. Discovered in the late 20th century, these channels were initially identified in the fruit fly (*Drosophila melanogaster*) as essential components for light perception (Nilius *et al.*, 2007). Since then, numerous TRP channels have been identified in mammals, including humans, where they are

involved in a broad spectrum of biological processes. These channels are present in the cell membranes of numerous cell types, where they act as sensors for external stimuli such as changes in temperature, chemical signals, mechanical pressure, and osmotic pressure (Cao, 2020). Functionally, TRP channels are permeable to cations such as Ca^{2+} and Na^{+}, which allows regulation of electrical and biochemical signals in cells (Wang *et al.*, 2020). This permeability is crucial for the transmission of signals that enable cells to adapt to changes in their environment. TRP channels can be classified into several subfamilies based on their structural features and functional properties. These include the TRPC (canonical), TRPV (vanilloid), TRPM (melastatin), TRPA (ankyrin), TRPP (polycystin), TRPML (mucolipin), and TRPN (*Drosophila NOMPC*, found mostly in non-mammalian species) (Venkatachalam and Montell, 2007). Each subfamily has distinct characteristics, however, they share the common functionality of being non-selective cation channels. Among these subfamilies, the TRPM (melastatin) group is particularly significant due to its involvement in multiple physiological and pathological processes. The TRPM family is comprised of eight members (TRPM1 to TRPM8), each of which has specialized functions. These channels are involved in various processes such as thermosensation, pain perception, insulin secretion, and ion homeostasis (Fleig and Penner, 2004).

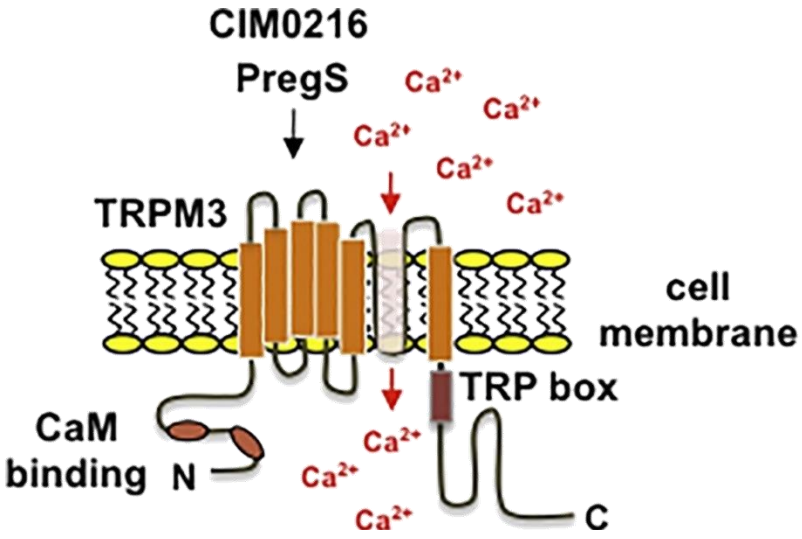

Figure 1.7. Modular structure, membrane topology, and expression of TRPM3. TRPM3 has six transmembrane domains with a pore-forming domain between transmembrane regions 5 and 6. Both the N- and C-termini are located in the cytosol. The N-terminus contains two calmodulin binding sites encompassing amino acids 35–124 and 291–382. The C-terminus contains the TRP domain on the C-terminal side of the sixth transmembrane domain. *Reprinted from "Transient receptor potential TRPM3 channels: Pharmacology, signaling, and biological functions", Gerald Thiel et.al. 2017, with permission from Elsevier (Thiel et al., 2017).*

The general structure of TRPM channels includes six transmembrane domains with a pore-forming region between the fifth and sixth segments. Additionally, they have large intracellular domains at both the N- and C-termini, which play important roles in regulating channel activity and interacting with other cellular proteins (Himmel and Cox, 2020). As non-selective cation channels, TRPM members allow the passage of various ions, including Ca^{2+}, Na^{+}, and Mg^{2+}, in response to diverse stimuli. Different TRPM channels are activated by distinct triggers; for instance, TRPM1 is crucial for retinal function and vision, while TRPM2 functions as a sensor for oxidative stress and has

roles in the immune response (Chubanov *et al.*, 2024). TRPM4 and TRPM5 are essential for Ca^{2+}-activated cation currents, which influence electrical signaling in the heart and pancreas. TRPM6 and TRPM7 are necessary for magnesium balance and are critical for cellular growth and survival. TRPM8 is well-known as a cold receptor, sensitive to cool temperatures and menthol.

Within this family, TRPM3 has garnered attention for its distinctive functions in thermal sensation, pain detection and modulation (Aloi *et al.*, 2023; Vriens *et al.*, 2011). TRPM3 is a non-selective cation channel that exhibits the typical structural features of TRP channels. It possesses six transmembrane domains and has a pore region that is vital for ion permeation (Figure 1.7). The channel can exist in multiple isoforms due to alternative splicing, which enables the performance of diverse functions in different tissues. TRPM3 is highly permeable to Ca^{2+}, which is critical for its involvement in cellular signaling pathways. This channel is broadly expressed across the body, including in the brain, sensory DRG neurons, retina, pancreatic β cells, as well as in smooth muscle and kidney cells. The functions of TRPM3 are varied, with its role as a thermosensitive channel being one of the most prominent (Uchida, 2024). In DRG neurons, TRPM3 channels are highly involved in nociception, particularly responding to noxious heat and chemical stimuli (Vriens *et al.*, 2011). Studies have demonstrated that TRPM3 activation plays a significant role in inflammatory pain. In mouse models, TRPM3-deficient mice exhibit a marked reduction in inflammatory heat hyperalgesia, indicating that TRPM3 is essential for the sensitization of pain under inflammatory conditions (Vriens *et al.*, 2011). TRPM3 is expressed in a large subset of TRPV1-expressing sensory neurons, and Trpm3 −/− mice show reduced heat sensitivity at both cellular and behavioral levels. Interestingly, double knockout (DKO) mice lacking both TRPM3 and TRPV1 exhibit only mild heat sensitivity deficits, suggesting compensatory mechanisms involving other heat-sensitive channels (Vandewauw *et al.*, 2018). However, triple knockout

(TKO) mice lacking TRPM3, TRPV1, and TRPA1 display profound deficits in heat sensing, confirming the complementary roles of these channels in acute noxious heat detection and their interplay in maintaining thermosensitivity. When exposed to inflammatory stimuli, TRPM3 channels become sensitized, leading to enhanced pain perception. This makes TRPM3 a potential therapeutic target for treating inflammatory pain disorders. For instance, antagonists that inhibit TRPM3 activation alleviate thermal and mechanical hyperalgesia in animal models, suggesting that TRPM3 inhibitors could provide relief in conditions such as neuropathic and inflammatory pain (Krügel *et al.*, 2017).

Beyond its role in nociception, TRPM3 is also involved in metabolic processes, particularly in pancreatic beta cells (Thiel *et al.*, 2013). In these cells, TRPM3 activation by pregnenolone sulphate (PS) enhances glucose-induced insulin secretion, linking this ion channel to glucose metabolism and insulin regulation. This suggests that TRPM3 could play a role in metabolic disorders such as diabetes, where impaired insulin secretion is a hallmark. The channel's presence in various tissues, including the kidney, retina, and brain, indicates that its physiological functions are not limited to pain perception but extend to other critical cellular processes. Emerging evidence connects TRPM3 to neurodevelopmental disorders as well, particularly developmental and epileptic encephalopathies (DEE), which are characterized by epilepsy, intellectual disabilities, and musculoskeletal abnormalities (Burglen *et al.*, 2023; Zhao *et al.*, 2020). Rare *de novo* mutations in the TRPM3 gene have been identified in individuals with DEE, revealing gain-of-function effects that result in increased basal activity of the channel. Functional studies in mammalian cells and frog oocytes demonstrate that these mutations make TRPM3 more sensitive to heat and chemical activators, such as PS, while also elevating baseline calcium permeability even in the absence of stimuli. This aberrant calcium influx leads to intracellular calcium overload,

which is a known driver of neuronal damage and dysfunction. Patients with DEE-associated TRPM3 mutations exhibit a spectrum of neurological and developmental symptoms, including global developmental delay, epilepsy, altered pain perception, and cerebellar abnormalities such as ataxia and hypotonia. These findings suggest that TRPM3-mediated calcium dysregulation contributes to both developmental impairments and neuronal excitability. Notably, the antiseizure medication primidone, a TRPM3 antagonist, reduced the basal hyperactivity of mutant channels, providing a potential therapeutic avenue for managing DEE-related symptoms (Zhao *et al.*, 2020).

Although the role of TRPM3 in the human brain remains incompletely understood, its gain-of-function mutations in DEE highlight its critical involvement in neuronal calcium signaling and developmental processes. These findings emphasize TRPM3's broader physiological significance and reinforce its potential as a therapeutic target in diverse conditions ranging from sensory and metabolic disorders to severe neurodevelopmental diseases.

1.9.2 TRPM3 pharmacology

The pharmacological modulation of the TRPM3 channel offers a compelling avenue to explore its multifaceted roles in sensory, metabolic, and neurological systems. TRPM3 channels respond to diverse endogenous and synthetic modulators that influence its gating mechanisms, specificity, and physiological outcomes (Held *et al.*, 2015a). TRPM3 activation involves conformational changes in the channel's structure through two distinct permeation pathways - a canonical central pore and a non-canonical alternative pathway, each with unique biophysical and pharmacological characteristics. The canonical pathway refers to the conventional ion-conducting pore located at the center of the TRPM3 tetrameric channel structure. Activation of this pore is typically induced by classical agonists such as the endogenous neurosteroid pregnenolone sulfate (PS) and synthetic

ligands like nifedipine (Grimm *et al.*, 2003; Held *et al.*, 2015a; Vriens *et al.*, 2011; Wagner *et al.*, 2008). Ion conduction via this pore primarily facilitates the influx of divalent cations, notably Ca^{2+}, along with Na^{+} and Mg^{2+}. Electrophysiological recordings show this pathway exhibits an outwardly rectifying current-voltage (I–V) relationship, characterized by increase in current significantly at positive membrane potentials. In contrast, the non-canonical permeation pathway represents a functionally and structurally distinct ion route within TRPM3 (Vriens *et al.*, 2014). This pathway becomes active only under specific conditions — most notably, co-stimulation with PS and the antifungal agent clotrimazole (Clt) (Held *et al.*, 2015a; Vriens *et al.*, 2014). Unlike the central pore, the non-canonical pathway shows preference for monovalent cations such as Na^{+} and is characterized by an inwardly rectifying I–V profile, indicating a larger inward current at negative potentials.

CIM0216, a synthetic agonist with exceptional potency, provides an invaluable tool for dissecting TRPM3's dual pore functionality (Held *et al.*, 2015a). Unlike PS, which requires Clt for full activation of the non-canonical pathway, CIM0216 independently activates both permeation pathways, inducing robust inward and outward rectifying currents. Interestingly, CIM0216 lacks the acidic substituents critical for PS-mediated activation, suggesting a distinct binding mechanism. Its structure, consisting of three aromatic rings around a central linking moiety, shares basic similarities with Clt, potentially enabling its interaction with specific domains of TRPM3 that regulate the non-canonical pore. The dual activation by CIM0216 significantly augments intracellular Ca^{2+} signals, particularly in excitable cells such as sensory neurons and pancreatic β cells. This mechanism facilitates Na^{+}-driven membrane depolarization, which in turn activates voltage-gated calcium channels, amplifying Ca^{2+} influx and enhancing downstream signaling, including vesicular release.

In contrast, TRPM3 antagonists, including isosakuranetin and primidone, counteract the channel's activation by blocking ion influx or altering its conformation (Krügel *et al.*, 2017; Straub *et al.*, 2013). Isosakuranetin, a flavonoid with high specificity for TRPM3, effectively blocks both the canonical and non-canonical pathways by inhibiting ion flux induced by endogenous and synthetic agonists (Straub *et al.*, 2013). Its specificity for TRPM3 over other TRP channels makes it a valuable tool for studying TRPM3's role in sensory and inflammatory processes. Similarly, primidone, an anticonvulsant drug, has shown efficacy in inhibiting TRPM3-mediated calcium influx, reducing neurogenic inflammation and pain (Krügel *et al.*, 2017). These antagonists demonstrate significant potential in treating neuropathic pain and inflammatory conditions, providing critical tools for investigating TRPM3's roles in disease.

1.9.3 GPCR regulation of TRPM3 channels

One of the unique features of TRPM3 is its ability to be modulated by GPCRs through intricate mechanisms that influence function in pain, inflammation, and other sensory processes. The interaction between TRPM3 and GPCR pathways is a key mechanism through which opioid analgesics exert their peripheral effects. The binding of Gβγ to TRPM3 effectively gates the channel and prevents its activation, providing a molecular basis for how opioids can modulate pain at the sensory neuron level (Badheka *et al.*, 2017; Quallo *et al.*, 2017). Similarly, Gq- and Gs-coupled receptors, including prostaglandin EP2 and bradykinin B2 receptors, inhibit TRPM3, highlighting the channel's central role in nociceptive signaling. These findings underscore TRPM3 as a promising therapeutic target for managing pain and inflammation. TRPM3 regulation extends beyond Gβγ-mediated inhibition. The channel is dynamically modulated by phosphoinositides, particularly PIP_2 (Badheka *et al.*, 2015; Tóth *et al.*, 2015). PIP_2 not only enhances TRPM3 activity but also plays a pivotal role in promoting recovery from channel desensitization. This recovery is

facilitated by phosphatidylinositol kinases (PI-Ks), which resynthesize PIPs in the plasma membrane, thus reactivating TRPM3 functionality. Among the phosphoinositides, phosphatidylinositol (3,4,5)-trisphosphate (PIP_3) and PIP_2 exhibit the highest efficacy in potentiating TRPM3 activity, while phosphatases that deplete these lipids act as inhibitory factors. This lipid-mediated regulation underscores the critical importance of maintaining appropriate PIP levels to ensure TRPM3 functionality.

1.9.4 Effect of TRPM3 activation

Activation of TRPM3 by physiological stimuli or pharmacological agents initiates a robust influx of Ca^{2+}, surpassing that observed through depolarization-induced pathways such as voltage-gated Ca^{2+} channels (Held *et al.*, 2015a). This Ca^{2+} influx has profound implications for mitochondrial function, intracellular signaling and neuronal adaptation, positioning TRPM3 as a central player in linking Ca^{2+} dynamics with metabolic and transcriptional regulation. Ca^{2+} entry through TRPM3 channels triggers the binding of Ca^{2+} to calmodulin, a key Ca^{2+} sensor that modulates TRPM3 activity (Thiel and Rössler, 2023). Calmodulin directly interacts with TRPM3 channels, facilitating their activation and subsequent intracellular signaling (Holakovska *et al.*, 2012). Through its EF-hand motifs, calmodulin binds Ca^{2+} ions, and the Ca^{2+}-bound form is essential for modulating TRPM3 activity and downstream signaling pathways. Importantly, this interaction serves as a feedback mechanism: Ca^{2+} influx through TRPM3 activates calmodulin, which in turn activates calcineurin, a Ca^{2+}/calmodulin-dependent phosphatase that acts as a negative regulator of TRPM3 signaling. This dual role of calmodulin ensures precise control of TRPM3-induced signaling cascades.

Following TRPM3 activation, mitochondria rapidly buffer approximately 40% of the incoming Ca^{2+} (Wang *et al.*, 2022). This buffering leads to a steady-state elevation of mitochondrial Ca^{2+} levels, a phenomenon that is further amplified by the neurotrophic factor - nerve growth factor (NGF), which enhances TRPM3 activity and slows the clearance of intracellular Ca^{2+}. The delayed recovery of cytosolic Ca^{2+} extends the duration of Ca^{2+}-dependent signaling cascades, underscoring the unique role of TRPM3 in modulating intracellular Ca^{2+} homeostasis. This sustained Ca^{2+} signaling and buffering of Ca^{2+} within the mitochondrial matrix could play a role in activating enzymes in the TCA cycle, including pyruvate dehydrogenase (PDH) and isocitrate dehydrogenase (IDH), which in turn accelerate ATP production to meet the high metabolic demands of neurons. These findings indicate a potential role for TRPM3 in modulating mitochondrial respiration and neuronal metabolism. In DSPN, where chronic hyperglycemia and oxidative stress are known to impair mitochondrial function, TRPM3-mediated Ca^{2+} buffering emerges as a promising mechanism to maintain Ca^{2+} homeostasis and enhance mitochondrial energy production. By supporting these processes, TRPM3 may aid in neuronal recovery, particularly in contexts of injury or degeneration. However, its precise role in DSPN, including whether it mitigates or exacerbates Ca^{2+} dysregulation, mitochondrial dysfunction, or neuronal degeneration, remains unclear. This highlights the need for further investigation into the mechanistic contribution of TRPM3 in diabetic neuropathy.

1.10 Rationale, hypothesis and aims

DSPN is characterized by a progressive "dying-back" axonal degeneration, leading to sensory deficits and debilitating neuropathic pain. M_1R antagonism was first demonstrated experimentally by our lab to promote neurite outgrowth and enhance mitochondrial function via activation of the AMPK pathway in DRG sensory neurons. The antimuscarinic drugs effectively prevented or

reversed key indices of peripheral neuropathy, such as depletion of sensory nerve terminals, thermal hypoalgesia, and nerve conduction slowing across diverse rodent models of diabetes. M_1R is linked to numerous processes including axonal sprouting and mitochondrial function. Conversely, aberrant M_1R activation disrupts these processes by inhibiting microtubule polymerization and impairing mitochondrial trafficking in DRG neurons. Genetic ablation of M_1R increases the sensitivity of DRG neurons to neurotrophic stimuli, enhancing neurite outgrowth. Neurons from M_1R knockout mice display significantly improved mitochondrial function, evidenced by elevated maximal oxygen consumption rate and spare respiratory capacity, both mediated through AMPK activation. Enhanced spare respiratory capacity allows mitochondria to meet acute ATP demands, crucial for energy-dependent processes such as axonal growth and repair. M_1R antagonists such as pirenzepine and oxybutynin exhibit robust neuroprotective effects in both *in vitro* and *in vivo* models of CIPN and HIV-associated neuropathy. Clinical trials further validate these findings, with topical oxybutynin demonstrating increased IENF density and improved scores on clinical neuropathy, pain and quality of life scales in type 2 diabetes patients. Mechanistically, M_1R antagonism activates AMPK via its upstream regulator CaMKKβ. This process is initiated by a slow but sustained rise in intracellular Ca^{2+}, which is dependent on extracellular Ca^{2+} influx rather than release from intracellular stores such as the ER. A potential source of this extracellular Ca^{2+} is the TRPM3 channel, a non-selective cation channel that remains closed under low levels of PIP_2. Based on these findings, I hypothesized that M_1R antagonism-induced blockade of G protein signaling increases PIP_2 levels, activating TRPM3 channels and leading to enhanced mitochondrial function and axonal regeneration. This hypothesis is divided into two specific aims **(I & II)** and presented in **chapters 3 & 4** respectively.

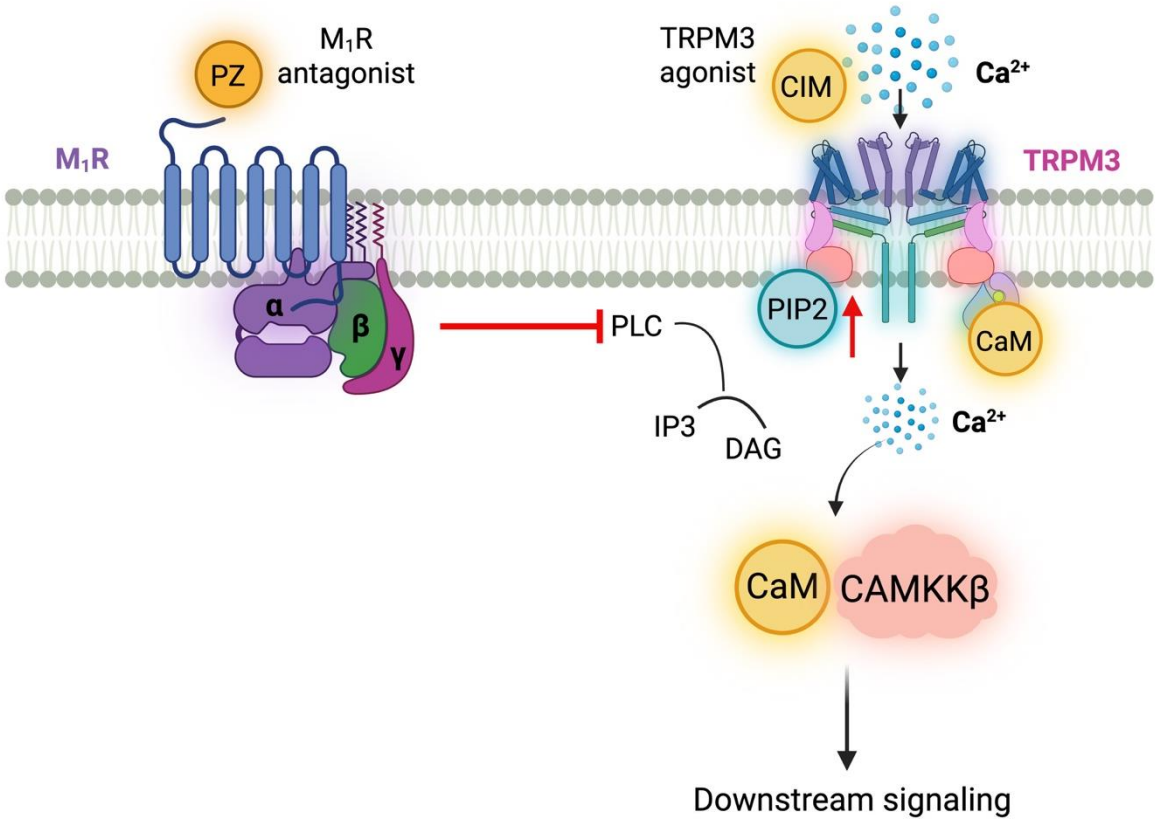

Figure 1.8: Hypothetical model of M_1R-mediated regulation of TRPM3 signaling via calcium influx and downstream pathways. This schematic represents a proposed mechanism in which M_1R signaling negatively regulates TRPM3 channel activity. Upon activation, M_1R couples to G proteins (α, β, γ subunits) and stimulates phospholipase C (PLC), leading to hydrolysis of PIP_2 into IP_3 and DAG. This reduces membrane PIP_2 levels, a critical factor for TRPM3 activation. TRPM3, activated by the agonist CIM, allows calcium (Ca^{2+}) influx, which binds to calmodulin (CaM), subsequently activating CaMKKβ and initiating downstream signaling. Antagonism of M_1R by PZ is hypothesized to prevent PLC activation, preserve PIP_2 levels, and enhance TRPM3-mediated Ca^{2+} signaling.

Specific Aims:

Aim I: To determine whether direct activation of TRPM3 channels promotes axonal repair and recapitulates the neuroprotective effects of M_1R antagonism in DRG sensory neurons.

TRPM3 channels regulate Ca^{2+} influx and mitochondrial dynamics; however, their precise impact on neuronal metabolism and repair processes remains poorly understood. This aim tested whether TRPM3 activation via specific agonists, pregnenolone sulfate (PS) and CIM0216, promoted Ca^{2+} influx, activated AMPK, and enhanced mitochondrial respiration in DRG sensory neurons. Using a combination of live-cell Ca^{2+} imaging, mitochondrial functional assays (e.g., OCR and ATP production), and metabolomic profiling (via mass spectrometry), we demonstrated that TRPM3 activation improves mitochondrial function, supports neuronal metabolism, and promotes neurite outgrowth. To validate the findings, we employed TRPM3-specific knockdown models and cultures derived from M_1R knockout mice, confirming that TRPM3 activation is required for the antimuscarinic-mediated enrichment of mitochondrial function and axonal regeneration. This work provides mechanistic insights into the role of TRPM3 channels in mediating the beneficial effects of M_1R antagonism on mitochondrial function and axonal repair. This work provides critical mechanistic insights into the interplay between TRPM3 channels and the CaMKKβ-AMPK signaling pathway, identifying a potential therapeutic strategy for treating peripheral neuropathies such as DSPN, CIPN, and HIV-associated neuropathy. The data supporting **Aim I** comprise a published research article in Molecular Metabolism titled: "*Muscarinic acetylcholine type 1 receptor antagonism activates TRPM3 to augment mitochondrial function and drive axonal repair in adult sensory neurons.*" This publication forms **Chapter 3** of this thesis and addresses the following key questions:

1) Does TRPM3 activation using specific agonists induce Ca^{2+} influx and activate downstream signaling pathways?
2) How does TRPM3 activation modulate mitochondrial metabolism and promote axonal regeneration?
3) What is the mechanistic link between M_1R antagonism and TRPM3 activation?

This aim establishes a novel pathway linking Ca^{2+} signaling via TRPM3 activation to mitochondrial function and axonal repair, providing a foundation for future therapeutic approaches for peripheral neuropathies.

Aim II: To determine the *in vivo* role of TRPM3 activation in mediating the neuroprotective and axonal repair effects of M_1R antagonism in a mouse model of diabetic neuropathy.

Pirenzepine (PZ), a selective M_1R antagonist, promoted axonal repair and reversed nerve degeneration in diabetic neuropathy. Topical PZ effectively treats peripheral neuropathy in diabetic mice by promoting axonal repair. Furthermore, PZ is currently in clinical trials for the treatment of diabetic neuropathy (phase III to be performed in 2025), as well as neuropathies induced by HIV or chemotherapeutics, highlighting its therapeutic potential across diverse neuropathic conditions. Following the findings in **Aim I** where PZ mediated its effects through TRPM3 activation, we sought to investigate the role of TRPM3 in mediating these neuroprotective effects *in vivo*. This aim utilized a diabetic neuropathy mouse model of type 1 diabetes induced by STZ to examine whether TRPM3 activation is essential for PZ-mediated nerve repair and functional recovery. In this aim, female Swiss webster mice were divided into seven experimental groups, including control and STZ-induced diabetic groups with and without PZ treatment, as well as combinations with TRPM3 inhibitors primidone and isosakuranetin. PZ including other drugs

were administered either topically (to the cornea) or subcutaneously. To determine the effects of these treatments, we assessed nerve conduction velocity (NCV), corneal nerve density, tactile and thermal sensitivity over time at 4, 8 and 16 weeks post-treatment. This aim addresses critical questions related to the *in vivo* role of TRPM3 in mediating the neuroprotective effects of M_1R antagonism and provides mechanistic insights into peripheral nerve repair in diabetic neuropathy. Data supporting this aim forms **Chapter 4** of this thesis and addresses the following questions:

1) Does PZ treatment promote nerve repair and functional recovery in a diabetic mouse model?
2) Is TRPM3 activation required for the neuroprotective effects of PZ *in vivo*?
3) How do corneal and systemic routes of PZ administration differ in their impact on nerve repair?

This aim provides insights into the translational relevance of findings from *in vitro* studies to more complex *in vivo* systems. While *in vitro* studies have demonstrated that PZ promotes axonal repair via TRPM3 activation, *in vivo* models offer a more realistic perspective on the challenges of translating these mechanisms to whole-organism physiology. Factors such as systemic drug distribution, localized effects, immune responses, and the involvement of other cellular pathways can influence outcomes in ways not well explained in in-vitro system. By utilizing a diabetic neuropathy mouse model, this aim bridges the gap between cellular mechanisms and their application in living systems, emphasizing the interplay of multiple biological factors that may modulate the therapeutic efficacy of PZ and TRPM3 activation in the context of peripheral neuropathy. This approach highlights the complexity and variability of *in vivo* models, providing a more comprehensive understanding of the therapeutic potential and limitations of targeting the M_1R-TRPM3 axis.

Chapter 2

Experimental methods and materials

Chapter 2 includes all the methods to maintain a concise and easy-to-read thesis. The content has been compiled from chapters 3 (published in Molecular metabolism, Dec 2024) and 4 (manuscript in progress). The described experimental procedures were carried out either independently by me or in collaboration with the co-authors. Contributions from other authors are detailed at the end of chapter 3 and 4.

2.1 Adult rodent DRG sensory neuron culture

The Canadian Committee on Animal Care (CCAC) guidelines were carefully followed for all animal protocols. As described previously, intact DRG were isolated and dissociated from adult age matched male control and 3-4-month streptozotocin (STZ)-induced diabetic Sprague–Dawley rats, wild type (Callender and Newton) C57BL/6 mice and M_1R knockout (KO) mice (the latter a kind gift from Dr. Jürgen Wess at NIDDK, USA) (Fernyhough *et al.*, 1993; Mulderry and Lindsay, 1990; Urban *et al.*, 2012). Type 1 diabetes was induced by injection of STZ (Millipore Sigma Canada Ltd, Oakville, Ontario, Canada) in 0.9% saline after overnight fast at a single dose of 90 mg/kg for rats. Blood glucose levels were confirmed 4–7 days later in samples obtained by tail prick and measured using a strip-operated reflectance meter (Alpha TRAK2, Zoetis Canada inc., Kirkland, Quebec, Canada). Our previous studies reveal that neurons isolated from type 1 diabetic rats exhibit key components of the diabetic phenotype and mimicking some aspects of the neurodegenerative process associated with diabetic neuropathy (Schartner *et al.*, 2018; Zherebitskaya *et al.*, 2009). Neurons were cultured in defined Hams F-12 media in the presence of

N2 supplement (0.1 mg/mL transferrin, 20 nM progesterone, 100 μM putrescine, 30 nM sodium selenite, 0.1 mg/mL BSA; MilliporeSigma Canada Ltd, Oakville, Ontario, Canada supplied the additives; Wisent Inc, Saint-Jean-Baptiste, Quebec, Canada provided the culture medium), insulin (MilliporeSigma Canada Ltd, Oakville, Ontario, Canada) and low-dose cocktail of neurotrophic factors (0.1 ng/mL NGF, 1.0 ng/mL GDNF, and 0.1 ng/mL NT-3; all from Peprotech, Cranbury, NJ, USA) (Calcutt *et al.*, 2017). By delivering growth factors, the goal was to mimic the level of neurotrophic support that sensory neurons receive *in vivo*. The enrichment of neurons was accomplished by centrifuging in a 15% BSA (Thermo Fisher Scientific, Carlsbad, California, USA) column (Gavazzi *et al.*, 1999). Most of the fibroblasts and Schwann cells were removed during this process, but a minimal number of satellite cells accounted for approximately 5%–10% of total cells in the final culture (mostly directly associated with sensory neurons). Cells were plated onto poly-d-l-ornithine hydrobromide (MilliporeSigma Canada, Oakville, Ontario, Canada), and laminin-coated 12 mm glass cover slips for neurite outgrowth and microscopy studies, black-96 well clear bottom plates for Ca^{2+} imaging using confocal microscopy, NUNC plastic tissue culture multi-well dishes for immunoblot analysis and custom 24-well plastic dishes for assessing mitochondrial bioenergetics using a Seahorse Biosciences XFe24 Analyser (laminin, cover slips, and plates from Thermo Fisher Scientific, Carlsbad, California, USA, Seahorse products from Agilent Technologies Inc, Santa Clara, California, USA). In all studies neurons from age matched control mice and rats were cultured in the presence of 10 mM d-glucose (MilliporeSigma Canada Ltd, Oakville, Ontario, Canada) and 0.1 nM insulin and neurons from diabetic rats were maintained in medium containing no insulin and 25 mM d-glucose.

2.2 Neuroblastoma SH-SY5Y cell line culture

The human neuroblastoma SH-SY5Y cell line (ATCC CRL-2266, Virginia, USA) was a kind gift from Dr. Jun-Feng Wang, University of Manitoba. The cells were cultured in DMEM/F12 (1:1) media supplemented with heat inactivated 10% FBS (DMEM/F12 and FBS from Thermo Fisher Scientific, Carlsbad, California, USA) and 1× antibiotic antimycotic solution (MilliporeSigma Canada Ltd, Oakville, Ontario, Canada).

2.3 AAV-PHP.S mediated knockdown of TRPM3

The DRG neurons were seeded in culture plates and incubated at 37 °C with 5% CO2 for 18–20 h. Custom AAV.PHP.s (Chan *et al.*, 2017) vectors encoding a scrambled sequence or carrying shRNA to TRPM3 (CGAGACATGGGCCCTCAAATA) under the U6 promoter were generated by Vector Builder (Chicago, IL, USA), with a final titer exceeding 1 × 10ˆ12 genome copies per milliliter (GC/ml). The culture medium was removed from the DRG neurons, and neurons were infected with the AAV vector at a multiplicity of infection (MOI) corresponding to 1 × 10ˆ5 viral particles per neuron. After 8 h of viral exposure, the medium was replaced with fresh complete culture medium, and cells were again incubated at 37 °C in a 5% CO2 incubator overnight. Analysis was performed 24–48 h post-transduction and levels of transduction were verified based upon GFP and RFP expression.

2.4 Real-time intracellular Ca^{2+} imaging

For acute measurements, as shown in Figure 3.1, Figure 3.2 (Chapter-3rd), neurons were cultured in 96-well plates (black clear-bottomed; Thermo Fisher Scientific, Carlsbad, California, United States) overnight. The following day or after 48 h, the cells were washed with HBSS with Ca^{2+} or HBSS without Ca^{2+} and then loaded with 3 μM of Ca^{2+}sensitive dye fluo-4 AM (all from Thermo Fisher Scientific, Carlsbad, California, United States). After 1 h of incubation, the cells were

washed with HBSS again. The temperature of the stage was maintained at 37 °C using a heating block. The 96-well plate was then placed in a Zeiss LSM 510 META Confocal microscope with on-stage incubator. Baseline signals were collected (excitation at 494 nm and emission 516 nm; 20 × and 100 × objectives) followed by addition of drugs such as CIM0216 (Bio-Techne Canada, Toronto, ON, Canada; and referred to as CIM), pregnenolone sulphate (PS), primidone, isosakuranetin, pirenzepine (PZ), muscarine (Millipore Sigma Canada, Oakville, Ontario, Canada) and MT7 (Alomone labs, Jerusalem, Israel). Regions of interest (ROIs) containing individual neuron cell bodies or axons were selected and fluorescence intensities were quantified using Zen 2009 software. For calcium measurements at ×20 magnification 10–15 ROIs from perikarya/axons per field or well of a 96-well plate were selected. The graphed data is the average of individual perikaryal or axon ROI signals from 7 to 10 replicate wells. For ×100 imaging, multiple ROIs within the perikaryal or axons were derived from 1 to 2 neurons. This process was performed in 3–5 wells of a 96 well plate. The data is presented as change in intensity of fluo-4 fluorescence (ΔF/F) and the area under the curve (Maalmi *et al.*). The ΔF/F was calculated as $\Delta F/F = (F–F0)/F0$, where F is the fluorescence at a given time and F0 is the baseline fluorescence signal averaged over a 10s period corresponding to the lowest fluorescence signal over the recording period. The data was plotted as the average intensity of perikaryal or axon signal from 3 to 5 replicate wells. AUC was calculated individually as $(S1+S2)/2 \times (t2-t1)$ where $(S1+S2)/2$ gives the average calcium signal between the two time points t1 and t2. Once the individual areas were computed for all time intervals, the average of these areas was taken to represent the total AUC.

2.5 Assessment of total neurite outgrowth

Adult rat or mouse neurons grown on glass coverslips were fixed with 2% paraformaldehyde in PBS (pH 7.4) for 15 min at room temperature and permeabilized with 0.3% Triton X-100 in PBS

for 5 min (products from Thermo Fisher Scientific, Carlsbad, California, USA). Neurons were then incubated in blocking buffer (Roche, Basel, Switzerland) diluted with FBS and 1.0 mM PBS (1:2:7) for 1 h, then rinsed 3 times with PBS. The primary antibody used was against β-tubulin isotype III (MilliporeSigma Canada, Oakville, Ontario, Canada; 1:1000), which is neuron specific. Plates were incubated at 4 °C overnight. The following day, the coverslips were incubated with Cy3-conjugated secondary antibodies (Jackson ImmunoResearch Laboratories, West Grove, Pennsylvania, USA) for 1 h at room temperature and then mounted and imaged using a Carl Zeiss Axioscope-2 fluorescence microscope equipped with an AxioCam camera. Random images were captured using Axio-Vision4.8 software. Quantification of total neurite outgrowth was performed by measuring the mean pixel area of captured images using ImageJ software and adjusted for the cell body signal. All values were adjusted for neuronal number. The level of total neurite outgrowth in this culture system has been validated to be similar to collateral sprouting *in vivo* and directly related to arborizing axonal plasticity (Smith and Skene, 1997).

2.6 Quantitative Western blotting

Cultured sensory neurons derived from rat DRG and SH-SY5Y cells were harvested after treatments in ice-cold RIPA buffer, 1 mM PMSF and protease inhibitor cocktail and were stored at − 80 °C (Fernyhough *et al.*, 1999) (products from Thermo Fisher Scientific, Carlsbad, California, USA). Protein concentration was measured using the DC protein assay (Bio-Rad, Hercules, CA, USA), and the lysates from the culture were resolved on a 10% sodium dodecyl sulphate–polyacrylamide gel electrophoresis [SDS-PAGE; 8% for TRPM3 and 15% for mitochondrial OXPHOS proteins] and electroblotted onto nitrocellulose membrane. The blots were blocked with 2% (for p-AMPK and T-AMPK) and 5% (for TRPM3, TRPM2 and mitochondrial OXPHOS proteins) non-fat dry milk, rinsed in TBS-T and incubated with antibodies

to the following proteins: TRPM3 (anti-TRPM3 antibody, ab56171; 1:200, Abcam, Waltham, Massachusetts, USA and anti-TRPM3 extracellular, PA5-77327; 1:200, Thermo Fisher Scientific, Carlsbad, California, USA), anti-TRPM2 antibody (NB110–81601SS; 1:500, Bio-Techne, Toronto, Ontario, Canada), p-AMPK (Thr172; 9101s; 1:1000, New England Biolabs, Whitby, ON, Canada), total-AMPK (T-AMPK; SC25792; 1:1000, Santa Cruz Biotechnology Inc., Dallas, Texas, USA), and mitochondrial OXPHOS cocktail (Oxphos WB-antibody cocktail; 45–8099; 1:1000, Thermo Fisher Scientific, Carlsbad, California, USA). After overnight incubation, the blots were washed 3 times with TBS-T for 10 min each, followed by addition of secondary antibodies at a dilution of 1:2000 for 1 h at room temperature. The blots were rinsed, incubated in Western Blotting ClarityTM Western ECL substrate (Bio-rad, Hercules, California, USA), or SignalFire™ Elite ECL reagent (Cell Signaling, Danvers, Massachusetts, USA) for a few minutes and imaged using a Chemi Doc (Bio-Rad, Hercules, California, USA).

2.7 Measurement of mitochondrial respiration

The neuronal bioenergetic function was measured using an XFe24 Seahorse Analyzer (Agilent Technologies Inc, Santa Clara, California, USA). The XFe24 creates a transient 7-µl chamber in specialized 24-well microplates that allows for oxygen consumption rate (OCR) to be monitored in real time (Hill *et al.*, 2009). A change of culture medium to unbuffered DMEM (pH 7.4) supplemented with 1 mM pyruvate and 10 mM d-glucose (for control) or 25 mM d-glucose (for diabetic rat-derived cultures) was performed 1 h before the assay. OCR was linear in the range of 2,500–5,000 neurons per well. We sequentially injected oligomycin (1 µM), carbonyl cyanidep-trifluorocarbonyl-cyanide methoxyphenyl hydrazone (FCCP) (1 µM), and rotenone (1 µM) plus antimycin A (1 µM) through ports in the Seahorse Flux Pak cartridges (Roy Chowdhury *et al.*, 2012) (chemicals from MilliporeSigma, Canada, Oakville, Ontario, Canada). Each loop began

with mixing for 3 min, was delayed for 2 min, and had OCR measured for 3 min. This allowed determination of the basal level of OCR, the amount of oxygen consumption linked to ATP production, the maximal respiration capacity, and the non-mitochondrial oxygen consumption (Brand and Nicholls, 2011; Hill *et al.*, 2009). Afterwards, the cells were suspended in RIPA buffer, PMSF and a cocktail of protease inhibitor. After centrifugation at 14000g for 10 min, the lysate was collected, and the DC protein assay was run followed by data analysis normalizing OCR to mg total protein.

2.8 Immunofluorescence

Cultured DRG neurons and SH-SY5Y cells were fixed on coverslips with paraformaldehyde (2%). The slides and coverslips were then washed with phosphate buffer saline (PBS) 3 times followed by treatment with 0.03% Tween-20 for 5 min to permeabilize the cells. The slides and cover slips were washed again and blocked with blocking buffer diluted with FBS and 1.0 mM PBS (1:2:7). The primary antibody against TRPM3 (rabbit anti-TRPM3 antibody, ab56171; 1:200), p-AMPK (Thr172, p-AMPK; SC3352; 1:1000) and phosphatidylinositol 4,5-bisphosphate monoclonal antibody (2C11 clone anti-PIP2 antibody; MA3-500, 1:200 dilution, Thermo Fisher Scientific, Carlsbad, California, USA) were added for overnight incubation. On the following day, the secondary antibody-goat anti-Mouse, Alexa Fluor™ 488 (A-11029, 1:500 dilution; Thermofisher Scientific, Waltham, Massachusetts, United States) was added and then the slides were mounted using PermaFlour mountant (Thermo Fisher Scientific, Carlsbad, California, USA). For double staining, after the addition of secondary antibody, the cover slips were blocked again followed by addition of the second primary antibody (mouse anti-β tubulin III). After overnight incubation, the second secondary antibody (anti-mouse) was added, and the coverslips were mounted on slides

using PermaFlour mountant. For each case, one slide was incubated with blocking buffer instead of the primary antibody or secondary antibody as a negative control.

2.9 Assessment of mitochondrial membrane potential (MMP) in cultured neurons

To quantify the effect of PS or CIM on MMP, double emission imaging of the JC-1 ratio (590/530 nm) was utilized to determine changes in mitochondrial membrane potential ($\Delta\Psi m$) induced by drugs and in response to acute +/− 200 μM FCCP treatment (to completely depolarize the inner mitochondrial membrane). Sensory neurons were loaded with 5 μM JC-1 for 20 min and then washed with Ham's F12 media in response to pre-treatment for 3 h of PS and CIM. The excitation wavelength was set at 485 ± 11 nm (for simultaneous aggregate and monomer excitation). The emission wavelength was set at 590 ± 15 nm (aggregate emission) and 530 ± 15 nm (monomer emission) on the Biotek Synergy Neo2 multimode plate reader (Agilent Technologies Inc, Santa Clara, California, USA) and the baseline fluorescence followed by addition of FCCP was recorded.

2.10 Untargeted metabolomics

Cultured DRG neurons were prepared in 6-well plates and allocated into two experimental groups: control and CIM-treated. Neurons were incubated for 24 h before sample collection. For untargeted metabolomics, cell pellets were resuspended in 1 mL of ice-cold 80% methanol, followed by vigorous vortexing for 1 min. The samples were then subjected to sonication in an Ultrasonic Bath (Branson Ultrasonics, Danbury, Connecticut, USA) filled with ice-cold water for 15 min to ensure complete cell lysis and efficient metabolite extraction. Post-sonication, the samples were centrifuged at 12,000 rpm for 15 min at 4 °C to separate the supernatant from the cell debris. The clear supernatant was transferred to clean tubes and dried under a gentle nitrogen flow to evaporate the solvent. The dried residues were reconstituted in 100 μL of methanol: water (4:1, v/v), vortexed

for 2 min, and centrifuged to remove any insoluble material. The final clear supernatant was transferred into 200 μL micro vial inserts for subsequent analysis. The metabolomic analysis was performed using a Rapid Resolution LC system (1260 Infinity, Agilent Technologies, Santa Clara, California, USA) coupled to a 6538 UHD Accurate QTOF mass spectrometer (Agilent Technologies, Santa Clara, California, USA) with dual electrospray ionization (Hall *et al.*) in both positive (+) and negative (−) modes. Chromatographic separation was achieved using a ZORBAX SB-Aq column (4.6 × 100 mm, 1.8 μm, Agilent) maintained at 55 °C. The mobile phases consisted of water (A) and acetonitrile (B), both containing 0.1% formic acid (all from Thermo Fisher Scientific, Carlsbad, California, USA). The flow rate was set at 0.45 mL/min with the following gradient: 2% B from 0 to 1 min, increased linearly to 98% B over 11 min, maintained at 98% B for 2 min, decreased back to 2% B over 4 min, maintained at 2% B for 1 min, followed by a 1-minute post-run. To minimize carryover, the needle was washed for 15 s with water: acetonitrile (1:1, v/v). 4 μL of each extract were injected for analysis. Mass spectrometry was conducted with the following parameters: capillary voltage at 4000V, fragmentor voltage at 175V, skimmer voltage at 50V, and Oct 1 RF Vpp at 750V. Nitrogen was used as the drying gas at a flow rate of 11 L/min and a gas temperature of 300 °C, while the nebulizer was set to 45 psig (pressure unit). A full-range mass scan from 50 to 3000 m/z was performed. Data acquisition and analysis were executed using MassHunter Workstation version 10 (Agilent Technologies, Santa Clara, California, USA). Metabolite identification was performed utilizing the integrated Metlin database, encompassing over 200,000 known endogenous compounds. This methodological approach ensured comprehensive extraction, identification, and analysis of metabolites from DRG neurons, facilitating a detailed untargeted metabolomic profile.

2.11 Targeted metabolomics

Standard solution preparation for GC–MS/MS analysis involved preparing stock solutions of fumarate, malate, lactate, and α-ketoglutarate in methanol, while all other compounds were prepared in water at 1 mg/mL. A cocktail solution was made by combining all the stock solutions. Working standard solutions were obtained by serial dilutions of the cocktail solution with methanol (Supplementary Table 3.S1, chapter-3rd). Subsequently, 30 µL of BSTFA with 1% TMCS was added at 37 °C for 30 min. Then 60 µL was transferred into a micro-vial insert and kept at −80 °C until analysis. The SH-SY5Y cells were treated upon reaching 90% confluency with 1 µM CIM for 1 h and 3 h and CIM (1 µM), primidone (10 µM) or isosakuranetin (10 µM) for 3 h post 4 h starvation. Cell culture media was removed, and cells were washed with 2 mL of PBS. Subsequently, 500 µL of 75% methanol-MTBE (9:1, v/v) was added containing 1,2 13C2 myristic acid at 5 µg/mL. Then cells were detached from plates and transferred to 1.5 mL centrifuge tubes. Cell lysis was performed using a X3 freeze and thaw cycle and centrifuged at 12000rpm for 10 min at 4 °C. The supernatant was dried under a gentle flow of nitrogen and stored at −80 °C. The GC–MS analysis was performed using a 7890B gas chromatograph (Agilent Technologies, Santa Clara, California, USA) with 7000D Triple-quadrupole mass spectrometer (Agilent Technologies), equipped with 7693 Autosampler (Agilent Technologies, Santa Clara, California, USA). The column used was an HP-5MS (0.25 mm, 30m, 0.25 µm, Agilent Technologies, Santa Clara, California, USA), with a split ratio of 18:1 and injection volume of 1 µL. The GC oven temperature initially was set at 60 °C, maintained for 1 min, ramped up to 100 °C at 30 °C/min, and ramped up to 300 °C at 20 °C/min and maintained for 2 min. Carrier gas was helium (99.999% purity), with a flow rate of 1.2mL/min and nitrogen (99.999% purity) was used as the collision cell gas. A period of 3.8 min for solvent delay was employed for each sample run and for mass range of 50–750 m/z.

Source temperature was set at 300 °C. For a targeted study with CIM, primidone and isosakuranetin, 4 μg of each analyte was spiked into the cell matrix as a reference, and metabolite concentrations were quantified directly from these standardized readings. Calibration curves were generated to evaluate the metabolite concentrations. A full scan mode was used for determination of retention time for each analyte (Supplementary Table 3.S2, chapter-3rd). The software used for data analysis was Mass Professional Profiler (MPP, 15.1).

2.12 Animal model and treatments

Adult female Swiss Webster mice (21–25 g; Envigo, CA, USA) were housed in groups of five per cage with fresh bedding in a controlled vivarium environment (12-hour light/dark cycle) and provided with unrestricted access to food and water. To induce diabetes, a randomly selected cohort received intraperitoneal injections of streptozotocin (STZ) (Sigma-Aldrich, United States) at 105 mg/kg in 0.9% saline for two consecutive days following an overnight fast. Mice with non-fasting blood glucose levels exceeding 15 mmol/L, confirmed via tail-prick blood sampling and measurement with a one touch ultra-glucometer (LifeScan Inc., United States), were classified as diabetic (Casselini *et al.,* 2024). Treatments commenced following the confirmation of diabetic status, typically 3–5 days post-injection. A total of 70 mice were divided into seven groups (n = 10 per group). Five groups received daily topical eye drop treatments (25 μL) containing either a vehicle control (0.9% sterile saline/ hydrogel) or drug solutions diluted in the vehicle. The remaining two groups were administered daily subcutaneous injections of either the vehicle or drug formulations. Drug treatments consisted of topical pirenzepine (20 mg/mL), primidone (1 μg/day), or isosakuranetin (1 μg/day), and subcutaneous injections of pirenzepine (10 mg/kg/day) or primidone (1 mg/kg/day) (all drugs from Sigma-Aldrich, United States). Daily treatments (5 days/week) were administered between 8:00 and 11:00 AM to conscious, manually restrained mice

in their home cages for a period of 16 weeks. On behavioral testing days, treatments were administered after the completion of all behavioral measurements to prevent acute drug effects from influencing test outcomes. Animal identification codes ensured blinding during all behavioral and physiological assessments. Diabetic status was reconfirmed at the conclusion of the study through non-fasting blood glucose measurements and body weight monitoring. All procedures were performed in Dr. Nigel A. Calcutt's lab at University of California, San Diego (UCSD) under his supervision and adhered to protocols approved by the institutional animal care and use committee at UCSD.

2.13 Thermal sensitivity assessment

Hind paw thermal nociception was evaluated using the Hargreaves apparatus with floor temperature started at 30 °C (Jolivalt *et al.*, 2016). Mice were placed individually in plexiglass chambers on a glass surface, and an infrared heat source (temperature increasing at 1 °C/second) was directed toward the plantar surface of the right hind paw. Withdrawal latencies were automatically recorded. Each paw was tested three times at five-minute intervals, and the average was calculated. Testing was conducted at 4, 8 and 16 weeks after diabetes confirmation and treatment initiation, between 9:00 AM and 3:00 PM.

2.14 Tactile sensitivity testing

Mechanical sensitivity was evaluated using von Frey filaments to measure the 50% paw withdrawal threshold. Mice were placed in individual restraint chambers on a testing stand and allowed to acclimatize for 15 minutes. A series of calibrated von Frey filaments (3.22, 3.61, 3.84, 4.08, 4.31, 4.56 and 4.74 g) were used, starting with the 3.84 g filament (Jolivalt *et al.*, 2016). Each filament was applied perpendicularly to the plantar surface of the right hind paw with enough

pressure to cause buckling for 1 second. This application was repeated five times, ensuring continuous contact with the paw unless a withdrawal response occurred. A paw lift was recorded as a positive response, prompting the use of the next lighter filament. If no response was observed after 5 seconds, the next heavier filament was applied. This sequence continued until four measurements were recorded following a change in behavior or until five consecutive negative responses (scored as 15 g) or four consecutive positive responses (scored as 0.25 g) were obtained. The 50% paw withdrawal threshold was interpolated from the pattern of positive and negative responses.

2.15 Electrophysiological measurements

Peripheral nerve conduction was assessed using standard electrophysiological techniques. Under isoflurane anesthesia, stimulating electrodes were placed at the sciatic notch and Achilles tendon of the left hind limb, while recording electrodes were positioned in the ipsilateral foot's interosseous muscles (Jolivalt *et al.*, 2016). Nerve temperature was maintained at 37°C. Single square-wave pulses were delivered sequentially to the sciatic notch and Achilles tendon. The peak-to-peak latencies of the resulting M waves were used to calculate motor nerve conduction velocity (MNCV) based on the distance between stimulation sites. Each measurement was performed in triplicate, and the median value was used for analysis.

2.16 Quantification of corneal nerve fiber density

Corneal nerve imaging was performed to assess sub-basal nerve plexus integrity. Isoflurane-anesthetized mice underwent corneal nerve imaging at baseline (pre-diabetes) and at 4, 8 and 16 weeks post-diabetes induction and drug treatments using a corneal confocal microscope (HRT3 with Rostock corneal module; Heidelberg Engineering, Germany) (Casselini *et al.*, 2024). Images

were acquired coded to prevent bias. Five consecutive corneal images (2 μm intervals) spanning from the superficial corneal epithelium to the stroma were analyzed using an 8 × 8 grid overlay to quantify nerve fiber occupancy (Jolivalt *et al.,* 2016).

2.17 Motor coordination testing (rotarod)

To rule out motor impairments that could confound sensory testing results, motor coordination was evaluated using a rotarod apparatus (Stoelting Co.). Mice were placed on a rotating rod (1.25-inch diameter) that accelerated from 4 to 40 revolutions per minute (RPM) over 120 seconds, followed by a consistent 40 RPM rotation for 180 seconds. Each mouse underwent an acclimation trial before the test session.

2.18 Statistical analysis

We used one rat or mouse (age-matched normal or diabetic) for each neuronal culture experiment, and 300,000 SH-SY5Y cells per well in 6 well plate and such experiments were independently repeated at least 2–3 times. In dose–response experiments and in comparisons of treatment groups to a single control group (*including behavioral studies*), data are expressed as mean ± SEM and analyzed by one-way ANOVA with Dunnett's test for post hoc comparisons. For comparisons between multiple treatment groups, Tukey's post hoc test was used. The statistical analysis was performed using GraphPad Prism software. For the untargeted metabolomics study in DRG neurons, Bonferroni FWER analysis was used using t-test for statistical analysis (Supplementary Figure 3.S9, chapter-3rd). For the targeted metabolomics study, Benjamini-Hochberg statistical analysis was performed using one-way ANOVA with $p < 0.05$ (Figure 3.8, chapter-3rd) and one-way ANOVA, $p < 0.05$, Bonferroni FWER for statistical analysis in Supplementary Figure 3.S10 (Chapter-3rd).

Chapter 3

Muscarinic acetylcholine type 1 receptor antagonism activates TRPM3 to augment mitochondrial function and drive axonal repair in adult sensory neurons

Sanjana Chauhan[1,2], Darrell R. Smith[1], Shiva Shariati-Ievari[1,3], Abhay Srivastava[4,5], Sanjiv Dhingra[4,5], Michel Aliani[1,3], and Paul Fernyhough[1,2*]

Published as an original article in the journal of "Molecular metabolism"

1) Division of Neurodegenerative Disorders, St. Boniface Hospital Albrechtsen Research Centre, University of Manitoba, Winnipeg, Canada. 2) Department of Pharmacology and Therapeutics, Max Rady College of Medicine, Rady Faculty of Health Sciences, University of Manitoba, Winnipeg, Canada. 3) Department of Food and Human Nutritional Sciences, Faculty of Agricultural and Food Sciences, University of Manitoba, Winnipeg, Canada 4) Institute of Cardiovascular Sciences, St. Boniface Hospital Albrechtsen Research Centre, University of Manitoba, Winnipeg, Canada. 5) Department of Physiology and Pathophysiology, Max Rady College of Medicine, Rady Faculty of Health Sciences, University of Manitoba, Winnipeg, Canada.

*** Corresponding author:**
Dr. Paul Fernyhough,
Professor, Department of Pharmacology & Therapeutics,
Rady Faculty of Health Sciences, University of Manitoba,
Director, Division of Neurodegenerative Disorders,
St. Boniface Hospital Albrechtsen Research Centre,
R4046 – 351 Tache Avenue,
Winnipeg, Manitoba, R2H 2A6, Canada.
E-mail: pfernyhough@sbrc.ca

3.1 Abstract

Objective. Antagonism of the muscarinic acetylcholine type 1 receptor (M_1R) promotes sensory axon repair and is protective in peripheral neuropathy, however, the mechanism remains elusive. We investigated the role of the heat-sensing transient receptor potential melastatin-3 (TRPM3) cation channel in M_1R antagonism-mediated nerve regeneration and explored the potential of TRPM3 activation to facilitate axonal plasticity.

Methods. Dorsal root ganglion (DRG) neurons from adult control or diabetic rats were cultured and treated with TRPM3 agonists (CIM0216, pregnenolone sulfate) and M_1R antagonists pirenzepine (PZ) or muscarinic toxin 7 (MT7). Ca^{2+} transients, mitochondrial respiration, AMP-activated protein kinase (AMPK) expression, and mitochondrial inner membrane potential were analyzed. The effect of M_1R activation or blockade on TRPM3 activity mediated by phosphatidylinositol 4,5-bisphosphate (PIP_2) was studied. Metabolic profiling of DRG neurons and human neuroblastoma SY-SY5Y cells was conducted.

Results. M_1R antagonism induced by PZ or MT7 increased Ca^{2+} influx in DRG neurons and was inhibited by TRPM3 antagonists or in the absence of extracellular Ca^{2+}. TRPM3 agonists elevated Ca^{2+} levels, augmented mitochondrial respiration, AMPK activation and neurite outgrowth. M_1R antagonism stimulated TRPM3 channel activity through inhibition of PIP_2 hydrolysis to activate Ca^{2+}/calmodulin-dependent protein kinase kinase β (CaMKKβ)/AMPK, leading to augmented mitochondrial function and neuronal metabolism. DRG neurons with AAV-mediated shRNA knockdown of TRPM3 exhibited suppressed antimuscarinic drug-induced neurite outgrowth. TRPM3 agonists increased glycolysis and TCA cycle metabolites, indicating enhanced metabolism in DRG neurons and SH-SY5Y cells.

Conclusion. Activation of the TRPM3/CaMKKβ/AMPK pathway promoted collateral sprouting of sensory axons, positioning TRPM3 as a promising therapeutic target for peripheral neuropathy.

Keywords: axonal regeneration; bioenergetics; diabetic neuropathy; GPCR; metabolomics; mitochondria; neuronal metabolism

3.2 Introduction

Axonal plasticity is dependent upon modulation of intracellular Ca^{2+} concentration $[Ca^{2+}]_i$ within the growth cone and is a well-characterized controller of motility [1]. Early work in *Aplysia* and *Xenopus* showed growth cones release quantal packets of acetylcholine (ACh; both spontaneous and evoked) and modulate Ca^{2+}-dependent motility via cholinergic nicotinic (+ve) and muscarinic (-ve) receptors [2-6]. Studies in embryonic sensory neurons further demonstrated that ACh signaling via muscarinic receptors (MR's), and associated mobilization of Ca^{2+} from internal stores, regulates growth cone motility during development [7-10]. It is notable that both adult sensory ganglia and epidermal keratinocytes, synthesize and secrete ACh [11-15]. Indeed, keratinocytes exhibit a rich cholinergic phenotype with expression of choline acetyltransferase (ChAT), acetylcholinesterase (AChE) and a range of muscarinic receptor (MR) subtypes [12; 14; 16]. Adult sensory neurons express a peripheral form of ChAT (pChAT), exhibit ChAT activity, have low AChE activity and express multiple MR sub-types including the muscarinic acetylcholine type 1 receptor (M_1R) [9; 11; 17].

The five subtypes of muscarinic receptor (M1–M5) have been divided into two classes according to their G protein coupling preference [18]. The M1, M3 and M5 subtypes couple to the Gq/G11 G proteins, whereas the M2 and M4 subtypes link to Gi/Go G proteins [19]. M_1R activation of Gq G protein induces phospholipase-Cβ and hydrolysis of phosphoinositides, such as phosphatidylinositol 4,5-bisphosphate (PIP_2), which triggers endoplasmic reticulum (ER)-dependent Ca^{2+} release via D-myo-inositol-1,4,5-triphosphate (IP_3)-mediated opening of IP_3 receptors [19; 20]. A variety of drugs block M_1R activation, including pirenzepine (a selective orthosteric antagonist) and muscarinic toxin 7 (MT7; a specific negative allosteric modulator) [21; 22].

A report from our laboratory demonstrated that selective or specific antagonists of the M_1R enhanced neurite outgrowth in cultured adult dorsal root ganglia (DRG) neurons [23]. In addition, M_1R antagonists improved mitochondrial function, normalized thermal sensitivity, and reversed intraepidermal fiber (IENF) density loss in various rodent models of peripheral neuropathy [23]. Interestingly, antagonizing M_1R resulted in a slow rise in $[Ca^{2+}]_i$ [23] which was associated with the activation of Ca^{2+}/calmodulin-dependent protein kinase kinase β (CaMKKβ) and mobilization of AMP-activated protein kinase (AMPK), which augmented mitochondrial function and enhanced neuroprotection in animal models of diabetic neuropathy and chemotherapy-induced peripheral neuropathy [24; 25]. This work has progressed to human clinical trials where topical antimuscarinic treatment reversed loss of IENF density in the skin and improved clinical signs of neuropathy in persons with type 2 diabetes [26].

Among the ion channels that allow influx of extracellular Ca^{2+} into neurons, the transient receptor potential (TRP) channel family is of particular interest as their activity is triggered both as a direct response to extracellular stimuli and also indirectly via signals from muscarinic receptors [27-29]. The majority of TRP channels open under conditions of low local PIP_2, as happens during canonical G protein-mediated signaling where Gq protein-mediated signaling activates phospholipase Cβ (PLCβ) to trigger hydrolysis of phosphoinositides and suppress PIP_2 levels. A TRP member is the transient receptor potential melastatin 3 (TRPM3), which is functionally expressed in a large subpopulation of sensory neurons and contributes to transduction of thermal stimuli [27; 30; 31]. This Ca^{2+} channel is unusual as it opens when local PIP_2 is high [32; 33] and release of activated G protein subunit βγ is suppressed [34]; as occurs when M_1R activation is blocked by an antagonist. Finally, another interesting feature of TRPM3 biology is

the presence of intracellular binding sites for Ca^{2+} and calmodulin that could combine to act as a scaffold for CaMKKβ activation [35].

In the current study we hypothesized that opening TRPM3 could trigger neurite outgrowth by activating the CaMKKβ/AMPK pathway and mimic the effects of antimuscarinic drugs. To investigate if M_1R antagonist-mediated effects are channeled through TRPM3 activation, our study first focused on observing the Ca^{2+} influx induced by M_1R antagonists. Following this, we examined the Ca^{2+} response specifically attributed to TRPM3 agonists (pregnenolone sulphate (PS) and CIM0216 (CIM) which are selective and specific TRPM3 agonists, respectively [36], aiming to establish a connection between M_1R receptor antagonism and subsequent TRPM3 channel activation. Further to these studies, we assessed whether activation of TRPM3 channels could mobilize signal transduction pathways associated with control of mitochondrial function. Finally, by blocking TRPM3 channels, the pathways downstream of M_1R signaling pathways were analyzed, leading to the conclusion that TRPM3 channels are actively involved in augmenting axonal outgrowth mediated by M_1R antagonists.

3.3 Materials and methods

3.3.1 Adult rodent DRG sensory neuron culture

The Canadian Committee on Animal Care (CCAC) guidelines were carefully followed for all animal protocols. As described previously, intact DRG were isolated and dissociated from adult age matched male control and 3-4-month STZ-induced diabetic Sprague-Dawley rats, wild type C57BL/6 mice and M_1R knock-out (KO) mice (the latter a kind gift from Dr. Jürgen Wess at NIDDK, USA) [37-39]. Type 1 diabetes was induced by injection of STZ (MilliporeSigma Canada Ltd, Oakville, Ontario, Canada) in 0.9% saline after overnight fast at a single dose of 90 mg/kg for rats. Blood glucose levels were confirmed 4 to 7 days later in samples obtained by tail prick and measured using a strip-operated reflectance meter (Alpha TRAK2, Zoetis Canada inc., Kirkland, Quebec, Canada). Our previous studies reveal that neurons isolated from type 1 diabetic rats exhibit key components of the diabetic phenotype and mimicking some aspects of the neurodegenerative process associated with diabetic neuropathy [40; 41]. Neurons were cultured in defined Hams F-12 media in the presence of N2 supplement (0.1 mg/ml transferrin, 20 nM progesterone, 100 μM putrescine, 30 nM sodium selenite, 0.1 mg/ml BSA; MilliporeSigma Canada Ltd, Oakville, Ontario, Canada supplied the additives; Wisent Inc, Saint-Jean-Baptiste, Quebec, Canada provided the culture medium), insulin (MilliporeSigma Canada Ltd, Oakville, Ontario, Canada) and low-dose cocktail of neurotrophic factors (0.1 ng/ml NGF, 1.0 ng/ml GDNF, and 0.1 ng/ml NT-3; all from Peprotech, Cranbury, NJ, USA) [23]. By delivering growth factors, the goal was to mimic the level of neurotrophic support that sensory neurons receive *in vivo*. The enrichment of neurons was accomplished by centrifuging in a 15% BSA (Thermo Fisher Scientific, Carlsbad, California, USA) column [42]. Most of the fibroblasts and Schwann cells were removed during this process, but a minimal number of satellite cells accounted for approximately 5% to

10% of total cells in the final culture (mostly directly associated with sensory neurons). Cells were plated onto poly-D-L-ornithine hydrobromide (MilliporeSigma Canada, Oakville, Ontario, Canada), and laminin-coated 12 mm glass cover slips for neurite outgrowth and microscopy studies, black-96 well clear bottom plates for Ca^{2+} imaging using confocal microscopy, NUNC plastic tissue culture multi-well dishes for immunoblot analysis and custom 24-well plastic dishes for assessing mitochondrial bioenergetics using a Seahorse Biosciences XFe24 Analyser (Laminin, cover slips, and plates from Thermo Fisher Scientific, Carlsbad, California, USA, Seahorse products from Agilent Technologies Inc, Santa Clara, California, USA). In all studies neurons from age matched control rats were cultured in the presence of 10 mM D-glucose (MilliporeSigma Canada Ltd, Oakville, Ontario, Canada) and 0.1 nM insulin and neurons from diabetic rats were maintained in medium containing no insulin and 25 mM D-glucose.

3.3.2 Neuroblastoma SH-SY5Y cell line culture

The human neuroblastoma SH-SY5Y cell line (ATCC CRL-2266, Virginia, USA) was a kind gift from Dr. Jun-Feng Wang, University of Manitoba. The cells were cultured in DMEM/F12 (1:1) media supplemented with heat inactivated 10% FBS (DMEM/F12 and FBS from Thermo Fisher Scientific, Carlsbad, California, USA) and 1X antibiotic antimycotic solution (MilliporeSigma Canada Ltd, Oakville, Ontario, Canada).

3.3.3 AAV-PHP.S mediated knockdown of TRPM3

The DRG neurons were seeded in culture plates and incubated at 37°C with 5% CO2 for 18-20 hours. Custom AAV.PHP.s [43] vectors encoding a scrambled sequence or carrying shRNA to TRPM3 (CGAGACATGGGCCCTCAAATA) under the U6 promoter were generated by Vector

Builder (Chicago, IL, USA), with a final titer exceeding 1x10^12 genome copies per milliliter (GC/ml). The culture medium was removed from the DRG neurons, and neurons were infected with the AAV vector at a multiplicity of infection (MOI) corresponding to 1x10^5 viral particles per neuron. After 8 hours of viral exposure, the medium was replaced with fresh complete culture medium, and cells were again incubated at 37°C in a 5% CO2 incubator overnight. Analysis was performed 24-48 hours post-transduction and levels of transduction were verified based upon GFP expression.

3.3.4 Real-time intracellular Ca^{2+} imaging

For acute measurements, as shown in Figures 3.1 and 3.2, neurons were cultured in 96-well plates (black clear-bottomed; Thermo Fisher Scientific, Carlsbad, California, United States) overnight. The following day or after 48 hours, the cells were washed with HBSS with Ca^{2+} or HBSS without Ca^{2+} and then loaded with 3μM of Ca^{2+}-sensitive dye fluo-4 AM (All from Thermo Fisher Scientific, Carlsbad, California, United States). After 1 hour of incubation, the cells were washed with HBSS again. The temperature of the stage was maintained at 37°C using a heating block. The 96-well plate was then placed in a Zeiss LSM 510 META Confocal microscope with on-stage incubator. Baseline signals were collected (excitation at 494 nm and emission 516 nm; 20× and 100× objective) followed by addition of drugs such as CIM 0216 (Bio-Techne Canada, Toronto, ON, Canada), pregnenolone sulphate (PS), primidone, isosakuranetin, pirenzepine (PZ), muscarine (Millipore Sigma Canada, Oakville, Ontario, Canada) and MT7 (Alomone labs, Jerusalem, Israel). Regions of interest (ROIs) containing individual neuron cell bodies or axons were selected and fluorescence intensities quantified using Zen 2009 software. For calcium measurements at x20 magnification 10-15 ROIs from perikarya/axons per field or well of a 96 well

plate were selected. The graphed data is the average of individual perikaryal or axon ROI signals from 7-10 replicate wells. For x100 imaging, multiple ROIs within the perikaryal or axons were derived from 1-2 neurons. This process was performed in 3-5 wells of a 96 well plate. The data is presented as change in intensity of fluo-4 fluorescence (ΔF/F) and the area under the curve (AUC). The ΔF/F was calculated as ΔF/F= (F-F0)/F0, where F is the fluorescence at a given time and F0 is the baseline fluorescence signal averaged over a 10s period corresponding to the lowest fluorescence signal over the recording period. The data was plotted as the average intensity of perikaryal or axon signal from 3-5 replicate wells. AUC was calculated individually as (S1+S2)/2 ×(t2−t1) where (S1+S2)/2 gives you the average calcium signal between the two time points t1 and t2. Once the individual areas were computed for all time intervals, the average of these areas was taken to represent the total AUC.

3.3.5 Assessment of total neurite outgrowth

Adult rat or mouse neurons grown on glass coverslips were fixed with 2% paraformaldehyde in PBS (pH 7.4) for 15 minutes at room temperature and permeabilized with 0.3% Triton X-100 in PBS for 5 minutes (Products from Thermo Fisher Scientific, Carlsbad, California, USA). Neurons were then incubated in blocking buffer (Roche, Basel, Switzerland) diluted with FBS and 1.0 mM PBS (1:1:3) for 1 hour, then rinsed 3 times with PBS. The primary antibody used was against β-tubulin isotype III (MilliporeSigma Canada, Oakville, Ontario, Canada; 1:1000), which is neuron specific. Plates were incubated at 4°C overnight. The following day, the coverslips were incubated with Cy3-conjugated secondary antibodies (Jackson ImmunoResearch Laboratories, West Grove, Pennsylvania, USA) for 1 hour at room temperature and then mounted and imaged using a Carl Zeiss Axioscope-2 fluorescence microscope equipped with an AxioCam camera. Random images

were captured using Axio-Vision4.8 software. Quantification of total neurite outgrowth was performed by measuring the mean pixel area of captured images using ImageJ software and adjusted for the cell body signal. All values were adjusted for neuronal number. The level of total neurite outgrowth in this culture system has been validated to be similar to collateral sprouting *in vivo* and directly related to arborizing axonal plasticity [44].

3.3.6 Quantitative Western blotting

Cultured sensory neurons derived from rat DRG and SH-SY5Y cells were harvested after treatments in ice-cold RIPA buffer, 1mM PMSF and protease inhibitor cocktail and were stored at − 80 °C [45] (Products from Thermo Fisher Scientific, Carlsbad, California, USA). Protein concentration was measured using the DC protein assay (Bio-Rad, Hercules, CA, USA), and the lysates from the culture were resolved on a 10% sodium dodecyl sulphate–polyacrylamide gel electrophoresis gel [SDS-PAGE; 8% for TRPM3 and 15% for mitochondrial OXPHOS proteins] and electroblotted onto nitrocellulose membrane. The blots were blocked with 2% (for P-AMPK and T-AMPK) and 5% (for TRPM3, TRPM2 and mitochondrial OXPHOS proteins) non-fat dry milk, rinsed in TBS-T and incubated with antibodies to the following proteins: TRPM3 (anti-TRPM3 antibody, ab56171; 1:200, Abcam, Waltham, Massachusetts, USA and anti-TRPM3 extracellular (PA5-77327; 1:200, Thermo Fisher Scientific, Carlsbad, California, USA), anti-TRPM2 antibody (NB110-81601SS; 1:500, Bio-Techne, Toronto, Ontario, Canada), p-AMPK (Thr172; SC3352; 1:1000, Santa Cruz Biotechnology Inc. Dallas, Texas, USA), total-AMPK (T-AMPK; SC25792; 1:1000, Santa Cruz Biotechnology Inc., Dallas, Texas, USA), and mitochondrial OXPHOS cocktail (Oxphos WB-antibody cocktail; 45-8099; 1:1000, Thermo Fisher Scientific, Carlsbad, California, USA). After overnight incubation, the blots were washed

3 times with TBS-T for 10 mins each, followed by addition of secondary antibodies at a dilution of 1:2000 for 1 hour at room temperature. The blots were rinsed, incubated in Western Blotting ClarityTM Western ECL substrate (Bio-rad, Hercules, California, USA), or SignalFire ™ Elite ECL reagent (Cell Signaling, Danvers, Massachusetts, USA) for a few minutes and imaged using a Chemi Doc (Bio-Rad, Hercules, California, USA).

3.3.7 Measurement of mitochondrial respiration

The neuronal bioenergetic function was measured using an XFe24 Analyzer (Agilent Technologies Inc, Santa Clara, California, USA). The XFe24 creates a transient 7-µl chamber in specialized 24-well microplates that allows for oxygen consumption rate (OCR) to be monitored in real time [46]. A change of culture medium to unbuffered DMEM (pH 7.4) supplemented with 1 mM pyruvate and 10 mM D-glucose (for control) 25 mM D-glucose (for diabetic rat-derived cultures) and was made one hour before the assay. OCR was linear in the range of 2,500-5,000 neurons per well. We sequentially injected oligomycin (1 µM), carbonyl cyanidep-trifluorocarbonyl-cyanide methoxyphenyl hydrazone (FCCP) (1 µM), and rotenone (1 µM) plus antimycin A (1 µM) through ports in the Seahorse Flux Pak cartridges [24] (Chemicals from MilliporeSigma, Canada, Oakville, Ontario, Canada). Each loop began with mixing for 3 minutes, was delayed for 2 minutes, and had OCR measured for 3 minutes. This allowed determination of the basal level of oxygen consumption rate (OCR), the amount of oxygen consumption linked to ATP production, the maximal respiration capacity, and the nonmitochondrial oxygen consumption [46; 47]. Afterwards, the cells were suspended in RIPA buffer, PMSF and a cocktail of protease inhibitor. After centrifugation at 14000g for 10 minutes, the lysate was collected, and the DC protein assay was run followed by data analysis normalizing OCR to mg total protein.

3.3.8 Immunofluorescence

Cultured DRG neurons and SH-SY5Y cells were fixed on cover slips with paraformaldehyde (2%). The slides and cover slips were then washed with phosphate buffer saline (PBS) 3 times followed by treatment with 0.03% Tween-20 for 5 minutes to permeabilize the cells. The slides and cover slips were washed again and blocked with blocking buffer diluted with FBS and 1.0 mM PBS (1:1:3). The primary antibody against TRPM3 (rabbit anti-TRPM3 antibody, ab56171; 1:200), p-AMPK (Thr172, p-AMPK; SC3352; 1:1000) and phosphatidylinositol 4,5-bisphosphate monoclonal antibody (2C11 clone anti-PIP2 antibody; MA3-500, 1:200 dilution, Thermo Fisher Scientific, Carlsbad, California, USA) was added for overnight incubation. On the following day, the secondary antibody- goat anti-Mouse, Alexa Fluor™ 488 (A-11029, 1:500 dilution; Thermofisher Scientific, Waltham, Massachusetts, United States) was added and then the slides were mounted using PermaFlour mountant (Thermo Fisher Scientific, Carlsbad, California, USA). For double staining, after the addition of secondary antibody, the cover slips were blocked again followed by addition of the second primary antibody (mouse anti- β tubulin III). After overnight incubation, the second secondary antibody (anti-mouse) was added and the cover slips were mounted on slides using PermaFlour mountant. For each case, one slide was incubated with blocking buffer instead of the primary antibody or secondary antibody as a negative control.

3.3.9 Assessment of mitochondrial membrane potential (MMP) in cultured neurons

To quantify the effect of PS or CIM on MMP, double emission imaging of the JC-1 ratio (590/530 nm) was utilized to determine changes in mitochondrial membrane potential ($\Delta\Psi m$) induced by drugs and in response to acute +/- 200 μM FCCP treatment (to completely depolarize the inner

mitochondrial membrane). Sensory neurons were loaded with 5 μM JC-1 for 20 minutes and then washed with Ham's F12 media in response to pre-treatment for 3 hours of PS and CIM. The excitation wavelength was set at 485 ± 11 nm (for simultaneous aggregate and monomer excitation). The emission wavelength was set at 590 ± 15 nm (aggregate emission) and 530 ± 15 nm (monomer emission). On the Biotek Synergy Neo2 multimode plate reader (Agilent Technologies Inc, Santa Clara, California, USA), the baseline fluorescence followed by addition of FCCP was recorded.

3.3.10 Untargeted metabolomics

Cultured DRG neurons were prepared in 6-well plates and allocated into two experimental groups: control and CIM-treated. Neurons were incubated for 24 hours before sample collection. For untargeted metabolomics, cell pellets were resuspended in 1 mL of ice-cold 80% methanol, followed by vigorous vortexing for one minute. The samples were then subjected to sonication in an Ultrasonic Bath (Branson Ultrasonics, Danbury, Connecticut, USA) filled with ice-cold water for 15 minutes to ensure complete cell lysis and efficient metabolite extraction. Post-sonication, the samples were centrifuged at 12,000 RPM for 15 minutes at 4°C to separate the supernatant from the cell debris. The clear supernatant was transferred to clean tubes and dried under a gentle nitrogen flow to evaporate the solvent. The dried residues were reconstituted in 100 μL of methanol: water (4:1, v/v), vortexed for 2 minutes, and centrifuged to remove any insoluble material. The final clear supernatant was transferred into 200 μL micro vial inserts for subsequent analysis. The metabolomic analysis was performed using a Rapid Resolution LC system (1260 Infinity, Agilent Technologies, Santa Clara, California, USA) coupled to a 6538 UHD Accurate QTOF mass spectrometer (Agilent Technologies, Santa Clara, California, USA) with dual

electrospray ionization (ESI) in both positive (+) and negative (−) modes. Chromatographic separation was achieved using a ZORBAX SB-Aq column (4.6 x 100 mm, 1.8 µm, Agilent) maintained at 55°C. The mobile phases consisted of water (A) and acetonitrile (B), both containing 0.1% formic acid (All from Thermo Fisher Scientific, Carlsbad, California, USA). The flow rate was set at 0.45 mL/min with the following gradient: 2% B from 0-1 min, increased linearly to 98% B over 11 minutes, maintained at 98% B for 2 minutes, decreased back to 2% B over 4 minutes, maintained at 2% B for 1 minute, followed by a 1-minute post-run. To minimize carryover, the needle was washed for 15 seconds with water: acetonitrile (1:1, v/v). 4µl of each extract were injected for analysis. Mass spectrometry was conducted with the following parameters: capillary voltage at 4000V, fragmentor voltage at 175V, skimmer voltage at 50V, and Oct 1 RF Vpp at 750V. Nitrogen was used as the drying gas at a flow rate of 11 L/min and a gas temperature of 300°C, while the nebulizer was set to 45 psig (pressure unit). A full-range mass scan from 50–3000 m/z was performed. Data acquisition and analysis were executed using MassHunter Workstation version 10 (Agilent Technologies, Santa Clara, California, USA). Metabolite identification was performed utilizing the integrated Metlin database, encompassing over 200,000 known endogenous compounds. This methodological approach ensured comprehensive extraction, identification, and analysis of metabolites from DRG neurons, facilitating a detailed untargeted metabolomic profile.

3.3.11 Targeted metabolomics

Standard solution preparation for GC–MS/MS analysis involved preparing stock solutions of fumarate, malate, lactate, and α-ketoglutarate in methanol, while all other compounds were prepared in water at 1 mg/ml. A cocktail solution was made by combining all the stock solutions.

Working standard solutions were obtained by serial dilutions of the cocktail solution with methanol (Supplementary Table 3.S1). Subsequently, 30 µL of BSTFA with 1% TMCS was added at 37°C for 30 minutes. Then 60µL was transferred into a micro-vial insert and kept at -80°C until analysis. The SH-SY5Y cells were treated upon reaching 90% confluency with 1µm CIM for 1 hour and 3 hours and CIM (1 µm), primidone (10 µm) or isosakuranetin (10µm) for 3 hours post 4 hours starvation. Cell culture media was removed, and cells were washed with 2mL of PBS. Subsequently, 500 µL of 75% methanol-MTBE (9:1, v/v) was added containing 1,2 $^{13}C_2$ myristic acid at 5µg/mL. Then cells were detached from plates and transferred to 1.5mL centrifuge tubes. Cell lysis was performed using a X3 freeze and thaw cycle and centrifuged at 12000rpm for 10 minutes at 4°C. The supernatant was dried under gentle flow of nitrogen and stored at -80°C. The GC-MS analysis was performed using a 7890B gas chromatograph (Agilent Technologies, Santa Clara, California, USA) with 7000D Triple-quadrupole mass spectrometer (Agilent Technologies), equipped with 7693 Autosampler (Agilent Technologies, Santa Clara, California, USA). The column used was an HP-5MS (0.25mm, 30m, 0.25µm, Agilent Technologies, Santa Clara, California, USA), with a split ratio of 18:1 and injection volume of 1µL. The GC oven temperature initially was set at 60°C, maintained for 1 minute, ramped up to 100°C at 30°C/ min, and ramped up to 300°C at 20°C/min and maintained for 2 minutes. Carrier gas was helium (99.999% purity), with a flow rate of 1.2mL/ min and nitrogen (99.999% purity) were used as the collision cell gas. A period of 3.8 min for solvent delay was employed for each sample run and for mass range of 50-750 m/z. Source temperature was set at 300°C. For a targeted study with CIM, primidone and isosakuranetin, 4 µg of each analyte was spiked into the cell matrix as a reference, and metabolite concentrations were quantified directly from these standardized readings. Whereas study analysing the effect of CIM on SH-SY5Y metabolism time dependently, calibration curve was generated to

evaluate the metabolite concentrations. A full scan mode was used for determination of retention time for each analyte (Supplementary Table 3.S2). The software used for data analysis was Mass Professional Profiler (MPP, 15.1).

3.3.12 Statistical analysis

We used one rat or mouse (age-matched normal or diabetic) for each neuronal culture experiment, and 300,000 SH-SY5Y cells per well in 6 well plate and such experiments were independently repeated at least 2–3 times. In dose-response experiments and in comparisons of treatment groups to a single control group, data are expressed as mean ± SEM and analyzed by one-way ANOVA with Dunnett's test for *post hoc* comparisons. For comparisons between multiple treatment groups, Tukey's *post hoc* test was used. The statistical analysis was performed using GraphPad Prism software. For the untargeted metabolomics study in DRG neurons, Bonferroni FWER analysis was used using t-Test for statistical analysis (Supplementary Figure 3.S9). For the targeted metabolomics study, Benjamini-Hochberg statistical analysis was performed using one-way ANOVA with $p < 0.05$ (Figure 3.8) and one-way ANOVA, $p < 0.05$, Bonferroni FWER for statistical analysis in Supplementary Figure 3.S10.

3.4 Results

3.4.1 TRPM3 agonists induce Ca^{2+} influx in adult rat DRG sensory neurons

Confirming previous studies [31; 36] TRPM3 agonists induced a significant increase in intracellular Ca^{2+} levels in cultured adult rat DRG sensory neurons (Figure 3.1 and Supplementary Figure 3.S1). Both TRPM3 agonists CIM (25 μM) and PS (50 μM) elevated intracellular Ca^{2+} in the presence of Ca^{2+}-containing media, but not in Ca^{2+}-free media, indicating that the source of Ca^{2+} influx was extracellular. At this concentration of CIM there is limited interaction with other TRPM type channels, although some blocking effect may be expected at TRPM2 and TRPM5 [36]. PS at concentrations up to 50 μM was quite selective for TRPM3 with no current generation observed in TRPM3 KO DRG neuron cultures [31]. These relatively high concentrations were used to enable effective mixing of drug for acute Ca^{2+} measurements. In all subsequent longer-term treatment studies, these agonists are used at 1 μM concentration. Approximately 50-60% of the DRG sensory neurons responded to the TRPM3 agonists with increased intracellular Ca^{2+} levels and suggesting differential TRPM3 expression in the cultured neurons in support of previous studies [31; 48]. The specificity of the TRPM3-induced Ca^{2+} influx was further confirmed using TRPM3 inhibitors, primidone and isosakuranetin (both at 100 μM) [49; 50] (Figure 3.1H-L and Supplementary Figure 3.S2). These relatively high concentrations of antagonists were required for rapid mixing and for induction of acute blockade of Ca^{2+} transients. Generally, the optimal concentrations are in the range of 1-10 μM where both drugs show good selectivity for TRPM3 [49-51]. At 100 μM isosakuranetin would be expected to activate TRPA1 [51]. For the consequent longer-term treatment studies, we use 10 μM primidone which has no effect on TRPV1, TRPM8 or TRPA1 [49-51].

3.4.2 TRPM3 activation leads to Ca^{2+} influx in cell body and axons of sensory neurons

A significant increase in $[Ca^{2+}]_i$ in both the axonal and cell body regions of DRG sensory neurons was observed in response to TRPM3 agonist CIM (25 μM) (Figure 3.2A-C). This increase was only evident in the presence of extracellular Ca^{2+}. The elevation in Ca^{2+} levels was comparable between the axons and cell bodies.

3.4.3 M_1R blockade induced a slow rise in intracellular Ca^{2+} in the axons of DRG sensory neurons

M_1R agonists, such as ACh, typically induce a rapid increase in intracellular Ca^{2+} levels. However, in the presence of extracellular Ca^{2+}, M_1R antagonists, surprisingly induced a slow, time-dependent increase in Ca^{2+} in DRG neurons (Figure 3.2D-L). Pirenzepine (PZ; at 30 μM) and MT7 (100 nM), selective and specific antagonists at M_1R, respectively, led to a significant rise in intracellular Ca^{2+}. PZ is only selective for M_1R and at 30 μM it would be expected to also bind to the M2-M5 muscarinic receptors [52], however, Ca^{2+} transients in response to PZ were absent in DRG neuron cultures from M_1R KO mice (Supplementary Figure 3.S3). This high concentration of PZ was chosen to ensure rapid mixing for these acute studies. In all future studies we use 1 μM PZ where there is more restricted binding to M2-M5 muscarinic receptors [52]. We can also confirm that sensory neurons derived from wild-type vs M_1R KO mice exhibited similar densities and viabilities as previously demonstrated [23].

3.4.4 M_1R-mediated increase in intracellular Ca^{2+} is TRPM3 dependent

The selective TRPM3 channel inhibitors, primidone and isosakuranetin (both at 100 μM), completely blocked the M_1R antagonist-mediated Ca^{2+} influx (Figure 3.2J-R). To further validate

the interaction between M_1R and TRPM3, we again compared DRG cultures derived from wild-type vs M_1R KO mice [53]. In DRG sensory neurons from wild-type mice, a significant increase in Ca^{2+} influx was observed upon CIM treatment, whereas this response was markedly attenuated in cultures derived from M_1R KO mice (Figure 3.3A-C). It should be noted that we are studying relative changes in intracellular Ca^{2+} through use of the fluo-4 dye, this approach is not ratiometric and does not permit the basal/resting levels or absolute concentrations of Ca^{2+} to be compared between cultures derived from wild-type and M_1R KO mice. Thus, it is quite feasible that basal levels of Ca^{2+} are higher in the M_1R KO cultures due to suppression of PLC activation and raised PIP_2 levels. M_1R agonism lowers PIP_2 levels [32; 33], and thus a build-up in PIP_2 would be expected to activate TRPM3 channels. Thus, we treated with the broad-spectrum muscarinic agonist muscarine (at 1 μM) and observed a decrease in PIP_2 level in DRG neurons (Figure 3.3D-G), while the M_1R antagonist PZ caused an increase in PIP_2 levels in DRG neurons.

3.4.5 TRPM3 opening activates AMPK, elevates mitochondrial function, and enhances neurite outgrowth

We hypothesized that Ca^{2+} entry via TRPM3 could activate the AMPK pathway and enhance neuronal bioenergetics, a key target of antimuscarinic drug action at M_1R [23; 25]. Activation of TRPM3 channels using specific agonists CIM and PS (both at 1 μM) in DRG neurons resulted in a two-fold increase in phosphorylation of AMPK at Thr172 (primary activation site) (Figure 3.4). Our previous work has demonstrated that cultured DRG neurons derived from 3-4 month streptozotocin (STZ)-induced type 1 diabetic rats exhibit neurodegenerative features with evidence of oxidative stress, impaired AMPK activation and suppressed axonal outgrowth [40; 41]. Therefore, we studied role of TRPM3 activation in AMPK signaling in DRG cultures derived from

aged-matched control or diabetic rats. PS and CIM were able to activate AMPK in control and diabetic cultures (Figure 3.4). We used AAV delivery of shRNA to knockdown TRPM3. The successful knockdown of TRPM3 was validated through Western blotting and immunocytochemistry, both of which showed a significant reduction in TRPM3 protein levels (Supplementary Figure 3.S4). Importantly, the expression of TRPM2 remained unchanged, indicating the specificity of the shRNA for TRPM3. The neurotropic AAV.PHP.s [43] delivered shRNA to TRPM3 and blocked the CIM-induced elevation in p-AMPK (Figure 3.4J-K). Both TRPM3 agonists at 1 μM also increased mitochondrial function, as measured by the oxygen consumption rate (OCR) (Figure 3.5 and Supplementary Figure 3.S5). Application of CIM led to increased maximal respiration and spare respiratory capacity in DRG cultures derived from both control and diabetic animals, indicating enhanced mitochondrial capacity to meet energy demands, particularly under stress conditions (Figure 3.5C, E, I and K). Similar results were observed with PS (Supplementary Figure 3.S5). This observation is consistent with the role of AMPK as a key regulator of mitochondrial biogenesis and function [54]. CIM and PS also elevated the inner mitochondrial membrane potential in cultured neurons as detected using JC-1 dye (Figure 3.5M-Q). Further investigation into mitochondrial activity revealed that the expression of components of the respiratory chain, including oxidative phosphorylation (OXPHOS) proteins, significantly increased in the presence of agonists CIM and PS (Figure 3.5R-W). We also performed studies in human neuroblastoma SH-SY5Y cells in order to prepare for metabolomic studies (see later). SH-SY5Y cells exhibited relatively high expression of TRPM3 and responded to CIM with Ca^{2+} transients (Supplementary Figure 3.S6). Finally, we also confirmed in human neuroblastoma SH-SY5Y cells that CIM and PS could activate AMPK, elevate mitochondrial function, and enhance respiratory chain protein expression (Supplementary Figures 3.S7-8).

3.4.6 Pirenzepine elevates neurite outgrowth through activation of TRPM3 channels

The activation of TRPM3 channels by 1 μM CIM or PS also stimulated neurite outgrowth in DRG neurons derived from both control and diabetic animals (Figure 3.6A-C and F). As discussed above, M_1R antagonism mediated elevation of $[Ca^{2+}]_i$ is transmitted through opening of TRPM3 channels. To prove the mechanistic role of TRPM3 in mediating M_1R antagonism, we used AAV-PHP.s to deliver shRNA to knockdown TRPM3 in DRG neuron cultures derived from diabetic rats. PZ (1 μM) treatment led to a significant increase in neurite outgrowth and TRPM3 channel knockdown completely blocked this effect (Figure 3.6D-E). To support this study, we used the selective inhibitor of TRPM3 channel, primidone (10 μM), which also resulted in a complete blockage of PZ-mediated neurite outgrowth in DRG neurons (Figure 3.6H). In Figure 3.6G we show that TRPM3 knockdown also inhibited CIM-induced neurite outgrowth. This demonstrates that TRPM3 channel activation can replicate the effects of M_1R antagonism to drive axonal regeneration in cultured adult rat sensory neurons.

3.4.7 TRPM3 channels activate AMPK via the CaMKKβ pathway

To investigate whether the observed effects of TRPM3 activation are mediated through the CaMKKβ pathway, we used the CaMKKβ selective inhibitor STO-609 and assessed the downstream effects on AMPK activation and neurite outgrowth in the presence of CIM and PS. No increase in AMPK activation or neurite outgrowth was observed when STO-609 (1 μM) was applied, indicating that TRPM3 activation involves the CaMKKβ pathway to augment mitochondrial function and neurite outgrowth (Figure 3.7).

3.4.8 Untargeted and targeted metabolomics reveals TRPM3 activation leads to enhanced neuronal metabolism

To comprehensively understand the effects of TRPM3 activation on neuronal metabolism, we conducted untargeted metabolomics on DRG cultured neurons treated with CIM. Among the 497 detected metabolites, 97 were significantly enriched, as determined by t-test analysis ($p < 0.05$). Principal component analysis (PCA) revealed a clear separation between the control and CIM-treated groups, indicating distinct metabolic profiles. Several metabolic pathways exhibited significant alterations following CIM treatment. Specifically, the arachidonic acid and galactose pathways demonstrated reduced activity. Similarly, the phospholipid pathway and lactose metabolism showed decreased activity, whereas ubiquinone levels increased. These findings suggest an overall impact on mitochondrial function and glycolysis. These pathway alterations are visualized in the heat map provided in Supplementary Figure 3.S9. To further investigate the specific effects on the tricarboxylic acid (TCA) cycle and glycolysis, we performed targeted metabolomics using the SH-SY5Y cell line due to limitations in DRG cell numbers. We analyzed three experimental groups: control, 1-hour CIM treatment, and 3-hour CIM treatment. Partial least square (PLS) indicated distinct metabolic profiles among these groups, as further illustrated by the heat map (Supplementary Figure 3.S10A). Metabolites involved in the TCA cycle and glycolysis, such as glucose, pyruvate, and citrate, showed increased levels after 1 hour of treatment, with a more pronounced increase observed after 3 hours (Supplementary Figure 3.S10C). To verify that TRPM3 activation drives this metabolic enhancement, SH-SY5Y cells were co-treated with CIM (1 μM) and the TRPM3 inhibitors primidone and isosakuranetin (both at 10 μM) (Figure 3.8). These inhibitors completely blocked the CIM-induced increases in glycolysis and TCA cycle

metabolites (Figure 3.8C). These results demonstrate that TRPM3 activation significantly upregulates neuronal metabolism, particularly affecting the TCA cycle and glycolysis pathways.

3.5 Discussion

3.5.1 Ca^{2+} response of DRG neurons to direct activation of TRPM3

We investigated the intracellular Ca^{2+} response of DRG neurons upon direct activation of TRPM3 channels using PS and CIM (Figure 3.1 and Supplementary Figure 3.S1). Employing live Ca^{2+} confocal imaging with fluo-4 AM dye, we observed a significant Ca^{2+} influx in approximately 50-60% of the neurons, in line with previous work [36]. Our time-course analysis revealed that the peak Ca^{2+} influx occurred within 10-15 seconds post-application of either PS or CIM. This rapid activation of TRPM3 channels corroborates previous findings [31; 36], including studies in freshly isolated human DRG neurons and human stem cell-derived sensory neurons [55]. CIM is particularly noteworthy as it uniquely opens distinct cation permeation pathways and represents one of the most potent TRPM3 activators identified to date [36]. Our observations indicated a rapid, transient influx of Ca^{2+} triggered by PS, characterized by an initial sharp increase, followed by a brief period at its peak, and subsequently stabilizing at a slightly reduced but elevated level (Supplementary Figure 3.S1B). In contrast, the Ca^{2+} influx induced by CIM was sustained, maintaining elevated levels over 3-4 min (Figure 3.1B). This differential response underscores distinct kinetics of TRPM3 activation by PS and CIM. To verify that TRPM3 mediates Ca^{2+} influx, we utilized isosakuranetin and primidone, which are well characterized selective inhibitors of TRPM3. Previous studies demonstrate isosakuranetin (10 μM) and primidone (10 μM) inhibit TRPM3-evoked Ca^{2+} responses [49-51]. In our study, pre-treatment with isosakuranetin (100 μM) or primidone (100 μM) completely abolished the Ca^{2+} influx induced by CIM and PS (Figure 3.1 and Supplementary Figure 3.S2). The use of higher concentrations was selected since prior studies indicated that pharmacological inhibition was reversible.

3.5.2 PZ and MT7 induce a relatively slow rise in intracellular Ca^{2+}

Our study demonstrates that PZ and MT7 induce a relatively slow rise in intracellular Ca^{2+} levels in the axons of DRG neurons. Activation of M_1R by agonists, such as ACh, typically results in a marked increase in intracellular Ca^{2+} levels [56]. However, while M_1R antagonists, such as PZ, acutely block muscarine-induced ER Ca^{2+} responses over a 10-20 second period, longer-term undefined mechanisms contribute to a delayed increase in Ca^{2+} levels [23]. Treatment with PZ (30 μM) or MT7 (100 nM) increased axonal intracellular Ca^{2+} levels after 5-10 minutes (Figure 3.2). Muscarinic receptor activation regulates PIP_2 levels, with muscarinic activation decreasing PIP_2 levels in HEK293 cells and oocytes over-expressing TRPM3 [32; 33]. Our observations support these findings, noting a significant increase in PIP_2 levels after 1-2 min of M_1R antagonism mediated by PZ or MT7 (Figure 3.3D-G). This increase in PIP_2 is crucial for the regulation of TRPM3 channel activity and subsequent Ca^{2+} dynamics, consistent with demonstration that PIP_2 can directly activate TRPM3 channels [32; 33]. To understand the mechanism behind the M_1R-mediated slow Ca^{2+} uptake via TRPM3, we employed a TRPM3-selective inhibitor followed by PZ/MT7 treatment. This approach resulted in no time-dependent Ca^{2+} uptake (Figure 3.2M-R).

It should be noted that treatment with PZ or MT7 should lead to a complete blockade of G protein activation at M_1R and thereby eliminating the potential inhibitory effect of βγ G protein signaling on TRPM3 channel opening in this culture system [34; 57]. This suppression of βγ G protein signaling could combine with raised PIP_2 levels to maximally activate TRPM3. Future studies could test this hypothesis by directly blocking PLC activation using pharmacological agents or down-regulation of PLC β expression. However, a notable limitation is that U73122, the most commonly used PLC inhibitor, directly modulates TRPM channels [58].

M_1R signaling and subsequent interaction with downstream signaling proteins is critical for prolonged cellular responses [59; 60]. This complex signaling process may explain, in part, why the axonal Ca^{2+} response peaked around 16-18 min and then decreased to baseline by 26-28 min (Figure 3.2D-I). Following TRPM3 activation, the Ca^{2+}/calmodulin complex activates the Ca^{2+}-dependent phosphorylase calcineurin, which dephosphorylates Elk-1, and reduces c-Fos expression to down-regulate TRPM3 expression [61]. This negative feedback mechanism that regulates TRPM3-induced gene transcription may be responsible for the bell-shaped Ca^{2+} response curve and presumably maintains cellular Ca^{2+} homeostasis [61].

3.5.3 Novel activation of AMPK via TRPM3

We have demonstrated for the first time that the activation of TRPM3 channels can lead to the activation of AMPK in DRG neurons. A previous study in clear cell renal carcinoma cells did uncover a link between TRPM3 activation and stimulation of the CaMKKβ/AMPK pathway and control of autophagy [62]. CIM and PS induced phosphorylation of AMPK at 3 and 6 hour post-treatment in DRG neurons (Figure 3.4), lagging behind the observed Ca^{2+} influx following TRPM3 activation at 10-20 minutes. Treatment with STO-609, a selective inhibitor of CaMKK, prior to CIM and PS in DRG neurons, reduced P-AMPK activation, indicating that the calmodulin-dependent process is crucial for sustained AMPK activity (Figure 3.7). The slow kinetics of AMPK activation suggests the involvement of a complex mechanism, likely mediated by Ca^{2+}-dependent binding of calmodulin to TRPM3 and subsequent mobilization of CaMKKβ, which activates AMPK [63; 64]. Calmodulin interacts with at least 5 binding sites with varying affinities within the intracellular domain of the N-terminus of TRPM3, co-operativity between these sites may lead to a complex multilevel modulation of TRPM3 downstream signaling [65]. To further confirm

the effect of TRPM3 activation on AMPK, we employed SH-SY5Y cells. Our findings are consistent with those of Naznin *et al* [66], who reported an elevation of P-AMPK within 1 hour of PZ and MT7 treatment in SH-SY5Y cells (Supplementary Figure 3.S7).

PS induced an increase in P-AMPK at 6 hours in control DRG neurons whereas in diabetic DRG neurons, this effect was seen at 3 hours (Figure 3.4). Similarly, CIM induced P-AMPK activation within 3 hours in diabetic DRG neurons. Both PS and CIM also result in increased total AMPK (T-AMPK) levels at 24 hours in DRG neurons from both control and diabetic models. In diabetes, chronic hyperglycemia and oxidative stress typically downregulate AMPK activity, impairing energy metabolism and exacerbating metabolic dysfunctions [24]. Additionally, the overall increase in T-AMPK appears be a compensatory mechanism to meet higher metabolic demands in diabetic neurons [67].

3.5.4 TRPM3 activation augmented mitochondrial function

In our study, we demonstrated that both PS and CIM significantly enhance mitochondrial function in DRG neurons, primarily through mechanisms involving Ca^{2+} dynamics and metabolic regulation. This finding aligns with existing literature that underscores the pivotal role of mitochondrial Ca^{2+} in regulating cellular metabolism. Mitochondria in DRG neurons are strategically positioned near the plasma membrane, facilitating efficient buffering of Ca^{2+} entering through channels such as TRPM3. Notably, TRPM3 activation induces a more pronounced Ca^{2+} influx compared to depolarization-induced pathways, including voltage-gated Ca^{2+} channels (VGCC's) [68]. Mitochondria can buffer up to 40% of this Ca^{2+} load, which is crucial for maintaining cytosolic Ca^{2+} homeostasis and supporting the high energy demands of neurons. Mitochondrial Ca^{2+} uptake plays a key role in modulating intracellular Ca^{2+} signaling, contributing

to delayed cytosolic Ca^{2+} recovery. This delay results from the gradual release of sequestered Ca^{2+} back into the cytosol, prolonging Ca^{2+} dependent signaling and influencing various cellular functions. Prolonged Ca^{2+} signaling enhances ATP production by stimulating key enzymes within the TCA cycle, such as pyruvate dehydrogenase (PDH), isocitrate dehydrogenase (IDH), and α-ketoglutarate dehydrogenase (α-KGDH). These enzymes enhance the throughput of the TCA cycle, boosting ATP production, which is essential for meeting the high metabolic demands of neurons, particularly in maintaining elevated metabolic activity [69]. Similarly, our study also highlights that TRPM3 activation significantly increased OXPHOS protein expression in DRG neurons and the SH-SY5Y cell line (Figure 3.5 and Supplementary Figure 3.S8), driving heightened metabolic activity, likely due to the delayed Ca^{2+} release following TRPM3 activation. Although PS had a subtle effect on P-AMPK activation, it exhibited increased mitochondrial activity through enhanced basal respiration (Supplementary Figure 3.S5). CIM markedly enhanced basal respiration in both control and diabetic DRG neurons, suggesting its potential to improve mitochondrial function under varying physiological conditions (Figure 3.5).

Additionally, the study demonstrated that PS and CIM elevated mitochondrial membrane potential (MMP), which is crucial for maintaining mitochondrial energy homeostasis (Figure 3.5). MMP is essential for driving ATP production through oxidative phosphorylation, and an elevated MMP indicates highly energized mitochondrial membranes. Enhanced MMP, coupled with improved basal respiration, signifies greater mitochondrial efficiency, which is vital for supporting the metabolic demands of neurons.

3.5.5 Metabolomics data support TRPM3 as a major stimulator of neuronal metabolism

The impact of TRPM3 activation by CIM on the kinetics of glycolytic and TCA pathways in neurons has not been previously described. Therefore, we performed a joint untargeted and targeted LC/MS-MS-based metabolomics screen to investigate these pathways. Our findings revealed a significant increase in ubiquinone levels following CIM treatment in DRG neurons. The specific increase in ubiquinone (coenzyme Q10) levels is significant, given its crucial role in mitochondrial electron transport and ATP synthesis [70]. Additionally, we observed a decrease in galactose metabolism and lactic acid levels, along with a reduction in arachidonic acid metabolism (Supplementary Figure 3.S9). Galactose metabolism is essential for providing energy and structural components for neuronal cells. A decrease in galactose metabolism, as observed in our study, suggests a metabolic shift away from glycolytic pathways towards more efficient energy production mechanisms [71]. The reduction in lactic acid levels supports this shift, indicating a decrease in anaerobic glycolysis. Anaerobic glycolysis is often upregulated in hypoxic or dysfunctional neuronal environments [72]. This shift from lactic acid production to other pathways suggests a more efficient use of glucose, thereby reducing the lactate burden on cells and lowering the risk of lactic acidosis, a condition detrimental to neuronal health [73]. Furthermore, the decrease in arachidonic acid metabolism suggests reduced pro-inflammatory signaling. Arachidonic acid is a precursor for inflammatory mediators, and its reduction could mitigate neuroinflammatory responses, promoting neuronal survival and function [74].

CIM treatment led to an upregulation of key TCA cycle metabolites such as citrate, isocitrate, and pyruvate in SH-SY5Y cells (Supplementary Figure 3.S10). The TCA cycle is fundamental for generating reducing equivalents (NADH, FADH2) used in oxidative phosphorylation to produce ATP [75]. Citrate and isocitrate are not only critical for energy production but also for the synthesis of fatty acids and cholesterol, which are vital components of

neuronal membranes [76]. Our findings suggest that TRPM3 activation could potentially overcome metabolic deficits observed in diabetic neuropathy by enhancing mitochondrial function and metabolic efficiency. In diabetes, metabolism is impaired due to a combination of insulin resistance, hyperglycemia, and mitochondrial dysfunction. This results in reduced TCA cycle activity and a decrease in ATP production, leading to impaired neuronal function and survival [77]. TRPM3 activation appears to promote a feedback loop between the mitochondria and the TCA cycle, providing substrates to the mitochondria, thereby permitting high energization of the mitochondrial membrane and ATP synthesis. Interestingly, when the effects of CIM treatment were abolished by co-treatment with primidone or isosakuranetin, TRPM3 antagonists, the upregulation of TCA cycle metabolites and mitochondrial function was completely mitigated. This indicates that the observed metabolic enhancements are directly mediated through TRPM3 activation and its downstream effects. These findings reinforce the hypothesis that TRPM3 plays a central role in regulating neuronal metabolic resilience by restoring TCA cycle activity and mitochondrial efficiency.

3.5.6 Elevated axonal outgrowth follows activation of TRPM3 and mobilization of the CaMKKβ/AMPK pathway

The present findings demonstrate for the first time that the activation of the TRPM3 channel significantly impacts the structure of DRG neurons. This effect of TRPM3 activation is mediated primarily via neuronal TRPM3 channels since there is no evidence of TRPM3 expression or function in Schwann cells or satellite cells [31; 48; 78]. Activation of TRPM3 enhances mitochondrial function and metabolism within these neurons, as previously discussed. This enhancement is particularly important due to the critical role of ATP in supporting growth cone

motility and axonal construction via requirement for actin treadmilling [79]. ATP serves as a vital energy source for various cellular processes, including the polymerization of cytoskeletal components necessary for axonal elongation and the trafficking of growth-promoting molecules [80]. Our prior research has demonstrated that muscarinic antagonist-induced neurite outgrowth occurs, in part, through the blockade of ACh-dependent constraint of extracellular signal-regulated kinase 1/2 (ERK1/2), resulting in the phosphorylation of the nuclear effector cyclic AMP response element-binding protein (CREB) [81]. The interplay between TRPM3 activation and the ERK/ATF3 pathway could provide a synergistic mechanism promoting axonal outgrowth and regeneration. The significance of TRPM3 in sensory neuron function is further emphasized by Vriens *et al* [31] who demonstrated that TRPM3 knockout (KO) mice exhibited a pronounced loss of thermal sensation. However, in this instance the sensory deficit observed in TRPM3 KO mice could not be attributed to loss of sensory innervation given a previous study in TRPM3, TRPV1, TRPA1 triple KO mice where histological analysis did not reveal any significant difference vs wild type in the nerve bundles innervating the hindpaw skin [82].

At present our *in vitro* and *in vivo* data are limited to demonstrating repair and/or enhancement of collatoral sprouting of sensory fibers in the skin. It remains unknown if this muscarinic signaling pathway via TRPM3 could also contribute to nerve fiber regeneration. Pathways such as the phosphatase and tensin homolog deleted on chromosome 10 (PTEN) pathway that inhibit nerve regeneration via, in part, suppression of PI3-K/Akt signaling [83] would appear to operate in isolation from the M_1R/TRPM3/AMPK axis described herein. Interestingly, the Rho/Rock pathway, a known negative regulator of axon regeneration [84], is activated by agonist action at M_1R leading to augmentation of tubulin depolymerization. In our previous work we revealed that antagonism of M_1R could enhance tubulin polymerization, possibly via inhibition

of Rho/Rock signaling [81]. Thus, it is feasible that M_1R blockade and suppression of G protein signaling could enhance axonal regeneration while the activation of TRPM3 and subsequent AMPK mobilization could elevate collateral sprouting via augmentation of mitochondrial function.

3.5.7 Limitations of this study

Despite the promising findings, several limitations need to be addressed in this study. First, while the *in vitro* model provided useful insights, the complexity of *in vivo* environments and their potential effects on TRPM3 activity and axon sprouting and nerve regeneration remain unexplored. Animal models would be crucial to confirm the translational value of TRPM3 activation under actual neuropathic conditions. Additionally, studies in diabetic neuropathy animal models would establish if TRPM3 activation did exacerbate any pain phenotype (as discussed below). Furthermore, while our study has established the role of the TRPM3/CaMKKβ/AMPK signaling pathway in axonal sprouting, other pathways or interacting proteins could also play significant roles in this process (see discussion above relating to Rho/Rock and PTEN signaling). Finally, while Ca^{2+} influx can activate AMPK and then augment mitochondrial function it is feasible the rise of intracellular Ca^{2+} could also be buffered by mitochondria and effect bioenergetics directly (via modulation of Ca^{2+}-dependent enzymes in the mitochondrial matrix) [85]. Wang et al show that approximately 40% of the Ca^{2+} entering via TRPM3 can be localized to the mitochondria with PS inducing a significant mitochondrial Ca^{2+} transient in cultured DRG neurons [68]. Thus, our future studies should include direct imaging of Ca^{2+} transients in mitochondria in response to M_1R antagonism and TRPM3 agonism and whether it differs in control vs diabetic neurons. In addition, future intracellular Ca^{2+} studies would benefit from the use of a ratiometric approach, e.g. using

fura-2AM, in order to clearly delineate the impact of M_1R loss or blockade on steady state and transient changes in Ca^{2+} regulated by TRPM3 function. Such an approach would also permit a more accurate comparison between Ca^{2+} transients in control vs diabetic cultures. It remains unknown in the current study if TRPM3 activation and subsequent Ca^{2+} influx is altered in diabetic neurons. Previous work in cultured neurons derived from type 1 and type 2 diabetic rodents revealed raised resting intracellular Ca^{2+} levels, in part, due to impaired loading into the ER [86; 87]. Thus, one might expect a reduced ability of TRPM3 opening to further augment AMPK activity, however, our data in Figure 3.4 did not show any significant differences for this endpoint in control vs diabetic neurons treated with PS or CIM.

3.6 Conclusions

Our findings suggest that TRPM3 activation could be a strategic intervention for reversing distal nerve fiber loss observed in diabetic neuropathy, potentially driving nerve repair and regeneration. The clinical success of muscarinic receptor antagonists, such as oxybutynin, for treatment of diabetic neuropathy highlights the advantages of topical delivery methods [26]. Oxybutynin's shift from oral to topical formulations for overactive bladder demonstrated significant benefits by bypassing first-pass metabolism, reducing side effect-related metabolites, and maintaining therapeutic levels of the parent compound [26]. Similarly, topical pirenzepine effectively treated peripheral neuropathy in diabetic mice [23]. These examples suggest that TRPM3 agonists could be similarly applied topically for diabetic neuropathy. One concern, of course, would be that activation of TRPM3 while enhancing sensory fiber outgrowth could also elevate responses to thermal stimuli. Since approximately 15-20% of persons with diabetic neuropathy exhibit a variety of pain phenotypes [88] this could become a major factor limiting any therapy. However, studies

in animal models [23] and now in humans [26] demonstrate that long term blockade of M_1R does reduce pain and so repairing the peripheral projections of the nervous system could suppress any aberrant sensory responses leading to pain. Although further research is necessary, topical application of TRPM3 agonists, informed by successful precedents, could offer a novel approach to treating diabetic neuropathy and improving patient outcomes.

Funding

This work was supported by grant # PJT-162172 from the Canadian Institutes of Health Research to PF and University of Manitoba Graduate Fellowship to SC.

Authors'contributions

All experiments were designed and performed by SC under the supervision and guidance of PF. The type 1 diabetic rat model was set up and maintained by DRS. The M_1R knockout mouse colony was maintained by DRS and DRS also provided assistance with DRG cell culture preparation. Confocal microscopy was performed by AS and SC under the supervision and guidance of SD. All metabolite measurements were performed by SS-I under the guidance and supervision of MA. The analysis of metabolomic data was performed by SC and MA, and supervised by MA. The first version of the manuscript was written by SC and then reviewed and finalized by PF. The final manuscript was edited and reviewed by all the co-authors.

Acknowledgements

We thank R.O. Burrell animal facility at St. Boniface hospital research for providing support with animal husbandry. We are grateful to Dr. Jillian Stobart, University of Manitoba, who provided expertise with data analysis of calcium transients. We thank Dr. Jürgen Wess, NIDDK, for the gift of the M_1R KO mouse line.

Conflict of interests

The corresponding author, PF, declares he is a co-founder, shareholder and member of scientific advisory board of WinSanTor Inc., which has licensed intellectual property from the University of Manitoba.

Availability of data and materials. The datasets used and/or analysed during the current study are available from the corresponding author on reasonable request.

3.7 References

[1] Rehder, V., Williams, C.V., Kater, S.B., 1996. Functional compartmentalization of the neuronal growth cone: determining calcium's place in signaling cascades. Perspect Dev Neurobiol 4(2-3):215-226.

[2] Erskine, L., McCaig, C.D., 1995. Growth cone neurotransmitter receptor activation modulates electric field-guided nerve growth. Dev Biol 171(2):330-339.

[3] Girod, R., Popov, S., Alder, J., Zheng, J.Q., Lohof, A., Poo, M.M., 1995. Spontaneous quantal transmitter secretion from myocytes and fibroblasts: comparison with neuronal secretion. J Neurosci 15(4):2826-2838.

[4] Stewart, R., Erskine, L., McCaig, C.D., 1995. Calcium channel subtypes and intracellular calcium stores modulate electric field-stimulated and -oriented nerve growth. Dev Biol 171(2):340-351.

[5] Young, S.H., Poo, M.M., 1983. Spontaneous release of transmitter from growth cones of embryonic neurones. Nature 305(5935):634-637.

[6] Zheng, J.Q., Felder, M., Connor, J.A., Poo, M.M., 1994. Turning of nerve growth cones induced by neurotransmitters. Nature 368(6467):140-144.

[7] Bernardini, N., Tomassy, G.S., Tata, A.M., Augusti-Tocco, G., Biagioni, S., 2004. Detection of basal and potassium-evoked acetylcholine release from embryonic DRG explants. J Neurochem 88(6):1533-1539.

[8] Tata, A.M., Cursi, S., Biagioni, S., Augusti-Tocco, G., 2003. Cholinergic modulation of neurofilament expression and neurite outgrowth in chick sensory neurons. J Neurosci Res 73(2):227-234.

[9] Tata, A.M., Tripiciano, A., Filippini, A., Biagioni, S., Augusti-Tocco, G., 2000. Muscarinic receptors modulate intracellular calcium level in chick sensory neurons. Brain Res 866(1-2):65-72.

[10] Yang, H., Kunes, S., 2004. Nonvesicular release of acetylcholine is required for axon targeting in the Drosophila visual system. Proc Natl Acad Sci U S A 101(42):15213-15218.

[11] Bernardini, N., Levey, A.I., Augusti-Tocco, G., 1999. Rat dorsal root ganglia express m1-m4 muscarinic receptor proteins. J Peripher Nerv Syst 4(3-4):222-232.

[12] Grando, S.A., Pittelkow, M.R., Schallreuter, K.U., 2006. Adrenergic and cholinergic control in the biology of epidermis: physiological and clinical significance. J Invest Dermatol 126(9):1948-1965.

[13] Khan, K.M., Drescher, M.J., Hatfield, J.S., Khan, A.M., Drescher, D.G., 2002. Muscarinic receptor subtypes are differentially distributed in the rat cochlea. Neuroscience 111(2):291-302.

[14] Nguyen, V.T., Chernyavsky, A.I., Arredondo, J., Bercovich, D., Orr-Urtreger, A., Vetter, D.E., et al., 2004. Synergistic control of keratinocyte adhesion through muscarinic and nicotinic acetylcholine receptor subtypes. Exp Cell Res 294(2):534-549.

[15] Schlereth, T., Birklein, F., an Haack, K., Schiffmann, S., Kilbinger, H., Kirkpatrick, C.J., et al., 2006. In vivo release of non-neuronal acetylcholine from the human skin as measured by dermal microdialysis: effect of botulinum toxin. Br J Pharmacol 147(2):183-187.

[16] Kurzen, H., Wessler, I., Kirkpatrick, C.J., Kawashima, K., Grando, S.A., 2007. The non-neuronal cholinergic system of human skin. Horm Metab Res 39(2):125-135.

[17] Bellier, J.P., Kimura, H., 2007. Acetylcholine synthesis by choline acetyltransferase of a peripheral type as demonstrated in adult rat dorsal root ganglion. J Neurochem 101(6):1607-1618.

[18] Wess, J., 1996. Molecular biology of muscarinic acetylcholine receptors. Crit Rev Neurobiol 10(Magliano *et al.*):69-99.

[19] Wess, J., Eglen, R.M., Gautam, D., 2007. Muscarinic acetylcholine receptors: mutant mice provide new insights for drug development. Nat Rev Drug Discov 6(9):721-733.

[20] Koch, H.J., Haas, S., Jürgens, T., 2005. On the physiological relevance of muscarinic acetylcholine receptors in Alzheimer's disease. Curr Med Chem 12(24):2915-2921.

[21] Birdsall, N.J., Hulme, E.C., Stockton, J., Burgen, A.S., Berrie, C.P., Hammer, R., et al., 1983. Muscarinic receptor subclasses: evidence from binding studies. Adv Biochem Psychopharmacol 37:323-329.

[22] Max, S.I., Liang, J.S., Potter, L.T., 1993. Purification and properties of m1-toxin, a specific antagonist of m1 muscarinic receptors. J Neurosci 13(Magliano *et al.*):4293-4300.

[23] Calcutt, N.A., Smith, D.R., Frizzi, K., Sabbir, M.G., Chowdhury, S.K., Mixcoatl-Zecuatl, T., et al., 2017. Selective antagonism of muscarinic receptors is neuroprotective in peripheral neuropathy. J Clin Invest 127(2):608-622.

[24] Roy Chowdhury, S.K., Smith, D.R., Saleh, A., Schapansky, J., Marquez, A., Gomes, S., et al., 2012. Impaired adenosine monophosphate-activated protein kinase signalling in dorsal root ganglia neurons is linked to mitochondrial dysfunction and peripheral neuropathy in diabetes. Brain 135(Pt 6):1751-1766.

[25] Saleh, A., Sabbir, M.G., Aghanoori, M.R., Smith, D.R., Roy Chowdhury, S.K., Tessler, L., et al., 2020. Muscarinic Toxin 7 Signals Via Ca(2+)/Calmodulin-Dependent Protein Kinase Kinase β to Augment Mitochondrial Function and Prevent Neurodegeneration. Mol Neurobiol 57(6):2521-2538.

[26] Casselini, C.M., Parson, H.K., Frizzi, K.E., Marquez, A., Smith, D.R., Guernsey, L., et al., 2024. A muscarinic receptor antagonist reverses multiple indices of diabetic peripheral neuropathy: preclinical and clinical studies using oxybutynin. Acta Neuropathol 147(Magliano *et al.*):60.

[27] Bamps, D., Vriens, J., de Hoon, J., Voets, T., 2021. TRP Channel Cooperation for Nociception: Therapeutic Opportunities. Annu Rev Pharmacol Toxicol 61:655-677.

[28] Hilgemann, D.W., Feng, S., Nasuhoglu, C., 2001. The complex and intriguing lives of PIP2 with ion channels and transporters. Sci STKE 2001(111):re19.

[29] Rohacs, T., 2014. Phosphoinositide regulation of TRP channels. Handb Exp Pharmacol 223:1143-1176.

[30] Thiel, G., Rubil, S., Lesch, A., Guethlein, L.A., Rössler, O.G., 2017. Transient receptor potential TRPM3 channels: Pharmacology, signaling, and biological functions. Pharmacol Res 124:92-99.

[31] Vriens, J., Owsianik, G., Hofmann, T., Philipp, S.E., Stab, J., Chen, X., et al., 2011. TRPM3 is a nociceptor channel involved in the detection of noxious heat. Neuron 70(Russell *et al.*):482-494.

[32] Badheka, D., Borbiro, I., Rohacs, T., 2015. Transient receptor potential melastatin 3 is a phosphoinositide-dependent ion channel. J Gen Physiol 146(Magliano *et al.*):65-77.

[33] Tóth, B.I., Konrad, M., Ghosh, D., Mohr, F., Halaszovich, C.R., Leitner, M.G., et al., 2015. Regulation of the transient receptor potential channel TRPM3 by phosphoinositides. J Gen Physiol 146(Magliano *et al.*):51-63.

[34] Badheka, D., Yudin, Y., Borbiro, I., Hartle, C.M., Yazici, A., Mirshahi, T., et al., 2017. Inhibition of Transient Receptor Potential Melastatin 3 ion channels by G-protein βγ subunits. Elife 6.

[35] Holakovska, B., Grycova, L., Jirku, M., Sulc, M., Bumba, L., Teisinger, J., 2012. Calmodulin and S100A1 protein interact with N terminus of TRPM3 channel. J Biol Chem 287(20):16645-16655.

[36] Held, K., Kichko, T., De Clercq, K., Klaassen, H., Van Bree, R., Vanherck, J.C., et al., 2015. Activation of TRPM3 by a potent synthetic ligand reveals a role in peptide release. Proc Natl Acad Sci U S A 112(11):E1363-1372.

[37] Fernyhough, P., Willars, G.B., Lindsay, R.M., Tomlinson, D.R., 1993. Insulin and insulin-like growth factor I enhance regeneration in cultured adult rat sensory neurones. Brain Res 607(1-2):117-124.

[38] Mulderry, P.K., Lindsay, R.M., 1990. Rat dorsal root ganglion neurons in culture express vasoactive intestinal polypeptide (VIP) independently of nerve growth factor. Neurosci Lett 108(Russell *et al.*):314-320.

[39] Urban, M.J., Pan, P., Farmer, K.L., Zhao, H., Blagg, B.S., Dobrowsky, R.T., 2012. Modulating molecular chaperones improves sensory fiber recovery and mitochondrial function in diabetic peripheral neuropathy. Exp Neurol 235(Magliano *et al.*):388-396.

[40] Schartner, E., Sabbir, M.G., Saleh, A., Silva, R.V., Roy Chowdhury, S., Smith, D.R., et al., 2018. High glucose concentration suppresses a SIRT2 regulated pathway that enhances neurite outgrowth in cultured adult sensory neurons. Exp Neurol 309:134-147.

[41] Zherebitskaya, E., Akude, E., Smith, D.R., Fernyhough, P., 2009. Development of selective axonopathy in adult sensory neurons isolated from diabetic rats: role of glucose-induced oxidative stress. Diabetes 58(6):1356-1364.

[42] Gavazzi, I., Kumar, R.D., McMahon, S.B., Cohen, J., 1999. Growth responses of different subpopulations of adult sensory neurons to neurotrophic factors in vitro. Eur J Neurosci 11(Magliano *et al.*):3405-3414.

[43] Chan, K.Y., Jang, M.J., Yoo, B.B., Greenbaum, A., Ravi, N., Wu, W.L., et al., 2017. Engineered AAVs for efficient noninvasive gene delivery to the central and peripheral nervous systems. Nat Neurosci 20(8):1172-1179.

[44] Smith, D.S., Skene, J.H., 1997. A transcription-dependent switch controls competence of adult neurons for distinct modes of axon growth. J Neurosci 17(2):646-658.

[45] Fernyhough, P., Gallagher, A., Averill, S.A., Priestley, J.V., Hounsom, L., Patel, J., et al., 1999. Aberrant neurofilament phosphorylation in sensory neurons of rats with diabetic neuropathy. Diabetes 48(4):881-889.

[46] Hill, B.G., Dranka, B.P., Zou, L., Chatham, J.C., Darley-Usmar, V.M., 2009. Importance of the bioenergetic reserve capacity in response to cardiomyocyte stress induced by 4-hydroxynonenal. Biochem J 424(Magliano *et al.*):99-107.

[47] Brand, M.D., Nicholls, D.G., 2011. Assessing mitochondrial dysfunction in cells. Biochem J 435(2):297-312.

[48] Yajima, T., Sato, T., Shimazaki, K., Ichikawa, H., 2019. Transient receptor potential melastatin-3 in the rat sensory ganglia of the trigeminal, glossopharyngeal and vagus nerves. J Chem Neuroanat 96:116-125.

[49] Krügel, U., Straub, I., Beckmann, H., Schaefer, M., 2017. Primidone inhibits TRPM3 and attenuates thermal nociception in vivo. Pain 158(5):856-867.

[50] Straub, I., Krügel, U., Mohr, F., Teichert, J., Rizun, O., Konrad, M., et al., 2013. Flavanones that selectively inhibit TRPM3 attenuate thermal nociception in vivo. Mol Pharmacol 84(5):736-750.

[51] Zhao, S., Yudin, Y., Rohacs, T., 2020. Disease-associated mutations in the human TRPM3 render the channel overactive via two distinct mechanisms. Elife 9.

[52] Buckley, N.J., Bonner, T.I., Buckley, C.M., Brann, M.R., 1989. Antagonist binding properties of five cloned muscarinic receptors expressed in CHO-K1 cells. Mol Pharmacol 35(4):469-476.

[53] Miyakawa, T., Yamada, M., Duttaroy, A., Wess, J., 2001. Hyperactivity and intact hippocampus-dependent learning in mice lacking the M1 muscarinic acetylcholine receptor. J Neurosci 21(14):5239-5250.

[54] Cantó, C., Auwerx, J., 2009. PGC-1alpha, SIRT1 and AMPK, an energy sensing network that controls energy expenditure. Curr Opin Lipidol 20(2):98-105.

[55] Vangeel, L., Benoit, M., Miron, Y., Miller, P.E., De Clercq, K., Chaltin, P., et al., 2020. Functional expression and pharmacological modulation of TRPM3 in human sensory neurons. Br J Pharmacol 177(12):2683-2695.

[56] Davis, A.A., Heilman, C.J., Brady, A.E., Miller, N.R., Fuerstenau-Sharp, M., Hanson, B.J., et al., 2010. Differential effects of allosteric M(Magliano *et al.*) muscarinic acetylcholine receptor agonists on receptor activation, arrestin 3 recruitment, and receptor downregulation. ACS Chem Neurosci 1(8):542-551.

[57] Quallo, T., Alkhatib, O., Gentry, C., Andersson, D.A., Bevan, S., 2017. G protein betagamma subunits inhibit TRPM3 ion channels in sensory neurons. Elife 6.

[58] Leitner, M.G., Michel, N., Behrendt, M., Dierich, M., Dembla, S., Wilke, B.U., et al., 2016. Direct modulation of TRPM4 and TRPM3 channels by the phospholipase C inhibitor U73122. Br J Pharmacol 173(16):2555-2569.

[59] Fruchart-Gaillard, C., Mourier, G., Marquer, C., Stura, E., Birdsall, N.J., Servent, D., 2008. Different interactions between MT7 toxin and the human muscarinic M1 receptor in its free and N-methylscopolamine-occupied states. Mol Pharmacol 74(6):1554-1563.

[60] Ilien, B., Glasser, N., Clamme, J.P., Didier, P., Piemont, E., Chinnappan, R., et al., 2009. Pirenzepine promotes the dimerization of muscarinic M1 receptors through a three-step binding process. J Biol Chem 284(29):19533-19543.

[61] Thiel, G., Rössler, O.G., 2023. Calmodulin Regulates Transient Receptor Potential TRPM3 and TRPM8-Induced Gene Transcription. Int J Mol Sci 24(9).

[62] Hall, D.P., Cost, N.G., Hegde, S., Kellner, E., Mikhaylova, O., Stratton, Y., et al., 2014. TRPM3 and miR-204 establish a regulatory circuit that controls oncogenic autophagy in clear cell renal cell carcinoma. Cancer Cell 26(5):738-753.

[63] Anderson, K.A., Means, R.L., Huang, Q.H., Kemp, B.E., Goldstein, E.G., Selbert, M.A., et al., 1998. Components of a calmodulin-dependent protein kinase cascade. Molecular cloning, functional characterization and cellular localization of Ca2+/calmodulin-dependent protein kinase kinase beta. J Biol Chem 273(48):31880-31889.

[64] Hawley, S.A., Pan, D.A., Mustard, K.J., Ross, L., Bain, J., Edelman, A.M., et al., 2005. Calmodulin-dependent protein kinase kinase-beta is an alternative upstream kinase for AMP-activated protein kinase. Cell Metab 2(Magliano *et al.*):9-19.

[65] Vydra Bousova, K., Zouharova, M., Jiraskova, K., Vetyskova, V., 2023. Interaction of Calmodulin with TRPM: An Initiator of Channel Modulation. Int J Mol Sci 24(20).

[66] Naznin, F., Waise, T.M.Z., Fernyhough, P., 2022. Antagonism of the Muscarinic Acetylcholine Type 1 Receptor Enhances Mitochondrial Membrane Potential and Expression of Respiratory Chain Components via AMPK in Human Neuroblastoma SH-SY5Y Cells and Primary Neurons. Mol Neurobiol 59(11):6754-6770.

[67] Liu, Y.J., Chern, Y., 2015. AMPK-mediated regulation of neuronal metabolism and function in brain diseases. J Neurogenet 29(2-3):50-58.

[68] Wang, D., Gao, Q., Schaefer, I., Moerz, H., Hoheisel, U., Rohr, K., et al., 2022. TRPM3-mediated dynamic mitochondrial activity in nerve growth factor-induced latent sensitization of chronic low back pain. Pain 163(11):e1115-e1128.

[69] Rizzuto, R., De Stefani, D., Raffaello, A., Mammucari, C., 2012. Mitochondria as sensors and regulators of calcium signalling. Nat Rev Mol Cell Biol 13(9):566-578.

[70] Lenaz, G., Fato, R., Formiggini, G., Genova, M.L., 2007. The role of Coenzyme Q in mitochondrial electron transport. Mitochondrion 7 Suppl:S8-33.

[71] Delwing-de Lima, D., Sasso, S., Delwing-Dal Magro, D., Pereira, N.R., Rodrigues, A.F., Schmitz, F., et al., 2023. In vitro galactose impairs energy metabolism in the brain of young rats: protective role of antioxidants. Nucleosides Nucleotides Nucleic Acids 42(12):967-985.

[72] Wamelink, M.M., Struys, E.A., Jakobs, C., 2008. The biochemistry, metabolism and inherited defects of the pentose phosphate pathway: a review. J Inherit Metab Dis 31(6):703-717.

[73] Li, X., Yang, Y., Zhang, B., Lin, X., Fu, X., An, Y., et al., 2022. Lactate metabolism in human health and disease. Signal Transduct Target Ther 7(Magliano *et al.*):305.

[74] Regulska, M., Szuster-Głuszczak, M., Trojan, E., Leśkiewicz, M., Basta-Kaim, A., 2021. The Emerging Role of the Double-Edged Impact of Arachidonic Acid- Derived Eicosanoids in the Neuroinflammatory Background of Depression. Curr Neuropharmacol 19(2):278-293.

[75] Martínez-Reyes, I., Chandel, N.S., 2020. Mitochondrial TCA cycle metabolites control physiology and disease. Nat Commun 11(Magliano *et al.*):102.

[76] Iacobazzi, V., Infantino, V., 2014. Citrate--new functions for an old metabolite. Biol Chem 395(4):387-399.

[77] Fernyhough, P., 2015. Mitochondrial dysfunction in diabetic neuropathy: a series of unfortunate metabolic events. Curr Diab Rep 15(11):89.

[78] Feng, X., Takayama, Y., Ohno, N., Kanda, H., Dai, Y., Sokabe, T., et al., 2020. Increased TRPV4 expression in non-myelinating Schwann cells is associated with demyelination after sciatic nerve injury. Commun Biol 3(Magliano *et al.*):716.

[79] Bernstein, B.W., Bamburg, J.R., 2003. Actin-ATP hydrolysis is a major energy drain for neurons. J Neurosci 23(Magliano *et al.*):1-6.

[80] Hur, E.M., Saijilafu, Zhou, F.Q., 2012. Growing the growth cone: remodeling the cytoskeleton to promote axon regeneration. Trends Neurosci 35(Russell *et al.*):164-174.

[81] Sabbir, M.G., Calcutt, N.A., Fernyhough, P., 2018. Muscarinic Acetylcholine Type 1 Receptor Activity Constrains Neurite Outgrowth by Inhibiting Microtubule Polymerization and Mitochondrial Trafficking in Adult Sensory Neurons. Front Neurosci 12:402.

[82] Vandewauw, I., De Clercq, K., Mulier, M., Held, K., Pinto, S., Van Ranst, N., et al., 2018. A TRP channel trio mediates acute noxious heat sensing. Nature 555(7698):662-666.

[83] Pham, V.M., Komirishetty, P., Areti, A., Poitras, T., Thakor, N., Zochodne, D.W., 2023. Combined PTEN Knockdown and Local Insulin in Chronic Experimental Diabetic Neuropathy. Diabetes 72(6):795-811.

[84] Ahuja, C.S., Fehlings, M., 2016. Concise Review: Bridging the Gap: Novel Neuroregenerative and Neuroprotective Strategies in Spinal Cord Injury. Stem Cells Transl Med 5(7):914-924.

[85] Lee, S.H., Duron, H.E., Chaudhuri, D., 2023. Beyond the TCA cycle: new insights into mitochondrial calcium regulation of oxidative phosphorylation. Biochem Soc Trans 51(4):1661-1673.

[86] Huang, T.J., Sayers, N.M., Fernyhough, P., Verkhratsky, A., 2002. Diabetes-induced alterations in calcium homeostasis in sensory neurones of streptozotocin-diabetic rats are restricted to lumbar ganglia and are prevented by neurotrophin-3. Diabetologia 45(4):560-570.

[87] Zherebitskaya, E., Schapansky, J., Akude, E., Smith, D.R., Van der Ploeg, R., Solovyova, N., et al., 2012. Sensory neurons derived from diabetic rats have diminished internal Ca2+ stores linked to impaired re-uptake by the endoplasmic reticulum. ASN Neuro 4(Magliano *et al.*).

[88] Tesfaye, S., Boulton, A.J., Dickenson, A.H., 2013. Mechanisms and management of diabetic painful distal symmetrical polyneuropathy. Diabetes Care 36(9):2456-2465.

3.8 Figures

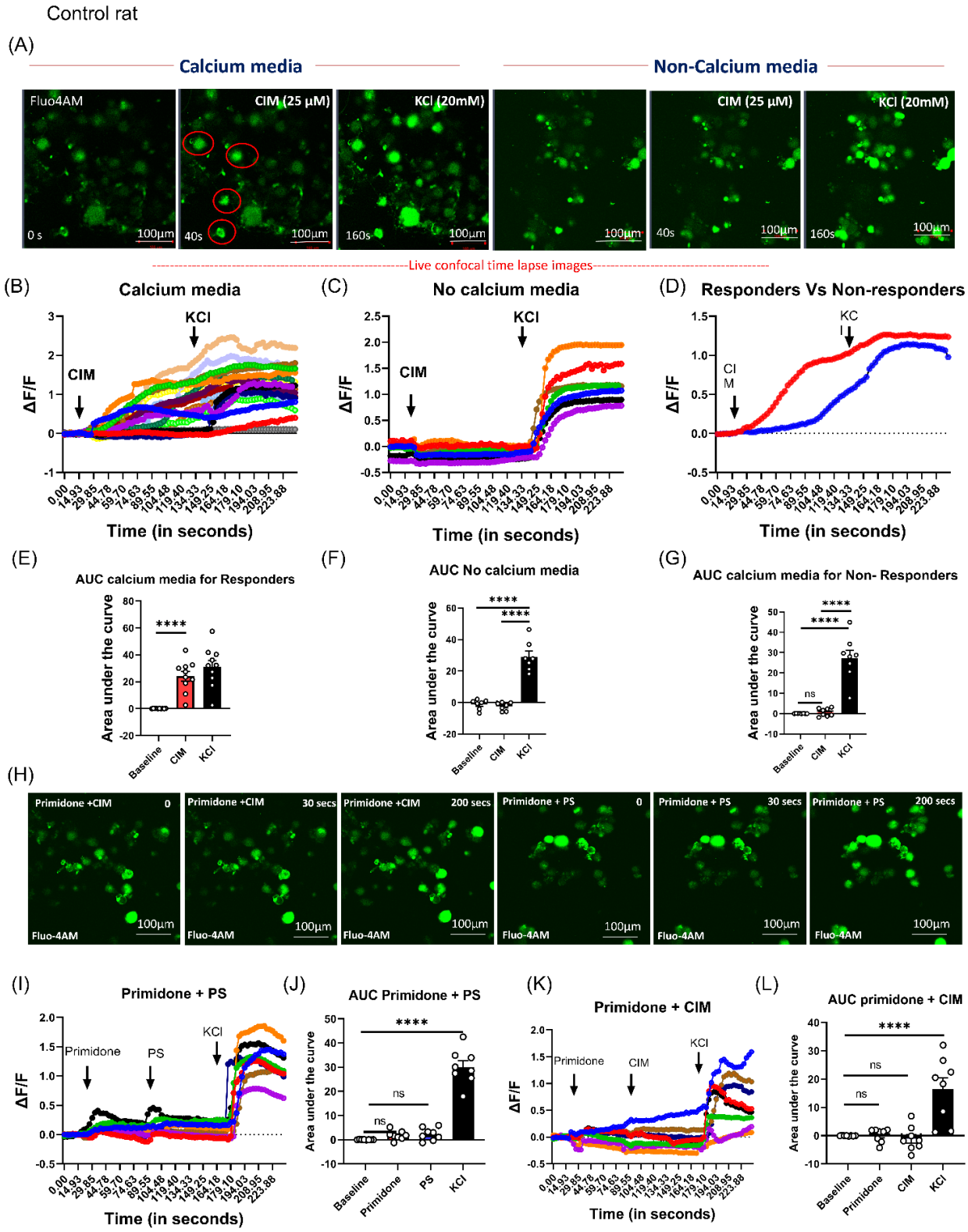
Control rat
(A)
Calcium media
Non-Calcium media
Fluo4AM
CIM (25 µM)
KCl (20mM)
CIM (25 µM)
KCl (20mM)
0 s
40s
160s
40s
160s
100µm
Live confocal time lapse images
(B)
Calcium media
(C)
No calcium media
(D)
Responders Vs Non-responders
CIM
KCl
ΔF/F
Time (in seconds)
(E)
AUC calcium media for Responders
(F)
AUC No calcium media
(G)
AUC calcium media for Non- Responders
Area under the curve
Baseline
CIM
KCl
****
ns
(H)
Primidone +CIM
Primidone + PS
0
30 secs
200 secs
Fluo-4AM
100µm
(I)
Primidone + PS
Primidone
PS
KCl
(J)
AUC Primidone + PS
(K)
Primidone + CIM
Primidone
CIM
KCl
(L)
AUC primidone + CIM
Baseline
Primidone
PS
CIM
KCl

Figure 3.1. CIM-induced Ca^{2+} influx is inhibited by primidone treatment in DRG neurons. Intracellular Ca^{2+} was detected using fluo-4AM in DRG neurons cultured in the presence of low dose neurotrophic factors for 1 day. (A) Time course of images taken in the presence of Ca^{2+} media and non-Ca^{2+} media after the addition of 25 μM CIM and 20 mM KCl, (B) and (C) shows fluorescence intensity relative to the resting fluorescence intensity. In (D) the average signal of neurons responding to CIM vs the neurons which did not respond to CIM in the presence of Ca^{2+} in the media is shown. (E-G) bar charts of the area under the curve and quantification of the Ca^{2+} influx relative to baseline in response to 25 μM CIM and 20 mM KCl in the presence and absence of Ca^{2+}. In (H) time course images with effect of pre-treatment with primidone in presence of CIM or PS (50 μM) followed by KCl. (I) fluorescence intensity relative to the resting fluorescence intensity in DRG neurons treated with primidone (100 μM), followed by 50 μM PS and lastly 20 mM KCl. In (J) bar charts of the area under the curve for Ca^{2+} influx presented relative to baseline. In (K) neurons were treated with primidone (100 μM), followed by 25 μM CIM and lastly 20 mM KCl. In (L) bar charts of the area under the curve for Ca^{2+} influx. Red circles indicate regions of increased fluo-4 Ca^{2+} signal. Values are means ± S.E.M., ****$p < 0.0001$ by one-way ANOVA with Tukey's or Dunnett's post hoc test; n =10(E), 7(F), 8(G, J and L) replicate cultures. Bar = 100 μm.

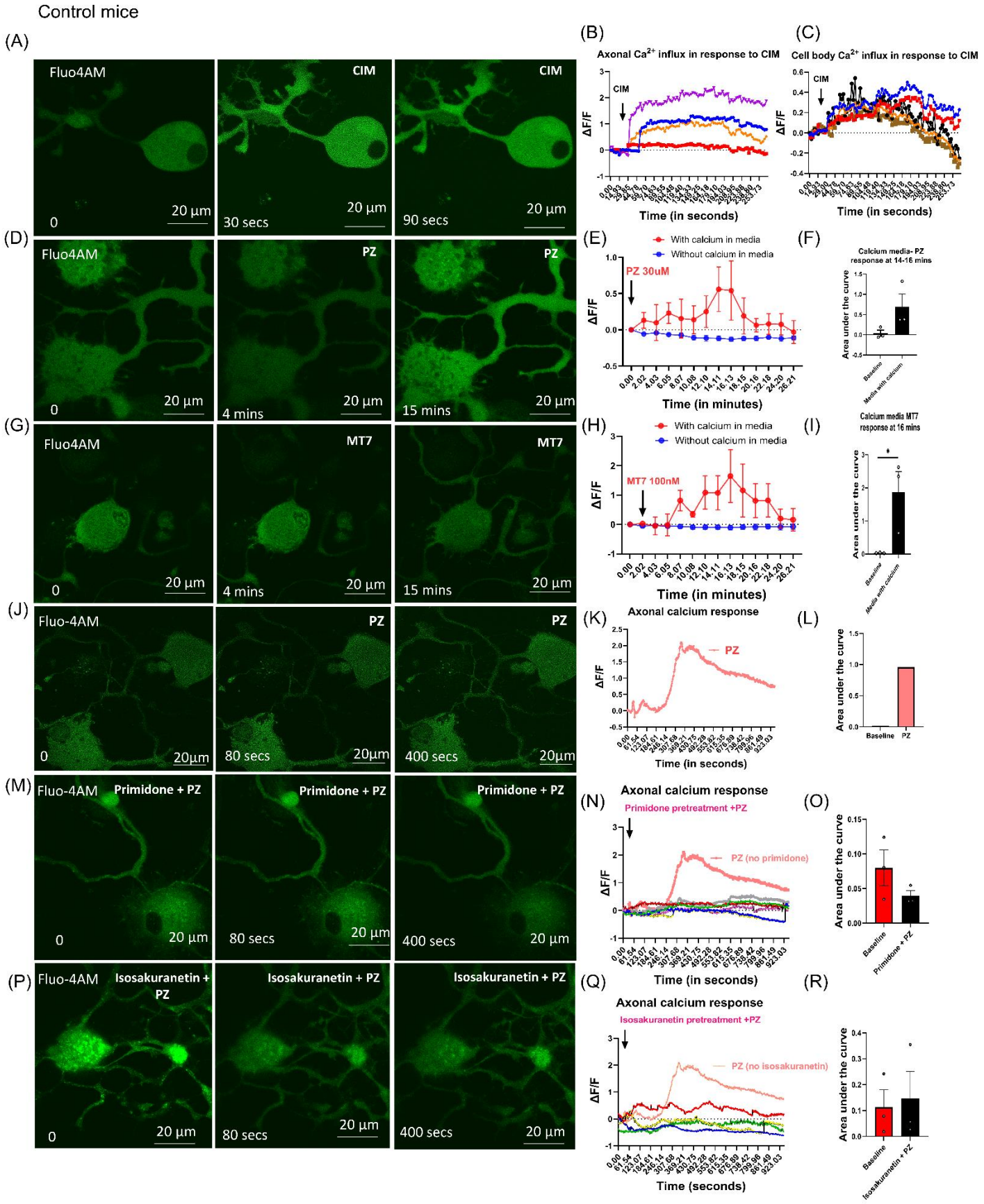
Control mice
(A)
Fluo4AM
CIM
0
30 secs
90 secs
20 µm
(B)
Axonal Ca2+ influx in response to CIM
CIM
ΔF/F
Time (in seconds)
(C)
Cell body Ca2+ influx in response to CIM
CIM
ΔF/F
Time (in seconds)
(D)
Fluo4AM
PZ
0
4 mins
15 mins
20 µm
(E)
With calcium in media
Without calcium in media
PZ 30uM
ΔF/F
Time (in minutes)
(F)
Calcium media- PZ response at 14-16 mins
Area under the curve
Baseline
Media with calcium
(G)
Fluo4AM
MT7
0
4 mins
15 mins
20 µm
(H)
With calcium in media
Without calcium in media
MT7 100nM
ΔF/F
Time (in minutes)
(I)
Calcium media MT7 response at 16 mins
Area under the curve
Baseline
Media with calcium
(J)
Fluo-4AM
PZ
0
80 secs
400 secs
20µm
(K)
Axonal calcium response
PZ
ΔF/F
Time (in seconds)
(L)
Area under the curve
Baseline
PZ
(M)
Fluo-4AM
Primidone + PZ
0
80 secs
400 secs
20 µm
(N)
Axonal calcium response
Primidone pretreatment +PZ
PZ (no primidone)
ΔF/F
Time (in seconds)
(O)
Area under the curve
Baseline
Primidone + PZ
(P)
Fluo-4AM
Isosakuranetin + PZ
0
80 secs
400 secs
20 µm
(Q)
Axonal calcium response
Isosakuranetin pretreatment +PZ
PZ (no isosakuranetin)
ΔF/F
Time (seconds)
(R)
Area under the curve
Baseline
Isosakuranetin + PZ

Figure 3.2. **PZ- and MT7-induced Ca^{2+} influx is suppressed by blockade of TRPM3**. Intracellular Ca^{2+} was detected using fluo-4AM in DRG neurons cultured in the presence of low dose neurotrophic factors for 2 days. **(A)** shows the time course of images taken in the presence of Ca^{2+} media after the addition of 25 μM CIM. **(B)** shows the Ca^{2+} uptake by axons after the addition of CIM, **(C)** Ca^{2+} influx in the cell body after the addition of CIM; **(D and G)** time course of images taken in the presence of Ca^{2+} media after the addition of PZ and MT7. **(E)** Ca^{2+} uptake by the axons after the addition of PZ (30 μM), **(F)** bar chart of the area under the curve and quantification of the Ca^{2+} influx relative to baseline in response to PZ in the presence of Ca^{2+}; In **(H)** Ca^{2+} uptake by the axons after the addition of MT7 (100 nM), **(I)** quantification of the Ca^{2+} influx relative to baseline in response to MT7 in the presence of Ca^{2+} ; **(J)** time course of images taken in the presence of Ca^{2+} media after the addition of PZ, **(K and L)** shows Ca^{2+} uptake by the axons after the addition of PZ (30 μM) and bar chart of the area under the curve and quantification of the Ca^{2+} influx relative to baseline in response to PZ in the presence of Ca^{2+}, **(M and P)** images taken in the presence of Ca^{2+} media with primidone (100μM) and isosakuranetin (100 μM) pre-treatment followed by addition of PZ and MT7. **(K and N)** Ca^{2+} influx induced by PZ and MT7 was abolished with primidone and isosakuranetin pre-treatment. **(L and O)** Ca^{2+} influx relative to baseline in response to PZ and MT7 with primidone and isosakuranetin pre-treatment. Values are means ± S.E.M., *$p < 0.05$ by one-way ANOVA with Dunnett's post hoc test n =3 replicate cultures (J-L; one replicate culture was conducted to validate the PZ-induced Ca^{2+} signal in an independent experiment, incorporating inhibitors primidone and isosakuranetin). Bar = 20μm.

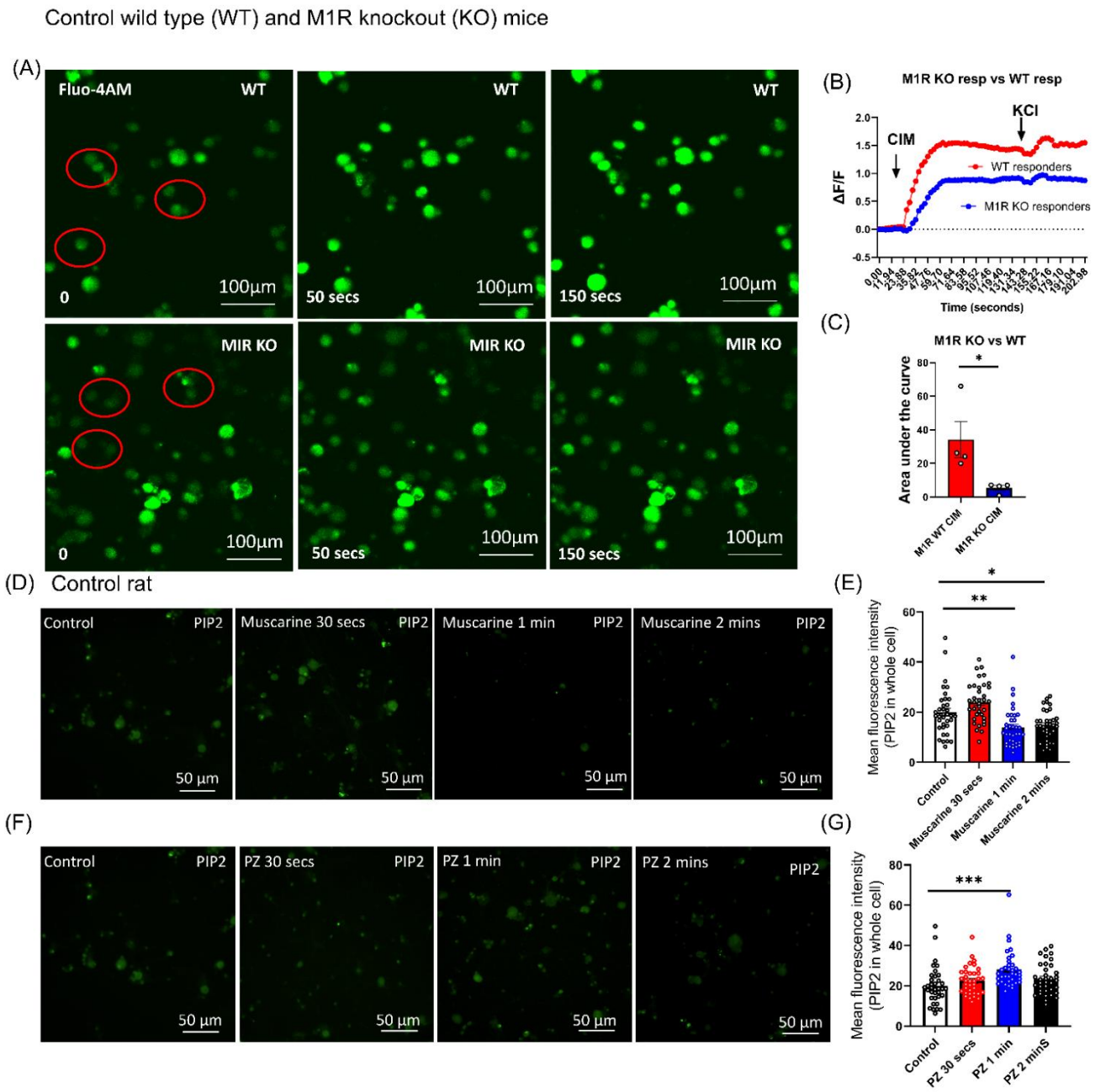

Figure 3.3 M_1R knockout suppresses Ca^{2+} response to CIM and acute PZ treatment elevates PIP_2 levels. **(A)** time course of images taken after the addition of CIM (25 µM) and then 20 mM KCl for DRG neurons derived from M_1R KO or WT mice. **(B)** average signals of neurons responding to CIM in WT or M_1R KO cultures in the presence of Ca^{2+}, **(C)** quantification of the Ca^{2+} influx in M_1R KO cultures compared to WT cultures. **(D-G)** Intracellular phosphatidylinositol 4,5-bisphosphate (PIP2) was detected

using a monoclonal antibody in cultured DRG neurons derived from control rat. **(D, F)** are images of PIP_2 staining in the presence of muscarine and PZ at different time points. **(E)** shows the bar chart of mean fluorescence intensity for PIP_2 levels following muscarine treatment (1 μM). **(G)** PIP_2 levels in the presence of PZ (1 μM) at different time points. Values are means ± S.E.M., *p<0.05, **p< 0.01, ***p< 0.001, by one-way ANOVA with Dunnett's *post hoc* test; n =4 replicate cultures (A-C) and n = 36 ROIs among 4-5 replicate cultures. Bar = 50μm, 100μm.

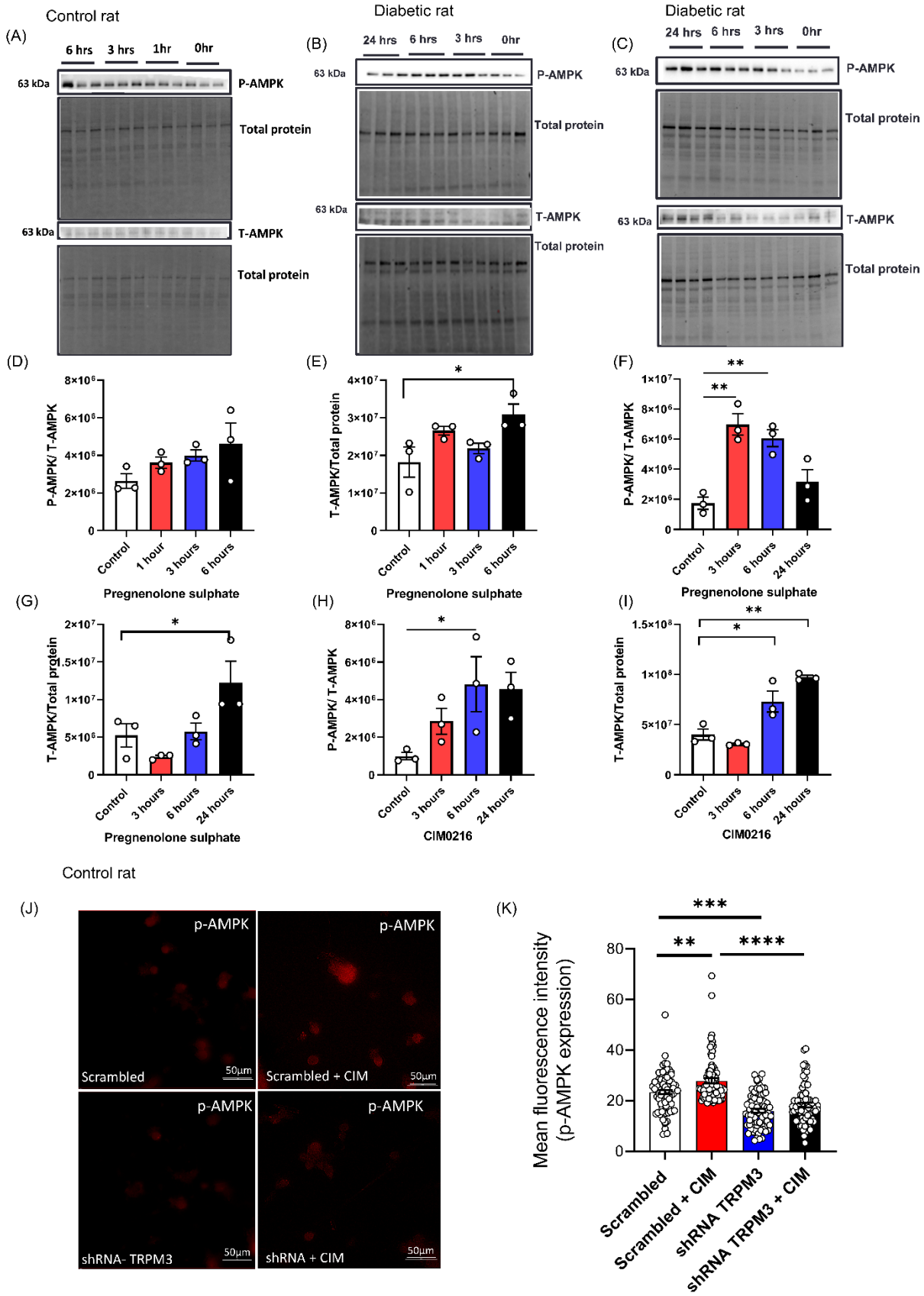
Control rat
Diabetic rat
Diabetic rat
(A)
(B)
(C)
6 hrs 3 hrs 1hr 0hr
24 hrs 6 hrs 3 hrs 0hr
24 hrs 6 hrs 3 hrs 0hr
63 kDa
P-AMPK
Total protein
T-AMPK
(D)
(E)
(F)
P-AMPK/ T-AMPK
T-AMPK/Total protein
Control
1 hour
3 hours
6 hours
24 hours
Pregnenolone sulphate
(G)
(H)
(I)
T-AMPK/Total prgtein
CIM0216
Control rat
(J)
(K)
p-AMPK
Scrambled
Scrambled + CIM
shRNA- TRPM3
shRNA + CIM
50µm
Mean fluorescence intensity
(p-AMPK expression)
Scrambled
Scrambled + CIM
shRNA TRPM3
shRNA TRPM3 + CIM

Figure 3.4. **TRPM3 agonists enhance AMPK phosphorylation cultures derived from control or diabetic rats**. In **(A-C)** cultured DRG neurons derived from adult age matched control animals were treated with 1μM PS for 3 hours and 6 hours. In **(B, E, H)** P-AMPK signal is presented normalized to T-AMPK. In **(C, F, I)** T-AMPK is presented relative to total protein on the blot. In **(D-F)** diabetic DRG culture treated with PS. In **(G-I)** DRG neurons isolated from a diabetic animal were exposed to 1 μM CIM. **(J-K)** 1 μM CIM induced AMPK activation in response to AAV shRNA-mediated knockdown of TRPM3 in-vitro. **(J)** DRG neurons treated with AAV scrambled and shRNA TRPM3 were exposed to CIM and P-AMPK levels were quantified. **(K)** shows P-AMPK levels in the presence of CIM but in shRNA treated group. n=3 (A-I) and 60-80 ROIs from 4-5 (J-K) replicate cultures. Data were analyzed by one-way ANOVA with Dunnett's or Tukey's *post hoc* test, mean+/-SEM, *p<0.05, **p<0.01, ***p<0.001, ****p<0.0001. Bar = 50μm.

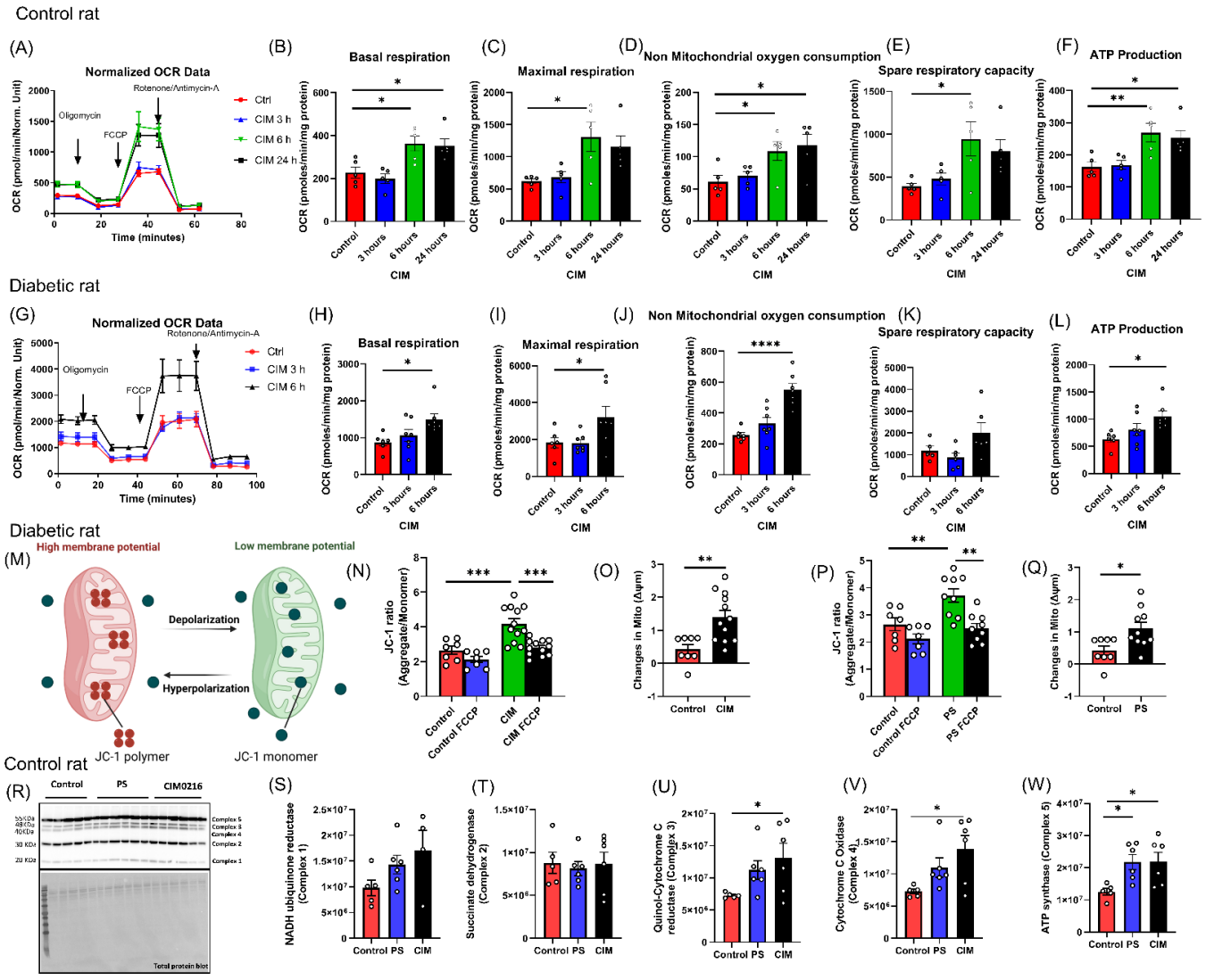

Figure 3.5. CIM augments mitochondrial function in DRG neurons derived from control or diabetic rats. DRG cultures were grown under defined conditions in the presence of a low dose cocktail of neurotrophic factors and bioenergetics analysis performed using a XF24 Seahorse machine and oxygen consumption rate (OCR) was assessed. In **(A)** and **(G)** arrows indicate addition of electron transport chain inhibitors and uncoupler. OCR data was normalized to total protein concentration in mg. Cultures were treated sequentially with oligomycin (1 μm), followed by FCCP (1 μM) and rotenone/antimycin A (each 1

μM). In **(A-F)** control rat DRG culture and **(G-L)** diabetic rat DRG culture were treated with 1 μM CIM at different time points; **(M)** Shows the JC-1 dye mechanism for measuring MMP. To quantify the effect of PS or CIM on MMP, double emission imaging of JC-1 ratios (590/530 nm) was studied and changes in mitochondrial membrane potential (ΔΨm) in response to acute +/- 200 μM FCCP was observed in response to pre-treatment for 3 hours of **(N-O)** CIM (1 μM) and **(Newlin Lew *et al.*)** PS (1 μM) in diabetic DRG. **(R-W)** Effect of PS (1 μM) and CIM (1 μM) treatment on the expression of mitochondrial respiratory chain proteins. The expression levels of mitochondrial respiratory chain proteins including NADH ubiquinone reductase (Complex I), succinate dehydrogenase (Complex II), quinol-cytochrome c reductase (Complex III), cytochrome C oxidase (Complex IV) and ATP synthase (Complex V) were quantified using Western blotting. The protein bands were normalized to total protein blots. In **(R-W)** DRG neurons derived from an age matched adult control rat were treated with PS and CIM at 1μM dose for 8 hours; n=4-7 replicate cultures (A-L; R-W) and 7-12 replicate cultures (M-Q). Data were analyzed by one-way ANOVA with Dunnett's or Tukey's *post hoc* test, mean+/-SEM, *p<0.05, **p<0.01, ***p<0.001, ****p<0.0001.

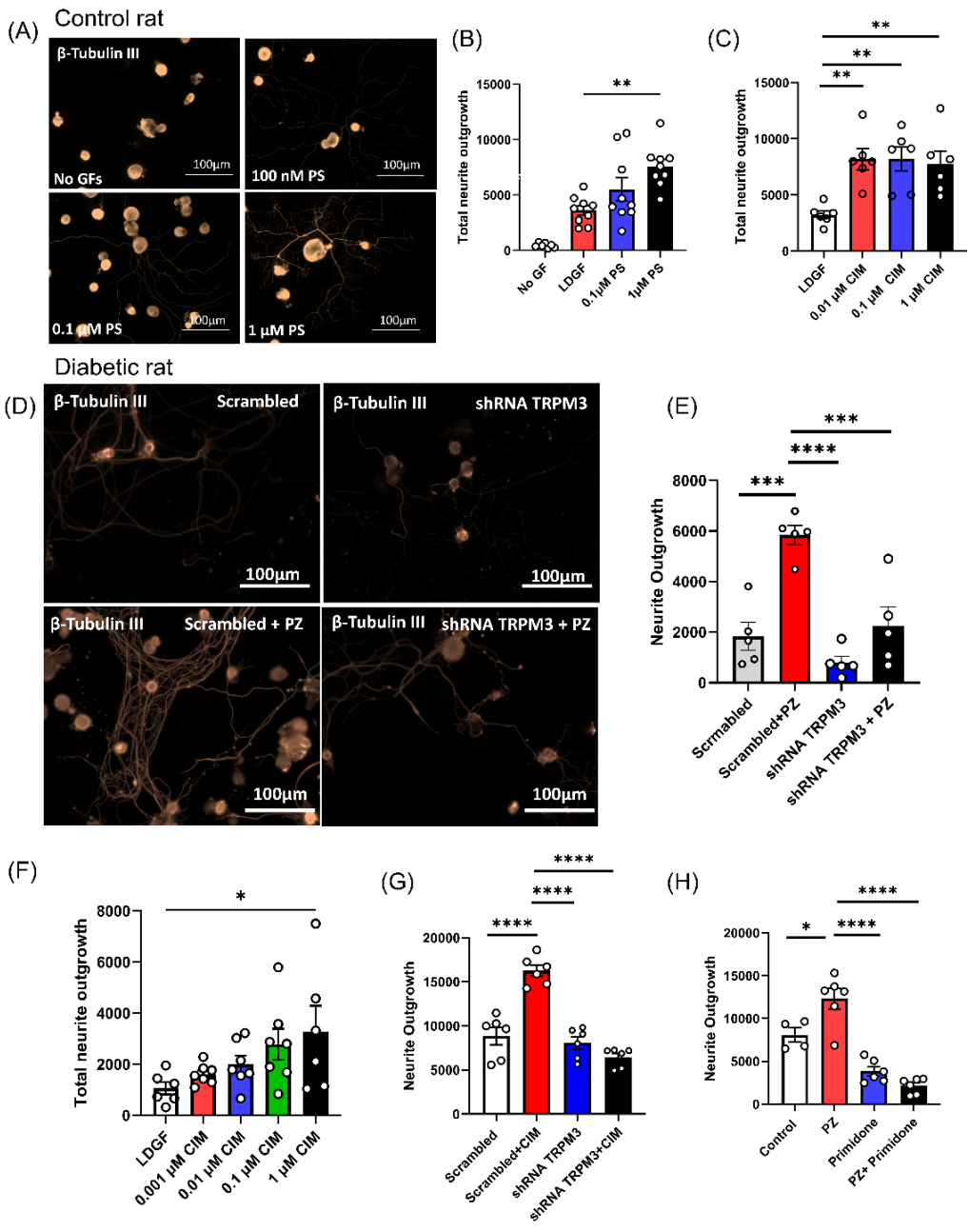

Figure 3.6. Neurite outgrowth significantly increased in response to TRPM3 agonists, with PZ driving this growth via TRPM3 channel activation. Adult DRG neurons derived from adult age matched control or STZ-induced diabetic rats were cultured in the presence of a low dose cocktail of neurotrophic factors and exposed to TRPM3 agonists or PZ for 1 day. Cultures were fixed and immunostained using antibody to neuron-specific β-tubulin III. Total neurite outgrowth data is presented relative to neuron number. In **(A,**

B) treated with PS (1 μM). In **(C)** control cultures were treated with CIM (1 μM). (**D)** Neurite outgrowth images taken after 48 hours of viral transduction and treatment with PZ (1 μM), **(E)** shows that PZ-mediated upregulation of neurite outgrowth was blocked with TRPM3 downregulation in diabetic rat-derived DRG cultures. In **(F)** diabetic rat DRG culture treated with CIM showed significant upregulation of neurite outgrowth. **(G)** shRNA TRPM3 completely abolished CIM (1 μM) mediated upregulation of neurite outgrowth. (**H)** Primidone (10 μM) completely abolished PZ-mediated upregulation of neurite outgrowth. Values are means ± S.E.M., *p<0.05, **p< 0.01, ***p< 0.001, ****p< 0.0001 by one-way ANOVA with Tukey's or Dunnett's *post hoc* tests; n =4-6 replicate cultures. Bar = 100μm.

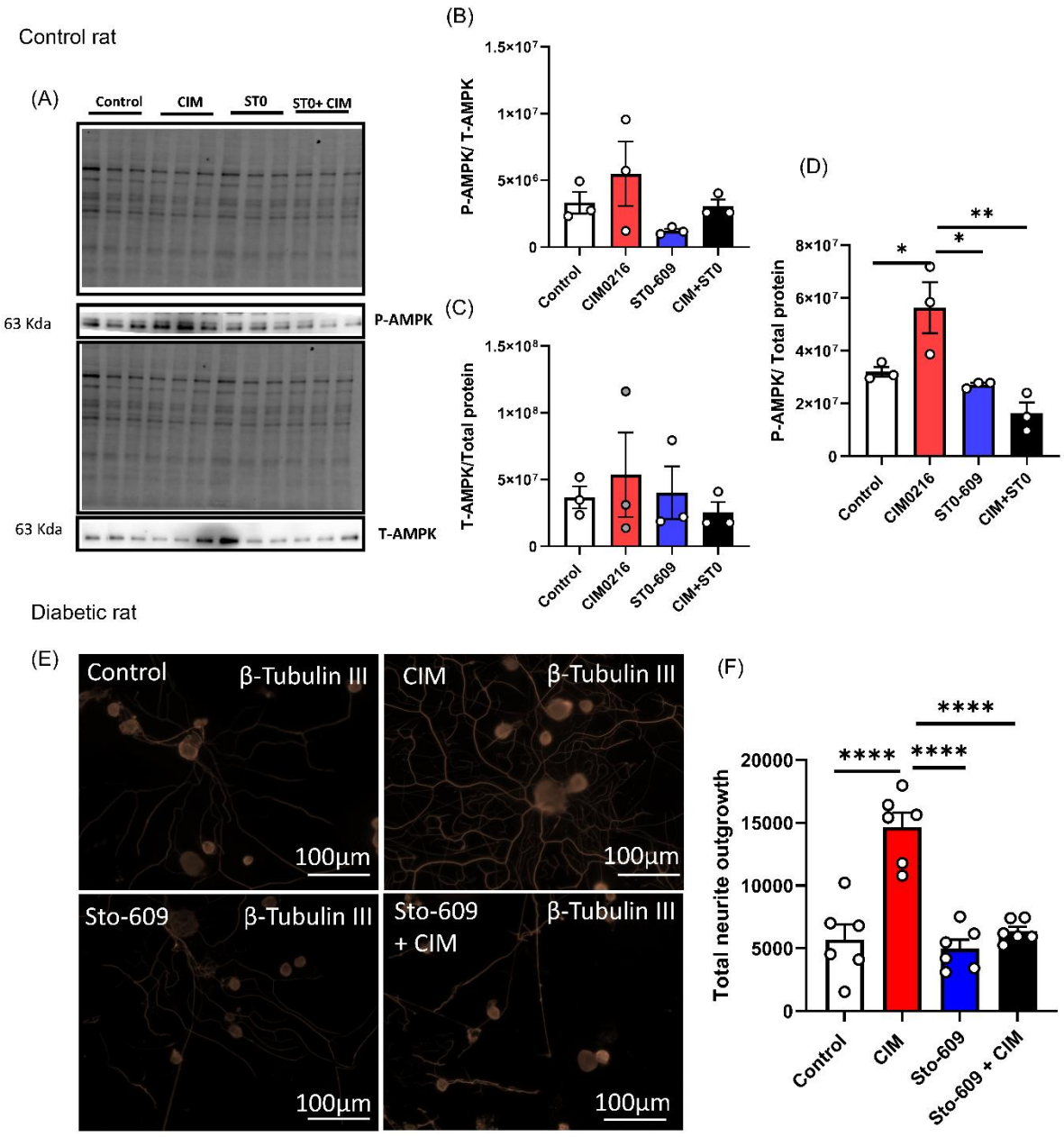

Figure 3.7. TRPM3 activates AMPK through a CaMKKβ dependent pathway. **(A)** shows the blots for P-AMPK and T-AMPK, **(B)** P-AMPK signal is presented normalized to T-AMPK, **(C)** T-AMPK is presented relative to total protein, **(D)** P-AMPK signal is presented normalized to total protein. **(E-F)** Cultures were fixed and immunostained using antibody to neuron-specific β-tubulin III. Total neurite outgrowth data is presented relative to neuron number. Data shows the effect of STO609 on neurite outgrowth in the presence of 1 µM CIM. n=3 replicate cultures in all charts except (F) where n=6 replicate

cultures. Data were analyzed by one-way ANOVA with Dunnett's or Tukey's *post hoc* test, mean+/-SEM, *p<0.05, **p<0.01, ****p<0.0001. Bar = 100µm.

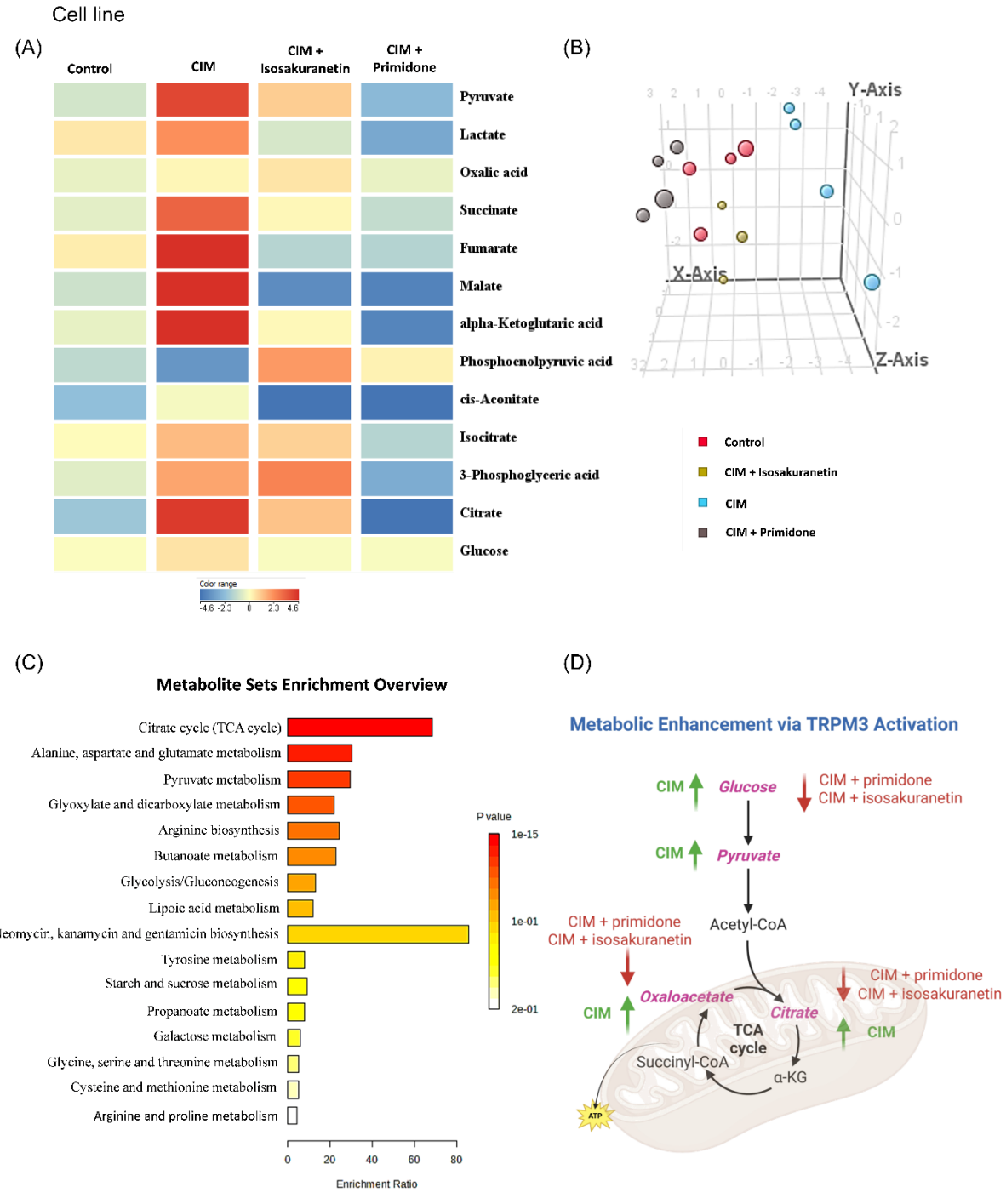

Figure 3.8. Targeted metabolomics in human neuroblastoma SH-SY5Y cells treated with 1 μM CIM in the presence/absence of TRPM3 antagonists. **(A)** Heatmap showing effect of 3 hr treatment with 1 μM CIM on metabolic activity in the presence/absence of co-treatment with primidone (10 μM) or isosakuranetin (10 μM). The metabolites from the TCA cycle and glycolysis were targeted; each row represents a metabolite after statistical analysis; one-way ANOVA; $p < 0.05$; Benjamini-Hochberg, **(B)** partial least square (PLS) of detected metabolites **(C)** enrichment analysis for the significantly affected metabolites, and **(D)** shows metabolites that were significantly increased with CIM treatment and decreased with co-treatment with primidone and isosakuranetin within the pathways for glycolysis and TCA cycle; n= 3-4 replicate cultures.

3.9 Supplementary figures

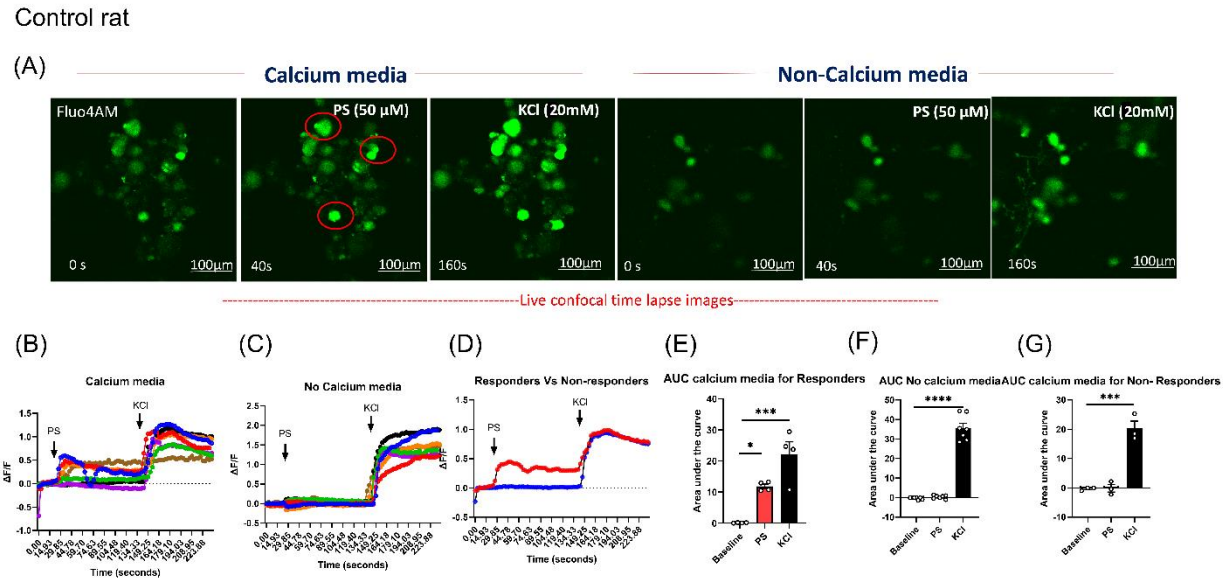

Figure 3.S1. Effect of PS on Ca^{2+} influx in cultured adult rat DRG neurons. Intracellular Ca^{2+} was detected using fluo-4AM in DRG neurons cultured in the presence of low dose neurotrophic factors for 1 day. **(A)** shows the time course of images taken in the presence of Ca^{2+} media and non-Ca^{2+} media after the addition of 50 µM PS and 20 mM KCl. In **(B)** fluorescence intensity relative to the resting fluorescence intensity in the presence of media containing Ca^{2+}. **(C)** in the presence of non-Ca^{2+} media. In **(D)** the average signal of neurons responding to PS vs the neurons which did not respond to PS in the presence of Ca^{2+} in the media is shown. **(E-G)** bar charts of the area under the curve and quantification of the Ca^{2+} influx relative to baseline in response to 50 µM PS and 20 mM KCl in the presence and absence of Ca^{2+}. Red circles indicate regions of increased fluo-4 Ca^{2+} signal. Values are means ± S.E.M., *p < 0.05, ***p < 0.001, ****p < 0.0001 by one-way ANOVA with Dunnett's *post hoc* test; n= 4(E), 7(F) and 3(G) replicate cultures. Bar = 100µm.

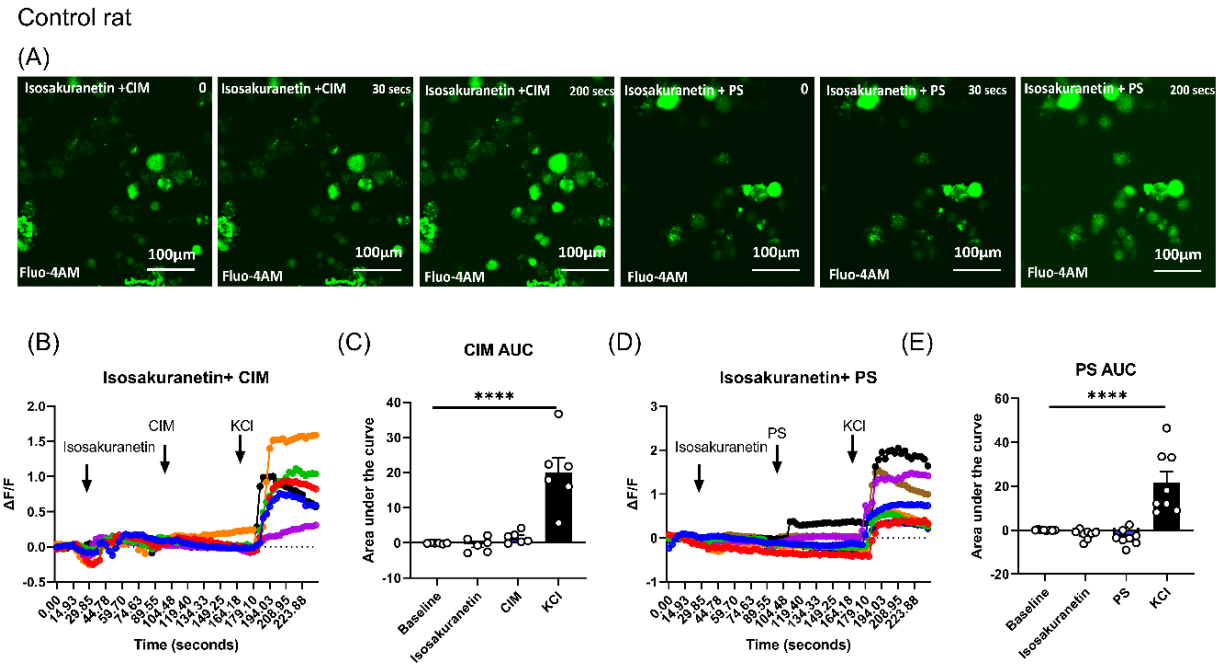

Figure 3.S2. PS and CIM induced Ca^{2+} influx was abolished by pre-treatment with TRPM3 inhibitor isosakuranetin. In **(A)** time course images are shown with the treatment of inhibitor and CIM/ PS followed by KCl. **(B)** Fluorescence intensity relative to the resting fluorescence intensity of DRG neurons treated with isosakuranetin (100 µM), followed by 25 µM CIM and lastly 20 mM KCl. In **(C)** bar charts of the area under the curve for Ca^{2+} influx presented relative to baseline. In **(D)** neurons were treated with primidone (100 µM), followed by 50 µM PS and lastly 20 mM KCl. In **(E)** bar charts of the area under the curve for Ca^{2+} influx. Values are means ± S.E.M., ****$p < 0.0001$ by one-way ANOVA with Dunnett's *post hoc* test; n =6-8 replicate cultures. Bar = 100µm.

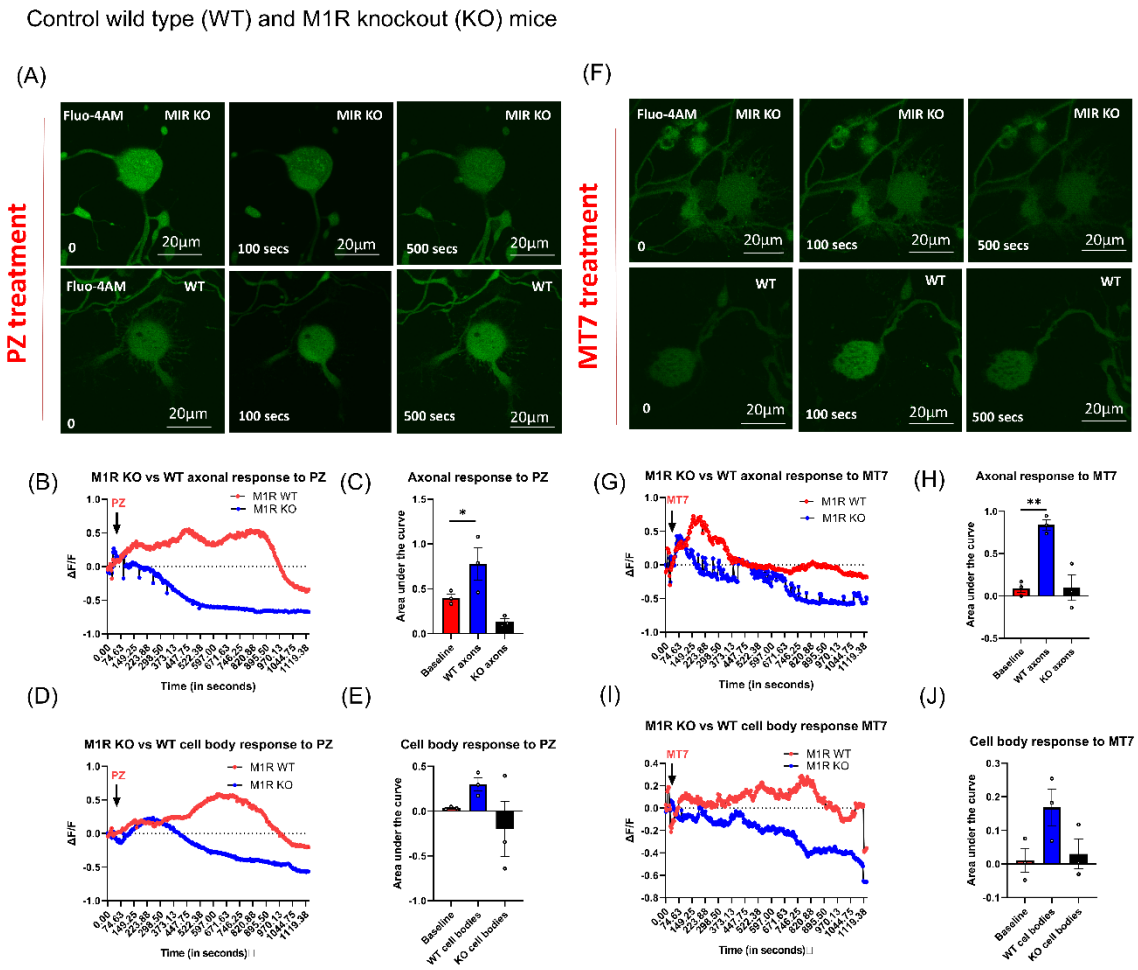

Figure 3.S3: PZ- and MT7-induced Ca^{2+} influx in M_1R KO and WT mice. Intracellular Ca^{2+} was detected using fluo-4AM in cultured DRG neurons derived from M_1R KO or WT mice in the presence of low dose neurotrophic factors for 2 days. **(A)** time course of images showing Ca^{2+} uptake by axons and cell bodies after the addition of PZ (30µM), **(F)** time course of images showing Ca^{2+} uptake by axons and cell bodies after the addition of MT7 (100nM), **(B)** average signals of neuronal axons responding to PZ in WT or M_1R KO cultures in the presence of Ca^{2+}, **(C)** quantification of the Ca^{2+} influx specific to axons in M_1R KO cultures compared to WT cultures in response to PZ. **(D)** average signals of neuronal cell bodies responding to PZ in WT or M_1R KO cultures in the presence of Ca^{2+}, **(E)** quantification of the Ca^{2+} influx specific to neuronal cell bodies in M_1R KO cultures compared to WT cultures in response to PZ. **(G)** average

signals of neuronal axons responding to MT7 in WT or M_1R KO cultures in the presence of Ca^{2+}, **(H)** quantification of the Ca^{2+} influx specific to axons in M_1R KO cultures compared to WT cultures in response to MT7. **(I)** average signals of neuronal cell bodies responding to MT7 in WT or M_1R KO cultures in the presence of Ca^{2+}, **(J)** quantification of the Ca^{2+} influx specific to neuronal cell bodies in M_1R KO cultures compared to WT cultures in response to MT7. Values are means ± S.E.M., *p<0.05, **p< 0.01, by one-way ANOVA with Dunnett's *post hoc* test; n =3 replicate cultures. Bar = 20μm.

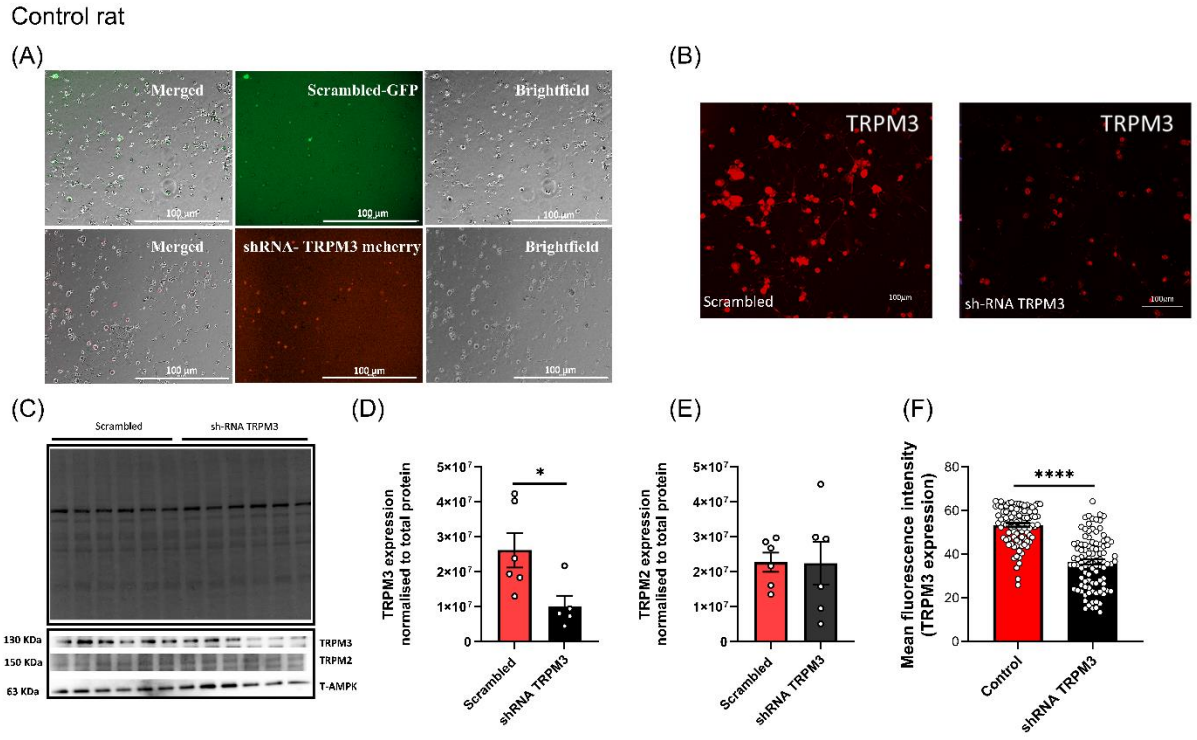

Figure 3.S4. AAV.shRNA-mediated knockdown of TRPM3 *in vitro*. **(A)** shows the transfected cells with scrambled and shRNA TRPM3 (labelling of primary DRGs transduced with AAV.PHP.s-shRNA-scrambled (green) or AAV.PHP.s-shRNA-TRPM3 (red)). **(B)** TRPM3 immunostaining (Cy7) of cells transduced with AAV.PHP.s-shRNA-TRPM3. **(F)** Quantitative analysis was performed to evaluate the TRPM3 expression. **(C-E)** DRG neurons were treated with AAVs and then TRPM3 expression was quantified. **(D and E)** show the downregulated expression of TRPM3 in AAV-shRNA-TRPM3 treated group. Values are means ± S.E.M., *p<0.05, ****p< 0.0001 by one-way ANOVA with Dunnett's *post hoc* test; n =80 (B, F) and 6 (C-E) replicate cultures, Bar = 100µm.

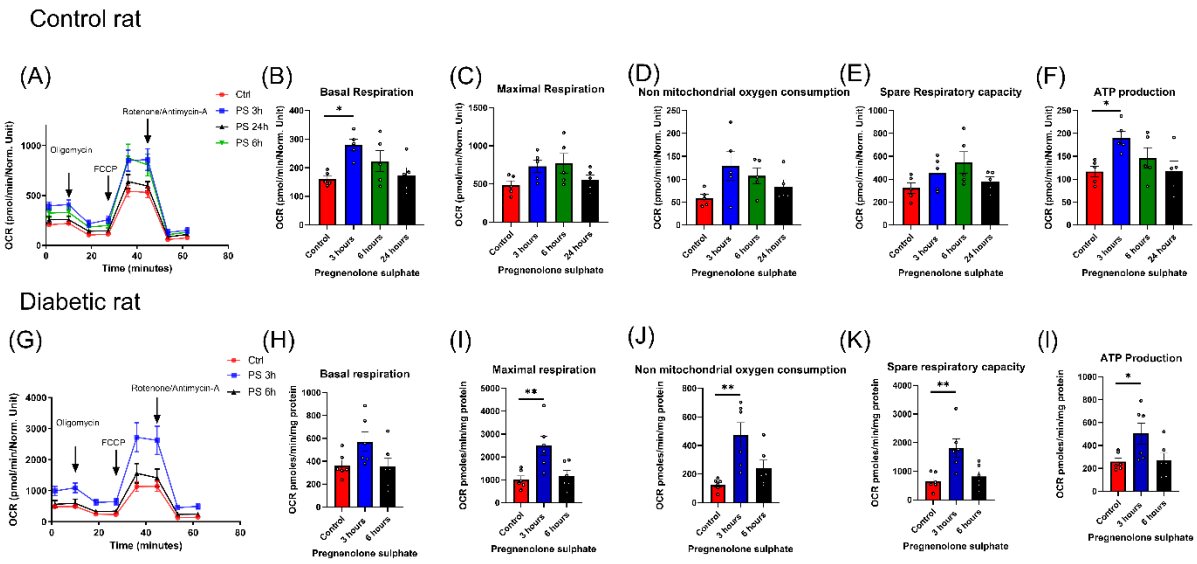

Figure 3.S5. PS enhanced mitochondrial function in cultured DRG neurons derived from age matched control or STZ-induced diabetic rats. DRG cultures were grown under defined conditions in the presence of a low dose cocktail of neurotrophic factors and bioenergetics analysis performed using a XF24 Seahorse machine and oxygen consumption rate (OCR) was assessed. In **(A)** and **(G)** arrows indicate addition of electron transport chain inhibitors and uncoupler. OCR data was normalized to total protein concentration in mg. Cultures were treated sequentially with oligomycin (1 μM), followed by FCCP (1 μM) and rotenone/antimycin A (each 1 μM). In **(A-F)** a control rat DRG culture and **(G-L)** diabetic rat DRG culture were treated with 1 μM PS at different time points. Values are means ± S.E.M., *p<0.05 **p<0.01, by one-way ANOVA with Dunnett's *post hoc* test; n=5-7 replicate cultures.

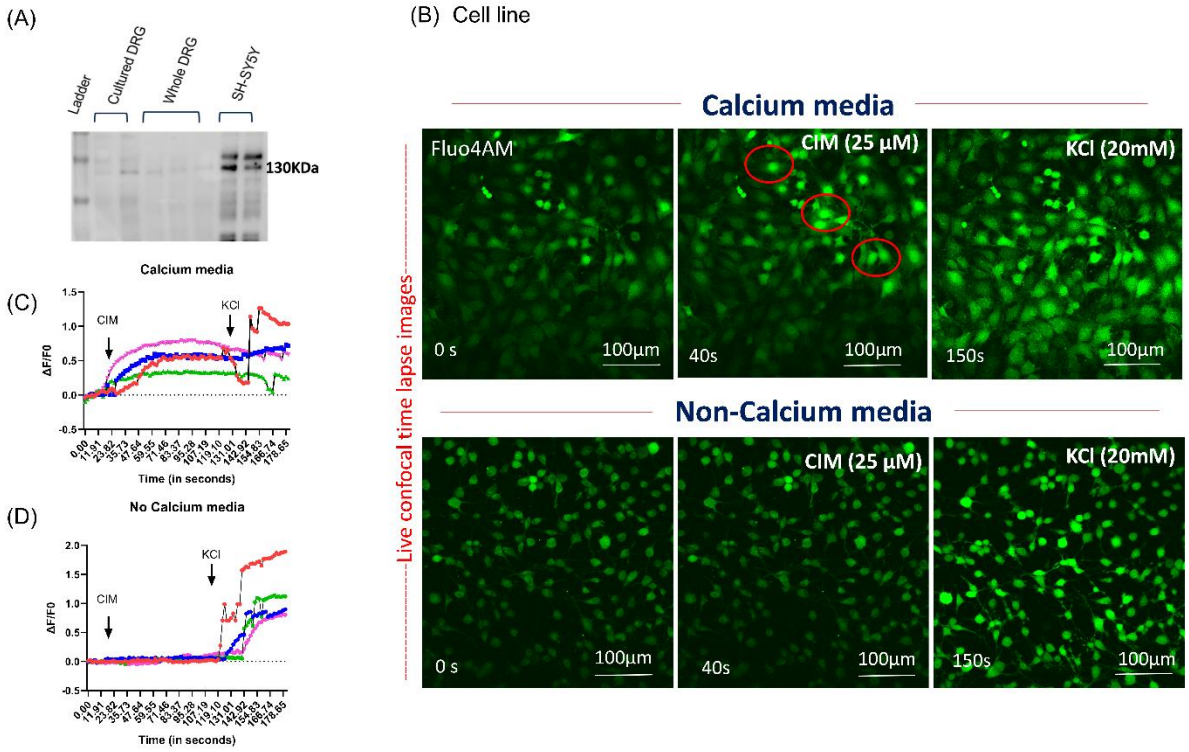

Figure 3.S6. TRPM3 expression and effect of CIM on Ca^{2+} influx in SH-SY5Y cells. **(A)** blot showing TRPM3 expression in DRG neurons and SH-SY5Y cells. Intracellular Ca^{2+} was detected using fluo-4AM in SH-SY5Y cells. **(B)** shows the time course of images taken in the presence of Ca^{2+} media and non-Ca^{2+} media after the addition of 25 µM CIM and 20 mM KCl. In **(C)** the average fluorescence intensity of the cells responding to CIM in the presence of media containing Ca^{2+}, **(D)** in the presence of non-Ca^{2+} media. Red circles indicate regions of increased fluo-4 Ca^{2+} signal. Data in (C) and (D) is presented as change in average intensity of Ca^{2+} signal in multiple ROIs from 4 replicate wells. Bar = 100µm.

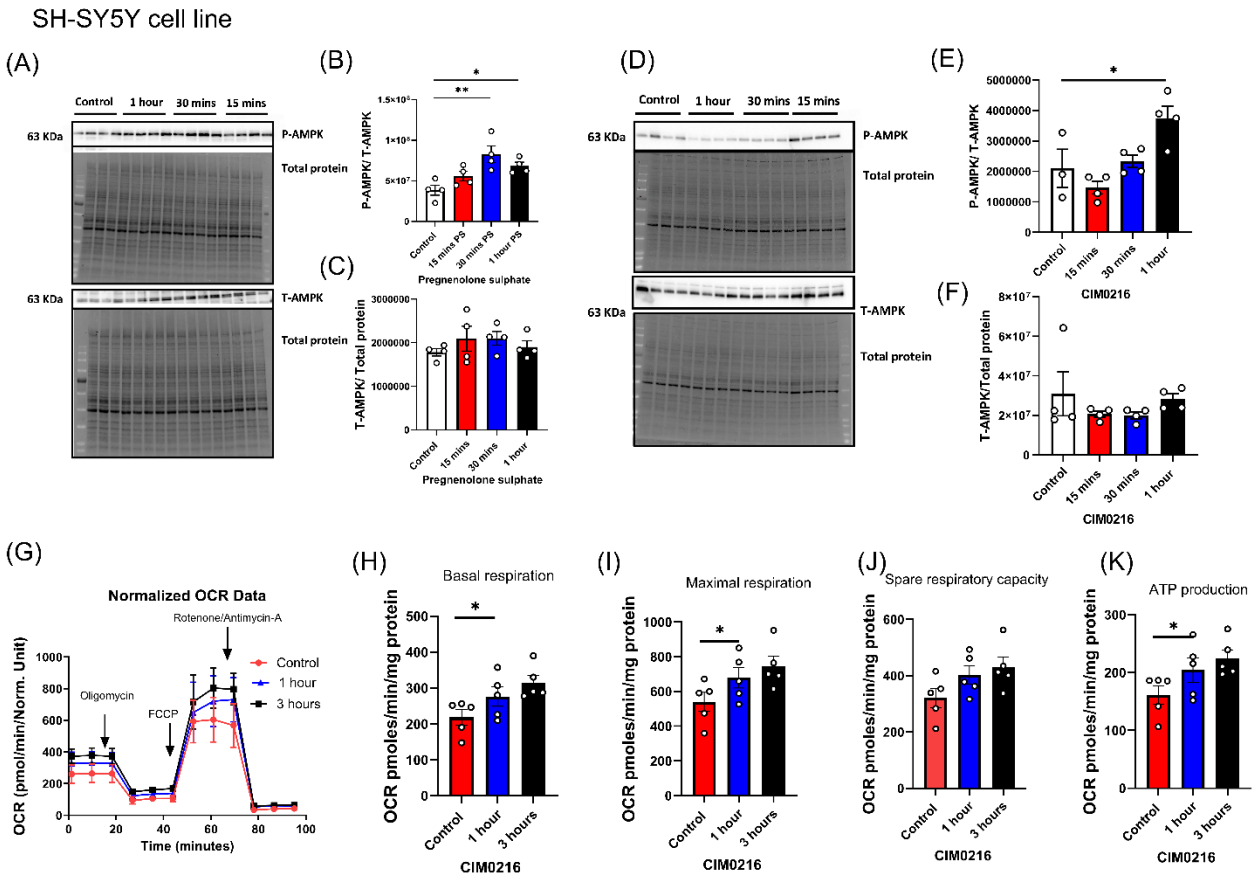

Figure 3.S7. **Effect of TRPM3 agonists on AMPK phosphorylation in SH-SY5Y cells**. In **(A and D)** total protein blots are shown. **(B)** represents the effect of 1 μM PS on P-AMPK normalized to T-AMPK, **(C)** shows the T-AMPK levels normalized to total protein in the presence of PS. **(E)** P-AMPK signal is presented normalized to T-AMPK, **(F)** T-AMPK is presented relative to total protein on the blot in the presence to 1 μM CIM. **(G-K)** Effect of CIM on mitochondrial function in SH-SY5Y cell line. Cells were plated and after 4 hours of serum starvation, bioenergetics analysis was performed using a XF24 Seahorse machine and OCR was assessed. In **(G)** arrows indicate addition of electron transport chain inhibitors and uncoupler. In **(H-K)** OCR measurements are presented as basal respiration, maximal respiration, spare respiratory capacity, and ATP production where cells were treated with 1 μM CIM at different time points. Values are means ± S.E.M., *p<0.05, **p<0.01, by one-way ANOVA with Dunnett's post hoc test; n=4-6 replicate cultures.

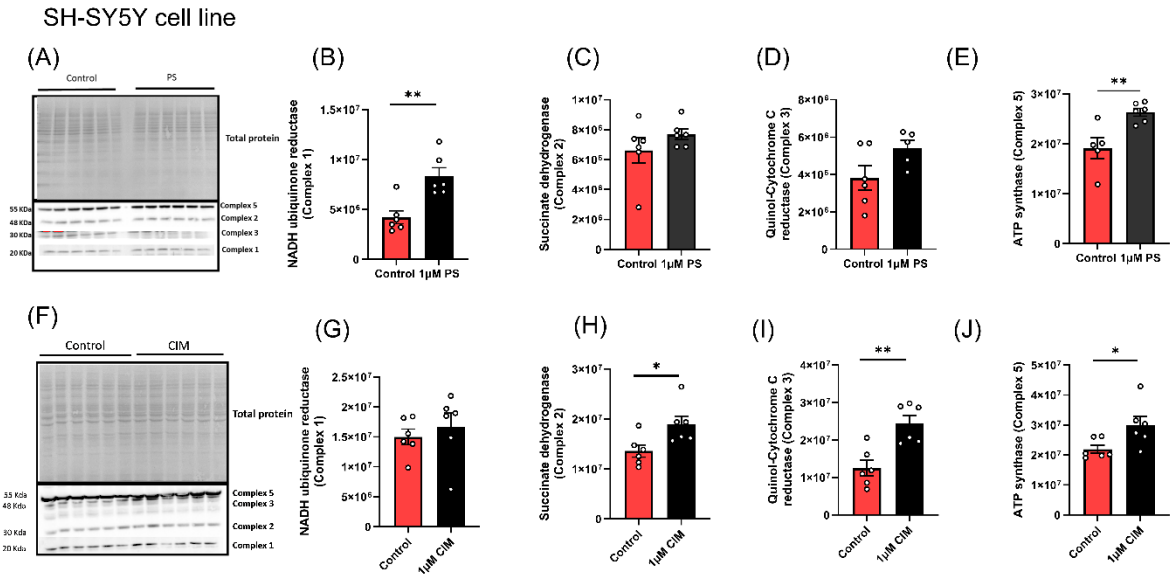

Figure 3.S8. Effect of PS and CIM treatment on the expression of mitochondrial respiratory chain proteins in SH-SY5Y cells. The expression levels of mitochondrial respiratory chain proteins including NADH ubiquinone reductase (Complex I), succinate dehydrogenase (Complex II), quinol-cytochrome c reductase (Complex III), cytochrome C oxidase (Complex IV) and ATP synthase (Complex V) were quantified using Western blotting. The protein bands were normalized to total protein blots. In **(A-E)** SH-SY5Y cells were treated with PS (1 μM) for 8 hours. In **(F-J)** SH-SY5Y cells were exposed to 1 μM CIM. Values are means ± S.E.M., *p<0.05 **p<0.01, by one-way ANOVA with Dunnett's *post hoc* test; n=6 replicate cultures.

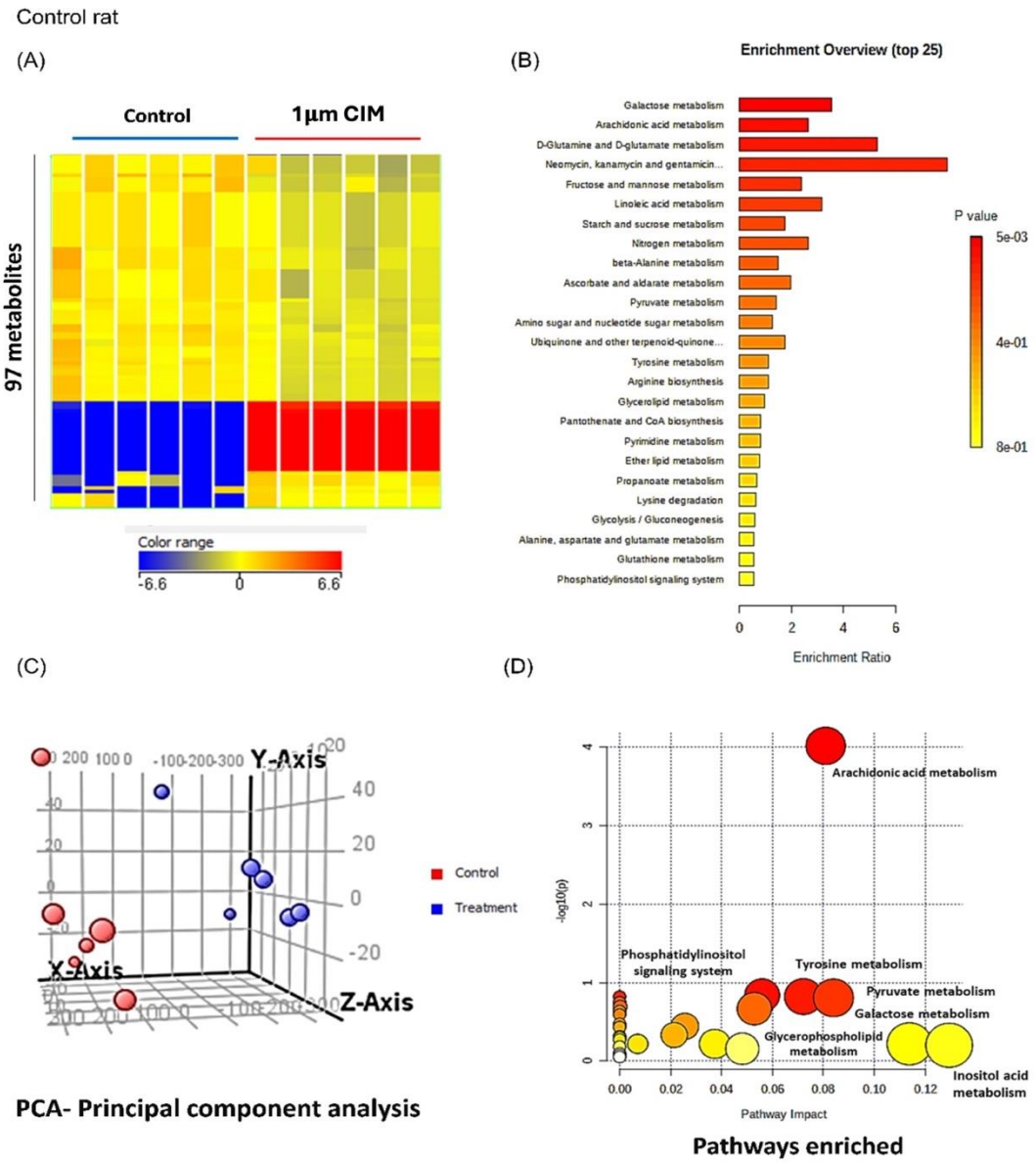

Figure 3.S9. Untargeted metabolomics in DRG neurons derived from control rat. DRG neurons were isolated from control rats and treated with 1 µM CIM for 3 hours. **(A)** Heatmap representing the significant effect of CIM. Each row represents a metabolite (total of 97 significant metabolites after statistical analysis; t-test; $p < 0.05$; Bonferroni FWER). **(B)** Enrichment analysis for the significantly affected metabolites, **(C)** principal component analysis (PCA) of detected metabolites. Each circle represents an individual sample and **(D)** pathway analysis of the enriched metabolites showing significantly affected metabolites. n= 6 replicate cultures.

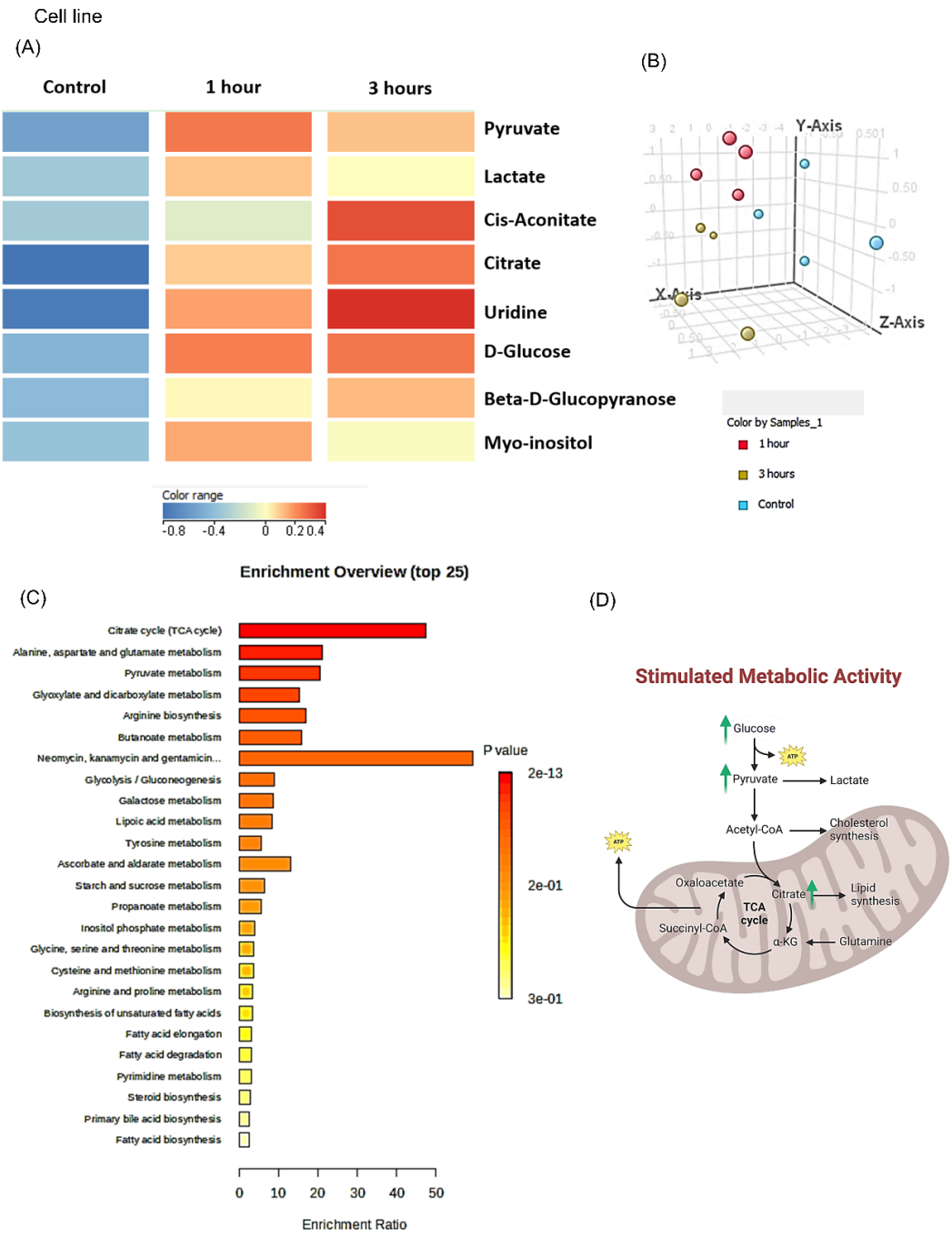

Figure 3.S10. Targeted metabolomics in human neuroblastoma SH-SY5Y cells treated with 1 µM CIM. (A) Shows heatmap representing the significant effect of CIM on metabolic activity. The metabolites from the TCA cycle and glycolysis were targeted; each row represents a metabolite after statistical analysis; one-way ANOVA; $p < 0.05$; Bonferroni FWER, **(B)** partial least square (PLS) of detected metabolites **(C)** enrichment analysis for the significantly affected metabolites, and **(D)** shows metabolites that were

significantly increased with CIM treatment within the pathways for glycolysis and TCA cycle; n= 4 replicate cultures.

3.10 Supplementary tables

Table 3.S1. The concentrations of the calibration standards were measured in µg/mL. Stock solutions of fumarate, malate, lactate, and α-ketoglutarate were individually prepared in methanol, whereas stock solutions of all other compounds were prepared in water at a concentration of 1 mg/mL. A cocktail solution was created by combining all the stock solutions. Working standard solutions were then obtained through serial dilutions of the cocktail solution using methanol. Calibration standards were prepared by spiking the treated matrix with appropriate amounts of the working standard solutions at eight different concentration levels, as detailed in ***Xu, Jia et al***. *"An optimized analytical method for cellular targeted quantification of primary metabolites in tricarboxylic acid cycle and glycolysis using gas chromatography-tandem mass spectrometry and its application in three kinds of hepatic cell lines." Journal of pharmaceutical and biomedical analysis vol. 171 (2019): 171-179. doi:10.1016/j.jpba.2019.04.022.*

Analyte	A	B	C	D	E	F	G	H
Pyruvate	5	2.5	1.25	0.625	0.312	0.156	0.0781	0.0391
Lactate	40	20	10	5	2.5	1.25	0.625	0.312
Succinate	20	10	5	2.5	1.25	0.625	0.312	0.156
Fumarate	3	1.5	0.75	0.375	0.188	0.0938	0.0469	0.0234
Malic acid	5	2.5	1.25	0.625	0.312	0.156	0.0781	0.0391
α-Ketoglutarate	10	5	2.5	1.25	0.625	0.312	0.156	0.0781
PhosphoenolPyruvate	3	1.5	0.75	0.375	0.188	0.0938	0.0469	0.0234
Cis-Aconitase	3	1.5	0.75	0.375	0.188	0.0938	0.0469	0.0234
3-Phosphoglycerate	5	2.5	1.25	0.625	0.312	0.156	0.0781	0.0391
Citrate	10	5	2.5	1.25	0.625	0.312	0.156	0.0781
Iso-Citrate	5	2.5	1.25	0.625	0.312	0.156	0.0781	0.0391
Glucose	80	40	20	10	5	2.5	1.25	0.625

Table 3.S2. Experimental conditions of the optimized GC–MS/MS method for the selected targeted compounds. The optimized parameters and retention time of each compound were summarized (T) using the quantifying ion (Q1- precursor ion and Q2- daughter ion) and collision energy (CE) parameters taken from the reference: **Xu, Jia et al**. "*An optimized analytical method for cellular targeted quantification of primary metabolites in tricarboxylic acid cycle and glycolysis using gas chromatography-tandem mass spectrometry and its application in three kinds of hepatic cell lines." Journal of Pharmaceutical and Biomedical Analysis (2019) 171: 171-179. doi:10.1016/j.jpba.2019.04.022.* The selection of Q1 and Q2 ensures high sensitivity and specificity in multiple reaction monitoring (MRM) mode, enhancing the method's performance. Retention times were optimized for precise compound identification, minimizing peak overlap and improving quantification accuracy.

Compounds	T (min)	Q1	Q3	CE
Pyruvate	4.14	174.1	74.1	14
Lactate	4.23	191.2	147.1	8
Succinate	5.98	147.1	73.1	14
Fumarate	6.19	245.1	73.1	18
Malate	7.15	233.1	73.1	10
α-Ketoglutarate	7.68	198.1	73.1	12
PEP	7.86	369.1	147.1	16
Cis-aconitate	8.66	229.1	147.1	10
3-phosphoglycerate	9.05	227.1	211.1	8
Citrate	9.1	273.1	73.1	18
Iso-citrate	9.11	245.1	73.1	16
Glucose	9.68	319.2	73.1	18
IS	9.16	119.1	75	10

Chapter 4

In vivo evaluation of TRPM3 channel dependency in M_1R antagonism-mediated neuroprotection in diabetic sensorimotor polyneuropathy

Sanjana Chauhan[1,2], Maria Rodriguez[3], Alireza Tayarani[3], Lucie Guernsey[3], Corinne G Jolivalt[3], Nigel A Calcutt[3] and Paul Fernyhough[1,2*]

Manuscript under preparation. A part of in-vivo study will be performed again and submitted to journal for publication.

1) Division of Neurodegenerative Disorders, St. Boniface Hospital Albrechtsen Research Centre, University of Manitoba, Winnipeg, Canada. 2) Department of Pharmacology and Therapeutics, Max Rady College of Medicine, Rady Faculty of Health Sciences, University of Manitoba, Winnipeg, Canada. 3) Department of Pathology, University of California San Diego, La Jolla, CA, USA.

*** Corresponding author:**
Dr. Paul Fernyhough,
Professor, Department of Pharmacology & Therapeutics,
Rady Faculty of Health Sciences, University of Manitoba,
Director, Division of Neurodegenerative Disorders,
St. Boniface Hospital Albrechtsen Research Centre,
R4046 – 351 Tache Avenue,
Winnipeg, Manitoba, R2H 2A6, Canada.
E-mail: pfernyhough@sbrc.ca

4.1 Introduction

Diabetic sensorimotor polyneuropathy (DSPN) is a prevalent and debilitating complication of diabetes mellitus, characterized by a progressive "dying-back" degeneration of distal axons in the peripheral nervous system (Feldman *et al.*, 2019). This axonopathy primarily affects the distal extremities, leading to significant sensory loss and chronic neuropathic pain. A similar pattern of axonal degeneration is observed in other peripheral neuropathies, such as chemotherapy-induced peripheral neuropathy (CIPN) and HIV-associated distal symmetric polyneuropathy, underscoring a shared vulnerability of peripheral neurons to metabolic and toxic insults (Bennett *et al.*, 2014; Cashman and Höke, 2015). Despite advances in glycemic management, the incidence and progression of DSPN remain challenging to mitigate due to the multifactorial pathophysiology and the absence of reliable, early-stage biomarkers to detect and track disease progression. Mitochondrial dysfunction in sensory neurons has been identified as a key driver of axonal degeneration, contributing to metabolic energy deficits, oxidative stress, and impaired axonal transport (Chowdhury *et al.*, 2013). Therefore, therapeutic strategies aimed at ameliorating mitochondrial impairments hold significant promise in addressing both neurodegenerative and neuropathic pain components of DSPN. Previous studies from our group have demonstrated that adult sensory neurons experience metabolic constraints mediated by activation of the muscarinic acetylcholine type 1 receptor (M_1R) (Sabbir *et al.*, 2018). However, M_1R signaling itself does not directly contribute to the underlying pathology of neuropathies such as DSPN, CIPN, or HIV-associated neuropathy. Interestingly, pharmacological inhibition of M_1R has demonstrated remarkable neuroprotective and regenerative properties.

Earlier findings from our research group revealed that M_1R antagonists such as pirenzepine (PZ) and muscarinic toxin 7 (MT7) trigger the activation of the AMP-activated protein

kinase/peroxisome proliferator-activated receptor gamma coactivator 1-alpha (AMPK/PGC-1α) signaling axis (Calcutt *et al.*, 2017; Saleh *et al.*, 2020). This cascade enhanced mitochondrial bioenergetics and promoted neurite outgrowth, offering a pathway to neuronal resilience. In rodent models of diabetic neuropathy PZ treatment effectively prevented and even reversed key pathological features of neuropathy by promoting axonal repair (Calcutt *et al.*, 2017). Subcutaneous administration of the M_1R antagonist oxybutynin significantly improved tactile and thermal sensory deficits in the STZ-induced type 1 diabetic mouse model, while topical applications of MT7 and oxybutynin restored corneal nerve fiber density and mitigated intraepidermal nerve fiber (IENF) loss in human diabetic subjects (Casselini *et al.*, 2024). The diabetic patients after 5 months of topical oxybutynin treatment demonstrated significant increases in IENF density, reduced neuropathic pain, and improved quality-of-life scores, reinforcing the therapeutic potential of M_1R antagonism in diabetic neuropathy. In a murine model of oxaliplatin-induced chemotherapy-induced peripheral neuropathy (CIPN), topical MT7 treatment effectively reversed corneal nerve fiber loss, suggesting its broader application in preserving small fiber integrity (Saleh *et al.*, 2020). Similarly, in the doxycycline-inducible HIV-TAT transgenic mouse model, systemic administration of PZ preserved corneal nerve density and prevented both tactile and thermal deficits by counteracting mitochondrial dysfunction induced by TAT expression (Han *et al.*, 2021). These restorative effects prompted further investigation into the underlying mechanisms driving this neuroprotection. Recent *in vitro* findings from our lab identified the transient receptor potential melastatin-3 (TRPM3) channel as a critical mediator of M_1R antagonist-induced neuroprotection (Chauhan *et al.*, 2025). TRPM3 channels, expressed on dorsal root ganglion (DRG) sensory neurons, are key regulators of nociceptive signaling, responding to noxious heat and chemical stimuli (Vriens *et al.*, 2011). Activation of TRPM3 channels facilitated

calcium influx, enhanced mitochondrial respiration, stimulated AMPK signaling, and promoted neurite outgrowth in DRG sensory neurons (Chauhan *et al.*, 2025). Crucially, pharmacological inhibition or genetic silencing of TRPM3 completely nullified the neuroprotective effects of M_1R antagonists. This finding highlights TRPM3 as an essential driver of the regenerative response elicited by M_1R blockade. Building upon these mechanistic insights, the present study sought to evaluate the *in vivo* dependency of M_1R antagonist-mediated neuroprotection on TRPM3 channel activity in a murine model of diabetic neuropathy. Utilizing a streptozotocin (STZ)-induced type 1 diabetes mouse model, we administered daily topical (to the cornea) or subcutaneous treatments of the M_1R antagonist PZ alongside TRPM3 antagonists- primidone and isosakuranetin over a 16-week period. Sensory and functional outcomes were assessed through tactile and thermal nociception tests, motor nerve conduction velocity (MNCV) measurements, and quantification of corneal nerve fiber density. Our results demonstrated that inhibition of TRPM3 channels negates the neuroprotective efficacy of M_1R antagonism in diabetic neuropathy, as evidenced by exacerbated sensory impairments. These findings suggest that TRPM3 channel activity plays a crucial role in mediating the protective effects of M_1R antagonism, and its inhibition disrupts key mechanisms underlying sensory and functional preservation in diabetic neuropathy.

4.2 Results

4.2.1 Effect of PZ treatment combined with TRPM3 inhibition on tactile sensitivity

At 4 weeks post-STZ induction, diabetic mice treated with vehicle control exhibited early signs of mechanical allodynia, as evidenced by a mild reduction in paw withdrawal threshold (PWT) compared to non-diabetic controls (Figure 4.1B). This observation aligns with previous studies demonstrating early-onset tactile hypersensitivity in diabetic neuropathy due to peripheral nerve

dysfunction (Calcutt *et al.*, 1996; Jolivalt *et al.*, 2016; Lee-Kubli *et al.*, 2014) . Given that PZ has been reported to require approximately 8 weeks of treatment to exert its therapeutic effects, no significant improvements in PWT (Figure 4.1B) were observed with topical administration at this early time point (Jolivalt *et al.*, 2022). However, co-treatment with the TRPM3 inhibitors primidone and isosakuranetin resulted in an increase in PWT, suggesting an early modulatory effect on mechanical hypersensitivity in STZ-induced neuropathy (Figure 4.1B). Additionally, subcutaneous administration of PZ (Figure 4.1E) introduced greater variability, suggesting inconsistencies in systemic absorption or distribution, which rendered it an unsuitable approach for preventive therapy during the early stages of diabetic neuropathy. At 8 weeks, vehicle-treated diabetic mice (STZ group) exhibited a transient increase in 50% PWT, indicating reduced tactile sensitivity (hypoalgesia) (Figure 4.2B). However, previous studies have demonstrated that tactile allodynia typically emerges within 2–4 weeks post-STZ injection and persists into late stages (≥16 weeks) due to progressive peripheral nerve damage and chronic neuroinflammation (Agarwal *et al.*, 2018). Thus, the observed increase in PWT at 8 weeks in the STZ group likely reflects a temporary shift in disease course, indicative of delayed neuropathic progression rather than a true reduction in pain sensitivity. Consequently, this complicates the interpretation of PZ's effects, as the apparent decrease in PWT in the PZ-treated STZ group may not necessarily indicate a protective effect. Similarly, the effects on PWT observed with primidone and isosakuranetin co-administration (Figure 4.2B,E) cannot be conclusively attributed to the induction of mechanical allodynia, given the underlying variability and slow progression in the STZ model. By 16-weeks, vehicle-treated diabetic mice (STZ group) displayed a significant reduction in PWT, reinforcing the persistence of mechanical allodynia (Figure 4.3B). In contrast, the control group exhibited the highest PWT values, reflecting intact tactile sensitivity. While this sustained decrease in PWT

suggested heightened pain sensitivity, there was no direct evidence of peripheral nerve fiber loss, as CCM measures remained unchanged (Figure 4.4). Instead, this was likely driven by maladaptive central mechanisms in the spinal dorsal horn. One key mechanism involves a pathological shift in GABAergic (Gamma-aminobutyric acid) signaling. Under normal conditions, GABA acts as an inhibitory neurotransmitter, but in diabetic models, its function can become excitatory due to the downregulation of the potassium-chloride co-transporter KCC2. This reduction in KCC2 expression disrupts chloride homeostasis, leading to increased intracellular chloride levels. As a result, activation of GABA-A receptors depolarizes rather than inhibits neurons, promoting pain hypersensitivity and contributing to the maintenance of allodynia (Jolivalt *et al.*, 2008). Interestingly, diabetic mice treated with PZ (topical and subcutaneous) exhibited an increase in PWT compared to the untreated STZ group, with subcutaneous administration resulting in a more pronounced improvement, supporting its long-term neuroprotective potential (Figure 4.3B, 4.3E). However, co-administration of TRPM3 inhibitors, isosakuranetin and primidone (Figure 4.3B) did not significantly alter the PZ mediated effects. Notably, when PZ was co-administered with primidone subcutaneously (Figure 4.3E), the PZ mediated PWT improvements were attenuated (but not statistically significant), suggesting that TRPM3 channels play a role in mediating M_1R antagonism-driven neuroprotection.

4 weeks data

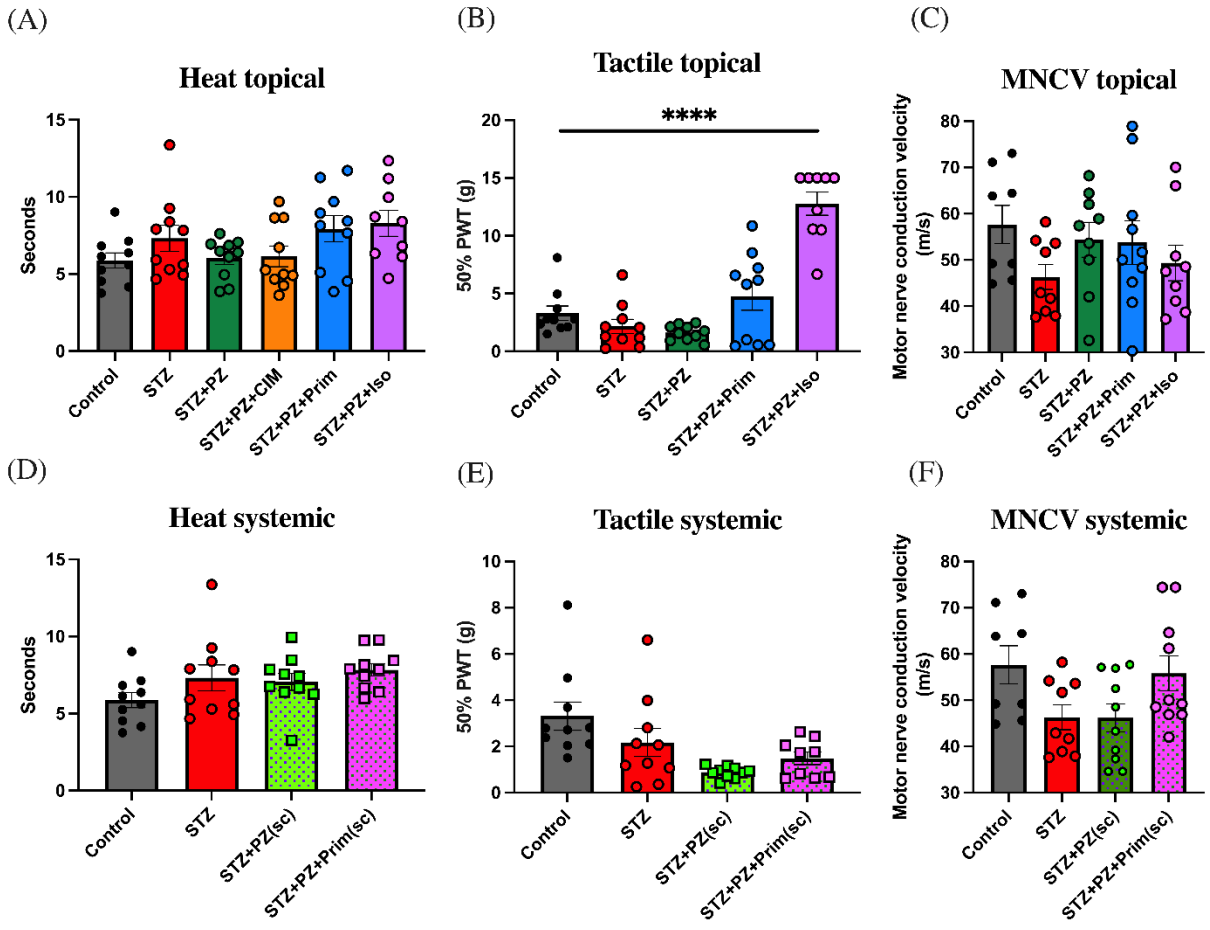

Figure 4.1. Effect of TRPM3 inhibitors on PZ induced protection against neuropathy in early stages of neuropathy development. (A,D) Paw withdrawal latency in response to heat using the Hargreaves apparatus, (B,E) Paw withdrawal frequencies to mechanical stimulation with von Frey filament test and (C,F) motor nerve conduction velocity measured after 4 weeks of diabetes, with daily topical drug treatment to the left eye with either vehicle (saline-25 µl), PZ (25 µl of 20 mg/ml) and isosakuranetin (25µl of 1µg dose solution) or primidone (25 µl of 1 µg dose solution), subcutaneous (systemic) drug treatment of PZ (10 mg/kg/day) or primidone (1 mg/kg/day). Data points are group mean ± SEM with in-between group analysis (7-10 animals per group) by one-way ANOVA followed by Dunnett's Post hoc test, ****$p < 0.0001$.

4.2.2 Thermal sensitivity in response to PZ and TRPM3 inhibitors

At 4 weeks post-STZ induction, diabetic mice exhibited a mild increase in latency to heat stimuli compared to non-diabetic controls (Figure 4.1A,D), indicating that thermal sensitivity remained largely intact at this stage. Similarly, at 8 weeks, no statistically significant differences in heat sensitivity were observed across all treatment conditions (Figure 4.2A,D). Previous reports suggest that an increase in paw thermal withdrawal latency in STZ-induced diabetic mice typically emerges as early as 4–8 weeks post-induction (Jolivalt *et al.*, 2016; Lee-Kubli *et al.*, 2014). However, in our model, no obvious changes in heat sensitivity were observed at 4 or 8 weeks, indicating a slower progression of neuropathy in this cohort (Figure 4.1A, 4.2A). This is consistent with the gradual development of mechanical allodynia, further supporting the delayed onset of sensory deficits. This slower progression of neuropathy may be attributed to the delayed neurotoxic effects of STZ, leading to an extended timeframe for the onset of fully developed neuropathy. By 16 weeks, clear neuropathic changes were observed in both topical and subcutaneous treatment groups. In the topical treatment group (Figure 4.3A), STZ-induced diabetic mice exhibited increased latency to heat stimuli compared to controls, confirming the progression of diabetic neuropathy. However, unlike previous studies that report earlier onset, thermal insensitivity in our model appears delayed, suggesting a slower disease progression (Beiswenger *et al.*, 2008). PZ treatment effectively reduced latency, indicating restored sensitivity and potential neuroprotection. However, co-administration with primidone (subcutaneously only, Figure 4.3D) and isosakuranetin (topically, Figure 4.3A) attenuated the PZ-mediated effect, with isosakuranetin demonstrating a stronger inhibitory effect, leading to a pronounced increase in latency.

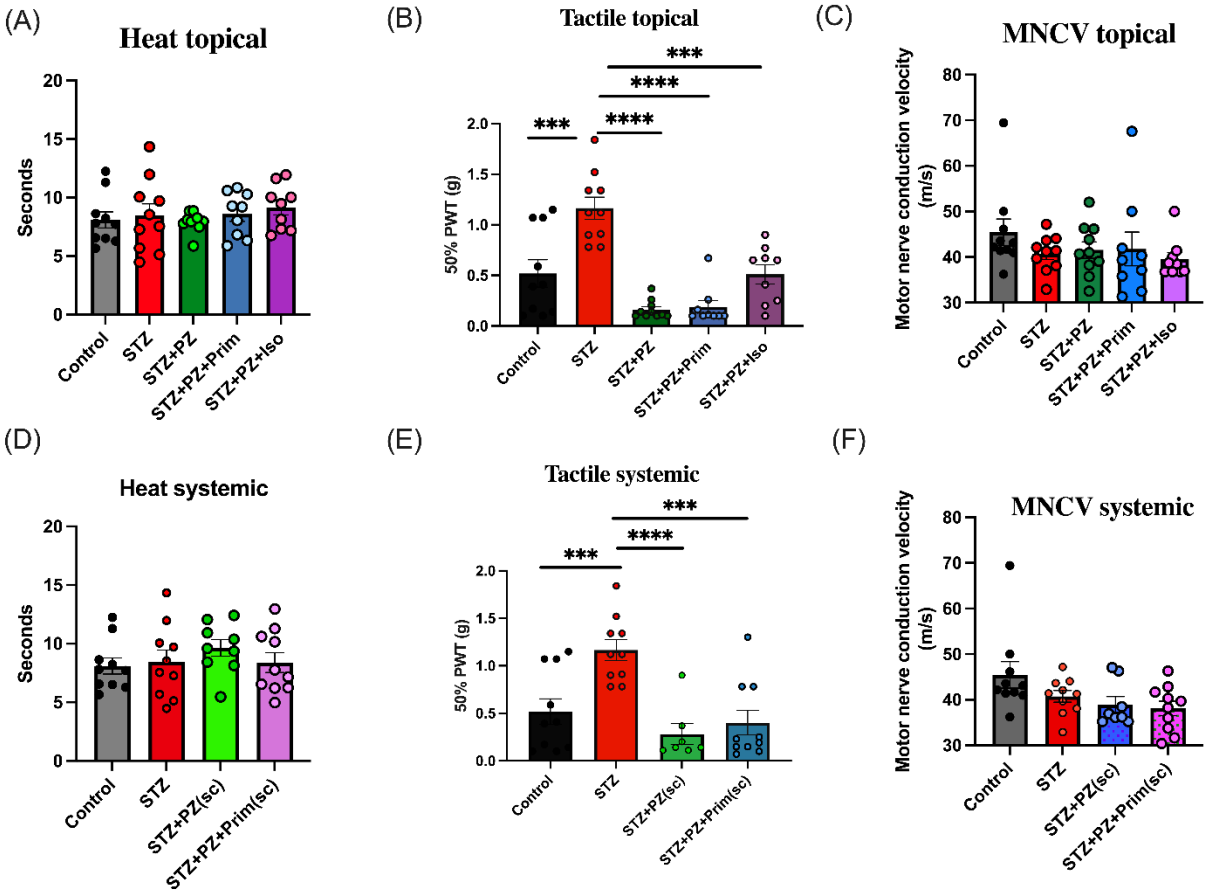

Figure 4.2. TRPM3 inhibition mediated effects on sensory and motor parameters post 8 weeks diabetes. (A,D) Paw withdrawal latency in response to heat using the Hargreaves apparatus, (B,E) Paw withdrawal frequencies to mechanical stimulation with von Frey filament test and (C,F) motor nerve conduction velocity measured after 4 weeks of diabetes, with daily topical drug treatment to the left eye with either vehicle (saline-25 µl), PZ (25 µl of 20 mg/ml) and isosakuranetin (25 µl of 1 µg dose solution) or primidone (25 µl of 1 µg dose solution), subcutaneous (systemic) drug treatment of PZ (10 mg/kg/day) or primidone (1 mg/kg/day). Data points are group mean ± SEM with in-between group analysis (7-10 animals per group) by one-way ANOVA followed by Dunnett's and Tukey's Post hoc test, ***$p < 0.001$, ****$p < 0.0001$.

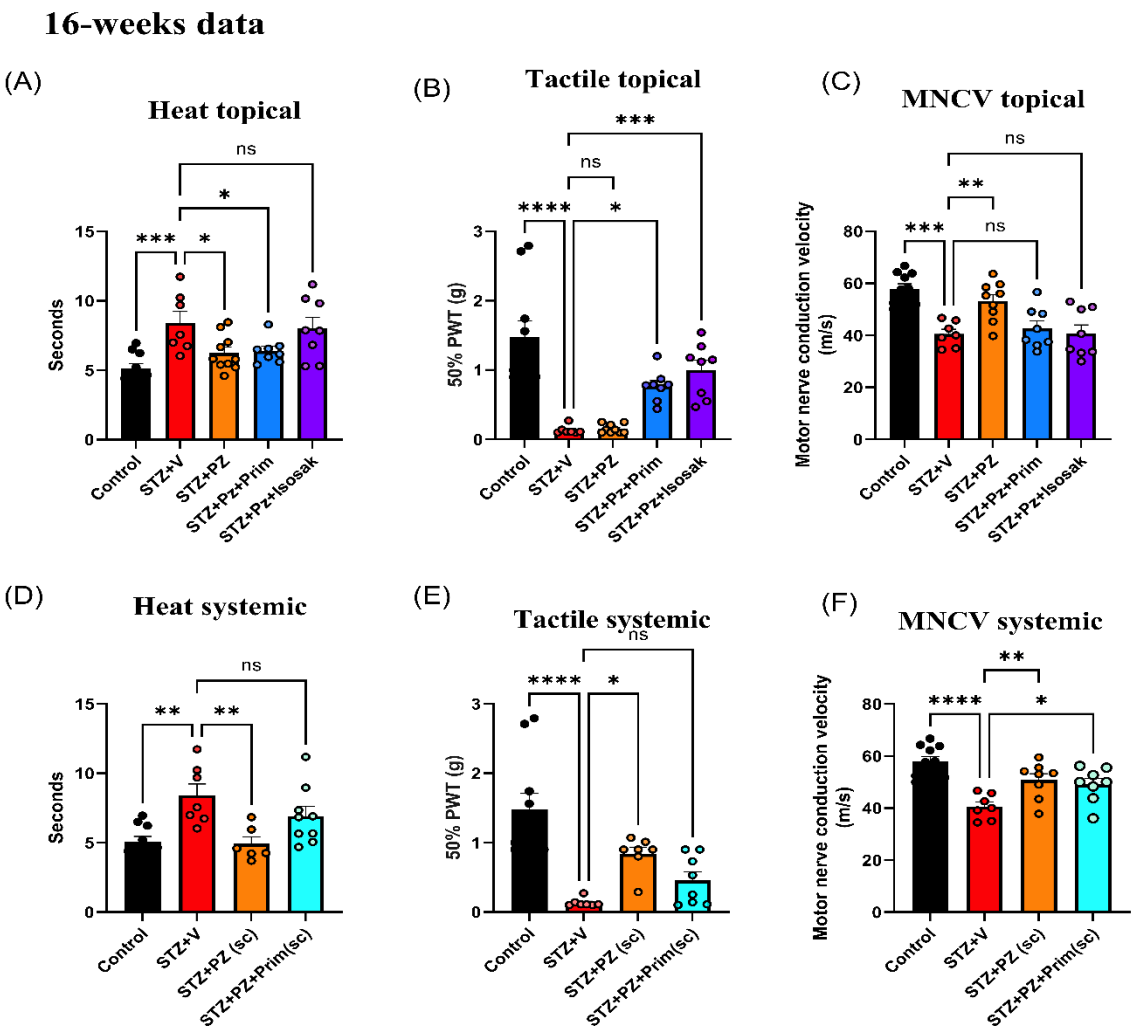

Figure 4.3. TRPM3 inhibition abolished PZ mediated neuroprotective effects post 16 weeks of diabetes. (A,D) Paw withdrawal latency in response to heat using the Hargreaves apparatus, (B,E) Paw withdrawal frequencies to mechanical stimulation with von Frey filament test and (C,F) motor nerve conduction velocity measured after 4 weeks of diabetes, with daily topical drug treatment to the left eye with either vehicle (saline-25 µl), PZ (25 µl of 20 mg/ml) and isosakuranetin (25 µl of 1 µg dose solution) or primidone (25 µl of 1 µg dose solution), subcutaneous (systemic) drug treatment of PZ (10 mg/kg/day) or primidone (1 mg/kg/day). Data points are group mean ± SEM with between group analysis (7-10 animals per group) by one-way ANOVA followed by Dunnett's and Tukey's Post hoc test. *p < 0.05, **p< 0.01, ***p < 0.001 and ns: non-significant.

4.2.3 Impact of PZ and TRPM3 inhibitors on motor nerve conduction velocity in diabetic neuropathy model

At 4 weeks post-STZ induction, motor nerve conduction velocity (MNCV) remained unchanged, showing no statistically significant differences between diabetic and control mice (Figure 4.1C,F). Similarly, at 8 weeks, MNCV remained stable across all treatment groups (Figure 4.2C,F), indicating that motor conduction deficits had not yet emerged. These findings are consistent with the slow progression of neuropathy observed in other sensory assessments, suggesting a delayed onset of nerve dysfunction in this STZ model compared to previously reported models (Jolivalt *et al.*, 2016). Collectively, these results reinforce the notion that the development of neuropathy was gradual in this cohort. By 16 weeks, diabetic mice treated with vehicle exhibited a pronounced decrease in MNCV compared to controls (Figure 4.3C), reflecting the expected progression of diabetic neuropathy. While this outcome aligns with previous studies (Obrosova *et al.*, 2004), neuropathy in this model developed at a slower pace, reinforcing the delayed onset observed in earlier time points. In the topical treatment group, PZ administration resulted in a significant improvement in MNCV (Figure 4.3C). However, the co-administration of TRPM3 inhibitors, primidone and isosakuranetin, attenuated PZ-mediated improvements. Although the reduction in PZ efficacy was not statistically significant, a clear trend toward decreased MNCV was observed, suggesting potential interactions between PZ and TRPM3 modulation. In contrast, subcutaneous administration of PZ resulted in a similar improvement in MNCV (Figure 4.3F), although the co-administration of TRPM3 inhibitors in the subcutaneous group did not significantly alter PZ-mediated improvements, indicating potential differences in pharmacokinetics between the two administration routes.

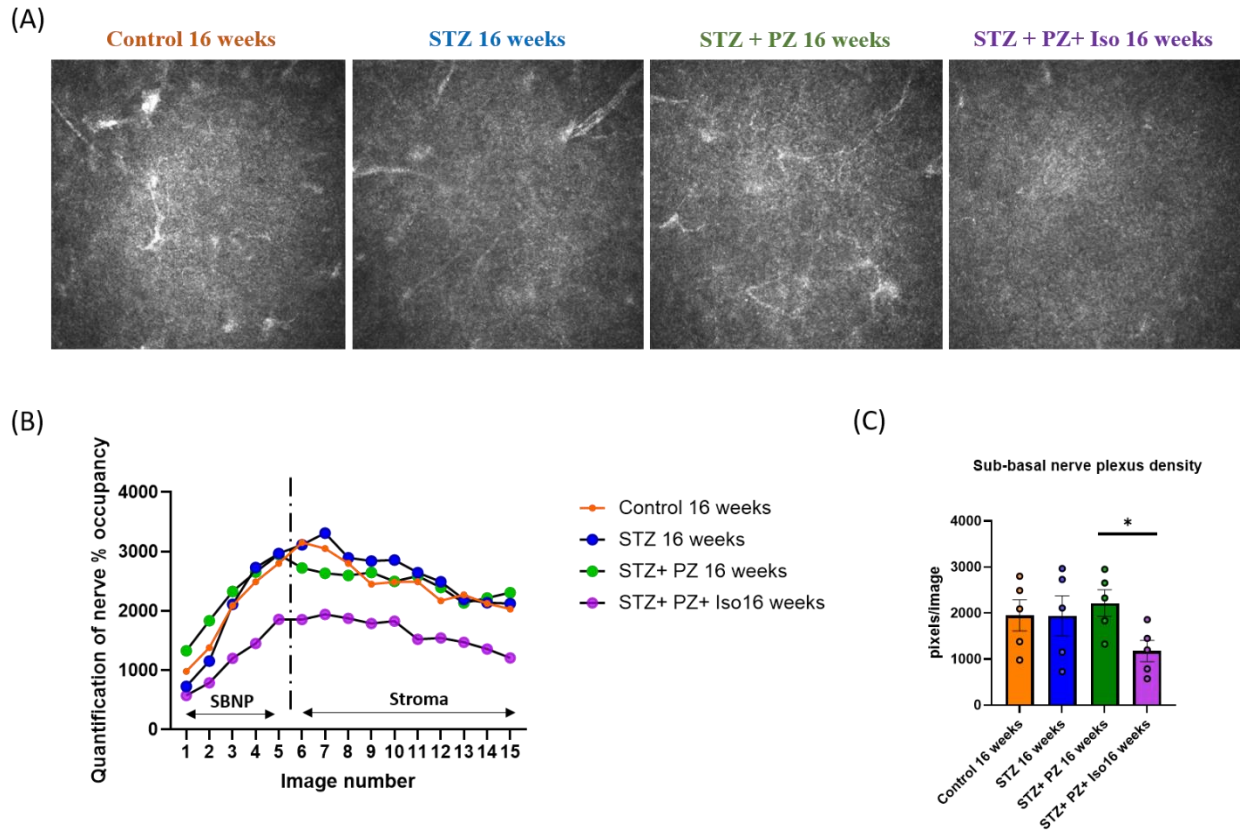

Figure 4.4. Effects of diabetic neuropathy progression on corneal nerve density. (A) Images of the sub-basal nerve plexus captured with Heidelberg Retina Tomograph III Rostock corneal module from the central cornea, (B) time course of sub-basal plexus nerve density (as percentage of occupancy) in mice that received daily eye drops of either vehicle (saline-25 µl), PZ (25 µl of 20 mg/ml) and isosakuranetin (25 µl of 1 µg dose solution) (C) quantification of sub-basal nerve plexus density among different treatment groups. Values are shown as mean ± SEM of n is the average of 5 images of sub-basal nerve plexus density among 7-10 animals each treatment group, *$p < 0.05$ by one-way ANOVA and Tukey's post-hoc test.

4.2.4 Corneal nerve density with disease progression and drug treatments

At baseline, control mice exhibited normal corneal nerve density, indicating healthy small fiber integrity (Figure 4.4A). Surprisingly, no significant progressive decline in corneal nerve density was observed over the 16-week period in STZ-induced diabetic mice compared to control mice

(Figure 4.4B,C). This suggests that while functional deficits such as tactile and thermal sensitivity impairments were present (Figure 4.3), they did not translate into significant structural damage to corneal nerves within this timeframe. PZ did not have any effect on corneal nerve density however TRPM3 inhibitor-isosakuranetin treatment resulted in a significant loss of corneal nerves (Figure 4.4B,C). These results indicated potential role of TRPM3 in maintaining corneal nerve integrity. Future studies should consider extending the duration of observation or utilizing more aggressive diabetic models to better elucidate the relationship between diabetic neuropathy progression and corneal nerve degeneration.

STZ+V	STZ+PZ	STZ+Pz+Prim	STZ+Pz+Isosak	STZ+PZ (sc)	STZ+PZ+Prim(sc)
599	599	599	519	599	119.00*
599	561	599	181.00*	599	379
510	599	599	599	585	147.00*
544	470	599	554	166.00*	406
599	134.00*	599	572	207.00*	408
599	468	599	599	550	591
599	599	599	599	599	599
	542	599	599	599	480
	544		599		465
	575				599

Table 4.1. **Blood glucose levels of experimental mouse groups**: Blood glucose (BG; mg/dL) measurements are shown for all treatment groups (V; vehicle, STZ; streptozotocin, PZ; pirenzepine, prim; primidone, isosak; isosakuranetin, sc; subcutaneous), across the study. BG levels reverted to normoglycemic range in some of the animals (*), indicating failure of sustained diabetic induction. These animals were excluded from analyses where persistent hyperglycemia was a prerequisite.

4.2.5 Body weight and sensorimotor function

Body weight and blood glucose levels were measured at baseline and after STZ injections, as well as following the administration of PZ, primidone, and isosakuranetin treatments to confirm the establishment of diabetes and to monitor potential β-cell regeneration over the course of the study. Consistent with previous reports, long-term STZ-induced diabetes may allow for partial β-cell regeneration, potentially impacting metabolic parameters and disease progression. However, in this study, no significant changes in blood glucose levels were observed following treatment, confirming the sustained diabetic state throughout the experiment. Sensorimotor coordination was assessed using the rotarod test to evaluate motor function in diabetic and non-diabetic control mice. The results showed no significant differences in rotarod performance between STZ-induced diabetic mice and control mice over the first 8 weeks of diabetes progression. Furthermore, daily administration of PZ, isosakuranetin, or primidone for 8 weeks did not result in any detectable improvement or impairment in motor coordination, suggesting that the treatments did not adversely affect motor function. The absence of significant differences persisted over time, with no notable changes in rotarod performance observed in STZ mice treated with vehicle, PZ alone, or in combination with isosakuranetin or primidone. The maintained rotarod performance across all experimental conditions suggests that diabetes-related motor deficits were not severe enough to confound the interpretation of sensory function outcomes.

4.3 Discussion

4.3.1 Topical and systemic treatments

Corneal confocal microscopy (CCM) has emerged as a powerful, non-invasive tool for evaluating small fiber neuropathy in diabetes (Chen *et al.*, 2013; Labbé *et al.*, 2006). The cornea is densely

innervated by small sensory fibers originating from the ophthalmic branch of the trigeminal nerve, making it a unique surrogate marker for systemic neuropathy. Unlike traditional diagnostic methods, which often require invasive skin biopsies or electrophysiological assessments with limited sensitivity to early neuropathic changes, CCM enables high-resolution imaging of corneal nerves with the ability to monitor disease progression and treatment efficacy longitudinally (Tavakoli *et al.*, 2010). Topical ocular administration allows for localized delivery to the cornea while also potentially exerting systemic effects via absorption through the ocular vasculature and trigeminal-autonomic pathways. In line with this, M_1R antagonist MT7, when given topically in rodent models of diabetes, effectively restored the corneal nerve density and enhanced AMPK activation in the ipsilateral trigeminal ganglia indicating a localized but systemically relevant response (Saleh *et al.*, 2020). These findings underscore the potential of corneal treatments to elicit broader neuroprotective effects by initiating signaling cascades at the distal nerve terminals that propagate to neuronal cell bodies, thereby promoting nerve regeneration and functional recovery. Similarly, ocular delivery of neurotrophic factors such as insulin or insulin-like growth factor-1 (IGF-1) not only restored corneal nerve density but also improved thermal hypoalgesia and mechanical allodynia in diabetic rodent models (Aghanoori *et al.*, 2019; Chen *et al.*, 2013).

Despite the promising localized effects of topical treatment, systemic administration remains the widely adopted therapeutic approach. Systemic treatments, such as subcutaneous administration of M_1R antagonists such as PZ, improved multiple indices of neuropathy, including MNCV, thermal sensitivity, and mechanical allodynia (Calcutt *et al.*, 2017). Systemic treatment offers the advantage of addressing generalized neuropathic pathology by enhancing neurotrophic signaling and reducing oxidative stress across multiple nerve territories, providing comprehensive neuroprotection. However, systemic administration often requires prolonged treatment durations

and higher doses to achieve therapeutic efficacy, which can increase the risk of systemic side effects and metabolic interactions that may limit its long-term use. Building on this concept, our study examined the differential impacts of topical ocular versus systemic delivery of the M_1R antagonist- PZ, and its interactions with TRPM3 inhibition in a diabetic neuropathy model.

4.3.2 Development of tactile allodynia

In our study, STZ-induced diabetic mice exhibited a mild reduction in paw withdrawal threshold (PWT), indicative of mechanical allodynia development starting at 4 weeks post-induction. The early decline in PWT at 4 weeks (Figure 4.1B,E) aligns with established findings that highlight the onset of diabetic neuropathy characterized by hyperexcitability of nociceptive pathways, primarily driven by metabolic and oxidative stress-induced sensitization of C-fibers and Aδ fibers (Calcutt and Chaplan, 1997; Jayaraj et al., 2018; Miyashita et al., 2023; Urban et al., 2012). The early phase of hypersensitivity in diabetic neuropathy results from peripheral nerve inflammation, mitochondrial dysfunction, and increased excitatory neurotransmission within the dorsal horn, contributing to exaggerated pain responses to mechanical stimuli (Feldman et al., 2019; Fernyhough and McGavock, 2014; Tesfaye et al., 2005). Interestingly, at 8 weeks post-STZ induction, we observed a transient increase in PWT, suggesting a temporary reduction in tactile sensitivity before a subsequent decline by 16 weeks (Figure 4.2B,E; 4.3B,E). Given that tactile allodynia is well-documented in various diabetic mouse models, including STZ-induced C57Bl/6J, 129S1/SvImJ, and Akita mice, as well as in ob/ob and high-fat diet-fed mice (models of type 2 diabetes and prediabetes), this transient increase in PWT at 8 weeks in the STZ group more likely represents a temporary shift in disease course, indicative of delayed neuropathic progression rather than a true reduction in pain sensitivity (Obrosova, 2009). Similar contradictory findings have been reported in experimental diabetic neuropathy models, where compensatory regenerative

mechanisms such as increased mitochondrial biogenesis, axonal sprouting, and alterations in central pain processing temporarily mask the progressive decline in sensory function (Vincent et al., 2010; Zochodne, 2014). This phenomenon may explain why some studies report reduced tactile sensitivity rather than mechanical allodynia in STZ-diabetic C57Bl/6J and db/db mice, reinforcing the variability in diabetic neuropathy presentations (Obrosova, 2009).

By 16 weeks, the STZ group exhibited a significant decrease in PWT, demonstrating persistent mechanical allodynia despite the absence of detectable peripheral nerve fiber loss (as measured in a surrogate fashion using CCM). The involvement of a central mechanism within the spinal dorsal horn contributes significantly to such sensory deficits. The maladaptive changes in the GABAergic inhibitory system, mediated by potassium-chloride cotransporter 2 (KCC2) downregulation explains the pathophysiology of tactile hypersensitivity in this model (Jolivalt *et al.*, 2008). A key upstream regulator of KCC2 downregulation in neuropathic pain conditions is the brain derived neurotrophic factor (BDNF)- tropomyosin receptor kinase B (TrkB) signaling pathway, which is closely linked to microglial activation (Coull *et al.*, 2005). Following chronic hyperglycemia, spinal microglia become activated, releasing BDNF, which then binds to its receptor TrkB on dorsal horn neurons. This interaction has been shown to suppress KCC2 expression, leading to increased intracellular chloride levels and excitatory GABAergic transmission (Hu *et al.*, 2023). This abnormal shift in GABA signaling leads to increased neuronal excitability, perpetuating the sensory hypersensitivity observed in diabetic neuropathy models. The other pathway that contributes significantly to the development of tactile allodynia is the involvement of C-X-C Motif Chemokine Ligand 12 (CXCL12) / C-X-C chemokine receptor type 4 (CXCR4) signaling axis which acts as critical modulator of neuronal excitability in sodium channel Na_v 1.8-positive DRG neurons (Jayaraj *et al.*, 2018). The binding of CXCL12 to its

receptor CXCR4 enhances neuronal hyperexcitability through increased intracellular calcium influx and functional alterations in Na_v 1.8. These modifications lower the threshold for action potential generation, making nociceptive neurons more responsive to normally non-noxious mechanical stimuli. Additionally, experimental evidence indicates that genetic deletion of CXCR4 in Na_v 1.8-positive neurons prevent the development of mechanical allodynia, further underscoring the role of this pathway in pain sensitization.

Previous studies have demonstrated that M_1R antagonists effectively reverse neuropathic deficits in diabetic models by enhancing mitochondrial function and promoting axonal regeneration (Calcutt *et al.*, 2017; Casselini *et al.*, 2024). However, in the present study, PZ-treated STZ mice when delivered topically (Figure 4.3B) exhibited a partial restoration of tactile sensitivity, as evidenced by a moderate increase in PWT compared to untreated diabetic mice (STZ group) at 16 weeks. Additionally, the subcutaneous group (Figure 4.3E) exhibited a sharper increase in PWT, suggesting that systemic administration may provide broader neuroprotection, possibly due to enhanced bioavailability and distribution across different nerve territories. Isosakuranetin, a potent TRPM3 antagonist, completely abolishes TRPM3 activation and its downstream signaling pathways (Straub *et al.*, 2013). However, in this study, topical treatment of TRPM3 inhibitors failed to suppress TRPM3 activation and instead, when co-administered with PZ, it increased PWT (Figure 4.3B). Conversely, primidone was able to abolish PZ-mediated neuroprotective effects, as evidenced by a reduced PWT in the subcutaneous treatment group (Figure 4.3E). This aligns with previous reports demonstrating that primidone directly inhibits TRPM3 by preventing calcium influx and reducing TRPM3-induced neuronal excitability (Krügel *et al.*, 2017). Tactile measurements in diabetic neuropathy models often yield inconsistent results, influenced by factors such as mouse strain, disease progression, and route of drug administration

(topical vs. systemic). However, in this study, the subcutaneous PZ-treated group provides a more consistent representation of neuropathic pain progression, reinforcing the TRPM3 dependency of PZ-mediated neuroprotection. This finding is consistent with emerging literature demonstrating that TRPM3 channels facilitate calcium influx, mitochondrial ATP production, and neuronal survival, all of which are critical for maintaining peripheral nerve function (Chauhan *et al.*, 2025; Held *et al.*, 2015b; Wang *et al.*, 2022).

4.3.3 Loss of thermal sensitivity

The progressive loss of heat sensation is a well-established hallmark of diabetic neuropathy, primarily attributed to the degeneration of small unmyelinated C-fibers that mediate thermal sensitivity (Boulton *et al.*, 2004). Previous studies have reported that STZ-induced diabetic mice exhibit increased latency to heat stimuli as early as 4–8 weeks post-induction (Jolivalt *et al.*, 2016; Lee-Kubli *et al.*, 2014). However, our study demonstrated a delayed onset, with significant changes in heat latency emerging only at 16 weeks (Figure 4.3A,D), suggesting a slow, plateaued progression of sensory deficits in this cohort. This prolonged trajectory could be attributed to several factors such as variability in STZ potency, potential heterogeneity in metabolic responses and differences in experimental conditions, which can influence diabetes severity and neuropathic progression. Previous work has demonstrated that both structural (IENF loss) and functional (thermal hypoalgesia) indices of small fiber neuropathy present in diabetic rodents were prevented and reversed by antimuscarinic drugs such as PZ and MT7 (Calcutt *et al.*, 2017; Casselini *et al.*, 2024; Saleh *et al.*, 2020). Consistent with these findings, PZ treatment significantly restored thermal sensitivity (Figure 4.3A), suggesting its potential neuroprotective effects in maintaining sensory nerve integrity. Pharmacological blockade of TRPM3 by isosakuranetin and primidone,

effectively abolished the neuroprotective effects of PZ in the topical treatment groups where isosakuranetin showed more pronounced inhibition (Figure 4.3A).

TRPM3 channels are known to play a pivotal role in thermosensation, regulating calcium influx in response to heat stimuli and modulating nociceptive signaling pathways in sensory neurons (Straub *et al.*, 2013; Vriens *et al.*, 2011). This notion is further supported by studies demonstrating that TRPM3 knockout (KO) mice exhibit significant impairments in heat perception. However, it is important to note that these deficits are not necessarily associated with sensory innervation loss, as evidenced by findings in TRPM3, TRPV1, and TRPA1 triple KO mice, where histological analysis did not reveal significant differences in nerve bundle density within the hind paw skin compared to wild-type controls (Vandewauw *et al.*, 2018). These findings suggest that TRPM3 channels primarily influence sensory processing and intracellular signaling rather than structural innervation. The observed inhibition of PZ-mediated neuroprotection by TRPM3 blockade suggests a mechanistic interplay between muscarinic signaling and TRPM3 activity in diabetic neuropathy. Given that TRPM3 channels facilitate intracellular calcium signaling in dorsal root ganglion neurons (Chauhan *et al.*, 2025; Held *et al.*, 2015b; Vriens *et al.*, 2011), their inhibition disrupts PZ's ability to restore calcium homeostasis, thereby attenuating its neuroprotective effects. In the subcutaneous treatment group PZ improved heat sensitivity at 16 weeks (Figure 4.3E) which was abolished with primidone co-administration. These findings underscore the crucial role of TRPM3 channels in the modulation of heat sensitivity and their potential interaction with PZ-mediated neuroprotection in diabetic neuropathy.

4.3.4 Motor nerve conduction velocity deficits

MNCV is a critical electrophysiological parameter widely used to assess the functional integrity of peripheral nerves, providing valuable insights into the extent of axonal damage and demyelination associated with diabetic neuropathy (Dyck, 1991). A decline in MNCV is indicative of progressive nerve fiber degeneration, myelin loss, and impaired impulse transmission, making it a widely used biomarker for evaluating both disease progression and therapeutic efficacy (Calcutt *et al.*, 2003). In the present study, STZ-induced diabetic mice did not exhibit a significant decline in MNCV at 4 weeks (Figure 4.1C) or 8 weeks (Figure 4.2C) post-induction. However, by 16 weeks, a progressive decline in MNCV was observed in untreated diabetic mice, suggesting that neuropathy in this cohort developed more slowly compared to previous reports (Figure 4.3C). Topical PZ treatment effectively prevented the MNCV decline observed in diabetic mice, with improvements evident at 16-week (Figure 4.3C,F). This suggests that PZ exerts neuroprotective effects, potentially through muscarinic receptor modulation. This effect is consistent with the ability of M_1R antagonists to enhance mitochondrial function, reduce oxidative stress, and support neurotrophic signaling pathways, which are essential for peripheral nerve maintenance and regeneration (Calcutt *et al.*, 2017; Saleh *et al.*, 2020). These findings align with previous studies demonstrating the beneficial effects of muscarinic receptor antagonists in improving nerve conduction and preserving peripheral nerve function in diabetic models.

To further investigate the role of TRPM3 in this neuroprotection, isosakuranetin was co-treated with PZ, which significantly attenuated the PZ mediated MNCV slowing, indicating the critical involvement of TRPM3 channels in M_1R antagonism mediated neuroprotective effects (Figure 4.3C). TRPM3 channels are integral regulators of calcium influx and neuronal excitability, and their inhibition likely disrupts calcium-dependent signaling pathways essential for nerve function and repair (Zhao and MacKinnon, 2023). Interestingly, co-administration of primidone,

another TRPM3 inhibitor, suppressed the neuroprotective effects of PZ when given topically (Figure 4.3C), but no effect when used via the subcutaneous route (Figure 4.3F), suggesting potential mechanistic differences in how these inhibitors interact with TRPM3 and muscarinic receptor signaling pathways through different absorption mechanisms. The differential effects observed with isosakuranetin, and primidone highlight the complexity of TRPM3 modulation and suggest distinct binding affinities or signaling pathway interactions that warrant further investigation (Krügel *et al.*, 2017). Isosakuranetin is a potent TRPM3 inhibitor with a flavanone pharmacophore which effectively reduces TRPM3-like signals in DRG neurons and demonstrated analgesic effects *in vivo* (Straub *et al.*, 2013). In contrast, primidone, an anticonvulsant, inhibits TRPM3 activation through allosteric modulation at lower concentrations than typically used for anticonvulsant effects (Vangeel *et al.*, 2020). While both compounds inhibit TRPM3, isosakuranetin is a plant-derived flavanone, whereas primidone is a clinically approved drug with distinct mechanisms and pharmacological profiles.

4.3.5 Corneal nerve density with disease progression

In the present study, despite the presence of functional deficits such as impaired tactile and thermal sensitivity, no significant progressive decline in corneal nerve density was observed over the 16-week period in STZ-induced diabetic mice compared to controls. The absence of a pronounced structural decline suggests that corneal nerve density may remain relatively preserved in the early stages of diabetic neuropathy, with functional impairments preceding detectable morphological changes. Small fiber dysfunction, as assessed by thermal and tactile sensitivity tests, often precedes observable nerve fiber loss (Ziegler *et al.*, 2014). The potential neuroprotective effects of topical PZ treatment on corneal nerves were not fully assessed in this study given the timeline. Although, isosakuranetin treatment (Figure 4.4B,C) significantly reduced the corneal nerve density. TRPM3

is expressed throughout the corneal epithelium and descends down to the stromal nerves (Brown *et al.*, 2015), suggesting that pharmacological blockade may have broad implications for corneal nerve health. While this study was limited in duration, future investigations should extend the observation period and explore more aggressive diabetic models to assess the long-term effects of TRPM3 modulation on corneal nerve integrity.

4.4 Conclusion

Our findings support the neuroprotective role of M_1R antagonist PZ and establish that its beneficial effects in diabetic neuropathy are mediated through TRPM3 activation. This aligns with our recent *in vitro* studies, which demonstrated that PZ exerts its neuroprotective effects by directly activating TRPM3, promoting axonal integrity and sensory function (Chauhan *et al.*, 2025). In the present study, topical PZ administration led to functional improvements across multiple sensory and motor indices, including MNCV, thermal sensitivity, and tactile allodynia, reinforcing its role in mitigating diabetes-induced neuropathy. To validate the TRPM3-dependent mechanism underlying PZ-mediated neuroprotection, we examined the effects of two distinct TRPM3 inhibitors, isosakuranetin and primidone. Isosakuranetin effectively abolished PZ-induced improvements, confirming its potent TRPM3 inhibitory properties and the direct reliance of PZ's effects on TRPM3 activation. In contrast, primidone, another TRPM3 inhibitor, exhibited weaker suppression of PZ-mediated neuroprotection *in vivo*, likely due to its broader pharmacological effects as an anti-epileptic drug, which may have influenced TRPM3-specific pathways differently in a complex biological system. Although corneal nerve fiber loss is considered an early marker of small fiber neuropathy, no significant decline in nerve fiber integrity was observed in the STZ group, suggesting that diabetic neuropathy progression in this cohort was slower than previously reported. As a result, the role of PZ in maintaining nerve structural integrity cannot be definitively

stated, though its functional benefits remain evident. However, isosakuranetin treatment led to a significant decline in corneal nerve density, reinforcing TRPM3's role in supporting sensory fibers and neurotrophic signaling. Given that TRPM3 channels are expressed along sensory fibers descending into the cornea (Brown *et al.*, 2015), their inhibition likely disrupts maintenance of axonal structure, leading to degeneration.

A key observation in this study was the delayed onset of sensory impairments, with clear deficits only emerging at 16 weeks, despite previous reports showing similar neuropathic changes as early as 4–8 weeks post-STZ induction. This discrepancy suggests that neuropathy in this cohort progressed at a slower rate, with some detectable fiber loss likely emerging much later than expected. Several factors discussed earlier may have contributed to this delayed progression. However, it is also important to acknowledge that this was the first time I performed these experiments, and limited time for training, optimization, and refinement of techniques may have influenced the observed outcomes. Future studies aimed at longer durations and greater experimental proficiency would provide valuable insight into the therapeutic efficacy of TRPM3 activation as a potential strategy for reversing neuropathic damage.

Funding

This work was supported by grant # PJT-162172 from the Canadian Institutes of Health Research to PF.

Authors'contributions

All experiments were designed and performed by SC under the supervision and guidance of NA-C, CG-J and PF. Diabetic mice were set up under the supervision of MR and NA-C. Corneal confocal microscopy, MNCV, thermal studies and tactile measurements were performed by SC,

MR and AT under the supervision and guidance of NA-C. The analysis of data was performed by SC with the help of LG and supervised by NA-C and PF. The manuscript was written by SC and then reviewed and finalized by PF.

Chapter 5

General discussion

The research presented in this thesis advanced our understanding of the role of TRPM3 activation in M_1R antagonism-mediated neuroprotection. By delving into the molecular mechanisms underlying TRPM3 activity, we have uncovered novel insights into its contribution to neuronal metabolism, axonal and functional integrity. These findings are particularly significant in the context of neurodegenerative disorders and neuropathies, where metabolic dysfunction, synaptic loss and dying back of axons are central pathological features. Since, we initially discovered that M_1R antagonism reversed the indices of peripheral neuropathy and promoted neuronal repair (Calcutt *et al.*, 2017), this study aimed to determine whether M_1R modulates TRPM3 activation to elicit these effects. Also, the study focused on elucidating whether TRPM3 activation alone was sufficient to provide neuroprotection.

M_1R is a type of G protein-coupled receptor that, when activated, can negatively affect the cytoskeleton, which is crucial for cell structure and function (Sabbir *et al.*, 2018). Overexpression of M_1R in neurons induced reduced neurite outgrowth and disrupted the tubulin cytoskeleton, which is essential for maintaining cell shape and facilitating intracellular transport. The disruption of the cytoskeleton by excessive M_1R signaling also impaired mitochondrial trafficking, reducing the movement and abundance of mitochondria in neurites. This can limit the energy supply necessary for neurite outgrowth and function. Previous reports from our lab suggested that blocking M_1R resulted in a gradual increase in intracellular Ca^{2+} levels, activating AMPK, an enzyme critical for cellular energy balance (Calcutt *et al.*, 2017; Saleh *et al.*, 2020). This Ca^{2+} increase occurred upstream of a pathway involving CaMKKβ, which activated AMPK independently of AMP, indicating an alternative mechanism of energy regulation. The enhanced

Ca^{2+} signaling triggered by M_1R blockade contributed to improved mitochondrial function and neurite outgrowth, which are essential for nerve repair and protection, particularly in conditions such as diabetic neuropathy.

In the first results section (Chapter 3), pharmacological activation of TRPM3 using specific agonists, such as CIM0216 (CIM) and pregnenolone sulfate (PS) was characterized using Ca^{2+} fluorometric assays. Both agonists produced an increase in intracellular Ca^{2+}, consistent with previous findings (Vriens *et al.*, 2014; Vriens *et al.*, 2011). PS-evoked Ca^{2+} signals were transient, whereas CIM-induced Ca^{2+} influx remained sustained over longer durations (Chauhan et al. 2025; Figure 3.1, 3.S1). The sustained Ca^{2+} over longer periods with CIM was particularly noteworthy due to its ability to open distinct cation permeation pathways, making it one of the most potent TRPM3 activators identified to date (Vriens *et al.*, 2014). To explore whether M_1R antagonism mediated the gradual increase in Ca^{2+} through TRPM3 activation, PIP_2 levels were measured following M_1R inhibition using Pirenzepine (PZ) and muscarinic toxin 7 (MT7) (M_1R antagonists). The results revealed a marked increase in PIP_2 levels within 1–2 minutes of treatment (Chauhan et al. 2025; Figure 3.3), supporting previous findings that M_1R antagonists enhanced PIP_2 accumulation (Howe *et al.*, 1986). Given that PIP_2 is a well-established regulator of TRPM3 gating, this suggested that M_1R inhibition indirectly facilitated TRPM3 activation via PIP_2 buildup (Badheka *et al.*, 2017; Tóth *et al.*, 2015; Vriens *et al.*, 2014). The established interaction between GPCRs and TRP channels further corroborated this mechanism, as GPCR-mediated signaling through Gβγ subunits inhibits TRPM3 activity via Gαq and Gαs (Quallo *et al.*, 2017). Thus, the blockade of M_1R by PZ likely disrupted this inhibitory signaling cascade, allowing TRPM3 activation to proceed. In support of this hypothesis, pharmacological inhibition of TRPM3 with

isosakuranetin and primidone completely abolished TRPM3-mediated Ca^{2+} influx following PZ or MT7 treatment, reinforcing the role of TRPM3 activation in M_1R antagonism.

Our study provided the first evidence that the activation of TRPM3 by its specific agonists CIM and PS led to time dependent phosphorylation of AMPK (3 and 6 hours) and the activation of the CAMKKβ pathway in dorsal root ganglion (DRG) neurons (Chauhan et al. 2025; Figure 3.4, 3.7). This pathway has long been associated with energy homeostasis and cellular resilience, and its activation by TRPM3 suggested a mechanism through which neuronal metabolism was fine-tuned under conditions that challenges the neuronal integrity. While prior research in clear cell renal carcinoma cells identified a connection between TRPM3 activation, CaMKKβ, and AMPK signaling, its relevance to neuronal function, metabolism, and mitochondrial regulation had not been established (Hall *et al.*, 2014). In my study, the effect of TRPM3 activation on AMPK signaling was confirmed using a CaMKK inhibitor STO-609, which reduced phosphorylation of AMPK when co-treated with CIM ((Chauhan *et al.*, 2025); Figure 3.7). The reduction in p-AMPK levels following CaMKKβ inhibition strongly indicated that CaMKKβ is necessary for sustaining AMPK activation downstream of TRPM3. Although TRPM3 activation caused rapid influx of Ca^{2+}, the increase in p-AMPK activity following PS and CIM treatment exhibited a notable delay. The lag between Ca^{2+} entry and AMPK phosphorylation suggested that TRPM3-mediated AMPK activation is not merely a direct consequence of calcium influx, but rather a multi-step process involving calmodulin (CaM) and CaMKKβ recruitment. Calmodulin possesses at least five distinct binding sites within the N-terminal intracellular domain of TRPM3, with different affinities for Ca^{2+} (Thiel and Rössler, 2023). The cooperative interaction between these binding sites suggested a complex multi-level modulation of TRPM3-dependent signaling. Rather than simply relaying Ca^{2+} influx, calmodulin likely served as an integrator of Ca^{2+} signaling dynamics, mobilizing

CaMKKβ, which in turn phosphorylated and activated AMPK. This intricate regulation allowed for sustained AMPK activation, even after the initial calcium wave had subsided, ensuring a prolonged metabolic response that supported neuronal integrity, mitochondrial function, and energy homeostasis.

Another important finding indicated that TRPM3 activation upregulated the expression of mitochondrial electron transport chain proteins and improved mitochondrial respiration in DRG neurons derived from both control and diabetic rats. Neurons rely on finely tuned Ca^{2+} signaling to regulate mitochondrial activity and optimize energy production (Hatsuda *et al.*, 2023). In DRG neurons, mitochondria are strategically positioned near the plasma membrane, allowing them to act as rapid Ca^{2+} buffers when Ca^{2+} enters through channels, such as TRPM3 (Wang *et al.*, 2022). Interestingly, TRPM3 activation induced a more substantial Ca^{2+} influx compared to depolarization-induced pathways, such as voltage-gated Ca^{2+} channels (VGCCs) (Bouron and Oberwinkler, 2014). This distinction is critical because mitochondria could buffer up to 40% of this Ca^{2+} load, preventing excessive cytosolic Ca^{2+} accumulation while ensuring sufficient Ca^{2+} availability for metabolic regulation. However, in the pathogenesis of painful diabetic neuropathy (PDN), mitochondrial calcium homeostasis becomes dysregulated due to the excessive influx of Ca^{2+} into the mitochondrial matrix through the mitochondrial calcium uniporter (MCU) (George *et al.*, 2022). While mitochondrial Ca^{2+} uptake is necessary for metabolic enzyme activation and ATP production, excessive MCU activity in DRG neurons has been associated with mitochondrial fragmentation, oxidative stress, and axonal degeneration. Notably, in HFD-induced diabetic mice, fragmented mitochondrial morphology was observed in DRG nociceptors as early as two weeks after diet initiation, preceding the onset of mechanical allodynia and small-fiber degeneration (George *et al.*, 2024). This finding highlighted mitochondrial dysfunction as an early pathological

event in PDN. The genetic deletion of MCU in Na v 1.8-expressing DRG neurons prevented mitochondrial fragmentation, restored normal mitochondrial morphology, and protected against mechanical allodynia and axonal degeneration. These findings indicated that MCU-mediated Ca^{2+} overload contributed to the development of PDN and that limiting mitochondrial Ca^{2+} influx through MCU deletion may mitigate neuropathic pain and neuronal degeneration.

Despite the pathological consequences of excessive MCU activity, controlled Ca^{2+} transfer to mitochondria is essential for maintaining oxidative phosphorylation and ATP synthesis. Mitochondria sequester Ca^{2+} from the cytosol during TRPM3 activation and gradually release it back, prolonging Ca^{2+}-dependent signaling (Wang *et al.*, 2022). This delayed Ca^{2+} recovery influenced a variety of neuronal functions, including metabolic enzyme activation, synaptic plasticity, and mitochondrial ATP production. Prolonged Ca^{2+} signaling stimulated ATP synthesis by activating key metabolic enzymes within the tricarboxylic acid (TCA) cycle, including pyruvate dehydrogenase (PDH), isocitrate dehydrogenase (IDH), and α-ketoglutarate dehydrogenase (α-KGDH). These enzymes increased the production of NADH and $FADH_2$, which fueled oxidative phosphorylation and ATP synthesis to support the energy-intensive demands of neurons (Rizzuto *et al.*, 2012). Our study demonstrated that pharmacological activation of TRPM3 using PS and CIM significantly enhanced mitochondrial function in DRG neurons ((Chauhan *et al.*, 2025); Figure 3.5, 3.S5). The increased Ca^{2+} influx following TRPM3 activation directly contributed to heightened oxidative phosphorylation (OXPHOS) protein expression, as observed in DRG neurons derived from control or diabetic rats. This upregulation of OXPHOS proteins was likely driven by the delayed mitochondrial Ca^{2+} release, which sustained the metabolic activity of neurons over an extended period. This finding suggested that TRPM3 activation can optimize

mitochondrial performance, ensuring neurons receive adequate ATP to meet their functional demands under diverse physiological conditions.

Quantitative imaging assays and mass spectrometry-based metabolic profiling revealed that TRPM3 activation enhanced glycolysis and TCA cycle metabolite levels in DRG neurons ((Chauhan *et al.*, 2025); Figure 3.S9). This metabolic shift suggested that TRPM3-mediated Ca^{2+} influx not only improved mitochondrial function but also stimulated glucose metabolism to meet the sustained energy demands of neurons. Our findings demonstrated a significant increase in ubiquinone (coenzyme Q10) levels in DRG neurons following CIM treatment ((Chauhan *et al.*, 2025); Figure 3.S9). This increase was particularly noteworthy given the essential role of ubiquinone in mitochondrial electron transport and ATP synthesis (Lenaz *et al.*, 2007). Ubiquinone functions as an electron carrier within the electron transport chain (ETC), directly influencing oxidative phosphorylation efficiency and ATP production. Its upregulation following TRPM3 activation suggested a metabolic adaptation favoring mitochondrial respiration over alternative energy-producing pathways.

Further supporting this notion, the activation of TRPM3 enhanced neurite outgrowth in DRG sensory neurons ((Chauhan *et al.*, 2025); Figure 3.6), a critical aspect of neuronal plasticity and regeneration. CaMKKβ inhibition effectively blocked the neurite-promoting effects of TRPM3 activation, reinforcing the downstream involvement of the Ca^{2+}-dependent CaMKKβ-AMPK signaling ((Chauhan *et al.*, 2025); Figure 3.7). Given that neurite outgrowth is crucial for ongoing plasticity or axonal repair following injury or neurodegenerative insult, these findings highlighted the therapeutic potential of TRPM3 modulation in neuroprotection and regeneration. The knockdown of TRPM3 using an AAV-shRNA method provided additional confirmation, as it significantly attenuated neurite outgrowth and reduced P-AMPK levels, demonstrating the

necessity of TRPM3 for sustaining neuronal integrity ((Chauhan *et al.*, 2025); Figure 3.S4). In exploring the molecular underpinnings of TRPM3 activation, human neuroblastoma SH-SY5Y cells were employed as a model. These cells mirrored the findings observed in DRG neurons, demonstrating increased intracellular calcium levels, unregulated phosphorylation of AMPK and enhanced mitochondrial function ((Chauhan *et al.*, 2025); Figure 3.S6, 3.S7, 3.S8). These observations were validated through live calcium imaging, Western blotting, membrane potential assays, and mass spectrometry studies. TRPM3 activation also enhanced glycolysis and TCA cycle metabolites indicating a shift towards upregulated metabolism and improved mitochondrial efficiency ((Chauhan *et al.*, 2025); Figure 3.8, 3.S10). The key TCA cycle intermediates such as citrate, isocitrate, and pyruvate were upregulated in SH-SY5Y cells, following CIM treatment. These metabolites are crucial not only for ATP production via oxidative phosphorylation but also for the synthesis of fatty acids and cholesterol, which are vital for neuronal membrane integrity and function. Given that diabetic neuropathy is often characterized by mitochondrial dysfunction, impaired metabolism, and reduced ATP production (Fernyhough, 2015), the ability of TRPM3 activation to restore TCA cycle activity suggested a potential mechanism for overcoming metabolic deficits associated with neuronal dysfunction. TRPM3 activation appeared to facilitate a feedback loop between the TCA cycle and mitochondria, ensuring a continuous supply of substrates for ATP generation. This is particularly important for maintaining neuronal survival, axon integrity, and functional energy demands in conditions where metabolic stress is present. Interestingly, when TRPM3 activation was blocked using specific inhibitors, primidone and isosakuranetin, the upregulation of TCA cycle metabolites and mitochondrial function was completely abolished ((Chauhan *et al.*, 2025); Figure 3.8). This confirmed that the observed metabolic improvements are directly mediated by TRPM3 activation and not through alternative

pathways. The consistency of these results across different neuronal systems reinforced the robustness of TRPM3's role in neuroprotection and metabolic regulation.

Having established the metabolic and neuroprotective effects of TRPM3 activation *in vitro*, the focus shifted towards investigating its role in an *in vivo* setting using a diabetic neuropathy model, as detailed in **Chapter 4** of this thesis. The streptozotocin (STZ)-induced diabetic neuropathy model was chosen due to its well-characterized ability to replicate key sensory deficits associated with diabetes-induced nerve damage (Murakami *et al.*, 2013). This model demonstrates reduction in corneal nerve density, slowing of motor nerve conduction velocity (MNCV), mechanical allodynia, and thermal hypoalgesia are hallmarks of diabetic neuropathy. These functional impairments reflect the progressive nature of neuropathy, making this model well-suited for assessing whether TRPM3 activation could contribute to M_1R antagonist-mediated neuroprotection. Antimuscarinic drugs such as PZ and MT7 prevented or reversed key indicators of peripheral neuropathy, including sensory nerve terminal depletion, thermal hypoalgesia, and slowed nerve conduction in various rodent models of diabetes (Calcutt *et al.*, 2017; Saleh *et al.*, 2020). Their protective effects extended beyond diabetes, as PZ and MT7 have also been effective against neuropathy induced by chemotherapeutic agents such as dichloroacetate and paclitaxel, as well as HIV envelope protein gp120 (Han *et al.*, 2021; Saleh *et al.*, 2020). Given these findings, this study aimed to determine whether the neuroprotective effects of PZ in reversing nerve fiber loss and sensory deficits were TRPM3-dependent. To validate this, TRPM3 inhibitors isosakuranetin and primidone were tested alongside PZ treatment. Sensory deficits were mild at 4–8 weeks but became pronounced by 16 weeks, with diabetic mice exhibiting mechanical allodynia, reduced MNCV, and increased thermal latency. PZ treatment effectively reversed these impairments, restoring sensory and motor responses closer to control levels, indicating functional

recovery (Figure 4.3). However, co-administration of TRPM3 inhibitors eliminated these improvements, confirming that PZ-mediated neuroprotection is TRPM3-dependent. Notably, differences in the extent of inhibition between the two TRPM3 inhibitors suggested that their distinct mechanisms of action may have influenced their inhibitory effects.

Corneal nerve loss, a well-established marker of diabetic neuropathy progression, serves as a critical indicator of sensory fiber degeneration (Tavakoli *et al.*, 2010). Although significant sensory deficits were observed, corneal nerve loss was less pronounced than expected within the study's timeframe, suggesting a slower progression of neuropathy compared to previous reports (Calcutt *et al.*, 1996; Calcutt *et al.*, 2017; Yorek *et al.*, 2014). This delayed degeneration allowed functional impairments to develop gradually before detectable fiber loss. However, treatment with isosakuranetin led to a significant reduction in corneal nerve density, highlighting TRPM3's role in maintaining sensory fiber integrity. Given that TRPM3 is widely expressed in the corneal epithelium and stromal nerves (Brown *et al.*, 2015), its pharmacological inhibition may have broader implications for corneal nerve health. Nevertheless, the study provided a strong foundation for future research exploring TRPM3 modulation as a potential therapeutic strategy against neurodegeneration. The implications of these findings extend beyond the immediate context of diabetic neuropathy. The ability of TRPM3 to modulate calcium signaling, mitochondrial function, and energy metabolism positions it as a crucial player in neuronal homeostasis. Dysregulation of these processes is a common feature in a range of neurodegenerative conditions, including Alzheimer's disease, Parkinson's disease, and peripheral neuropathies. By elucidating the pathways through which TRPM3 exerts its neuroprotective effects, this research opens new avenues for therapeutic strategies aimed at enhancing neuronal resilience under pathological conditions.

Limitations and future studies

Despite the promising insights gained, certain limitations must be acknowledged, and additional studies are warranted to deepen our understanding of TRPM3's role in neuroprotection and mitochondrial regulation in diabetic neuropathy.

- One major consideration is the dual role of TRPM3; while its activation appears neuroprotective, TRPM3 is also a well-characterized pain transduction channel. Overactivation could exacerbate nociceptive signaling, making it essential to achieve a balanced activation profile that promotes cellular resilience without inducing hyperalgesia.
- A significant technical limitation of the current study was the inability to perform dual immunostaining for M_1R and TRPM3 due to the lack of highly specific antibodies. Such staining would have allowed identification of neurons co-expressing both proteins and provided insight into how these neurons respond to combinatorial pharmacological manipulation (i.e., M_1R antagonism and TRPM3 activation).
- Another important limitation relates to systemic TRPM3 targeting in the *in-vivo model*. TRPM3 is expressed not only in sensory neurons but also in other tissues including the pancreas, kidneys, and retina- organs already vulnerable in diabetes. Therefore, systemic administration of TRPM3 modulators carries a risk of off-target effects. Targeted delivery approaches or neuron-specific modulation strategies should be explored to reduce unintended consequences.
- Furthermore, synergistic interactions between M_1R antagonists (such as PZ) and TRPM3 agonists (like CIM0216) were not evaluated. This represents a critical gap, as combined targeting of M_1R and TRPM3 may yield enhanced neuroprotective outcomes. Future

experiments should directly assess synergistic effects using combination treatments in both preventive and reversal paradigms of *in-vivo studies.*

- Additionally, the lack of multivariate statistical analysis, such as principal component analysis (PCA), limited the ability to comprehensively evaluate treatment effects across diverse *in vivo* endpoints. Employing PCA or other dimensionality reduction techniques in future studies could provide a more integrated understanding of group differences and treatment effects, especially when multiple behavioral, metabolic, and histological parameters are measured.
- Finally, the use of genetic models: such as sensory neuron-specific or inducible TRPM3 knockout mice—would enable definitive dissection of TRPM3's role in neuroprotection, independent of off-target systemic effects.

Moving forward, several key experimental directions should be pursued to further elucidate the role of TRPM3 in sensory neuron repair and mitochondrial regulation, including the following:

- Detailed calcium imaging in mitochondria: While this study demonstrated TRPM3-mediated increases in mitochondrial respiration, real-time Ca^{2+} imaging within mitochondria could reveal how TRPM3-dependent Ca^{2+} influx directly influences ATP production and mitochondrial dynamics. The use of genetically encoded Ca^{2+} indicators (GECIs) targeted to mitochondria (e.g., mito-GCaMP) could allow for high-resolution tracking of mitochondrial Ca^{2+} fluctuations following TRPM3 activation (Wu *et al.*, 2014; Zhao *et al.*, 2011).
- Screening for novel TRPM3 agonists: Current TRPM3 activators, CIM0216 and pregnenolone sulfate (PS), exhibit suboptimal pharmacokinetics for therapeutic application. High-throughput compound screening should be performed to identify novel TRPM3 agonists with enhanced specificity, solubility, and bioavailability. Structure-activity relationship (SAR) studies could

optimize TRPM3-targeting molecules with improved stability and controlled activation properties.

- Use of TRPM3 mutants to dissect functional pathways: TRPM3 contains multiple functional domains that could be responsible for its effects on mitochondrial regulation. Generating domain-specific TRPM3 mutants (e.g., mutations in Ca^{2+} binding regions or PIP_2-interaction sites) would help elucidate the specific mechanisms linking TRPM3 activation to mitochondrial function and axonal repair.
- Transcriptomic and proteomic profiling of TRPM3 activated neurons: Single-cell RNA sequencing (scRNA-seq) could provide a global overview of gene expression changes following TRPM3 activation. Proteomic studies could reveal upregulated mitochondrial proteins and signaling pathways that drive neuroprotection in TRPM3-activated sensory neurons.
- In addition to sensory deficits, future studies should evaluate motor function, pain perception, and metabolic changes to assess the full spectrum of TRPM3-mediated neuroprotection.
- Electrophysiological studies, such as patch-clamp recordings from DRG neurons, could confirm whether TRPM3 activation enhances synaptic activity and neurotransmission in neuropathic conditions.
- Sustained activation of TRPM3 may affect calcium homeostasis and cellular metabolism, necessitating long-term safety studies.
- Future studies should assess whether co-therapy strategies further improve mitochondrial function and sensory recovery in neuropathic conditions.

Finally, in-vivo studies using alternative neuropathy models, long-term functional assessments, and combinatorial treatment strategies will be critical for advancing TRPM3-targeted therapies

toward clinical translation. Addressing these gaps in knowledge will help determine whether TRPM3 activation can serve as a viable long-term therapeutic approach for peripheral neuropathy and related neurodegenerative conditions.

Future translational approaches

Peripheral neuropathy encompasses a range of disorders with diverse etiologies, yet mitochondrial dysfunction is increasingly recognized as a key pathological driver across multiple neuropathies (Zong *et al.*, 2024). Loss of mitochondrial integrity within intraepidermal nerve fibers (IENF) is strongly correlated with sensory deficits and axonal degeneration, highlighting the need for therapeutic strategies that restore neuronal metabolism and energy homeostasis (Casanova-Molla *et al.*, 2012). Findings from this thesis demonstrate that TRPM3 activation enhances mitochondrial function, facilitates ATP production, and promotes sensory axon regeneration, presenting a promising translational pathway for the development of TRPM3-targeted neuroprotective therapies.

The modulation of TRPM3 and M_1R signaling provides a unique advantage over conventional neuropathy treatments, which primarily focus on symptom management rather than nerve repair. Pirenzepine (PZ), an M_1R antagonist, has demonstrated robust neuroprotective effects in preclinical models of diabetic neuropathy, restoring AMPK activity, improving mitochondrial function, and facilitating sensory nerve regeneration (Calcutt *et al.*, 2017; Saleh *et al.*, 2020). These findings have led to several ongoing clinical trials evaluating topical pirenzepine for HIV-associated neuropathy (NCT05005078), diabetic neuropathy (NCT04786340), and chemotherapy-induced peripheral neuropathy (NCT05488873). The established safety profile of

PZ, combined with its slow-release topical formulation, positions it as a strong candidate for clinical translation.

TRPM3 activation represents a complementary and alternative strategy to M_1R antagonism, given its role in mitochondrial calcium homeostasis, ATP production, and neuronal metabolism (Chauhan *et al.*, 2025; Wang *et al.*, 2022). By enhancing mitochondrial calcium buffering, TRPM3 activation supports neuronal resilience under metabolic stress, making it a promising therapeutic target for diabetic, chemotherapy-induced, and HIV-associated neuropathies. Additionally, TRPM3 regulates pain sensitization, offering the dual benefit of restoring sensory function while potentially alleviating neuropathic pain. Despite its strong therapeutic potential, direct TRPM3 activation faces several challenges, particularly in terms of drug delivery and pharmacokinetics. Current TRPM3 agonists, CIM0216 and pregnenolone sulfate, are highly lipophilic, which limits their solubility in aqueous formulations and prevents effective diffusion through the skin in depot-based delivery systems. Given these challenges, alternative approaches must be explored to optimize TRPM3 activation, while overcoming pharmacokinetic limitations, such as:

- Development of small-molecule TRPM3 agonists with improved bioavailability, solubility, and selective targeting.
- Prodrug strategies, where inactive TRPM3 agonists are converted into active compounds at the site of action, reducing systemic toxicity.
- Peptide-based TRPM3 modulators could provide greater specificity, reduce systemic exposure and simply concerns around drug metabolism.
- Designing lipid soluble TRPM3 agonists with improved membrane permeability, allowing for topical depot administration.

Potential drawbacks and considerations for TRPM3 therapies:

- TRPM3 is expressed in multiple tissues thereby systemic activation could lead to unintended metabolic or renal effects, necessitating highly selective targeting strategies (Fonfria *et al.*, 2006; Held *et al.*, 2015b).
- While TRPM3 activation promotes sensory recovery, it also plays a role in nociceptive pathways, meaning dose-dependent effects must be carefully studied to avoid exacerbating thermal sensitivity.
- Chronic TRPM3 activation may alter calcium homeostasis, necessitating long-term safety evaluations to assess potential metabolic consequences.

TRPM3 modulation holds strong potential for long-term neuroprotection across multiple neuropathies. Future translational research should bridge the gap between mechanistic discoveries and clinical application, ensuring that TRPM3-targeted therapies evolve into viable treatments for patients suffering from neuropathic conditions.

Summary

In conclusion, this thesis has uncovered novel insights into the role of TRPM3 activation in M_1R antagonism-mediated neuroprotection. The findings demonstrate that TRPM3 activation enhanced Ca^{2+} signaling, promoted mitochondrial function, and sustained neuronal metabolism, collectively supporting its role in neuronal integrity and repair. The in-vitro and in-vivo evidence confirms that M_1R-mediated neuroprotection is TRPM3-dependent, highlighting its significance in sensory neuron regeneration. Furthermore, TRPM3 activation augments energy metabolism through AMPK phosphorylation, reinforcing its role in maintaining neuronal resilience under metabolic stress. While certain limitations remain, the results provide a strong foundation for future

investigations into TRPM3 as a potential therapeutic target for neurodegenerative diseases and neuropathies.

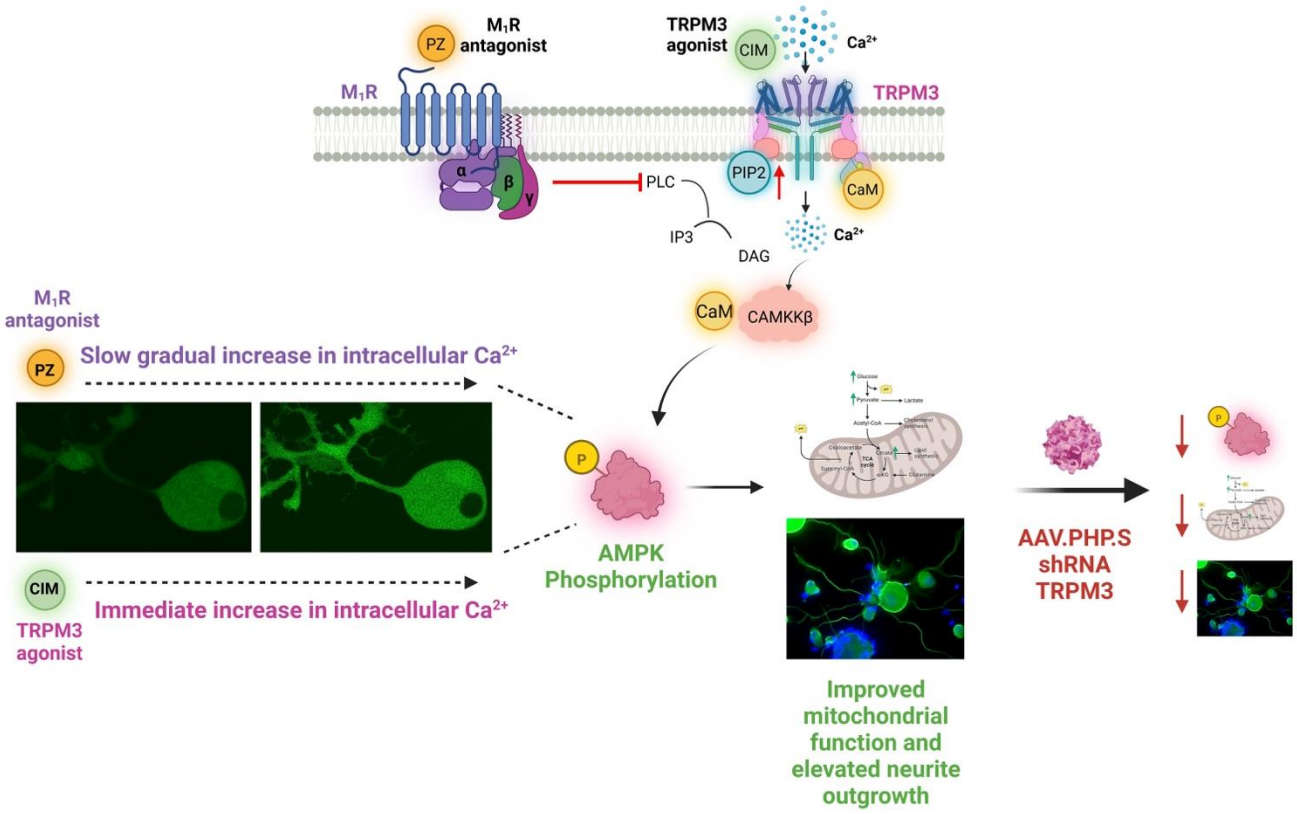

Figure 5.1: **Schematic representation of TRPM3 activation and its role in M_1R antagonist-mediated neuroprotection.** M_1R antagonism (PZ) prevents PIP_2 hydrolysis, leading to a gradual increase in intracellular Ca^{2+}, whereas TRPM3 agonists (CIM) induce an immediate Ca^{2+} influx. This Ca^{2+} signaling activates the CaMKKβ/AMPK pathway, enhancing mitochondrial function and promoting neurite outgrowth. TRPM3 knockdown using AAV-PHP.S shRNA reduces AMPK phosphorylation and metabolic activity, impairing neuronal growth and repair, indicating that the M_1R-mediated effects are TRPM3-dependent. *Created with BioRender*.

References

Abram, S.E., Yi, J., Fuchs, A., and Hogan, Q.H. (2006). Permeability of injured and intact peripheral nerves and dorsal root ganglia. Anesthesiology *105*, 146-153.

Agarwal, N., Helmstädter, J., Rojas, D.R., Bali, K.K., Gangadharan, V., and Kuner, R. (2018). Evoked hypoalgesia is accompanied by tonic pain and immune cell infiltration in the dorsal root ganglia at late stages of diabetic neuropathy in mice. Mol Pain *14*, 1744806918817975.

Aghanoori, M.R., Smith, D.R., Shariati-Ievari, S., Ajisebutu, A., Nguyen, A., Desmond, F., Jesus, C.H.A., Zhou, X., Calcutt, N.A., Aliani, M., *et al.* (2019). Insulin-like growth factor-1 activates AMPK to augment mitochondrial function and correct neuronal metabolism in sensory neurons in type 1 diabetes. Mol Metab *20*, 149-165.

Akude, E., Zherebitskaya, E., Chowdhury, S.K., Smith, D.R., Dobrowsky, R.T., and Fernyhough, P. (2011). Diminished superoxide generation is associated with respiratory chain dysfunction and changes in the mitochondrial proteome of sensory neurons from diabetic rats. Diabetes *60*, 288-297.

Aloi, V.D., Pinto, S., Van Bree, R., Luyten, K., Voets, T., and Vriens, J. (2023). TRPM3 as a novel target to alleviate acute oxaliplatin-induced peripheral neuropathic pain. Pain *164*, 2060-2069.

Amato, S., and Man, H.Y. (2011). Bioenergy sensing in the brain: the role of AMP-activated protein kinase in neuronal metabolism, development and neurological diseases. Cell Cycle *10*, 3452-3460.

Ang, L., Jaiswal, M., Martin, C., and Pop-Busui, R. (2014). Glucose control and diabetic neuropathy: lessons from recent large clinical trials. Curr Diab Rep *14*, 528.

Armstrong, D.G., and Lavery, L.A. (1998). Diabetic foot ulcers: prevention, diagnosis and classification. Am Fam Physician *57*, 1325-1332, 1337-1328.

Armstrong, D.G., Swerdlow, M.A., Armstrong, A.A., Conte, M.S., Padula, W.V., and Bus, S.A. (2020). Five year mortality and direct costs of care for people with diabetic foot complications are comparable to cancer. J Foot Ankle Res *13*, 16.

Atkinson, M.A., Eisenbarth, G.S., and Michels, A.W. (2014). Type 1 diabetes. Lancet *383*, 69-82.

Badheka, D., Borbiro, I., and Rohacs, T. (2015). Transient receptor potential melastatin 3 is a phosphoinositide-dependent ion channel. J Gen Physiol *146*, 65-77.

Badheka, D., Yudin, Y., Borbiro, I., Hartle, C.M., Yazici, A., Mirshahi, T., and Rohacs, T. (2017). Inhibition of Transient Receptor Potential Melastatin 3 ion channels by G-protein βγ subunits. Elife *6*.

Beggs, J., Johnson, P.C., Olafsen, A., and Watkins, C.J. (1992). Innervation of the vasa nervorum: changes in human diabetics. J Neuropathol Exp Neurol *51*, 612-629.

Beiswenger, K.K., Calcutt, N.A., and Mizisin, A.P. (2008). Dissociation of thermal hypoalgesia and epidermal denervation in streptozotocin-diabetic mice. Neurosci Lett *442*, 267-272.

Bellier, J.P., and Kimura, H. (2007). Acetylcholine synthesis by choline acetyltransferase of a peripheral type as demonstrated in adult rat dorsal root ganglion. J Neurochem *101*, 1607-1618.

Bennett, G.J., Doyle, T., and Salvemini, D. (2014). Mitotoxicity in distal symmetrical sensory peripheral neuropathies. Nat Rev Neurol *10*, 326-336.

Bernardini, N., Tomassy, G.S., Tata, A.M., Augusti-Tocco, G., and Biagioni, S. (2004). Detection of basal and potassium-evoked acetylcholine release from embryonic DRG explants. J Neurochem *88*, 1533-1539.

Bernstein, B.W., and Bamburg, J.R. (2003). Actin-ATP hydrolysis is a major energy drain for neurons. J Neurosci *23*, 1-6.

Berridge, M.J., and Irvine, R.F. (1989). Inositol phosphates and cell signalling. Nature *341*, 197-205.

Berta, T., Qadri, Y., Tan, P.H., and Ji, R.R. (2017). Targeting dorsal root ganglia and primary sensory neurons for the treatment of chronic pain. Expert Opin Ther Targets *21*, 695-703.

Bhandari, R., Sharma, A., and Kuhad, A. (2021). Novel Nanotechnological Approaches for Targeting Dorsal Root Ganglion (DRG) in Mitigating Diabetic Neuropathic Pain (DNP). Front Endocrinol (Lausanne) *12*, 790747.

Bierhaus, A., Fleming, T., Stoyanov, S., Leffler, A., Babes, A., Neacsu, C., Sauer, S.K., Eberhardt, M., Schnölzer, M., Lasitschka, F., *et al.* (2012). Methylglyoxal modification of Nav1.8 facilitates nociceptive neuron firing and causes hyperalgesia in diabetic neuropathy. Nat Med *18*, 926-933.

Bluestone, J.A., Buckner, J.H., Fitch, M., Gitelman, S.E., Gupta, S., Hellerstein, M.K., Herold, K.C., Lares, A., Lee, M.R., Li, K., *et al.* (2015). Type 1 diabetes immunotherapy using polyclonal regulatory T cells. Sci Transl Med *7*, 315ra189.

Boulton, A.J., Malik, R.A., Arezzo, J.C., and Sosenko, J.M. (2004). Diabetic somatic neuropathies. Diabetes Care *27*, 1458-1486.

Bouron, A., and Oberwinkler, J. (2014). Contribution of calcium-conducting channels to the transport of zinc ions. Pflugers Arch *466*, 381-387.

Boyman, L., Karbowski, M., and Lederer, W.J. (2020). Regulation of Mitochondrial ATP Production: Ca(2+) Signaling and Quality Control. Trends Mol Med *26*, 21-39.

Brand, M.D., and Nicholls, D.G. (2011). Assessing mitochondrial dysfunction in cells. Biochem J *435*, 297-312.

Brown, M.J., and Asbury, A.K. (1984). Diabetic neuropathy. Ann Neurol *15*, 2-12.

Brown, R.L., Xiong, W.H., Peters, J.H., Tekmen-Clark, M., Strycharska-Orczyk, I., Reed, B.T., Morgans, C.W., and Duvoisin, R.M. (2015). TRPM3 expression in mouse retina. PLoS One *10*, e0117615.

Brownlee, M. (2001). Biochemistry and molecular cell biology of diabetic complications. Nature *414*, 813-820.

Bugger, H., Chen, D., Riehle, C., Soto, J., Theobald, H.A., Hu, X.X., Ganesan, B., Weimer, B.C., and Abel, E.D. (2009). Tissue-specific remodeling of the mitochondrial proteome in type 1 diabetic akita mice. Diabetes *58*, 1986-1997.

Burglen, L., Van Hoeymissen, E., Qebibo, L., Barth, M., Belnap, N., Boschann, F., Depienne, C., De Clercq, K., Douglas, A.G.L., Fitzgerald, M.P., *et al.* (2023). Gain-of-function variants in the ion channel gene TRPM3 underlie a spectrum of neurodevelopmental disorders. Elife *12*.

Cade, W.T. (2008). Diabetes-related microvascular and macrovascular diseases in the physical therapy setting. Phys Ther *88*, 1322-1335.

Calcutt, N.A., Allendoerfer, K.L., Mizisin, A.P., Middlemas, A., Freshwater, J.D., Burgers, M., Ranciato, R., Delcroix, J.D., Taylor, F.R., Shapiro, R., *et al.* (2003). Therapeutic efficacy of sonic hedgehog protein in experimental diabetic neuropathy. J Clin Invest *111*, 507-514.

Calcutt, N.A., and Chaplan, S.R. (1997). Spinal pharmacology of tactile allodynia in diabetic rats. Br J Pharmacol *122*, 1478-1482.

Calcutt, N.A., Jorge, M.C., Yaksh, T.L., and Chaplan, S.R. (1996). Tactile allodynia and formalin hyperalgesia in streptozotocin-diabetic rats: effects of insulin, aldose reductase inhibition and lidocaine. Pain *68*, 293-299.

Calcutt, N.A., Smith, D.R., Frizzi, K., Sabbir, M.G., Chowdhury, S.K., Mixcoatl-Zecuatl, T., Saleh, A., Muttalib, N., Van der Ploeg, R., Ochoa, J., *et al.* (2017). Selective antagonism of muscarinic receptors is neuroprotective in peripheral neuropathy. J Clin Invest *127*, 608-622.

Callaghan, B.C., Cheng, H.T., Stables, C.L., Smith, A.L., and Feldman, E.L. (2012). Diabetic neuropathy: clinical manifestations and current treatments. Lancet Neurol *11*, 521-534.

Callender, J.A., and Newton, A.C. (2017). Conventional protein kinase C in the brain: 40 years later. Neuronal Signal *1*, Ns20160005.

Cameron, N.E., and Cotter, M.A. (2001). Diabetes causes an early reduction in autonomic ganglion blood flow in rats. J Diabetes Complications *15*, 198-202.

Cameron, N.E., Eaton, S.E., Cotter, M.A., and Tesfaye, S. (2001). Vascular factors and metabolic interactions in the pathogenesis of diabetic neuropathy. Diabetologia *44*, 1973-1988.

Cao, E. (2020). Structural mechanisms of transient receptor potential ion channels. J Gen Physiol *152*.

Casanova-Molla, J., Morales, M., Garrabou, G., Solà-Valls, N., Soriano, A., Calvo, M., Grau, J.M., and Valls-Solé, J. (2012). Mitochondrial loss indicates early axonal damage in small fiber neuropathies. J Peripher Nerv Syst *17*, 147-157.

Cashman, C.R., and Höke, A. (2015). Mechanisms of distal axonal degeneration in peripheral neuropathies. Neurosci Lett *596*, 33-50.

Casselini, C.M., Parson, H.K., Frizzi, K.E., Marquez, A., Smith, D.R., Guernsey, L., Nemmani, R., Tayarani, A., Jolivalt, C.G., Weaver, J., *et al.* (2024). A muscarinic receptor antagonist reverses

multiple indices of diabetic peripheral neuropathy: preclinical and clinical studies using oxybutynin. Acta Neuropathol *147*, 60.

Cerles, O., Gonçalves, T.C., Chouzenoux, S., Benoit, E., Schmitt, A., Bennett Saidu, N.E., Kavian, N., Chéreau, C., Gobeaux, C., Weill, B., *et al.* (2019). Preventive action of benztropine on platinum-induced peripheral neuropathies and tumor growth. Acta Neuropathol Commun *7*, 9.

Chan, K.Y., Jang, M.J., Yoo, B.B., Greenbaum, A., Ravi, N., Wu, W.L., Sánchez-Guardado, L., Lois, C., Mazmanian, S.K., Deverman, B.E., *et al.* (2017). Engineered AAVs for efficient noninvasive gene delivery to the central and peripheral nervous systems. Nat Neurosci *20*, 1172-1179.

Chauhan, S., Smith, D.R., Shariati-Ievari, S., Srivastava, A., Dhingra, S., Aliani, M., and Fernyhough, P. (2025). Muscarinic acetylcholine type 1 receptor antagonism activates TRPM3 to augment mitochondrial function and drive axonal repair in adult sensory neurons. Mol Metab *92*, 102083.

Chen, D.K., Frizzi, K.E., Guernsey, L.S., Ladt, K., Mizisin, A.P., and Calcutt, N.A. (2013). Repeated monitoring of corneal nerves by confocal microscopy as an index of peripheral neuropathy in type-1 diabetic rodents and the effects of topical insulin. J Peripher Nerv Syst *18*, 306-315.

Chen, L., Wang, J., Zhang, Y.Y., Yan, S.F., Neumann, D., Schlattner, U., Wang, Z.X., and Wu, J.W. (2012). AMP-activated protein kinase undergoes nucleotide-dependent conformational changes. Nat Struct Mol Biol *19*, 716-718.

Chen, X., Graham, J., Dabbah, M.A., Petropoulos, I.N., Ponirakis, G., Asghar, O., Alam, U., Marshall, A., Fadavi, H., Ferdousi, M., *et al.* (2015). Small nerve fiber quantification in the

diagnosis of diabetic sensorimotor polyneuropathy: comparing corneal confocal microscopy with intraepidermal nerve fiber density. Diabetes Care *38*, 1138-1144.

Choi, J., Chandrasekaran, K., Inoue, T., Muragundla, A., and Russell, J.W. (2014). PGC-1α regulation of mitochondrial degeneration in experimental diabetic neuropathy. Neurobiol Dis *64*, 118-130.

Chong, M.S., and Hester, J. (2007). Diabetic painful neuropathy: current and future treatment options. Drugs *67*, 569-585.

Chowdhury, S.K., Dobrowsky, R.T., and Fernyhough, P. (2011). Nutrient excess and altered mitochondrial proteome and function contribute to neurodegeneration in diabetes. Mitochondrion *11*, 845-854.

Chowdhury, S.K., Smith, D.R., and Fernyhough, P. (2013). The role of aberrant mitochondrial bioenergetics in diabetic neuropathy. Neurobiol Dis *51*, 56-65.

Chowdhury, S.K., Zherebitskaya, E., Smith, D.R., Akude, E., Chattopadhyay, S., Jolivalt, C.G., Calcutt, N.A., and Fernyhough, P. (2010). Mitochondrial respiratory chain dysfunction in dorsal root ganglia of streptozotocin-induced diabetic rats and its correction by insulin treatment. Diabetes *59*, 1082-1091.

Chubanov, V., Köttgen, M., Touyz, R.M., and Gudermann, T. (2024). TRPM channels in health and disease. Nat Rev Nephrol *20*, 175-187.

Chung, S.S., Ho, E.C., Lam, K.S., and Chung, S.K. (2003). Contribution of polyol pathway to diabetes-induced oxidative stress. J Am Soc Nephrol *14*, S233-236.

Clapham, D.E. (2007). Calcium signaling. Cell *131*, 1047-1058.

Coull, J.A., Beggs, S., Boudreau, D., Boivin, D., Tsuda, M., Inoue, K., Gravel, C., Salter, M.W., and De Koninck, Y. (2005). BDNF from microglia causes the shift in neuronal anion gradient underlying neuropathic pain. Nature *438*, 1017-1021.

Coy-Dibley, J., Jayaraj, N.D., Ren, D., Pacifico, P., Belmadani, A., Wang, Y.Z., Gebis, K.K., Savas, J.N., Paller, A.S., Miller, R.J., *et al.* (2024). Keratinocyte-Derived Exosomes in Painful Diabetic Neuropathy. bioRxiv.

Dasgupta, B., and Milbrandt, J. (2007). Resveratrol stimulates AMP kinase activity in neurons. Proc Natl Acad Sci U S A *104*, 7217-7222.

DeFronzo, R.A. (2004). Pathogenesis of type 2 diabetes mellitus. Med Clin North Am *88*, 787-835, ix.

Dhage, S., Ferdousi, M., Adam, S., Ho, J.H., Kalteniece, A., Azmi, S., Alam, U., Ponirakis, G., Petropoulos, I., Atkinson, A.J., *et al.* (2021). Corneal confocal microscopy identifies small fibre damage and progression of diabetic neuropathy. Sci Rep *11*, 1859.

Dia, M., Gomez, L., Thibault, H., Tessier, N., Leon, C., Chouabe, C., Ducreux, S., Gallo-Bona, N., Tubbs, E., Bendridi, N., *et al.* (2020). Reduced reticulum-mitochondria Ca(2+) transfer is an early and reversible trigger of mitochondrial dysfunctions in diabetic cardiomyopathy. Basic Res Cardiol *115*, 74.

Dunnigan, S.K., Ebadi, H., Breiner, A., Katzberg, H.D., Lovblom, L.E., Perkins, B.A., and Bril, V. (2013). Conduction slowing in diabetic sensorimotor polyneuropathy. Diabetes Care *36*, 3684-3690.

Dyck, P.J. (1991). Evaluative procedures to detect, characterize, and assess the severity of diabetic neuropathy. Diabet Med *8 Spec No*, S48-51.

Egan, D.F., Shackelford, D.B., Mihaylova, M.M., Gelino, S., Kohnz, R.A., Mair, W., Vasquez, D.S., Joshi, A., Gwinn, D.M., Taylor, R., *et al.* (2011). Phosphorylation of ULK1 (hATG1) by AMP-activated protein kinase connects energy sensing to mitophagy. Science *331*, 456-461.

el-Fakahany, E.E., Cioffi, C.L., Abdellatif, M.M., and Miller, M.M. (1986). Competitive interaction of pirenzepine with rat brain muscarinic acetylcholine receptors. Eur J Pharmacol *131*, 237-247.

Erskine, L., and McCaig, C.D. (1995). Growth cone neurotransmitter receptor activation modulates electric field-guided nerve growth. Dev Biol *171*, 330-339.

Esper, R.J., Nordaby, R.A., Vilariño, J.O., Paragano, A., Cacharrón, J.L., and Machado, R.A. (2006). Endothelial dysfunction: a comprehensive appraisal. Cardiovasc Diabetol *5*, 4.

Falkenburger, B.H., Jensen, J.B., and Hille, B. (2010). Kinetics of M1 muscarinic receptor and G protein signaling to phospholipase C in living cells. J Gen Physiol *135*, 81-97.

Feige, J.N., and Auwerx, J. (2007). Transcriptional coregulators in the control of energy homeostasis. Trends Cell Biol *17*, 292-301.

Feldman, E.L., Callaghan, B.C., Pop-Busui, R., Zochodne, D.W., Wright, D.E., Bennett, D.L., Bril, V., Russell, J.W., and Viswanathan, V. (2019). Diabetic neuropathy. Nat Rev Dis Primers *5*, 42.

Fernyhough, P. (2015). Mitochondrial dysfunction in diabetic neuropathy: a series of unfortunate metabolic events. Curr Diab Rep *15*, 89.

Fernyhough, P., and Calcutt, N.A. (2010). Abnormal calcium homeostasis in peripheral neuropathies. Cell Calcium *47*, 130-139.

Fernyhough, P., Gallagher, A., Averill, S.A., Priestley, J.V., Hounsom, L., Patel, J., and Tomlinson, D.R. (1999). Aberrant neurofilament phosphorylation in sensory neurons of rats with diabetic neuropathy. Diabetes *48*, 881-889.

Fernyhough, P., and McGavock, J. (2014). Mechanisms of disease: Mitochondrial dysfunction in sensory neuropathy and other complications in diabetes. Handb Clin Neurol *126*, 353-377.

Fernyhough, P., Willars, G.B., Lindsay, R.M., and Tomlinson, D.R. (1993). Insulin and insulin-like growth factor I enhance regeneration in cultured adult rat sensory neurones. Brain Res *607*, 117-124.

Fleig, A., and Penner, R. (2004). The TRPM ion channel subfamily: molecular, biophysical and functional features. Trends Pharmacol Sci *25*, 633-639.

Fonfria, E., Murdock, P.R., Cusdin, F.S., Benham, C.D., Kelsell, R.E., and McNulty, S. (2006). Tissue distribution profiles of the human TRPM cation channel family. J Recept Signal Transduct Res *26*, 159-178.

Galiero, R., Caturano, A., Vetrano, E., Beccia, D., Brin, C., Alfano, M., Di Salvo, J., Epifani, R., Piacevole, A., Tagliaferri, G., *et al.* (2023). Peripheral Neuropathy in Diabetes Mellitus: Pathogenetic Mechanisms and Diagnostic Options. Int J Mol Sci *24*.

Galloway, C.A., and Yoon, Y. (2013). Mitochondrial morphology in metabolic diseases. Antioxid Redox Signal *19*, 415-430.

Galvin, V.C., Yang, S.T., Paspalas, C.D., Yang, Y., Jin, L.E., Datta, D., Morozov, Y.M., Lightbourne, T.C., Lowet, A.S., Rakic, P., *et al.* (2020). Muscarinic M1 Receptors Modulate Working Memory Performance and Activity via KCNQ Potassium Channels in the Primate Prefrontal Cortex. Neuron *106*, 649-661.e644.

Gao, N., Li, M., Wang, W., Liu, Z., and Guo, Y. (2024). The dual role of TRPV1 in peripheral neuropathic pain: pain switches caused by its sensitization or desensitization. Front Mol Neurosci *17*, 1400118.

Garoushi, S., Johnson, M.I., and Tashani, O.A. (2019). A cross-sectional study to estimate the point prevalence of painful diabetic neuropathy in Eastern Libya. BMC Public Health *19*, 78.

Gavazzi, I., Kumar, R.D., McMahon, S.B., and Cohen, J. (1999). Growth responses of different subpopulations of adult sensory neurons to neurotrophic factors in vitro. Eur J Neurosci *11*, 3405-3414.

George, D.S., Hackelberg, S., Jayaraj, N.D., Ren, D., Edassery, S.L., Rathwell, C.A., Miller, R.E., Malfait, A.M., Savas, J.N., Miller, R.J., *et al.* (2022). Mitochondrial calcium uniporter deletion prevents painful diabetic neuropathy by restoring mitochondrial morphology and dynamics. Pain *163*, 560-578.

George, D.S., Jayaraj, N.D., Pacifico, P., Ren, D., Sriram, N., Miller, R.E., Malfait, A.M., Miller, R.J., and Menichella, D.M. (2024). The Mas-related G protein-coupled receptor d (Mrgprd) mediates pain hypersensitivity in painful diabetic neuropathy. Pain *165*, 1154-1168.

Geraldes, P., and King, G.L. (2010). Activation of protein kinase C isoforms and its impact on diabetic complications. Circ Res *106*, 1319-1331.

Gerich, J.E. (2003). Contributions of insulin-resistance and insulin-secretory defects to the pathogenesis of type 2 diabetes mellitus. Mayo Clin Proc *78*, 447-456.

Giorgi, C., Missiroli, S., Patergnani, S., Duszynski, J., Wieckowski, M.R., and Pinton, P. (2015). Mitochondria-associated membranes: composition, molecular mechanisms, and physiopathological implications. Antioxid Redox Signal *22*, 995-1019.

Gordois, A., Scuffham, P., Shearer, A., Oglesby, A., and Tobian, J.A. (2003). The health care costs of diabetic peripheral neuropathy in the US. Diabetes Care *26*, 1790-1795.

Gould, R.W., Dencker, D., Grannan, M., Bubser, M., Zhan, X., Wess, J., Xiang, Z., Locuson, C., Lindsley, C.W., Conn, P.J., *et al.* (2015). Role for the M1 Muscarinic Acetylcholine Receptor in Top-Down Cognitive Processing Using a Touchscreen Visual Discrimination Task in Mice. ACS Chem Neurosci *6*, 1683-1695.

Greer, E.L., Oskoui, P.R., Banko, M.R., Maniar, J.M., Gygi, M.P., Gygi, S.P., and Brunet, A. (2007). The energy sensor AMP-activated protein kinase directly regulates the mammalian FOXO3 transcription factor. J Biol Chem *282*, 30107-30119.

Grimm, C., Kraft, R., Sauerbruch, S., Schultz, G., and Harteneck, C. (2003). Molecular and functional characterization of the melastatin-related cation channel TRPM3. J Biol Chem *278*, 21493-21501.

Gumy, L.F., Bampton, E.T., and Tolkovsky, A.M. (2008). Hyperglycaemia inhibits Schwann cell proliferation and migration and restricts regeneration of axons and Schwann cells from adult murine DRG. Mol Cell Neurosci *37*, 298-311.

Haberberger, R.V., Kuramatilake, J., Barry, C.M., and Matusica, D. (2023). Ultrastructure of dorsal root ganglia. Cell Tissue Res *393*, 17-36.

Hagg, T. (2006). Collateral sprouting as a target for improved function after spinal cord injury. J Neurotrauma *23*, 281-294.

Hall, D.P., Cost, N.G., Hegde, S., Kellner, E., Mikhaylova, O., Stratton, Y., Ehmer, B., Abplanalp, W.A., Pandey, R., Biesiada, J., *et al.* (2014). TRPM3 and miR-204 establish a regulatory circuit that controls oncogenic autophagy in clear cell renal cell carcinoma. Cancer Cell *26*, 738-753.

Hamid, H.S., Mervak, C.M., Münch, A.E., Robell, N.J., Hayes, J.M., Porzio, M.T., Singleton, J.R., Smith, A.G., Feldman, E.L., and Lentz, S.I. (2014). Hyperglycemia- and neuropathy-induced changes in mitochondria within sensory nerves. Ann Clin Transl Neurol *1*, 799-812.

Han, M.M., Frizzi, K.E., Ellis, R.J., Calcutt, N.A., and Fields, J.A. (2021). Prevention of HIV-1 TAT Protein-Induced Peripheral Neuropathy and Mitochondrial Disruption by the Antimuscarinic Pirenzepine. Front Neurol *12*, 663373.

Hanada, K., Kishimoto, S., Bellier, J.P., and Kimura, H. (2013). Peripheral choline acetyltransferase in rat skin demonstrated by immunohistochemistry. Cell Tissue Res *351*, 497-510.

Hansen, C.S., Jensen, T.M., Jensen, J.S., Nawroth, P., Fleming, T., Witte, D.R., Lauritzen, T., Sandbaek, A., Charles, M., Fleischer, J., *et al.* (2015). The role of serum methylglyoxal on diabetic peripheral and cardiovascular autonomic neuropathy: the ADDITION Denmark study. Diabet Med *32*, 778-785.

Hardie, D.G. (2013). AMPK: a target for drugs and natural products with effects on both diabetes and cancer. Diabetes *62*, 2164-2172.

Hatsuda, A., Kurisu, J., Fujishima, K., Kawaguchi, A., Ohno, N., and Kengaku, M. (2023). Calcium signals tune AMPK activity and mitochondrial homeostasis in dendrites of developing neurons. Development *150*.

Hawley, S.A., Pan, D.A., Mustard, K.J., Ross, L., Bain, J., Edelman, A.M., Frenguelli, B.G., and Hardie, D.G. (2005). Calmodulin-dependent protein kinase kinase-beta is an alternative upstream kinase for AMP-activated protein kinase. Cell Metab *2*, 9-19.

Held, K., Kichko, T., De Clercq, K., Klaassen, H., Van Bree, R., Vanherck, J.C., Marchand, A., Reeh, P.W., Chaltin, P., Voets, T., *et al.* (2015a). Activation of TRPM3 by a potent synthetic ligand reveals a role in peptide release. Proc Natl Acad Sci U S A *112*, E1363-1372.

Held, K., Voets, T., and Vriens, J. (2015b). TRPM3 in temperature sensing and beyond. Temperature (Austin) *2*, 201-213.

Hernández-Beltrán, N., Moreno, C.B., and Gutiérrez-Álvarez, A.M. (2013). Contribution of mitochondria to pain in diabetic neuropathy. Endocrinol Nutr *60*, 25-32.

Hill, B.G., Dranka, B.P., Zou, L., Chatham, J.C., and Darley-Usmar, V.M. (2009). Importance of the bioenergetic reserve capacity in response to cardiomyocyte stress induced by 4-hydroxynonenal. Biochem J *424*, 99-107.

Himeno, T., Kamiya, H., Naruse, K., Harada, N., Ozaki, N., Seino, Y., Shibata, T., Kondo, M., Kato, J., Okawa, T., *et al.* (2011). Beneficial effects of exendin-4 on experimental polyneuropathy in diabetic mice. Diabetes *60*, 2397-2406.

Himmel, N.J., and Cox, D.N. (2020). Transient receptor potential channels: current perspectives on evolution, structure, function and nomenclature. Proc Biol Sci *287*, 20201309.

Holakovska, B., Grycova, L., Jirku, M., Sulc, M., Bumba, L., and Teisinger, J. (2012). Calmodulin and S100A1 protein interact with N terminus of TRPM3 channel. J Biol Chem *287*, 16645-16655.

Howe, P.H., Akhtar, R.A., Naderi, S., and Abdel-Latif, A.A. (1986). Correlative studies on the effect of carbachol on myo-inositol trisphosphate accumulation, myosin light chain phosphorylation and contraction in sphincter smooth muscle of rabbit iris. J Pharmacol Exp Ther *239*, 574-583.

Hu, Z., Yu, X., Chen, P., Jin, K., Zhou, J., Wang, G., Yu, J., Wu, T., Wang, Y., Lin, F., *et al.* (2023). BDNF-TrkB signaling pathway-mediated microglial activation induces neuronal KCC2 downregulation contributing to dynamic allodynia following spared nerve injury. Mol Pain *19*, 17448069231185439.

Huang, T.J., Price, S.A., Chilton, L., Calcutt, N.A., Tomlinson, D.R., Verkhratsky, A., and Fernyhough, P. (2003). Insulin prevents depolarization of the mitochondrial inner membrane in sensory neurons of type 1 diabetic rats in the presence of sustained hyperglycemia. Diabetes *52*, 2129-2136.

Huang, T.J., Sayers, N.M., Fernyhough, P., and Verkhratsky, A. (2002). Diabetes-induced alterations in calcium homeostasis in sensory neurones of streptozotocin-diabetic rats are restricted to lumbar ganglia and are prevented by neurotrophin-3. Diabetologia *45*, 560-570.

Hulme, E.C., Birdsall, N.J., and Buckley, N.J. (1990). Muscarinic receptor subtypes. Annu Rev Pharmacol Toxicol *30*, 633-673.

Inoki, K., Zhu, T., and Guan, K.L. (2003). TSC2 mediates cellular energy response to control cell growth and survival. Cell *115*, 577-590.

Jäger, S., Handschin, C., St-Pierre, J., and Spiegelman, B.M. (2007). AMP-activated protein kinase (AMPK) action in skeletal muscle via direct phosphorylation of PGC-1alpha. Proc Natl Acad Sci U S A *104*, 12017-12022.

Jayaraj, N.D., Bhattacharyya, B.J., Belmadani, A.A., Ren, D., Rathwell, C.A., Hackelberg, S., Hopkins, B.E., Gupta, H.R., Miller, R.J., and Menichella, D.M. (2018). Reducing CXCR4-mediated nociceptor hyperexcitability reverses painful diabetic neuropathy. J Clin Invest *128*, 2205-2225.

Jimenez-Andrade, J.M., Herrera, M.B., Ghilardi, J.R., Vardanyan, M., Melemedjian, O.K., and Mantyh, P.W. (2008). Vascularization of the dorsal root ganglia and peripheral nerve of the mouse: implications for chemical-induced peripheral sensory neuropathies. Mol Pain *4*, 10.

Jin, H.Y., Moon, S.S., and Calcutt, N.A. (2021). Lost in Translation? Measuring Diabetic Neuropathy in Humans and Animals. Diabetes Metab J *45*, 27-42.

Jolivalt, C.G., Frizzi, K.E., Guernsey, L., Marquez, A., Ochoa, J., Rodriguez, M., and Calcutt, N.A. (2016). Peripheral Neuropathy in Mouse Models of Diabetes. Curr Protoc Mouse Biol *6*, 223-255.

Jolivalt, C.G., Frizzi, K.E., Han, M.M., Mota, A.J., Guernsey, L.S., Kotra, L.P., Fernyhough, P., and Calcutt, N.A. (2020). Topical Delivery of Muscarinic Receptor Antagonists Prevents and Reverses Peripheral Neuropathy in Female Diabetic Mice. J Pharmacol Exp Ther *374*, 44-51.

Jolivalt, C.G., Han, M.M., Nguyen, A., Desmond, F., Alves Jesus, C.H., Vasconselos, D.C., Pedneault, A., Sandlin, N., Dunne-Cerami, S., Frizzi, K.E., *et al.* (2022). Using Corneal Confocal Microscopy to Identify Therapeutic Agents for Diabetic Neuropathy. J Clin Med *11*.

Jolivalt, C.G., Lee, C.A., Ramos, K.M., and Calcutt, N.A. (2008). Allodynia and hyperalgesia in diabetic rats are mediated by GABA and depletion of spinal potassium-chloride co-transporters. Pain *140*, 48-57.

Kalichman, M.W., Powell, H.C., and Mizisin, A.P. (1998). Reactive, degenerative, and proliferative Schwann cell responses in experimental galactose and human diabetic neuropathy. Acta Neuropathol *95*, 47-56.

Kambiz, S., van Neck, J.W., Cosgun, S.G., van Velzen, M.H., Janssen, J.A., Avazverdi, N., Hovius, S.E., and Walbeehm, E.T. (2015). An early diagnostic tool for diabetic peripheral neuropathy in rats. PLoS One *10*, e0126892.

Kamiya, H., Zhang, W., and Sima, A.A. (2006). Degeneration of the Golgi and neuronal loss in dorsal root ganglia in diabetic BioBreeding/Worcester rats. Diabetologia *49*, 2763-2774.

Kamiya, H., Zhang, W., and Sima, A.A. (2009). Dynamic changes of neuroskeletal proteins in DRGs underlie impaired axonal maturation and progressive axonal degeneration in type 1 diabetes. Exp Diabetes Res *2009*, 793281.

Karlsson, P., Hincker, A.M., Jensen, T.S., Freeman, R., and Haroutounian, S. (2019). Structural, functional, and symptom relations in painful distal symmetric polyneuropathies: a systematic review. Pain *160*, 286-297.

Karthiksaravanan, K., and Meriton, A.S. (2024). A study on prevalence of diabetic peripheral neuropathy in diabetic patients attending a rural health and training centre. J Family Med Prim Care *13*, 726-729.

Khawaja, K.I., Walker, D., Hayat, S.A., Boulton, A.J., and Malik, R.A. (2000). Clinico-pathological features of postural hypotension in diabetic autonomic neuropathy. Diabet Med *17*, 163-166.

Kikuchi, S., Shinpo, K., Moriwaka, F., Makita, Z., Miyata, T., and Tashiro, K. (1999). Neurotoxicity of methylglyoxal and 3-deoxyglucosone on cultured cortical neurons: synergism between glycation and oxidative stress, possibly involved in neurodegenerative diseases. J Neurosci Res *57*, 280-289.

Kim, S.J., Tang, T., Abbott, M., Viscarra, J.A., Wang, Y., and Sul, H.S. (2016). AMPK Phosphorylates Desnutrin/ATGL and Hormone-Sensitive Lipase To Regulate Lipolysis and Fatty Acid Oxidation within Adipose Tissue. Mol Cell Biol *36*, 1961-1976.

Kitabchi, A.E., Umpierrez, G.E., Miles, J.M., and Fisher, J.N. (2009). Hyperglycemic crises in adult patients with diabetes. Diabetes Care *32*, 1335-1343.

Klocke, B., Krone, K., Tornes, J., Moore, C., Ott, H., and Pitychoutis, P.M. (2023). Insights into the role of intracellular calcium signaling in the neurobiology of neurodevelopmental disorders. Front Neurosci *17*, 1093099.

Koerich, S., Parreira, G.M., de Almeida, D.L., Vieira, R.P., and de Oliveira, A.C.P. (2023). Receptors for Advanced Glycation End Products (RAGE): Promising Targets Aiming at the Treatment of Neurodegenerative Conditions. Curr Neuropharmacol *21*, 219-234.

Kolluru, G.K., Bir, S.C., and Kevil, C.G. (2012). Endothelial dysfunction and diabetes: effects on angiogenesis, vascular remodeling, and wound healing. Int J Vasc Med *2012*, 918267.

Kostyuk, E., Pronchuk, N., and Shmigol, A. (1995). Calcium signal prolongation in sensory neurones of mice with experimental diabetes. Neuroreport *6*, 1010-1012.

Krames, E.S. (2014). The role of the dorsal root ganglion in the development of neuropathic pain. Pain Med *15*, 1669-1685.

Krügel, U., Straub, I., Beckmann, H., and Schaefer, M. (2017). Primidone inhibits TRPM3 and attenuates thermal nociception in vivo. Pain *158*, 856-867.

Kruse, A.C., Kobilka, B.K., Gautam, D., Sexton, P.M., Christopoulos, A., and Wess, J. (2014). Muscarinic acetylcholine receptors: novel opportunities for drug development. Nat Rev Drug Discov *13*, 549-560.

Kukkonen, A., Peräkylä, M., Akerman, K.E., and Näsman, J. (2004). Muscarinic toxin 7 selectivity is dictated by extracellular receptor loops. J Biol Chem *279*, 50923-50929.

Kumar, A., Kaundal, R.K., Iyer, S., and Sharma, S.S. (2007). Effects of resveratrol on nerve functions, oxidative stress and DNA fragmentation in experimental diabetic neuropathy. Life Sci *80*, 1236-1244.

Kumar, A., and Sharma, S.S. (2010). NF-kappaB inhibitory action of resveratrol: a probable mechanism of neuroprotection in experimental diabetic neuropathy. Biochem Biophys Res Commun *394*, 360-365.

Labbé, A., Liang, H., Martin, C., Brignole-Baudouin, F., Warnet, J.M., and Baudouin, C. (2006). Comparative anatomy of laboratory animal corneas with a new-generation high-resolution in vivo confocal microscope. Curr Eye Res *31*, 501-509.

Latorraca, N.R., Venkatakrishnan, A.J., and Dror, R.O. (2017). GPCR Dynamics: Structures in Motion. Chem Rev *117*, 139-155.

Lee, K.T., Bulls, H.W., Hoogland, A.I., James, B.W., Colon-Echevarria, C.B., and Jim, H.S.L. (2024). Chemotherapy-Induced Peripheral Neuropathy (CIPN): A Narrative Review and Proposed Theoretical Model. Cancers (Basel) *16*.

Lee-Kubli, C.A., Mixcoatl-Zecuatl, T., Jolivalt, C.G., and Calcutt, N.A. (2014). Animal models of diabetes-induced neuropathic pain. Curr Top Behav Neurosci *20*, 147-170.

Lemaitre, D., Hurtado, M.L., De Gregorio, C., Oñate, M., Martínez, G., Catenaccio, A., Wishart, T.M., and Court, F.A. (2020). Collateral Sprouting of Peripheral Sensory Neurons Exhibits a Unique Transcriptomic Profile. Mol Neurobiol *57*, 4232-4249.

Lenaz, G., Fato, R., Formiggini, G., and Genova, M.L. (2007). The role of Coenzyme Q in mitochondrial electron transport. Mitochondrion *7 Suppl*, S8-33.

Leprivier, G., Remke, M., Rotblat, B., Dubuc, A., Mateo, A.R., Kool, M., Agnihotri, S., El-Naggar, A., Yu, B., Somasekharan, S.P., *et al.* (2013). The eEF2 kinase confers resistance to nutrient deprivation by blocking translation elongation. Cell *153*, 1064-1079.

Li, H.L., Yin, R., Chen, D., Liu, D., Wang, D., Yang, Q., and Dong, Y.G. (2007). Long-term activation of adenosine monophosphate-activated protein kinase attenuates pressure-overload-induced cardiac hypertrophy. J Cell Biochem *100*, 1086-1099.

Li, L., Yang, Y., Bai, J., Zhang, Y., Yang, H., Zhang, Y., and Lv, H. (2022). Impaired Vascular Endothelial Function is Associated with Peripheral Neuropathy in Patients with Type 2 Diabetes. Diabetes Metab Syndr Obes *15*, 1437-1449.

Li, S., and Sheng, Z.H. (2022). Energy matters: presynaptic metabolism and the maintenance of synaptic transmission. Nat Rev Neurosci *23*, 4-22.

Ma, J., Farmer, K.L., Pan, P., Urban, M.J., Zhao, H., Blagg, B.S., and Dobrowsky, R.T. (2014). Heat shock protein 70 is necessary to improve mitochondrial bioenergetics and reverse diabetic sensory neuropathy following KU-32 therapy. J Pharmacol Exp Ther *348*, 281-292.

Ma, J., Pan, P., Anyika, M., Blagg, B.S., and Dobrowsky, R.T. (2015). Modulating Molecular Chaperones Improves Mitochondrial Bioenergetics and Decreases the Inflammatory Transcriptome in Diabetic Sensory Neurons. ACS Chem Neurosci *6*, 1637-1648.

Maalmi, H., Strom, A., Petrera, A., Hauck, S.M., Strassburger, K., Kuss, O., Zaharia, O.P., Bönhof, G.J., Rathmann, W., Trenkamp, S., *et al.* (2023). Serum neurofilament light chain: a novel biomarker for early diabetic sensorimotor polyneuropathy. Diabetologia *66*, 579-589.

Maeda, K., Fernyhough, P., and Tomlinson, D.R. (1996). Regenerating sensory neurones of diabetic rats express reduced levels of mRNA for GAP-43, gamma-preprotachykinin and the nerve growth factor receptors, trkA and p75NGFR. Brain Res Mol Brain Res *37*, 166-174.

Magliano, D.J., Boyko, E.J., and committee, I.D.F.D.A.t.e.s. (2021). IDF Diabetes Atlas. In Idf diabetes atlas (Brussels: International Diabetes Federation

© International Diabetes Federation, 2021.).

Mahar, M., and Cavalli, V. (2018). Intrinsic mechanisms of neuronal axon regeneration. Nat Rev Neurosci *19*, 323-337.

Mannella, C.A. (2020). Consequences of Folding the Mitochondrial Inner Membrane. Front Physiol *11*, 536.

Martin, C.L., Albers, J.W., and Pop-Busui, R. (2014). Neuropathy and related findings in the diabetes control and complications trial/epidemiology of diabetes interventions and complications study. Diabetes Care *37*, 31-38.

Matsushima, Y., and Kaguni, L.S. (2012). Matrix proteases in mitochondrial DNA function. Biochim Biophys Acta *1819*, 1080-1087.

Meza, C.A., La Favor, J.D., Kim, D.H., and Hickner, R.C. (2019). Endothelial Dysfunction: Is There a Hyperglycemia-Induced Imbalance of NOX and NOS? Int J Mol Sci *20*.

Misra, S.L., Craig, J.P., Patel, D.V., McGhee, C.N., Pradhan, M., Ellyett, K., Kilfoyle, D., and Braatvedt, G.D. (2015). In Vivo Confocal Microscopy of Corneal Nerves: An Ocular Biomarker for Peripheral and Cardiac Autonomic Neuropathy in Type 1 Diabetes Mellitus. Invest Ophthalmol Vis Sci *56*, 5060-5065.

Miyashita, A., Kobayashi, M., Yokota, T., and Zochodne, D.W. (2023). Diabetic Polyneuropathy: New Strategies to Target Sensory Neurons in Dorsal Root Ganglia. Int J Mol Sci *24*.

Mizisin, A.P., Nelson, R.W., Sturges, B.K., Vernau, K.M., Lecouteur, R.A., Williams, D.C., Burgers, M.L., and Shelton, G.D. (2007). Comparable myelinated nerve pathology in feline and human diabetes mellitus. Acta Neuropathol *113*, 431-442.

Mizisin, A.P., Shelton, G.D., Wagner, S., Rusbridge, C., and Powell, H.C. (1998). Myelin splitting, Schwann cell injury and demyelination in feline diabetic neuropathy. Acta Neuropathol *95*, 171-174.

Mizukami, H., and Osonoi, S. (2020). Pathogenesis and Molecular Treatment Strategies of Diabetic Neuropathy Collateral Glucose-Utilizing Pathways in Diabetic Polyneuropathy. Int J Mol Sci *22*.

Modesti, L., Danese, A., Angela Maria Vitto, V., Ramaccini, D., Aguiari, G., Gafà, R., Lanza, G., Giorgi, C., and Pinton, P. (2021). Mitochondrial Ca(2+) Signaling in Health, Disease and Therapy. Cells *10*.

Mootha, V.K., Lindgren, C.M., Eriksson, K.F., Subramanian, A., Sihag, S., Lehar, J., Puigserver, P., Carlsson, E., Ridderstråle, M., Laurila, E., *et al.* (2003). PGC-1alpha-responsive genes involved in oxidative phosphorylation are coordinately downregulated in human diabetes. Nat Genet *34*, 267-273.

Mu, X., Yang, M., Ling, P., Wu, A., Zhou, H., and Jiang, J. (2022). Acylcarnitines: Can They Be Biomarkers of Diabetic Nephropathy? Diabetes Metab Syndr Obes *15*, 247-256.

Mulder, D.W., Lambert, E.H., Bastron, J.A., and Sprague, R.G. (1961). The neuropathies associated with diabetes mellitus. A clinical and electromyographic study of 103 unselected diabetic patients. Neurology *11(4)Pt 1*, 275-284.

Mulderry, P.K., and Lindsay, R.M. (1990). Rat dorsal root ganglion neurons in culture express vasoactive intestinal polypeptide (VIP) independently of nerve growth factor. Neurosci Lett *108*, 314-320.

Murakami, T., Iwanaga, T., Ogawa, Y., Fujita, Y., Sato, E., Yoshitomi, H., Sunada, Y., and Nakamura, A. (2013). Development of sensory neuropathy in streptozotocin-induced diabetic mice. Brain Behav *3*, 35-41.

Nathan, D.M., Buse, J.B., Davidson, M.B., Heine, R.J., Holman, R.R., Sherwin, R., and Zinman, B. (2006). Management of hyperglycemia in type 2 diabetes: A consensus algorithm for the initiation and adjustment of therapy: a consensus statement from the American Diabetes Association and the European Association for the Study of Diabetes. Diabetes Care *29*, 1963-1972.

Naznin, F., Waise, T.M.Z., and Fernyhough, P. (2022). Antagonism of the Muscarinic Acetylcholine Type 1 Receptor Enhances Mitochondrial Membrane Potential and Expression of Respiratory Chain Components via AMPK in Human Neuroblastoma SH-SY5Y Cells and Primary Neurons. Mol Neurobiol *59*, 6754-6770.

Newlin Lew, K., Arnold, T., Cantelmo, C., Jacque, F., Posada-Quintero, H., Luthra, P., and Chon, K.H. (2022). Diabetes Distal Peripheral Neuropathy: Subtypes and Diagnostic and Screening Technologies. J Diabetes Sci Technol *16*, 295-320.

Nilius, B., Owsianik, G., Voets, T., and Peters, J.A. (2007). Transient receptor potential cation channels in disease. Physiol Rev *87*, 165-217.

Nilius, B., Talavera, K., and Verkhratsky, A. (2006). T-type calcium channels: the never ending story. Cell Calcium *40*, 81-88.

Nishizuka, Y. (1995). Protein kinase C and lipid signaling for sustained cellular responses. Faseb j *9*, 484-496.

O'Donovan, K.J. (2016). Intrinsic Axonal Growth and the Drive for Regeneration. Front Neurosci *10*, 486.

Oakhill, J.S., Scott, J.W., and Kemp, B.E. (2012). AMPK functions as an adenylate charge-regulated protein kinase. Trends Endocrinol Metab *23*, 125-132.

Obrosova, I.G. (2009). Diabetic painful and insensate neuropathy: pathogenesis and potential treatments. Neurotherapeutics *6*, 638-647.

Obrosova, I.G., Li, F., Abatan, O.I., Forsell, M.A., Komjáti, K., Pacher, P., Szabó, C., and Stevens, M.J. (2004). Role of poly(ADP-ribose) polymerase activation in diabetic neuropathy. Diabetes *53*, 711-720.

Owen, M.R., Doran, E., and Halestrap, A.P. (2000). Evidence that metformin exerts its anti-diabetic effects through inhibition of complex 1 of the mitochondrial respiratory chain. Biochem J *348 Pt 3*, 607-614.

Pacifico, P., Coy-Dibley, J.S., Miller, R.J., and Menichella, D.M. (2023). Peripheral mechanisms of peripheral neuropathic pain. Front Mol Neurosci *16*, 1252442.

Palumbo, P.J., Elveback, L.R., and Whisnant, J.P. (1978). Neurologic complications of diabetes mellitus: transient ischemic attack, stroke, and peripheral neuropathy. Adv Neurol *19*, 593-601.

Paneque, A., Fortus, H., Zheng, J., Werlen, G., and Jacinto, E. (2023). The Hexosamine Biosynthesis Pathway: Regulation and Function. Genes (Basel) *14*.

Pang, L., Lian, X., Liu, H., Zhang, Y., Li, Q., Cai, Y., Ma, H., and Yu, X. (2020). Understanding Diabetic Neuropathy: Focus on Oxidative Stress. Oxid Med Cell Longev *2020*, 9524635.

Partanen, J., Niskanen, L., Lehtinen, J., Mervaala, E., Siitonen, O., and Uusitupa, M. (1995). Natural history of peripheral neuropathy in patients with non-insulin-dependent diabetes mellitus. N Engl J Med *333*, 89-94.

Pedreanez, A., Robalino, J., Tene, D., and Salazar, P. (2024). Advanced glycation end products of dietary origin and their association with inflammation in diabetes - A minireview. Endocr Regul *58*, 57-67.

Peng, W., Tan, C., Mo, L., Jiang, J., Zhou, W., Du, J., Zhou, X., Liu, X., and Chen, L. (2021). Glucose transporter 3 in neuronal glucose metabolism: Health and diseases. Metabolism *123*, 154869.

Petersen, E.A., Stauss, T.G., Scowcroft, J.A., Brooks, E.S., White, J.L., Sills, S.M., Amirdelfan, K., Guirguis, M.N., Xu, J., Yu, C., *et al.* (2022). High-Frequency 10-kHz Spinal Cord Stimulation Improves Health-Related Quality of Life in Patients With Refractory Painful Diabetic Neuropathy: 12-Month Results From a Randomized Controlled Trial. Mayo Clin Proc Innov Qual Outcomes *6*, 347-360.

Picciotto, M.R., Higley, M.J., and Mineur, Y.S. (2012). Acetylcholine as a neuromodulator: cholinergic signaling shapes nervous system function and behavior. Neuron *76*, 116-129.

Pirart, J. (1977). [Diabetes mellitus and its degenerative complications: a prospective study of 4,400 patients observed between 1947 and 1973 (3rd and last part) (author's transl)]. Diabete Metab *3*, 245-256.

Pop-Busui, R., Lu, J., Brooks, M.M., Albert, S., Althouse, A.D., Escobedo, J., Green, J., Palumbo, P., Perkins, B.A., Whitehouse, F., *et al.* (2013). Impact of glycemic control strategies on the progression of diabetic peripheral neuropathy in the Bypass Angioplasty Revascularization Investigation 2 Diabetes (BARI 2D) Cohort. Diabetes Care *36*, 3208-3215.

Powell, H.C., Rosoff, J., and Myers, R.R. (1985). Microangiopathy in human diabetic neuropathy. Acta Neuropathol *68*, 295-305.

Preston, F.G., Riley, D.R., Azmi, S., and Alam, U. (2023). Painful Diabetic Peripheral Neuropathy: Practical Guidance and Challenges for Clinical Management. Diabetes Metab Syndr Obes *16*, 1595-1612.

Qin, P., He, C., Ye, P., Li, Q., Cai, C., and Li, Y. (2023). PKCδ regulates the vascular biology in diabetic atherosclerosis. Cell Commun Signal *21*, 330.

Quallo, T., Alkhatib, O., Gentry, C., Andersson, D.A., and Bevan, S. (2017). G protein βγ subunits inhibit TRPM3 ion channels in sensory neurons. Elife *6*.

Rawat, A., and Morrison, B.M. (2021). Metabolic Transporters in the Peripheral Nerve-What, Where, and Why? Neurotherapeutics *18*, 2185-2199.

Rizzuto, R., De Stefani, D., Raffaello, A., and Mammucari, C. (2012). Mitochondria as sensors and regulators of calcium signalling. Nat Rev Mol Cell Biol *13*, 566-578.

Rodgers, J.T., Lerin, C., Gerhart-Hines, Z., and Puigserver, P. (2008). Metabolic adaptations through the PGC-1 alpha and SIRT1 pathways. FEBS Lett *582*, 46-53.

Román-Pintos, L.M., Villegas-Rivera, G., Rodríguez-Carrizalez, A.D., Miranda-Díaz, A.G., and Cardona-Muñoz, E.G. (2016). Diabetic Polyneuropathy in Type 2 Diabetes Mellitus: Inflammation, Oxidative Stress, and Mitochondrial Function. J Diabetes Res *2016*, 3425617.

Ross, F.A., MacKintosh, C., and Hardie, D.G. (2016). AMP-activated protein kinase: a cellular energy sensor that comes in 12 flavours. Febs j *283*, 2987-3001.

Rossi, G. (2010). [Diagnosis and classification of diabetes mellitus]. Recenti Prog Med *101*, 274-276.

Roy Chowdhury, S.K., Smith, D.R., Saleh, A., Schapansky, J., Marquez, A., Gomes, S., Akude, E., Morrow, D., Calcutt, N.A., and Fernyhough, P. (2012). Impaired adenosine monophosphate-

activated protein kinase signalling in dorsal root ganglia neurons is linked to mitochondrial dysfunction and peripheral neuropathy in diabetes. Brain *135*, 1751-1766.

Rüdiger, T., and Bolz, J. (2008). Acetylcholine influences growth cone motility and morphology of developing thalamic axons. Cell Adh Migr *2*, 30-37.

Rumora, A.E., Lentz, S.I., Hinder, L.M., Jackson, S.W., Valesano, A., Levinson, G.E., and Feldman, E.L. (2018). Dyslipidemia impairs mitochondrial trafficking and function in sensory neurons. Faseb j *32*, 195-207.

Russell, R.R., 3rd, Li, J., Coven, D.L., Pypaert, M., Zechner, C., Palmeri, M., Giordano, F.J., Mu, J., Birnbaum, M.J., and Young, L.H. (2004). AMP-activated protein kinase mediates ischemic glucose uptake and prevents postischemic cardiac dysfunction, apoptosis, and injury. J Clin Invest *114*, 495-503.

Ryan, K.C., Ashkavand, Z., and Norman, K.R. (2020). The Role of Mitochondrial Calcium Homeostasis in Alzheimer's and Related Diseases. Int J Mol Sci *21*.

Sabbir, M.G., Calcutt, N.A., and Fernyhough, P. (2018). Muscarinic Acetylcholine Type 1 Receptor Activity Constrains Neurite Outgrowth by Inhibiting Microtubule Polymerization and Mitochondrial Trafficking in Adult Sensory Neurons. Front Neurosci *12*, 402.

Saleh, A., Sabbir, M.G., Aghanoori, M.R., Smith, D.R., Roy Chowdhury, S.K., Tessler, L., Brown, J., Gedarevich, E., Kassahun, M.Z., Frizzi, K., *et al.* (2020). Muscarinic Toxin 7 Signals Via Ca(2+)/Calmodulin-Dependent Protein Kinase Kinase β to Augment Mitochondrial Function and Prevent Neurodegeneration. Mol Neurobiol *57*, 2521-2538.

Sapunar, D., Kostic, S., Banozic, A., and Puljak, L. (2012). Dorsal root ganglion - a potential new therapeutic target for neuropathic pain. J Pain Res *5*, 31-38.

Schartner, E., Sabbir, M.G., Saleh, A., Silva, R.V., Roy Chowdhury, S., Smith, D.R., and Fernyhough, P. (2018). High glucose concentration suppresses a SIRT2 regulated pathway that enhances neurite outgrowth in cultured adult sensory neurons. Exp Neurol *309*, 134-147.

Schmidt, R.E., Dorsey, D., Parvin, C.A., Beaudet, L.N., Plurad, S.B., and Roth, K.A. (1997). Dystrophic axonal swellings develop as a function of age and diabetes in human dorsal root ganglia. J Neuropathol Exp Neurol *56*, 1028-1043.

Schmidt, R.E., Green, K.G., Snipes, L.L., and Feng, D. (2009). Neuritic dystrophy and neuronopathy in Akita (Ins2(Akita)) diabetic mouse sympathetic ganglia. Exp Neurol *216*, 207-218.

Schmidt, R.E., Parvin, C.A., and Green, K.G. (2008). Synaptic ultrastructural alterations anticipate the development of neuroaxonal dystrophy in sympathetic ganglia of aged and diabetic mice. J Neuropathol Exp Neurol *67*, 1166-1186.

Schroer, J.A., Plurad, S.B., and Schmidt, R.E. (1992). Fine structure of presynaptic axonal terminals in sympathetic autonomic ganglia of aging and diabetic human subjects. Synapse *12*, 1-13.

Seager, R., Lee, L., Henley, J.M., and Wilkinson, K.A. (2020). Mechanisms and roles of mitochondrial localisation and dynamics in neuronal function. Neuronal Signal *4*, Ns20200008.

Sharma, S., and Rayman, G. (2023). Frontiers in diagnostic and therapeutic approaches in diabetic sensorimotor neuropathy (DSPN). Front Endocrinol (Lausanne) *14*, 1165505.

Shields, S.D., Ahn, H.S., Yang, Y., Han, C., Seal, R.P., Wood, J.N., Waxman, S.G., and Dib-Hajj, S.D. (2012). Nav1.8 expression is not restricted to nociceptors in mouse peripheral nervous system. Pain *153*, 2017-2030.

Singh, B., Singh, V., Krishnan, A., Koshy, K., Martinez, J.A., Cheng, C., Almquist, C., and Zochodne, D.W. (2014). Regeneration of diabetic axons is enhanced by selective knockdown of the PTEN gene. Brain *137*, 1051-1067.

Singh, R., Gholipourmalekabadi, M., and Shafikhani, S.H. (2024). Animal models for type 1 and type 2 diabetes: advantages and limitations. Front Endocrinol (Lausanne) *15*, 1359685.

Sloan, G., Selvarajah, D., and Tesfaye, S. (2021). Pathogenesis, diagnosis and clinical management of diabetic sensorimotor peripheral neuropathy. Nat Rev Endocrinol *17*, 400-420.

Smith, D.S., and Skene, J.H. (1997). A transcription-dependent switch controls competence of adult neurons for distinct modes of axon growth. J Neurosci *17*, 646-658.

Smith, S., Normahani, P., Lane, T., Hohenschurz-Schmidt, D., Oliver, N., and Davies, A.H. (2022). Pathogenesis of Distal Symmetrical Polyneuropathy in Diabetes. Life (Basel) *12*.

Soyoye, D.O., Abiodun, O.O., Ikem, R.T., Kolawole, B.A., and Akintomide, A.O. (2021). Diabetes and peripheral artery disease: A review. World J Diabetes *12*, 827-838.

Srinivasan, S., Stevens, M., and Wiley, J.W. (2000). Diabetic peripheral neuropathy: evidence for apoptosis and associated mitochondrial dysfunction. Diabetes *49*, 1932-1938.

Staehelin Jensen, T. (2023). The pathogenesis of painful diabetic neuropathy and clinical presentation. Diabetes Res Clin Pract *206 Suppl 1*, 110753.

Stancu, B., Ilyés, T., Farcas, M., Coman, H.F., Chiș, B.A., and Andercou, O.A. (2022). Diabetic Foot Complications: A Retrospective Cohort Study. Int J Environ Res Public Health *20*.

Steinmetz, J.D. (2024). Global, regional, and national burden of disorders affecting the nervous system, 1990-2021: a systematic analysis for the Global Burden of Disease Study 2021. Lancet Neurol *23*, 344-381.

Stevens, M.J., Zhang, W., Li, F., and Sima, A.A. (2004). C-peptide corrects endoneurial blood flow but not oxidative stress in type 1 BB/Wor rats. Am J Physiol Endocrinol Metab *287*, E497-505.

Straub, I., Krügel, U., Mohr, F., Teichert, J., Rizun, O., Konrad, M., Oberwinkler, J., and Schaefer, M. (2013). Flavanones that selectively inhibit TRPM3 attenuate thermal nociception in vivo. Mol Pharmacol *84*, 736-750.

Tavakoli, M., Quattrini, C., Abbott, C., Kallinikos, P., Marshall, A., Finnigan, J., Morgan, P., Efron, N., Boulton, A.J., and Malik, R.A. (2010). Corneal confocal microscopy: a novel noninvasive test to diagnose and stratify the severity of human diabetic neuropathy. Diabetes Care *33*, 1792-1797.

Tesfaye, S., Chaturvedi, N., Eaton, S.E., Ward, J.D., Manes, C., Ionescu-Tirgoviste, C., Witte, D.R., and Fuller, J.H. (2005). Vascular risk factors and diabetic neuropathy. N Engl J Med *352*, 341-350.

Thiel, G., Müller, I., and Rössler, O.G. (2013). Signal transduction via TRPM3 channels in pancreatic β-cells. J Mol Endocrinol *50*, R75-83.

Thiel, G., and Rössler, O.G. (2023). Calmodulin Regulates Transient Receptor Potential TRPM3 and TRPM8-Induced Gene Transcription. Int J Mol Sci *24*.

Thiel, G., Rubil, S., Lesch, A., Guethlein, L.A., and Rössler, O.G. (2017). Transient receptor potential TRPM3 channels: Pharmacology, signaling, and biological functions. Pharmacol Res *124*, 92-99.

Tóth, B.I., Konrad, M., Ghosh, D., Mohr, F., Halaszovich, C.R., Leitner, M.G., Vriens, J., Oberwinkler, J., and Voets, T. (2015). Regulation of the transient receptor potential channel TRPM3 by phosphoinositides. J Gen Physiol *146*, 51-63.

Tuncer, S., Dalkilic, N., Esen, H.H., and Avunduk, M.C. (2011). An early diagnostic tool for diabetic neuropathy: conduction velocity distribution. Muscle Nerve *43*, 237-244.

Uchida, K. (2024). TRPM3, TRPM4, and TRPM5 as thermo-sensitive channels. J Physiol Sci *74*, 43.

Urban, M.J., Pan, P., Farmer, K.L., Zhao, H., Blagg, B.S., and Dobrowsky, R.T. (2012). Modulating molecular chaperones improves sensory fiber recovery and mitochondrial function in diabetic peripheral neuropathy. Exp Neurol *235*, 388-396.

Ureshino, R.P., Erustes, A.G., Bassani, T.B., Wachilewski, P., Guarache, G.C., Nascimento, A.C., Costa, A.J., Smaili, S.S., and Pereira, G. (2019). The Interplay between Ca(2+) Signaling Pathways and Neurodegeneration. Int J Mol Sci *20*.

Vandewauw, I., De Clercq, K., Mulier, M., Held, K., Pinto, S., Van Ranst, N., Segal, A., Voet, T., Vennekens, R., Zimmermann, K., *et al.* (2018). A TRP channel trio mediates acute noxious heat sensing. Nature *555*, 662-666.

Vangeel, L., Benoit, M., Miron, Y., Miller, P.E., De Clercq, K., Chaltin, P., Verfaillie, C., Vriens, J., and Voets, T. (2020). Functional expression and pharmacological modulation of TRPM3 in human sensory neurons. Br J Pharmacol *177*, 2683-2695.

Varughese, J.T., Buchanan, S.K., and Pitt, A.S. (2021). The Role of Voltage-Dependent Anion Channel in Mitochondrial Dysfunction and Human Disease. Cells *10*.

Venkatachalam, K., and Montell, C. (2007). TRP channels. Annu Rev Biochem *76*, 387-417.

Verkhratsky, A., and Fernyhough, P. (2008). Mitochondrial malfunction and Ca2+ dyshomeostasis drive neuronal pathology in diabetes. Cell Calcium *44*, 112-122.

Vincent, A.M., Edwards, J.L., McLean, L.L., Hong, Y., Cerri, F., Lopez, I., Quattrini, A., and Feldman, E.L. (2010). Mitochondrial biogenesis and fission in axons in cell culture and animal models of diabetic neuropathy. Acta Neuropathol *120*, 477-489.

Vincent, A.M., Olzmann, J.A., Brownlee, M., Sivitz, W.I., and Russell, J.W. (2004). Uncoupling proteins prevent glucose-induced neuronal oxidative stress and programmed cell death. Diabetes *53*, 726-734.

Vinik, A.I., Maser, R.E., Mitchell, B.D., and Freeman, R. (2003). Diabetic autonomic neuropathy. Diabetes Care *26*, 1553-1579.

Vriens, J., Held, K., Janssens, A., Tóth, B.I., Kerselaers, S., Nilius, B., Vennekens, R., and Voets, T. (2014). Opening of an alternative ion permeation pathway in a nociceptor TRP channel. Nat Chem Biol *10*, 188-195.

Vriens, J., Owsianik, G., Hofmann, T., Philipp, S.E., Stab, J., Chen, X., Benoit, M., Xue, F., Janssens, A., Kerselaers, S., *et al.* (2011). TRPM3 is a nociceptor channel involved in the detection of noxious heat. Neuron *70*, 482-494.

Wada, R., and Yagihashi, S. (2005). Role of advanced glycation end products and their receptors in development of diabetic neuropathy. Ann N Y Acad Sci *1043*, 598-604.

Wagner, T.F., Loch, S., Lambert, S., Straub, I., Mannebach, S., Mathar, I., Düfer, M., Lis, A., Flockerzi, V., Philipp, S.E., *et al.* (2008). Transient receptor potential M3 channels are ionotropic steroid receptors in pancreatic beta cells. Nat Cell Biol *10*, 1421-1430.

Wang, D., Gao, Q., Schaefer, I., Moerz, H., Hoheisel, U., Rohr, K., Greffrath, W., and Treede, R.D. (2022). TRPM3-mediated dynamic mitochondrial activity in nerve growth factor-induced latent sensitization of chronic low back pain. Pain *163*, e1115-e1128.

Wang, H., Fan, D., Wang, W., Zhang, S., and Wang, X. (2015). [Early diagnosis of diabetic autonomic neuropathy by corneal confocal microscopy]. Zhonghua Yi Xue Za Zhi *95*, 2851-2856.

Wang, R., Tu, S., Zhang, J., and Shao, A. (2020). Roles of TRP Channels in Neurological Diseases. Oxid Med Cell Longev *2020*, 7289194.

Wang, Y., Dai, X., Li, H., Jiang, H., Zhou, J., Zhang, S., Guo, J., Shen, L., Yang, H., Lin, J., *et al.* (2023). The role of mitochondrial dynamics in disease. MedComm (2020) *4*, e462.

Way, K.J., Katai, N., and King, G.L. (2001). Protein kinase C and the development of diabetic vascular complications. Diabet Med *18*, 945-959.

Weis, W.I., and Kobilka, B.K. (2018). The Molecular Basis of G Protein-Coupled Receptor Activation. Annu Rev Biochem *87*, 897-919.

Wess, J., Eglen, R.M., and Gautam, D. (2007). Muscarinic acetylcholine receptors: mutant mice provide new insights for drug development. Nat Rev Drug Discov *6*, 721-733.

Willows, J.W., Gunsch, G., Paradie, E., Blaszkiewicz, M., Tonniges, J.R., Pino, M.F., Smith, S.R., Sparks, L.M., and Townsend, K.L. (2023). Schwann cells contribute to demyelinating diabetic neuropathy and nerve terminal structures in white adipose tissue. iScience *26*, 106189.

Wilson, D.F. (2017). Oxidative phosphorylation: regulation and role in cellular and tissue metabolism. J Physiol *595*, 7023-7038.

Woods, A., Johnstone, S.R., Dickerson, K., Leiper, F.C., Fryer, L.G., Neumann, D., Schlattner, U., Wallimann, T., Carlson, M., and Carling, D. (2003). LKB1 is the upstream kinase in the AMP-activated protein kinase cascade. Curr Biol *13*, 2004-2008.

Wu, J., Prole, D.L., Shen, Y., Lin, Z., Gnanasekaran, A., Liu, Y., Chen, L., Zhou, H., Chen, S.R., Usachev, Y.M., *et al.* (2014). Red fluorescent genetically encoded Ca2+ indicators for use in mitochondria and endoplasmic reticulum. Biochem J *464*, 13-22.

Xiao, B., Sanders, M.J., Underwood, E., Heath, R., Mayer, F.V., Carmena, D., Jing, C., Walker, P.A., Eccleston, J.F., Haire, L.F., *et al.* (2011). Structure of mammalian AMPK and its regulation by ADP. Nature *472*, 230-233.

Yorek, M.S., Obrosov, A., Shevalye, H., Lupachyk, S., Harper, M.M., Kardon, R.H., and Yorek, M.A. (2014). Effect of glycemic control on corneal nerves and peripheral neuropathy in streptozotocin-induced diabetic C57Bl/6J mice. J Peripher Nerv Syst *19*, 205-217.

Young, S.H., and Poo, M.M. (1983). Spontaneous release of transmitter from growth cones of embryonic neurones. Nature *305*, 634-637.

Zhang, L., Yu, C., Vasquez, F.E., Galeva, N., Onyango, I., Swerdlow, R.H., and Dobrowsky, R.T. (2010). Hyperglycemia alters the schwann cell mitochondrial proteome and decreases coupled respiration in the absence of superoxide production. J Proteome Res *9*, 458-471.

Zhang, M., Chen, T., Lu, X., Lan, X., Chen, Z., and Lu, S. (2024). G protein-coupled receptors (GPCRs): advances in structures, mechanisms, and drug discovery. Signal Transduct Target Ther *9*, 88.

Zhao, C., and MacKinnon, R. (2023). Structural and functional analyses of a GPCR-inhibited ion channel TRPM3. Neuron *111*, 81-91.e87.

Zhao, L.X., Ge, Y.H., Xiong, C.H., Tang, L., Yan, Y.H., Law, P.Y., Qiu, Y., and Chen, H.Z. (2018). M1 muscarinic receptor facilitates cognitive function by interplay with AMPA receptor GluA1 subunit. Faseb j *32*, 4247-4257.

Zhao, S., Yudin, Y., and Rohacs, T. (2020). Disease-associated mutations in the human TRPM3 render the channel overactive via two distinct mechanisms. Elife *9*.

Zhao, Y., Araki, S., Wu, J., Teramoto, T., Chang, Y.F., Nakano, M., Abdelfattah, A.S., Fujiwara, M., Ishihara, T., Nagai, T., *et al.* (2011). An expanded palette of genetically encoded Ca^{2+} indicators. Science *333*, 1888-1891.

Zherebitskaya, E., Akude, E., Smith, D.R., and Fernyhough, P. (2009). Development of selective axonopathy in adult sensory neurons isolated from diabetic rats: role of glucose-induced oxidative stress. Diabetes *58*, 1356-1364.

Zherebitskaya, E., Schapansky, J., Akude, E., Smith, D.R., Van der Ploeg, R., Solovyova, N., Verkhratsky, A., and Fernyhough, P. (2012). Sensory neurons derived from diabetic rats have diminished internal Ca2+ stores linked to impaired re-uptake by the endoplasmic reticulum. ASN Neuro *4*.

Zhu, J., Hu, Z., Luo, Y., Liu, Y., Luo, W., Du, X., Luo, Z., Hu, J., and Peng, S. (2023). Diabetic peripheral neuropathy: pathogenetic mechanisms and treatment. Front Endocrinol (Lausanne) *14*, 1265372.

Ziegler, D., Landgraf, R., Lobmann, R., Reiners, K., Rett, K., Schnell, O., and Strom, A. (2018). Painful and painless neuropathies are distinct and largely undiagnosed entities in subjects participating in an educational initiative (PROTECT study). Diabetes Res Clin Pract *139*, 147-154.

Ziegler, D., Papanas, N., Zhivov, A., Allgeier, S., Winter, K., Ziegler, I., Brüggemann, J., Strom, A., Peschel, S., Köhler, B., *et al.* (2014). Early detection of nerve fiber loss by corneal confocal microscopy and skin biopsy in recently diagnosed type 2 diabetes. Diabetes *63*, 2454-2463.

Zochodne, D.W. (2014). Mechanisms of diabetic neuron damage: Molecular pathways. Handb Clin Neurol *126*, 379-399.

Zochodne, D.W., and Ho, L.T. (1991). Unique microvascular characteristics of the dorsal root ganglion in the rat. Brain Res *559*, 89-93.

Zong, Y., Li, H., Liao, P., Chen, L., Pan, Y., Zheng, Y., Zhang, C., Liu, D., Zheng, M., and Gao, J. (2024). Mitochondrial dysfunction: mechanisms and advances in therapy. Signal Transduct Target Ther *9*, 124.

Outlook

Thank you for your order with RightsLink / Elsevier

From no-reply@email.copyright.com <no-reply@email.copyright.com>
Date Mon 12/16/2024 2:46 PM
To Sanjana Chauhan <chauhans@myumanitoba.ca>

Caution! This message was sent from outside the University of Manitoba.

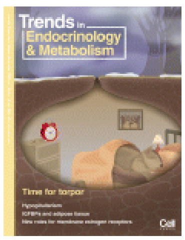

Thank you for your order!

Dear Ms. Sanjana Chauhan,

Thank you for placing your order through Copyright Clearance Center's RightsLink® service.

Order Summary

Licensee:	Ms. Sanjana Chauhan
Order Date:	Dec 16, 2024
Order Number:	5930941046231
Publication:	Trends in Endocrinology & Metabolism
Title:	AMPK functions as an adenylate charge-regulated protein kinase
Type of Use:	reuse in a thesis/dissertation
Order Total:	0.00 CAD

View or print complete details of your order and the publisher's terms and conditions.

Sincerely,

Outlook

Thank you for your order with RightsLink / Elsevier

From no-reply@email.copyright.com <no-reply@email.copyright.com>
Date Mon 12/16/2024 2:58 PM
To Sanjana Chauhan <chauhans@myumanitoba.ca>

Caution! This message was sent from outside the University of Manitoba.

Thank you for your order!

Dear Ms. Sanjana Chauhan,

Thank you for placing your order through Copyright Clearance Center's RightsLink® service.

Order Summary

Licensee:	Ms. Sanjana Chauhan
Order Date:	Dec 16, 2024
Order Number:	5930950265184
Publication:	Pharmacological Research
Title:	Transient receptor potential TRPM3 channels: Pharmacology, signaling, and biological functions
Type of Use:	reuse in a thesis/dissertation
Order Total:	0.00 CAD

View or print complete details of your order and the publisher's terms and conditions.

Sincerely,

Outlook

Thank you for your order with RightsLink / Wolters Kluwer Health, Inc.

From no-reply@email.copyright.com <no-reply@email.copyright.com>
Date Mon 3/3/2025 7:13 PM
To Sanjana Chauhan <chauhans@myumanitoba.ca>

Thank you for your order!

Dear Ms. Sanjana Chauhan,

Thank you for placing your order through Copyright Clearance Center's RightsLink® service.

Order Summary

Licensee:	Ms. Sanjana Chauhan
Order Date:	Mar 3, 2025
Order Number:	5981620655377
Publication:	Pain
Title:	Structural, functional, and symptom relations in painful distal symmetric polyneuropathies: a systematic review
Type of Use:	Dissertation/Thesis
Order Total:	0.00 CAD

View or print complete details of your order and the publisher's terms and conditions.